

Role of Intrinsic Disorder in Human Exonuclease1 Regulation

By

Aminu Umar Argungu

Submitted to

School of Bioscience

The University of Nottingham, UK

11th July 2016

Supervisor

Dr David J. Scott

Internal Assessor

Dr Jon Hobman

ABSTRACT

Human exonuclease1 (hExo1) is a member of the eukaryotic nuclease family that includes Rad2/Xeroderma pigmentosum complementation group G (XPG), flap endonuclease1 (FEN1) and gap endonuclease1 (GEN1). Human exonuclease1 is involved in multiple DNA metabolism processes, including DNA repair and replication. Most of the fundamental roles of Exo1 have been described in yeast. In this study, hExo1 protein was over expressed from both insect cells and bacteria and over expressed protein was purified to near homogeneity. In this research project, a biochemical characterization of full-length hExo1 is reported. As well as assaying hExo1 on different dsDNA substrates, the factors essential for the thermodynamic stability of hExo1 were determined. It is shown in this study that resection activity and stability of hExo1 on dsDNA is modulated by temperature, pH and salt concentration.

The DNA end resection process is a guiding principle to cellular response during DNA double strand break lesion and is pivotal for genome maintenance. Even though insufficient DNA resection restrains homology-directed repair mechanisms and the activation of ATR (ataxia telangiectasia and Rad3 related)-dependent checkpoint, over-resection results in production of an excessive single-stranded DNA that could lead to genomic instability. Nonetheless, the control mechanisms for DNA end resection are not yet understood fully. In this study it is shown that the major resection nuclease hExo1 is both positively and negatively controlled by protein-protein interactions to enable a proper DNA end resection mechanism. This report show that 14-3-3ζ 14-3-3ε proteins interact with the C-terminus region of hExo1 and allosterically control hExo1 DNA end-resection activity while PCNA sliding clamp increases the DNA end resection activity by hExo1.

Circular dichroism shows that the C-terminus region of hExo1 is intrinsically disordered with significant polyproline type II conformations. Dynamic Light Scattering and Sedimentation Velocity Analytical Ultracentrifugation results show that a monomeric, partly intrinsically disordered, form persists for hExo1 in solution with an expanded hydrodynamic radius of 118 Å. Taking into consideration the structural propensity of hExo1 and the fact that, more often the binding sites for the 14-3-3 proteins are found within the unstructured regions, this study propose that the disorder-to-order transition of the ligand molecule's structure might be a model of how hExo1 is negatively control by the 14-3-3 proteins. Results of this project work provide crucial insights into a pioneering process of DNA end resection regulation a critical event in genome maintenance and may be implicative in cancer treatment.

ACKNOWLEDGMENTS

I wish to express my profound gratitude to my supervisor **Dr David J. Scott** for giving me this great opportunity to work in his laboratory. I thank him for his enormous support and generosity both academically and personally. I say big thank to him for all the supports and guides he accorded to me, I very much appreciate his great and positive impact in making this research project a reality. The assistance from **Dr Stephen Carr** (Research Complex at Harwell) in the expression of hExo1 protein from insect cells and positive discussions are highly acknowledged. I thank **Gemma Harris** (Research Complex at Harwell) for her immense help and contribution in running SV-AUC experiment. The assistance and contribution from **Giuliano Siligardi** and **Rohanah Hussain** towards CD and DLS experiments at (Diamond B23, Research Complex at Harwell) are acknowledged and appreciated. I thank Professor Paul Modrich for the kind gift of hExo1 and PCNA clones. I thank Professor Lene Rasmussen for the kind gift of 14-3-3s clones. I thank **Karishma Asiani** for her support and helpful discussions. I wish to extend my gratitude to the School of Biosciences, The University of Nottingham United Kingdom Campus.

TABLE OF CONTENTS

Page

Chapter One: Introduction 1
1.0. Introduction 1
1.1. Sensing the DNA damage 2
1.2. DNA damage and repair 7
1.3. DNA resection 12
1.4. *In vitro* reconstitution of DNA resection 16
1.4.1. Interpreting the *in vitro* and *in vivo* observations of the DNA resection 17
1.4.2. Redundancy of Exo1 and Sgs1-Mediated Pathways 18
1.5. Exonuclease1 20
1.6. Proliferating Cell Nuclear Antigen (PCNA) 28
1.7. The 14-3-3 proteins 32
1.8. Intrinsically disordered proteins 39
1.9. Disorder prediction in hExo1 41
1.10. Analytical Ultracentrifugation (AUC) 43
1.11. Small Angle X-ray Scattering (SAXS) 44
1.12. Circular Dichroism (CD) 46
1.13. Dynamic Light Scattering (DLS) 46
1.14. Project Outline 48
Chapter Two: Materials and Methods 51
2.1.0. Materials 51
2.2.0. Methods 52
2.2.1. Cloning 52
2.2.1.1. Propagation of pFastbacI-hExo1 plasmid 52
2.2.1.2. Miniprep of the pFastbacI-hExo1 plasmid 52
2.2.1.3. Transforming DH10Bac™ *E. coli* 53
2.2.1.4. Isolating recombinant bacmid DNA 54
2.2.1.5. Analyzing recombinant bacmid DNA by PCR 56
2.2.1.6. Recombinant baculovirus production 57
2.2.1.7. Isolating P1 viral stock 58
2.2.1.8. Amplifying baculoviral stock 58
2.2.1.9. Preparing a viral plaque assay 59
2.2.1.10. Plaque assay procedure 59
2.2.1.11. Cloning hExo1 into pTXB1 vector 61
2.2.1.12. PCR for cloning full-length hExo1 into pTXB1 vector 61
2.2.1.13. Restriction digest of hExo1 PCR product 62
2.2.1.14. Ligation of the hExo1 PCR product into pTXB1 vector 63
2.2.1.15. Transformation of bacteria with ligated pTXB1 vector 64
2.2.1.16. Colony PCR screen for the ligated vector 64
2.2.1.17. Miniprep of the pTXB1-hExo1 plasmid 64
2.2.1.18. Cloning of Nt-hExo1 into pET28a vector 66
2.2.1.19. Cloning of PCNA, 14-3-3ζ and 14-3-3ε into pET28a vector 66
2.2.2.0. Recombinant protein expression 68
2.2.2.1. Expression of hExo1 protein from insect cells 68
2.2.2.2. Expression of hExo1 protein from bacteria 68
2.2.2.3. Expression of Nt-hExo1 protein 69

2.2.2.4. Expression of PCNA, 14-3-3ζ and 14-3-3ε proteins 69
2.2.3.0. Protein purification 71
2.2.3.1. Purification of hExo1 protein expressed from insect cells 71
2.2.3.2. Purification of hExo1 protein expressed from bacteria 72
2.2.3.3. Purification of His-tagged Nt-hExo1, PCNA, 14-3-3ζ & 14-3-3ε proteins.. 74
2.2.4.0. Mass spectrometry 75
2.2.4.1. Gel piece processing and tryptic digestions 75
2.2.4.2. Mass spectrometry 76
2.2.4.3. Data processing and database searching 76
2.2.5.0. *In vitro* DNA resection assays 77
2.2.5.1. DNA resection assay at different salt concentrations in reaction buffer .. 77
2.2.5.2. DNA resection assay at different pH conditions of the reaction buffer 77
2.2.5.3. DNA resection assay at different temperature conditions 78
2.2.5.4. DNA resection assay after pre-incubation of hExo1 78
2.2.5.5. DNA resection assay with different DNA end substrates 78
2.2.5.6. Time-course DNA resection assay of hExo1 78
2.2.5.7. DNA resection assay in the presence or absence of ATP and Mg^{2+} 78
2.2.5.8. DNA resection assay with Nt-hExo1 protein 79
2.2.5.9. DNA resection assay in the presence of PCNA 79
2.2.5.10. DNA resection assay in the presence of 14-3-3 proteins 79
2.2.5.11. Molar ratio assays of hExo1 with PCNA and 14-3-3 proteins 80
2.2.6. Sedimentation Velocity Analytical Ultracentrifugation analyses 80
2.2.7. Analyses of proteins by Small Angle X-ray Scattering 80
2.2.8. Analyses of proteins by Circular dichroism 81
2.2.9. Analyses of proteins by Dynamic light scattering 81
Chapter Three: Results for Cloning Studies 82
3.1.0. Cloning 82
3.1.1. Plasmid for hExo1 expression in insect cells 82
3.1.2. Transformation of *E. coli* DH10Bac™ 83
3.1.3. Plasmid for hExo1 protein expression in bacteria 87
3.1.4. Cloning of Nt-hExo1 into pET28a vector 89
3.1.5. Cloning of PCNA, 14-3-3ζ and 14-3-3ε into pET28a vector 91
3.2.0. Expression of recombinant proteins 93
3.2.1. Expression of hExo1 protein..... 93
3.2.2. Expression of Nt-hExo1 protein 96
3.2.3. Expression of PCNA, 14-3-3ζ and 14-3-3ε proteins 97
3.3.0. Purification of proteins 99
3.3.1. Purification of hExo1 protein expressed from insect cells and bacteria 99
3.3.2. Purification of Nt-hExo1 protein 101
3.3.3. Purification of PCNA, 14-3-3ζ and 14-3-3ε proteins 102
3.3.4. Quantification and Identification of proteins 103
Chapter Four: Results for the Kinetic Studies of hExo1 104
4.1.0. Kinetic studies 104
4.1.1. Ionic strength assay of hExo1 104
4.1.2. Human Exo1 is sensitive to change in temperature conditions 106
4.1.3. Human Exo1 is not stable at high temperature 107
4.1.4. Human Exo1 is sensitive to change in pH conditions 108
4.1.5. Human Exo1 is specific to 3′ overhang DNA substrate 109
4.1.6. The role of reaction incubation time on DNA resection activity of hExo1 ... 110
4.1.7. Human Exo1 activity depend on the presence of ATP and Mg^{2+} 112

4.2.0. Regulation of hExo1 DNA resection activity by PCNA and 14-3-3 proteins . 113
4.2.1. PCNA enhances DNA resection activity of hExo1 113
4.2.2. PCNA hinders DNA resection activity of Nt-hExo1 115
4.2.3. The 14-3-3 proteins inhibit hExo1 DNA resection activity 117
4.2.4. Interaction of the 14-3-3 proteins with hExo1 119
4.2.5. 14-3-3 proteins suppress PCNA binding to hExo1 121
4.2.6. Molar ratio of PCNA binding to hExo1 123
4.2.7. Molar ratio of 14-3-3ζ binding to hExo1 125
4.2.8. Molar ratio of 14-3-3ε binding to hExo1 126
4.2.9. Cooperative binding of 14-3-3 proteins to hExo1 127
Chapter Five: Results for the Biophysical Studies 131
5.1. Characterization of proteins by SV-AUC 131
5.2. Characterisation of proteins by SAXS 138
5.3. Characterisation of proteins by CD and DLS 146
Chapter Six: Discussion and Conclusions 160
6.1.0. Discussion 160
6.1.1. Thermodynamic and Kinetic properties of hExo1 160
6.1.2. Regulation of hExo1 by PCNA and 14-3-3 proteins 163
6.1.3. Biophysical studies and disorder prediction of hExo1 169
6.2.0. Conclusions 173
6.3.0. Future Studies 174
References 175
Appendices 197
Primary amino acid sequence of hExo1 197
DNA nucleotide sequence of hExo1 gene 197
Primary amino acid sequence of PCNA 199
DNA nucleotide sequence of PCNA gene 199
Primary amino acid sequence of the 14-3-3ζ 200
DNA nucleotide sequence of the 14-3-3ζ gene 200
Primary amino acid sequence of the 14-3-3ε 201
DNA nucleotide sequence of the 14-3-3ε gene 201
Map of pFastBac1-hExo1 plasmid 202
Map of pET28a vector 203
Map of pTXB1 vector 204

ACRONYMS AND ABBREVIATIONS

ATM - Ataxia Telangiectasia Mutated
ATR - Ataxia Telangiectasia and Rad3-related protein
ATRIP - ATR/ATR-interacting protein
CD - Circular Dichroism
CtIP – C-terminal Binding Protein-Interacting protein
DSB - Double Strand Break
DDR - DNA Damage Response
DLS - Dynamic Light Scattering
DNA-PK - DNA-dependent protein kinase
FEN1 - Flap Endonuclease1
GEN1 - Gap Endonuclease 1
hExo1 - Human Exonuclease1
HR - Homologous Recombination
MMR - Mismatch Repair
MRX/MRN - Mre11–Rad50–Xrs2/Mre11–Rad50–Nbs1
NHEJ - Nonhomologous End Joining
PARP - poly(ADP)ribose polymerase
PCNA - Proliferating Cell Nuclear Antigen
PCR - Polymerase Chain Reaction
PIKKs - Phosphatidylinositol 3-kinase-like Protein Kinases
SAP - Shrimp Alkaline Phosphatase
SAXS - Small Angle X-ray Scattering
STR - Sgs1–Top3–Rmi1
SV-AUC - Sedimentation Velocity Analytical Ultracentrifugation
XPG - Xeroderma Pigmentosum Complementation Group

LIST OF FIGURES

Page

Figure 1.1. Model of the DNA damage response 3
Figure 1.2. Schematic model for ATM and ATR activation 5
Figure 1.3. Pathways of DSB repair in *Mycobacteria* 8
Figure 1.4. Alternative DNA repair pathways involved in the repair of DSBs 10
Figure 1.5. Model of how distinct pathways resect DNA ends 13
Figure 1.6. FEN superfamily members bind the reacting duplex DNA 22
Figure 1.7. Schematic overview of full-length Exo1 and HEX-N2 23
Figure 1.8. Structure of the hExo1 catalytic domain 26
Figure 1.9. The Ribbon diagram of PCNA trimer 29
Figure 1.10. Crystal structure of the human 14-3-3ζ protein 35
Figure 1.11. Structural comparison of all seven human 14-3-3 proteins 35
Figure 1.12. Modes of action of the 14-3-3 proteins 38
Figure 1.13. PONDR prediction of unstructured regions in hExo1 42
Figure 1.14. Schematic representation of a typical SAXS experiment 45
Figure 1.15. Depiction of human Exo1 association with PCNA and 14-3-3s 49
Figure 3.1. Agarose gel image of isolated pFastBac-hExo1 83
Figure 3.2. S-Gal agar plates showing black/white colonies 84
Figure 3.3. Depiction of how forward and reverse pUC/M13 primers hybridize 85
Figure 3.4. Agarose gel image of the bacmid PCR product 85
Figure 3.5. Depiction of how recombinant baculovirus is generated 86
Figure 3.6. Agarose gel image of pTXB1-hExo1 construct 88
Figure 3.7. Agarose gel image of pET28a-Nt-hExo1 construct 90
Figure 3.8. Agarose gel image of PCNA and 14-3-3s constructs 92
Figure 3.9. SDS/PAGE gel image of hExo1 protein expression from insect cells ... 94
Figure 3.10. SDS/PAGE gel image of hExo1 protein expression from bacteria 95
Figure 3.11. SDS/PAGE gel image of Nt-hExo1 protein expression 96
Figure 3.12. SDS/PAGE gel image of PCNA protein expression 98
Figure 3.13. SDS/PAGE gel image of 14-3-3 protein expression 98
Figure 3.14. Chromatogram and SDS/PAGE gel image of purified hExo1 protein . 100
Figure 3.15. SDS/PAGE image of purified Nt-hExo1 101
Figure 3.16. SDS/PAGE gel image of purified PCNA and 14-3-3 proteins 102
Figure 4.1. Agarose gel image of the Ionic strength assay of hExo1 105
Figure 4.2. Agarose gel image of the temperature sensitivity assay of hExo1 106
Figure 4.3. Agarose gel image of the temperature stability assay of hExo1 107
Figure 4.4. Agarose gel image of the pH sensitivity assay of hExo1 108
Figure 4.5. Agarose gel image of the substrate specificity assay of hExo1 109
Figure 4.6. Agarose gel image of the time-course assay of hExo1 111
Figure 4.7. Agarose gel image of hExo1 activity with or without ATP and Mg^{2+} 112
Figure 4.8. Agarose gel image of hExo1 DNA resection activity with PCNA 114
Figure 4.9. Agarose gel image of Nt-hExo1 DNA resection activity with PCNA 116
Figure 4.10. Agarose gel image of hExo1 DNA resection activity with 14-3-3s 118
Figure 4.11. Agarose gel image of hExo1 and Nt-hExo1 activity with 14-3-3s..... 120
Figure 4.12. Agarose gel image of hExo1 activity with PCNA and 14-3-3s 122
Figure 4.13. Agarose gel image of the molar ratio binding of PCNA to hExo1 124
Figure 4.14. Agarose gel image of the molar ratio binding of 14-3-3ζ to hExo1 ... 125

Figure 4.15. Agarose gel image of the molar ratio binding of 14-3-3ε to hExo1 .. 126
Figure 4.16. Binding curve 129
Figure 5.1. Sedimentation coefficient distributions c(s) of hExo1 132
Figure 5.2. Sedimentation coefficient distributions c(s) of Nt-hExo1 133
Figure 5.3. Sedimentation coefficient distributions c(s) of PCNA 135
Figure 5.4. Sedimentation coefficient distributions c(s) of 14-3-3ζ 135
Figure 5.5. Sedimentation coefficient distributions c(s) of 14-3-3ε 136
Figure 5.6. SAXS scattering curves of hExo1 141
Figure 5.7. SAXS scattering curves of Nt-hExo1 142
Figure 5.8. Kratky plot of scattering data 143
Figure 5.9. Normalised Kratky plots of hExo1 and Nt-hExo1 143
Figure 5.10. Guinier fit plots of hExo1 and Nt-hExo1 145
Figure 5.11. Guinier plots 145
Figure 5.12. Far-UV CD spectra and DLS data of hExo1, PCNA and Nt-hExo1 150
Figure 5.13. Far-UV CD spectra of hExo1 and Nt-hExo1 151
Figure 5.14. Far-UV CD spectra and DLS data of the binary protein complexes ... 152
Figure 5.15. Far-UV CD spectra of the ternary protein complexes 153
Figure 5.16. Far-UV CD spectra of the quaternary protein mixture 156

LIST OF TABLES

Page

Table 2.1. pUC/M13 primers 56
Table 2.2. PCR reaction set up of the recombinant bacmid DNA 56
Table 2.3. PCR settings of the recombinant bacmid DNA 57
Table 2.4. Primers of the PCR of hExo1 61
Table 2.5. PCR reaction set up of hExo1 61
Table 2.6. PCR settings of hExo1 62
Table 2.7. Set up for the restriction digest of hExo1 PCR product 62
Table 2.8. Set up for the SAP treatment of the restriction digested pTBX1 vector 63
Table 2.9. Set up for the ligation of hExo1 PCR product into pTXB1 vector 63
Table 2.10. Primers for the PCR of Nt-hExo1 66
Table 2.11. Primers for the PCR of PCNA, 14-3-3ζ and 14-3-3ε 67
Table 3.1. Quantities of recombinant proteins obtained after purification 103
Table 4.1. Incubation times of hExo1 resection assay 110
Table 5.1: Calculated SV-AUC experimental parameters 134
Table 5.2. The calculated radius of gyration for hExo1 and Nt-hExo1 139
Table 5.3: Secondary Structure Estimation (SSE) by CONTINNL 157
Table 5.4: Sizes of proteins and their mixtures 158

CHAPTER ONE: INTRODUCTION

1.0. INTRODUCTION

There are a number of sophisticated surveillance and repair systems that safeguard the cellular genome in order to conserve the integrity and stability of genetic information. Amongst these various types of mechanisms, the repair of DNA double strand breaks (DSBs) is believed to be one of the most crucial, as unchecked, these DSBs can lead to cancer, genomic instability, premature aging and immunodeficiency (Hoeijmakers, 2009; Lord & Ashworth, 2012). DNA double strand breaks can arise accidentally during normal cell metabolism and/or when cells are exposed to exogenous agents, such as ionizing radiation (IR) or some classes of chemotherapeutic drugs. Moreover, during programmed recombination events, such as meiosis, budding yeast mating-type inter-conversion and lymphocyte development, DSBs serves as an essential intermediates (Paques & Haber, 1999; Soulas-Sprauel, *et al*., 2007).

The repair of DSBs is crucial to survival in all living organisms. It is lethal to have a scission of phosphodiester backbone in both strands of the DNA, as the loss of linear chromosome integrity compromises chromosome replication and will consequently hinder the duplication of the genome. Damage-tolerant DNA polymerases can bypass other types of DNA lesions, but there is no known mechanism for replication or transcription machinery in order to bypass a DSB. It is therefore, obligatory to repair them before replication or transcription can progress. From bacterial to human cells, multiple systems have metamorphosed to repair DSBs (Daley *et al*. 2005; Shuman & Glickman, 2007; Dillingham & Kowalczykowski, 2008; Yeeles & Dillingham, 2010; Lieber, 2010; Symington & Gautier, 2011).

1.1. Sensing the DNA Damage

Cells have developed mechanisms that detect DNA lesions, signal their presence and advance their repair in order to fight the threats posed by DNA damage. These mechanisms are collectively termed the DNA-damage response (DDR) (Rouse & Jackson, 2002; Harrison & Haber, 2006; Harper & Elledge, 2007). Although different classes of DNA lesions have different responses, they arise usually by a common general program (*Fig. 1.1*).

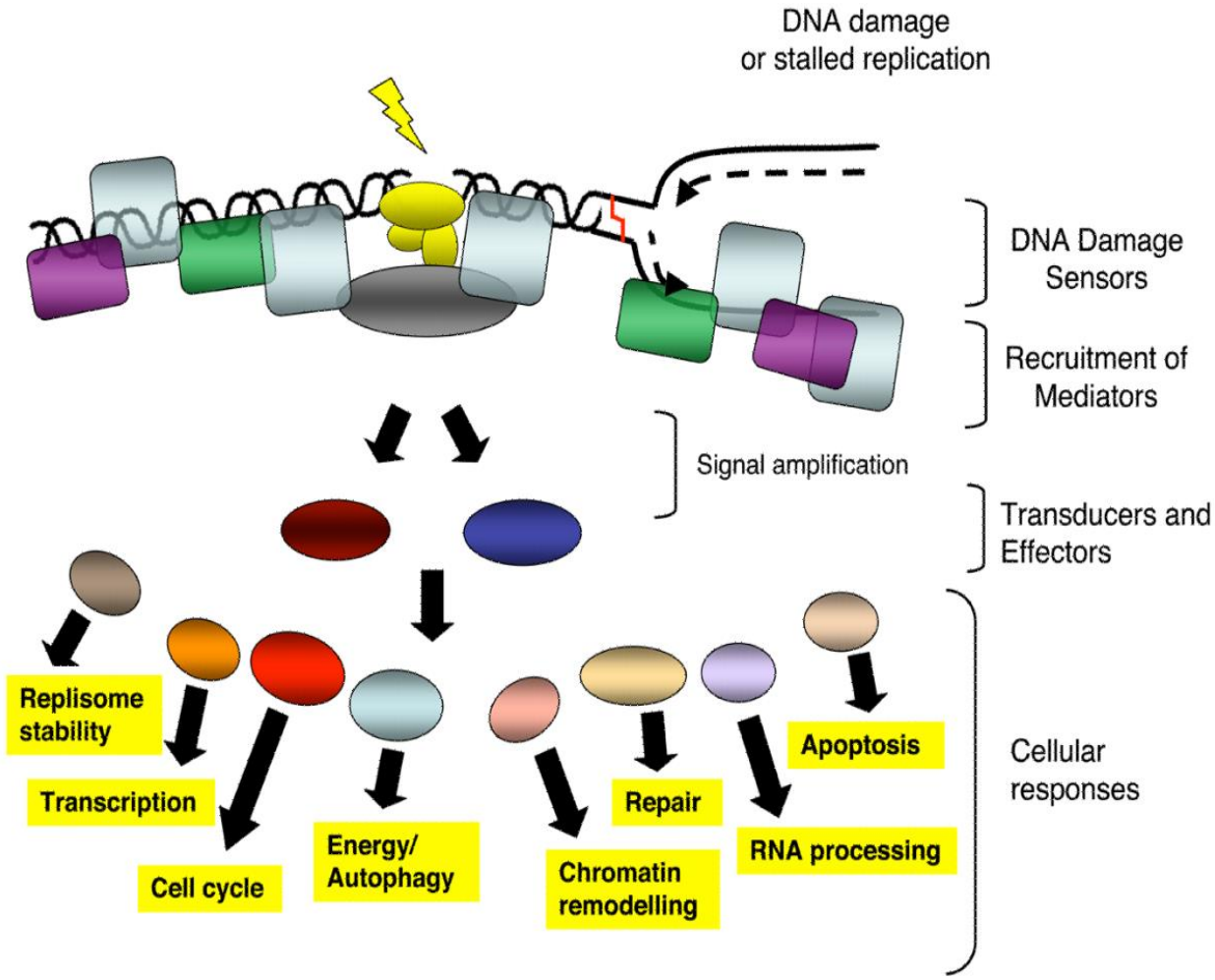


Figure 1.1. Model for the DNA Damage Response (DDR).

The presence of a lesion in the DNA, which can lead to replication stalling, is recognized by various sensor proteins. These sensors initiate signalling pathways that impact a wide variety of cellular processes. **(Figure reproduced with permission from Nature Publishing Group)**

Proteins of the phosphatidylinositol-3 kinase-like protein kinases (PIKKs) family [which includes Ataxia Telangiectasia Mutated (ATM), Ataxia Telangiectasia and Rad3-related protein (ATR) and DNA-dependent protein kinase (DNA-PK)] and members of the poly(ADP)ribose polymerase (PARP) family are the primary mediators of DDR. A DNA damaging agent such as ionizing radiation that creates DSBs activates ATM and DNA-PK (*Fig. 1.2A*) (Harper & Elledge, 2007; Meek *et al*., 2008). On the other hand, the ATR/ATR-interacting protein (ATRIP) complex is activated following recruitment to RPA-coated ssDNA regions that have resulted from stalled replication forks (*Fig. 1.2B*) and DSBs (Cimprich & Cortez, 2008).

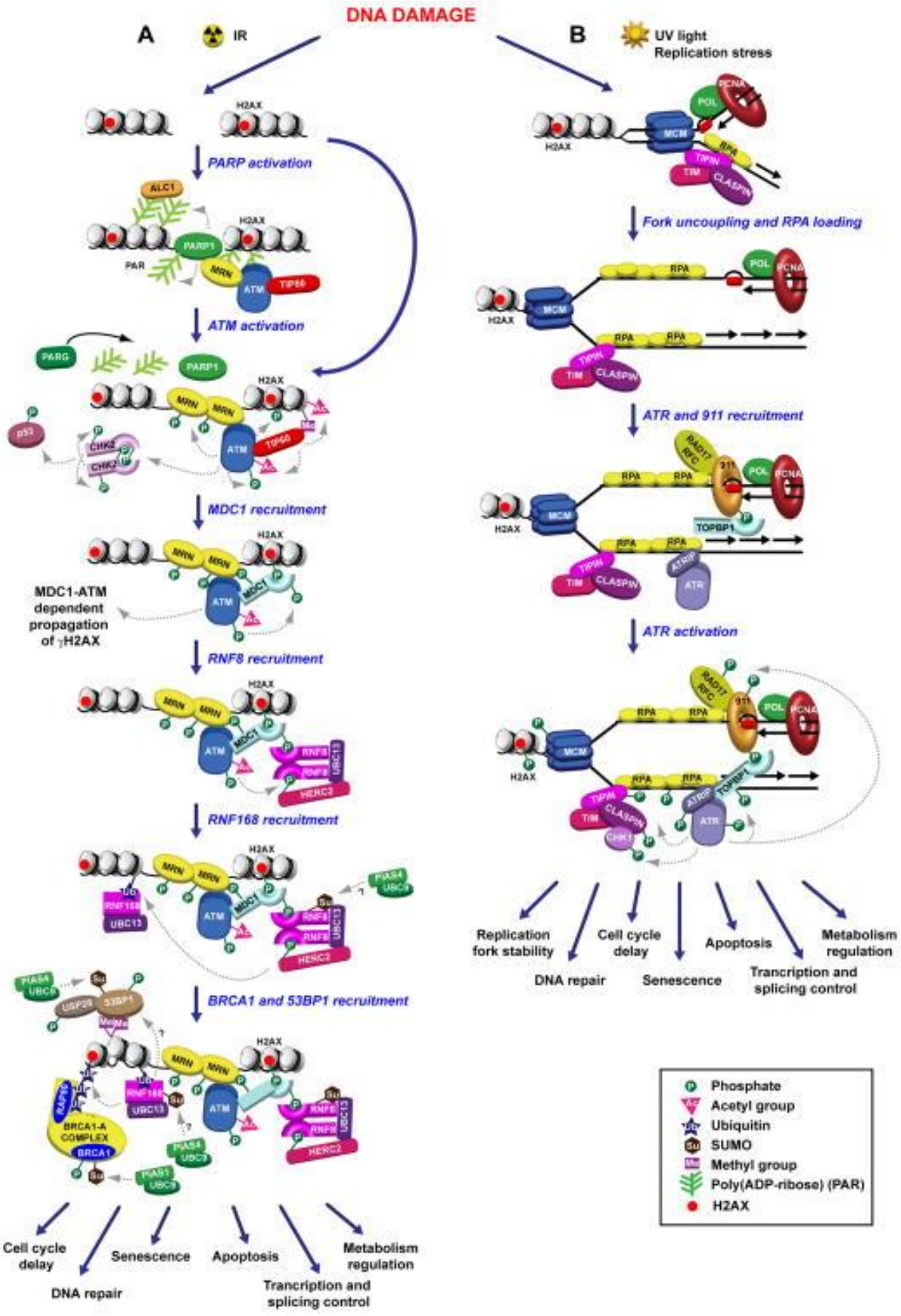

DNA DAMAGE
A
IR
B
UV light
Replication stress
H2AX
PARP activation
ALC1
PARP1
PAR
MRN
ATM
TIP60
ATM activation
PARG
p53
CHK2
MDC1 recruitment
MDC1-ATM dependent propagation of γH2AX
RNF8 recruitment
RNF8
UBC13
HERC2
RNF168 recruitment
RNF168
PIAS4
UBC9
BRCA1 and 53BP1 recruitment
USP28
53BP1
MdmX
RAP80
BRCA1-A COMPLEX
BRCA1
PIAS1
Fork uncoupling and RPA loading
PCNA
POL
MCM
RPA
TIPIN
TIM
CLASPIN
ATR and 911 recruitment
RAD17
RFC
911
TOPBP1
ATRIP
ATR
ATR activation
CHK1
Cell cycle delay
DNA repair
Senescence
Apoptosis
Metabolism regulation
Trancription and splicing control
Replication fork stability
Phosphate
Acetyl group
Ubiquitin
SUMO
Methyl group
Poly(ADP-ribose) (PAR)
H2AX

Figure 1.2. Schematic model for ATM and ATR activation in response to DNA damage.

(A) Formation of DSBs following IR treatment activates PARP1, which mediates the initial recruitment of the MRN/ATM complex at DSBs. Activation of the ATM kinase activity by MRN and TIP60 leads to the phosphorylation of CHK2 and p53, in addition to a wide number of other DDR factors, and the induction of the γH2AX-dependent signalling cascade, which results in the recruitment of MDC1, RNF8, RNF168, BRCA1 and 53BP1 to DSBs, as described in greater details in the main text. (B) DNA lesions induced by UV light or replication stress (denoted by red rectangular shapes) lead to replication fork stalling and accumulation of RPA-coated ssDNA regions, which recruit the ATR/ATRIP and the RAD17/RFC2-5 complexes. Loading of the 9-1-1 complex by RAD17/RFC2-5 and stimulation of the ATR kinase activity by the 9-1-1 associated protein TOPBP1 result in the activation of the ATR signalling cascade and CHK1 phosphorylation. Post-translational modifications of the DDR factors here depicted are represented by different coloured shapes, as indicated by the legend at the bottom of the figure. **(Figure reproduced with permission from the publishers of Molecular Cell)**

1.2. DNA Damage and Repair

Cells have evolved thorough mechanisms that can detect and repair various types of DNA lesions. This include DNA double strand break (DSB) which is one of the most cytotoxic classes of DNA damage (Aguilera, *et al*., 2008). DNA DSBs can emerge incidentally during normal cell metabolism, when exposed to DNA damaging agents, or as intermediates in programmed genome rearrangements. Prompt detection and the precise repair of DSBs is requisite to preserving the integrity of the genome. Highly conserved proteins are recruited to DSBs to activate checkpoint response systems and to subsequently repair DSBs. Inherited defects that result in sterility, developmental disorders, immune deficiencies and predisposition to cancer caused by the deficiencies in these factors highlights their importance (Aguilera, *et al*., 2008).

There are at least four independent pathways that can repair DSBs which includes homologous recombination (HR), non-homologous end joining (NHEJ), alternative-NHEJ (also known as microhomology mediated end-joining or MMEJ) and single-strand annealing (SSA). DNA end-processing is the main factor that determines the repair pathway choice. Classical NHEJ does not require DNA end resection, whereas alt-NHEJ, HR and SSA rely on DSB resection. This is limited for alt-NHEJ (5–25 nt), but more extensive for HR and SSA (Hartlerode & Scully, 2009). There are two general mechanisms for DNA break repair in bacteria: non-homologous end-joining (NHEJ) and homologous recombination (HR) (Lieber, 2010), although there exists a third mechanism in the *Mycobacteria* species which is referred to as single-strand annealing (SSA) (*Fig. 1.3*) (Glickman, 2014).

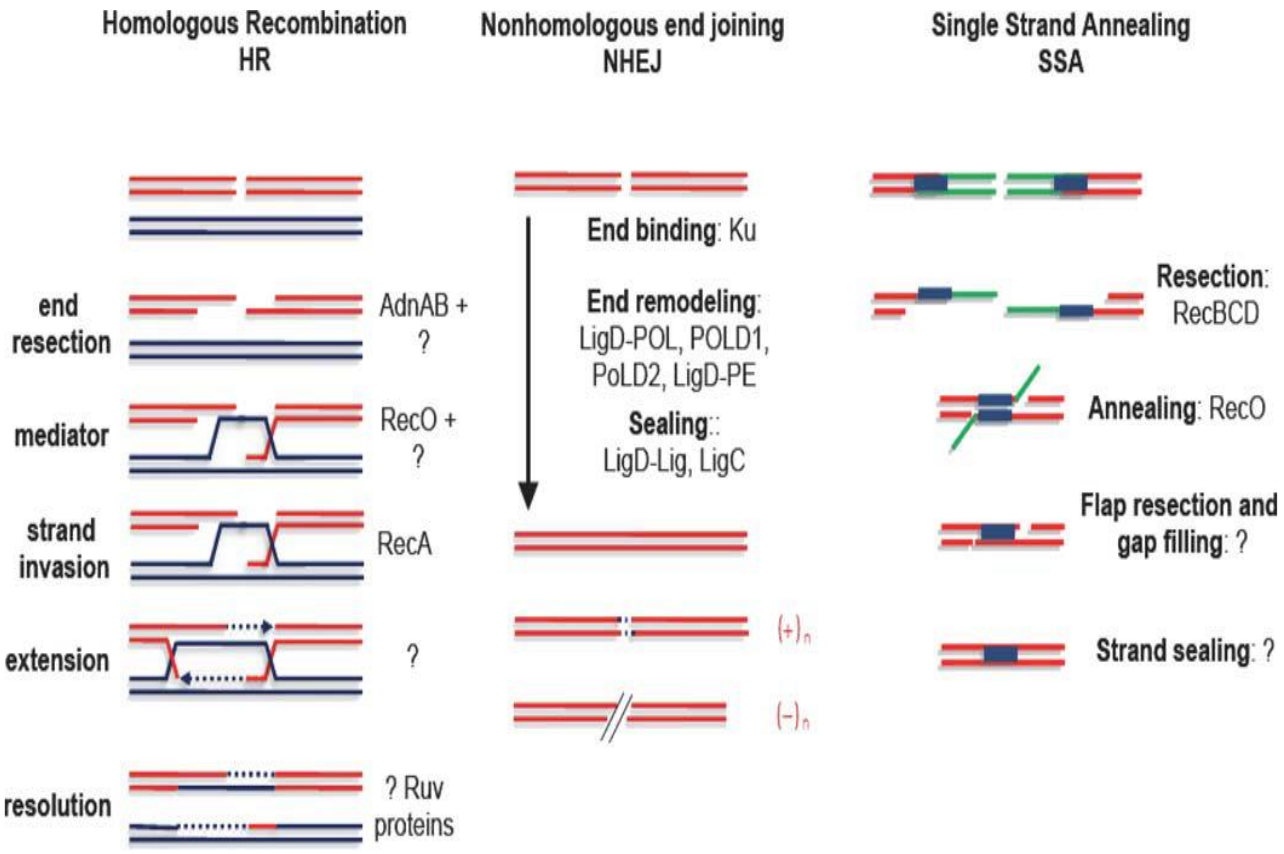


Figure 1.3. Pathways of DSB repair in *Mycobacteria*.

The three pathways shown are Homologous Recombination (HR), Non-homologous end Joining (NHEJ), and Single Strand Annealing (SSA). For each pathway, the major DNA processing events are depicted with the factors required for each step, when known. A question mark indicates that no specific experimental genetic data is available about that step, despite the presence of predicted proteins in *mycobacterial* chromosomes that may mediate these steps, or even biochemical activities consistent with a role in these pathways. In the NHEJ column the three outcomes below the arrow indicate faithful repair, nucleotide addition, and nucleotide trimming, respectively. In the SSA column, the blue rectangles indicate repeat sequences that flank the DSB. **(Figure reproduced with permission from the publishers of Cell)**

In eukaryotes, a DSB can be repaired by non-homologous end-joining (NHEJ) (*Fig. 1.4A*), homologous recombination (HR) (*Fig. 1.4B*), alternative-nonhomologous end joining (alt-NHEJ) (Fig. 1.4C) and single-strand annealing (SSA) (*Fig. 1.4D*) (Ciccia & Elledge, 2010). An intact homologous duplex DNA serve as a template for repair of the broken chromosome in HR, while NHEJ involves the religation of DSB ends with little or no homology. The preservation of the genetic sequence is the main feature of HR, because usually the sister chromatid is the donor sequence. On the other hand, NHEJ can be referred to as mutagenic due to the gain or loss of nucleotides that can occur at the junction (Daley, *et al*,. 2005).

In HR, DSBs repair requires the end to be processed to produce 3’ single-stranded DNA (ssDNA) tails that serve as substrates for the Rad51/RecA strand exchange protein (*Fig. 1.4B*). The conversion of DSB to limited ssDNA is a requisite in order to activate the ATR-mediated checkpoint response (Zou & Elledge 2003). Even though resected DNA ends restrain NHEJ, DNA end resection serves as the first step in differentiating between HR and NHEJ and it constitutes a vital point of control in the choice of repair pathway. Subsequently, the cell cycle components regulate DNA end resection to make certain that it occurs during the S and G2 phases of the cell cycle during which the uncondensed sister chromatid is present to serve as a template for a precise repair by HR (Aylon, *et al*,. 2004; Ira, *et al*,. 2004; Huertas, *et al*,. 2008).

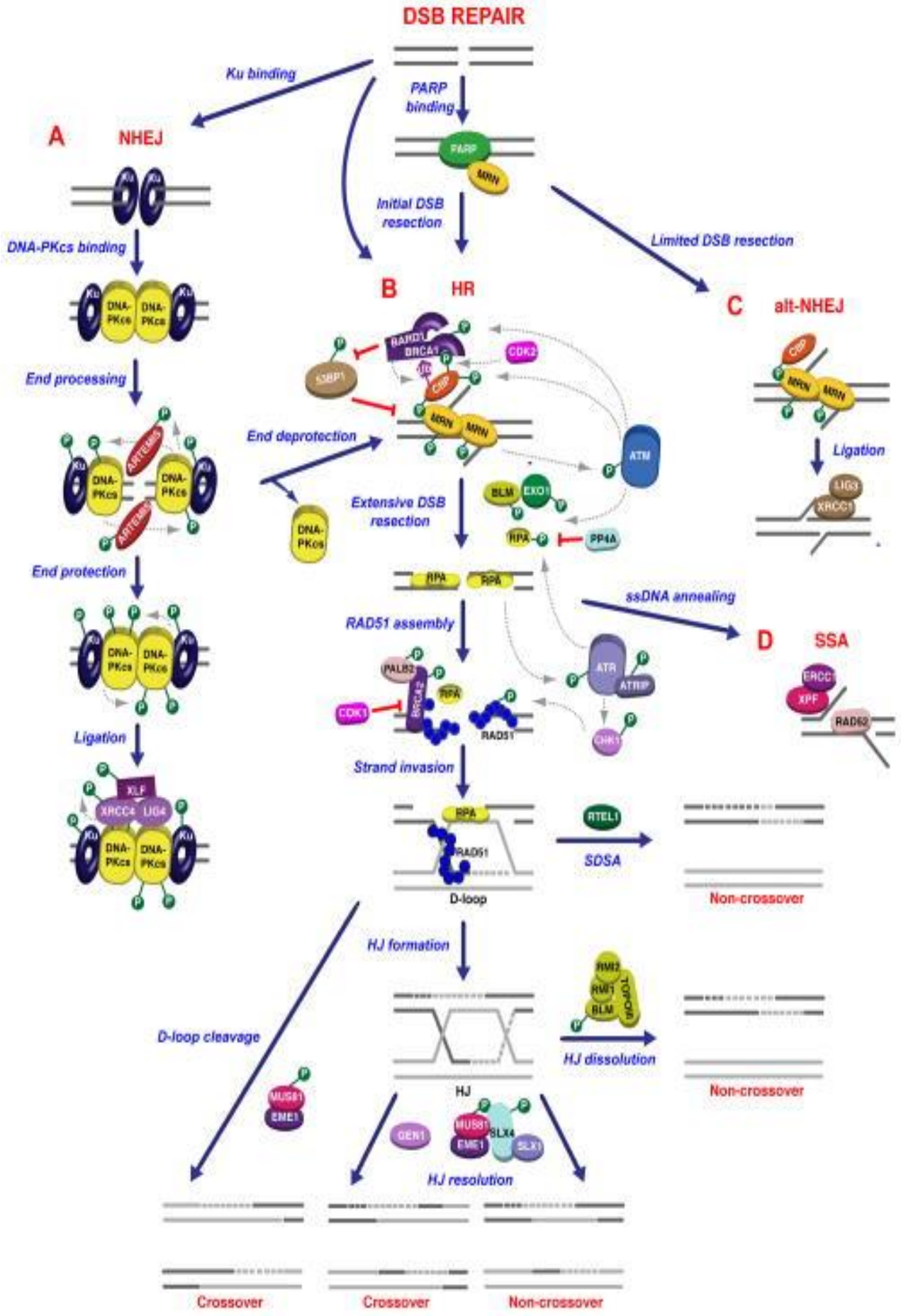

DSB REPAIR
Ku binding
PARP binding
A NHEJ
B HR
C alt-NHEJ
D SSA
DNA-PKcs binding
Initial DSB resection
Limited DSB resection
End processing
End deprotection
Extensive DSB resection
End protection
Ligation
RAD51 assembly
ssDNA annealing
Strand invasion
SDSA
D-loop
Non-crossover
HJ formation
D-loop cleavage
HJ dissolution
HJ
HJ resolution
Crossover
Crossover
Non-crossover

Figure 1.4. Alternative DNA repair pathways involved in the repair of eukaryotic double-strand breaks.

(A) Rapid association of Ku to DSBs promotes NHEJ by recruiting DNA-dependent protein kinase, catalytic subunit (DNA-PKcs). Sequential phosphorylation events on multiple DNA-PKc amino acid clusters favours the initial processing of DNA ends by ARTEMIS, followed by DNA-PKc-dependent protection of DNA ends required for DNA ligation. (B) Alternatively to NHEJ, MRN, which is initially recruited to DSBs by PARP in competition with Ku, mediates the initial stages of DSB resection together with CtIP and BRCA1 to promote homologous recombination in S and G2. The protein 53BP1 has an inhibitory role on DSB resection and is negatively regulated by BRCA1 by unknown mechanisms. The MRN/CtIP/BRCA1 complex can also promote DSB resection following deprotection of DNA ends when NHEJ fails. Extensive DSB resection and formation of RPA-coated 3'-ssDNA ends is induced by Exo1 and BLM. ATM plays a central role in the regulation of DSB resection as described in the main text. Displacement of RPA from the 3'-ssDNA ends and assembly of RAD51 filaments mediated by BRCA2 leads to strand invasion into homologous DNA sequences. Recruitment of RAD51 to ssDNA ends is regulated by the ATR pathway, which is activated following DSB resection. D-loop structures formed after strand invasion can be cleaved by MUS81/EME1 or displaced by RTEL1 during SDSA to generate crossover or non-crossover events, respectively. Non-crossovers are generated also by dissolution of Holliday junctions (HJs) by the BLM/TOPOIII complex, whereas HJ resolution by the nucleases GEN1 and SLX1/ SLX4, which associate with MUS81/EME1, can generate both crossover and non-crossover events. (C) Limited DSB resection carried out by CtIP and MRN in G1 results in alternative NHEJ. (D) Following DSB resection, 3'-ssDNA ends with homologous sequences can be directly annealed by RAD52. **(Figure reproduced with permission from the publishers of Molecular Cell)**

1.3. DNA Resection

DNA DSBs repair depends primarily on whether DNA end resection occur. A two-step model for a double strand break (DSB) resection has been proposed (*Fig. 1.5*) (Zhu *et al*, 2008; Gravel, *et al*, 2008; Mimitou & Symington, 2008). This involve an initial endonucleolytic cleavage that produce a short 3' overhang, then an extended resection follows to allow for repair by activating the HR and ATR checkpoint. The initial DNA resection is believed to be carried out by MRX/MRN and Sae2/CtIP. At the DNA break point, the endonucleolytic cleavage of the 5' strand is mediated by MRX/MRN and Sae2/CtIP. Even though the endonucleolytic cleavage step is not an absolute requirement to resect DSBs with 'clean' ends, it is a requisite to resect DSBs with covalently bound proteins and chemical adducts at their 5' ends. Two nucleases that carry out an extended long-range resection are Exo1 and Dna2 (Huertas, 2010; Mimitou & Symington, 2008; Mimitou & Symington, 2009; Zhu *et al*., 2008).

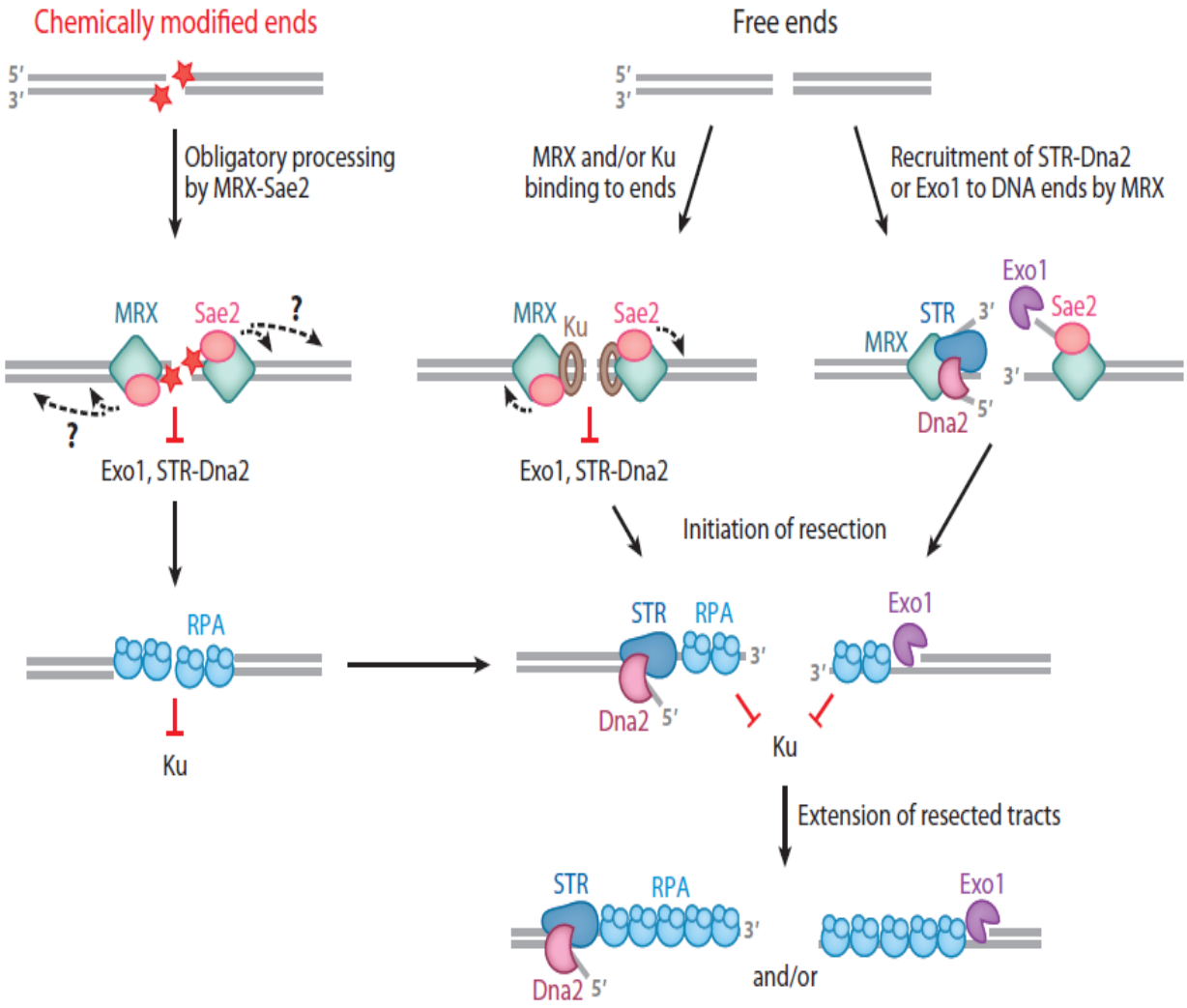


Figure 1.5. Model of how distinct pathways resect modified and free DNA ends.

MRX complex and Sae2 clip the ends endonucleolytically (*shown as dashed black arrows*) to release covalently modified ends. Ku binding is inhibited by partial resection, which enables the intermediates to undergo extensive resection by either STR-Dna2 or Exo1. Free ends are bound by Ku and/or MRX/N; clipping by MRX/N and Sae2/CtIP removes Ku, and can be processed further by Exo1 or STR-Dna2. Alternatively, MRX/N recruits Exo1 or STR-Dna2 to free ends to initiate resection directly, but this reaction is most efficient in the absence of Ku (Lorraine and Jean, 2011). **(Figure reproduced with permission from the publishers of Molecular Cell)**

Various laboratories have illustrated the molecular mechanisms of DSB end resection in *Saccharomyces cerevisiae* with a proposed two-step mechanism that involves nucleases and helicases (*Fig. 1.5*) (Mimitou & Symington, 2008; Zhu, *et al*, 2008). Several studies suggest that the initiation of end resection by MRX-Sae2 is the rate-limiting step for DSB processing (Frank-Vaillant & Marcand, 2002; Mimitou & Symington, 2008; Zhu, *et al*, 2008; Zierhut & Diffley, 2008). After MRX–Sae2 cleavage, the generated short 3' ssDNA tails undergo a second step of extensive resection effected through two pathways that are parallel to one another. One pathway depends on the 5'→3' exonuclease1 (Exo1) while the other is dependent on the concerted action of the Sgs1–Top3–Rmi1 (STR) complex and Dna2 endonuclease (*Fig. 1.5*) (Mimitou & Symington, 2008; Zhu, *et al*, 2008; Gravel, *et al*, 2008).

The absence of a sister chromatid (the preferred repair template) might theoretically result in the formation of long ssDNA tracts; an example is in the case where a HO endonuclease cleaves both sister chromatids. However, long ssDNA tracts are required for the activation of the G2/M checkpoint and it has been suggested that extensive resection serves to uphold repair fidelity (Zhu, *et al*, 2008; Chung, *et al*, 2010). In the absence of both Exo1 and STR, the processed intermediates that are MRX-Sae2 dependent can accumulate but can aid in mitotic gene conversion, even though this is inefficient (Mimitou & Symington, 2008; Zhu, *et al*, 2008). In wild-type cells, *de novo* telomere addition is an exceptional DSB repair event but in the absence of long range resection by Exo1 and STR–Dna2, it becomes persistent (Kramer & Haber, 1993; Chung, *et al*,. 2010; Lydeard, *et al*,. 2010).

It appears that the helicase–nuclease ensemble for DNA resection is a prevalent motif in DNA end-processing. Studies in *Escherichia coli* (Amundsen & Smith 2003; Dillingham & Kowalczykowski, 2008; Handa, *et al*, 2009), *Bacillus subtilis* (Yeeles & Dillingham, 2010) in archaea, *Pyrococcus furiosus* (Hopkins & Paull, 2008) and a more recent study in

Mycobacterium smegmatis (Sinha, *et al*, 2009) have all reported this common theme of a helicase–nuclease ensemble for DNA resection in DNA end-processing machinery. The RecQ family helicase role in resection seems to be conserved in *Xenopus* extracts and human cells. The mammalian BLM and Sgs1 homolog functions in a parallel pathway with Exo1 in aiding DSB resection (Gravel, *et al*, 2008), while *Xenopus* DNA2 nuclease degrades single strand tails in 5'→3' direction upon the DNA ends unwinding by the *Xenopus* WRN RecQ helicase (Liao, *et al*, 2008).

Although insufficient resection of broken double stranded DNA hinders HR and ATR checkpoint activation, excessive resection can have deleterious consequences because ssDNA is more prone to degradation. Also, the breakage of the 3’ strand DNA could cause a loss of genetic information (Chen *et al*, 2013). Likewise, persistent checkpoint signalling induced by excessive ssDNA could lead to cell death (Rossiello *et al* 2014). Mechanisms to prevent over-resection must exist in order to prevent genomic instability, yet little is known how the extent of DNA resectioning is properly controlled. Studies in different organisms have recently led to the discovery of various components involved in the process of DSB resection. These include MRN/MRX, CtIP/Sae2/Ctp1, Exo1, Dna2, BLM/Sgs1, RPA, LEDGF, SMARCAD1/Fun30, PCNA and SOSS1 (Minitou & Symington, 2009; Huertas 2010; Symington & Gautier 2011; Chen *et al*., 2013).

1.4. *In vitro* reconstitution of DSB resection

Recently, elements of the resection process have been reconstituted *in vitro* with purified *S. cerevisiae* proteins (Cejka, *et al*, 2010; Nicolette, *et al* 2010; Niu, *et al*, 2010). Some of the studies were focused on the Sgs1–Dna2 pathway and it was reported that the minimum set of proteins necessary for ATP-dependent resection was Sgs1, Dna2 and RPA (Cejka, *et al*, 2010; Niu, *et al*, 2010). Both studies highlighted the role of the MRX complex in the reconstituted end-resection assays. Other studies addressed the *in vitro* reconstitution of the Exo1-dependent pathway (Nicolette *et al* 2010). Nicolette *et al*., reported that the Exo1 catalysed 5'–3' degradation of a linear dsDNA substrate, and that this was in line with previous findings (Szankasi & Smith, 1992; Fiorentini, et al, 1997)

When purified MRX–Sae2 was added, Exo1-mediated degradation was stimulated in a concentration-dependent manner; at high concentrations, Exo1 exhibited its activity independent of MRX-Sae2, but at low concentrations, the Exo1 activity was strongly stimulated by MRX-Sae2 (60 to 300-fold). MRX and Sae2 could individually stimulate Exo1 activity, but when added simultaneously, they showed synergistic stimulation of Exo1 (Nicolette *et al* 2010). The MRX–Sae2 stimulation proportionally depended on the nuclease activity of Exo1, but depended only slightly on the nuclease activity of Mre11. This suggests that most of the resection activities observed in these reactions were largely carried out by Exo1.

Exo1 supports exonucleolytic 5' degradation and endonucleolytic 5' flap degradation, in which MRX–Sae2 was found to stimulate both activities (Nicolette *et al* 2010). Jointly, these results suggest that MRX–Sae2 affects Exo1 recruitment to the DNA ends, comparable to MRX-mediated Sgs1 recruitment as proposed by the other studies (Cejka, *et al*, 2010; Niu, *et al*, 2010). Contrary to Sgs1 and Dna2 interaction, there was no detection of any stable protein–protein interactions

between MRX or Sae2 and Exo1. Regardless, MRX, Sae2 and Exo1 formed complexes in the context of DNA, as revealed by their cooperative binding to the oligonucleotide substrates in the presence of all the proteins (Nicolette, *et al*, 2010). Exo1 interaction with a 5' strand was also strongly strengthened in the presence of MRX–Sae2 as revealed by strand-specific UV cross-linking (Nicolette, *et al*, 2010). It was therefore suggested that MRX–Sae2 facilitates the recruitment of Exo1 to the DNA end by creating a specific DNA structure in order to aid a higher affinity binding of Exo1 (Nicolette, *et al*, 2010).

1.4.1. *Interpreting the in vitro and in vivo observations of the DSB resection*

The *in vitro* studies described above suggest how the MRX complex may exert its stimulatory activity in aiding DSB processing through the pathways of Sgs1–Dna2 and Exo1. However, the MRX complex is a requisite for DSB resection under certain *in vivo* conditions. Looking at some genetic assays where some important MRX roles were demonstrated, there are several possible explanations that can be deduced. First, the DNA end clipping by MRX–Sae2 is critical for the removal of Spo11 and conceivably, other DNA end's modifications; *in vitro* studies used substrates with 'clean' ends only. Second, the necessity for MRX to recruit STR–Dna2 and/or Exo1 to the substrate is probably more rigorous *in vivo* than in the reconstituted systems. Finally, there are other proteins present in cells that can bind and block the access of resection machinery to DSBs, thereby increasing the necessity for the MRX–Sae2 activities. The heterodimeric Ku protein is such a factor. Ku forms a ring that binds DNA by sliding a DSB end through its opening. Once Ku binds, DNA it protects the ends from degradation and subsequently initiates the recruitment of downstream NHEJ factors (Daley, *et al*, 2005).

Recently, the interplay between Ku and the resection machinery in budding yeast was investigated *in vivo* (Shim, *et al*, 2010; Mimitou &

Symington, 2010). Chromatin immunoprecipitation (CHIP) assays were employed to investigate recruitment of the resection machinery at an inducible, unrepairable DSB (Shim, *et al*, 2010). Like the results seen in the *in vitro* studies, it was reported that MRX promotes Exo1 and Dna2 association to DSBs, and that Mre11 and Sae2 nuclease activities are nonessential for recruitment.

1.4.2. *Redundancy of Exo1 and Sgs1-mediated pathways*

Sgs1 and Dna2 have individual functions that are not related to DNA end resection. Sgs1 is an active DNA helicase that belongs to the RecQ family (Gangloff, *et al*., 1994; Cejka & Kowalczykowski, 2010), which functions in conjunction with Top3 and Rmi1 to dissolve double Holliday junctions in non-crossover products, thereby preventing sister chromatid exchanges and chromosome instability (Cejka, *et al*., 2010; Wu & Hickson, 2003). Dna2 is a bifunctional helicase-nuclease that functions in the removal of DNA flaps (a DNA duplex which has a single-stranded 5' overhang on one of the strands) that arises as result of strand displacement synthesis by DNA polymerase δ during the synthesis of the DNA lagging strand (Bae, *et al*., 2001). Sgs1 and Dna2 had not been implicated to function together before the seminal work by Zhu and colleagues (Zhu, *et al*., 2008).

A series of combined genetic and biochemical studies revealed the mechanism of DNA end resection by the Sgs1-Dna2 pathway. The helicase of Sgs1 unwinds dsDNA in a polarity of 3'→5' to produce a substrate for the ssDNA-specific Dna2 nuclease (Zhu, *et al*., 2008; Niu, *et al*., 2010; Cejka, *et al*., 2010). Distinct from Dna2 nuclease which is specific for ssDNA, Exo1 degrades the 5'-terminated strand within dsDNA (Tran, *et al*., 2002) and therefore does not require a helicase partner to unwind the DNA. Exo1 nuclease directly produces the required 3'-tailed DNA (Tran, *et al*., 2002; Cannavo, *et al*., 2013). To date, most studies that unravelled the mechanism of mitotic DSB resection reported redundancy between the Exo1 and Sgs1–Dna2

pathways, but work carried out recently on the resection of meiotic DSBs and telomeres suggested otherwise. (Tsubouchi & Ogawa, 2000; Keelagher *et al*., 2010; Manfrini *et al*., 2010; Zakharyevich *et al*., 2010).

In *S. cerevisiae,* the formation of meiotic DSBs is constricted with the resection and various evidence suggests the role played by Exo1 in the 'hyper-resection' of meiotic breaks has been observed in *dmc1Δ* mutants (Manfrini, *et al*, 2010; Tsubouchi & Ogawa, 2000). Moreover, it was shown that Sgs1–Dna2 contributed to the *dmc1Δ* hyper-resection in the absence of Exo1 (Manfrini, *et al*, 2010). Exo1 and/or Sgs1 roles in physiological meiotic DSB resection were unravelled by two recent studies using different assays to measure 5' strand resection of DSB ends formed at a meiotic hotspot. Both studies reported a notable role for Exo1 (Keelagher, *et al*, 2010; Zakharyevich, *et al*, 2010). Thus, Exo1 is required for meiotic DSB processing and, similarly to mitosis, it is nonessential for the initial resection which is presumed to depend on MRX–Sae2 (Keelagher, *et al*, 2010; Zakharyevich, *et al*, 2010).

1.5. Exonuclease1

Nuclease enzymes have been found to play a major role in a variety of cellular processes including DNA damage repair, DNA replication, recombination, and programmed cell death (apoptosis). Nucleases can execute their actions by generic binding to DNA (non-specific binding) or bind to a specific region on the DNA. Genetic instabilities such as cancer and premature ageing are some of examples of complex phenotypes that have been associated with nuclease function defects. From microorganisms such as bacteriophage to higher organisms such as humans, the RAD2 family of nucleases were found to be conserved (Lieber, 1997; Ceska & Sayers, 1998) and to exhibit different nuclease activities in various cellular pathways.

The N-terminal and internal domains are conserved in the RAD2 family of nucleases. On the basis of the amino acid sequences they contain, substrate specificity and the position of the N-terminal and internal domains, RAD2 family members have been classified into three groups. Class I comprises of the XPG-like proteins that are involved in nucleotide excision repair. Class II comprises of the FEN1-like proteins that exhibit a flap endonuclease-type activity while class III consists of Exo1-like proteins that had been reported in mammals, insects (flies) and yeast (Szankasi & Smith, 1995; Digilio *et al*, 1996; Wilson *et al*, 1998). Exo1 is a member of the RAD2 family of nucleases that was first identified by Szanki and Smith in 1992, as a meotically-induced 5’ to 3’ exonuclease in *Schizosaccharomyces pombe*. Subsequently, the Exo1 protein was discovered to be an interacting partner of the mismatch recognition protein Msh2 in *Saccharomyces cerevisiae* (Tishkoff *et al*, 1997).

The Human exonuclease1 (hExo1) is a member of the eukaryotic nuclease family that includes Rad2/Xeroderma pigmentosum complementation group G (XPG), flap endonuclease1 (FEN1) and gap endonuclease1 (GEN1) (Lee *et al* 2002; Orans *et al* 2011). The nuclease

domain of Rad2/XPG protein family is conserved through the species from phage to human. The EXO1 gene product exhibits both 5’ exonuclease and 5’ flap activity (Lee & Wilson, 1999; Lee *et al* 2002). Human Exo1 has a high affinity for processing double-stranded DNA (dsDNA) (Fig. 1.6), gaps, nicks and pseudo-Y structures and can resolve Holliday junctions due to its activity on the flap DNA (a DNA duplex which has a single-stranded 5' overhang on one of the strands) (Lee & Wilson, 1999; Qiu *et al* 1999; Genshel & Modrich 2003; Orans *et al*, 2011).

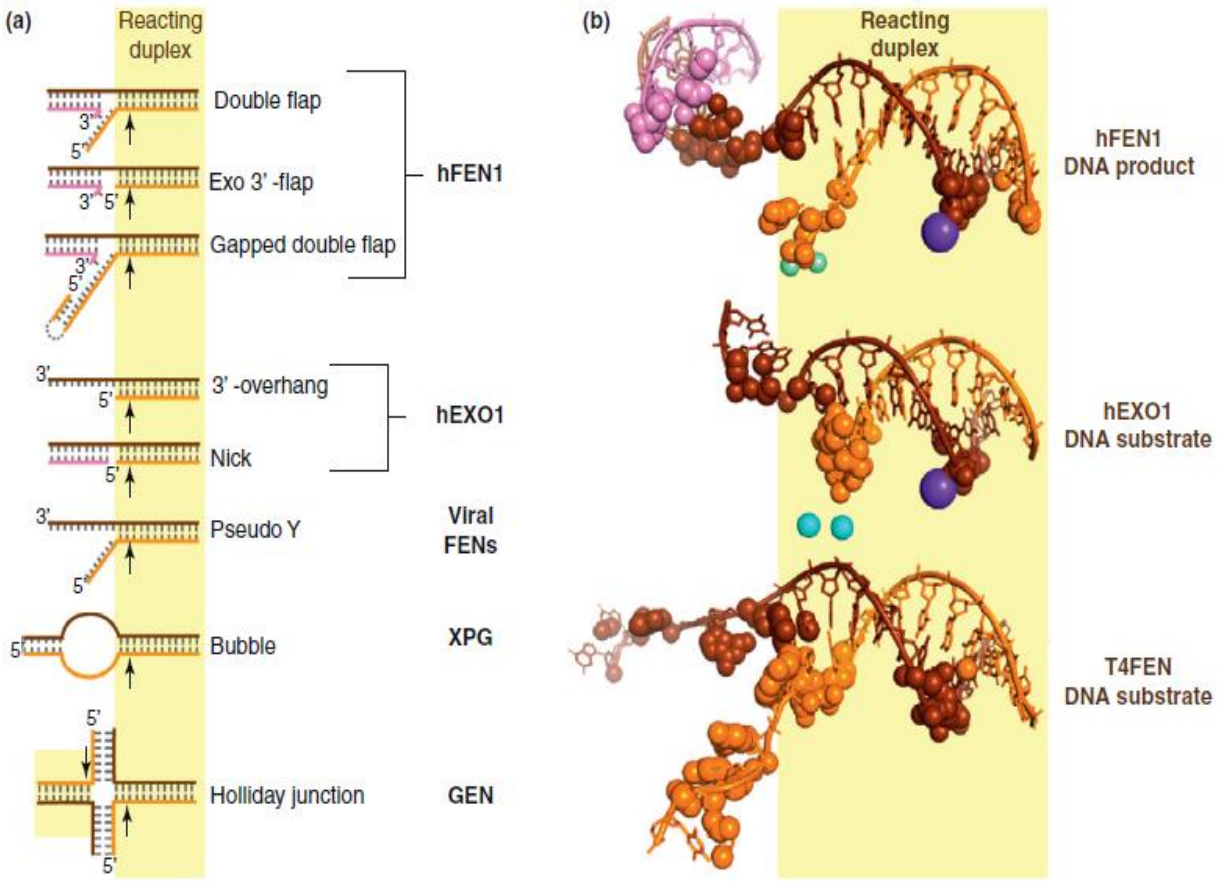


Figure 1.6. FEN superfamily members bind the reacting duplex DNA. (a) All FEN superfamily substrates include a duplex (yellow) that undergoes reaction (arrow). (b) The contacts between substrates and FEN superfamily proteins take place at a corresponding positions and forces substrate to bend. The figure illustrated DNA atoms located within 4 Å of the protein (brown spheres for complementary strand, orange spheres for incised strand, and pink spheres for 3' flap) with the reacting duplex highlighted (yellow), as observed in the structures of FEN1 bound to DNA substrate (PDB: 3Q8K), EXO1 (PDB: 3QE9, with divalent ions modelled in as in 3QEB), and T4FEN (PDB: 2IHN). Primarily, FEN superfamily proteins interact with the complementary strand and with the 5'-terminal nucleotides of the reacting strand; FEN1 is the only one that interact significantly with 3'-flap terminal nucleotide. The two major binding regions on the complementary strand (brown) are separated by ~1 helical turn, and this places the 5'-strand near the active site for incision. **(Figure reproduced with permission from the publishers of Trends in Biochemical Sciences)**

The Exo1 nuclease region is comprised of two subdomains: the NH_2 terminal (N) domain and the internal (I) domain which are separated by a spacer region (*Fig. 1.7*). The N-domain expedites Exo1 binding to the DNA, while the I-domain manifests multiple cysteine and glutamate residues necessary for Mg^{2+} binding. Prior to DNA hydrolysis, two Mg^{2+}'s are required to be loaded on to the I-domain to promote Exo1 binding to the phosphate groups on the DNA molecules (Orans, *et al*., 2011).

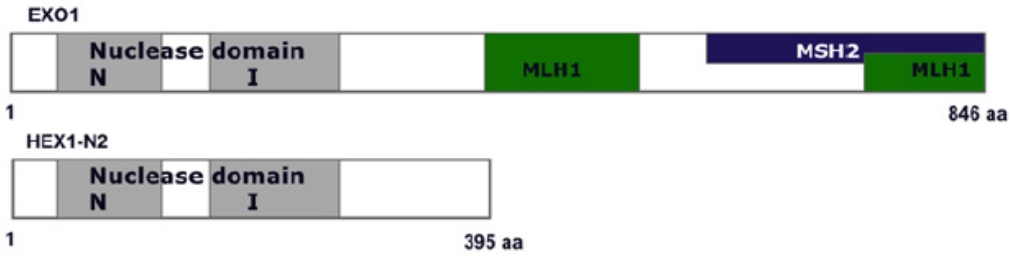


Figure 1.7. Schematic overview of full-length Exo1 and HEX-N2. Binding domains to MLH1 and MSH2 are indicated at the COOH-terminus of full-length Exo1. In both full-length Exo1 and HEX-N2, the nuclease domain contain two domains, N and I domain, separated by a spacer

It is therefore clear that Exo1 is associated with various sets of protein partners in mismatch repair (MMR) and double strand break (DSB) repair (Schmute, *et al*., 2001; Modrich, 2006; Minitou & Symington, 2009). Exo1 exhibits limited processivity in DSB resection *in vitro* and has a low abundance in cells, suggesting that there exists additional factors *in vivo* that promote its function in DNA end resection (Szankasi & Smith 1992; Fiorentini *et al*., 1997; Genschel & Modric 2003). Certainly, MRN/MRX, BLM, RPA, PCNA, SOSS1 and 9-1-1 all displayed stimulatory effects in the *in vitro* Exo1-mediated resection experiments by improving damage association and complementing the processivity (Nimonkar *et al*., 2008; Nicolette *et al*., 2010; Nimonkar *et al*., 2011; Cannavo *et al* 2013; Yang *et al* 2013; Chen, *et al*., 2013; Ngo, *et al*., 2014).

In vitro studies reported that both RecQ1 and WRN helicases interact and stimulate the enzymatic activity of Exo1 (Doherty *et al*., 2005; Sharma *et al*., 2003). It was found recently that Exo1 recruitment to any DNA double strand breaks depends on Mre11–Rad50–Nbs1 (MRN) and CtlP (Eid *et al*., 2010). This indicated the hExo1 role in double strand break early resection, as shown for the yeast homologue (Zhu *et al*., 2008; Mimitou & Symington, 2008). Recombinant CtlP interacts directly with hExo1 as shown in the resection reactions, but in this case, CtlP appeared to inhibit hExo1 nuclease activity *in vitro*. This may prevent excessive DNA degradation (Eid *et al*., 2010). The 5' resection activity of Exo1 has been demonstrated to be stimulated by MRX and Sae2 in a reconstitution reactions with a yeast homologue of the human Exo1. In these reconstitution reactions, MRX and Sae2 have been shown to facilitate Exo1 binding to the DNA ends and process the initial 5' strand (Nicollete *et al*, 2010). The excision activity of hExo1 is activated through direct interaction with the Bloom syndrome protein (BLM) (Nimonkar *et al*., 2008).

Recently, studies in both yeast and mammalian cells have identified 14-3-3 proteins as being interaction partners of Exo1 *in vivo* (Kim *et al*., 2011). Further to this, Sofie and their colleagues (Sofie, *et al*, 2012) in their recent study, have demonstrated direct and robust *in vitro* interaction between hExo1 and six out of the seven 14-3-3 isoforms. Although they showed that 14-3-3 interaction with Exo1 did not appear to have a direct influenced both *in vitro* hExo1 nuclease activity and DNA replication initiation, these results suggest a novel protein interaction network between DNA repair and cell cycle control. It is also suggestive that the interactions may be associated with the regulation of hExo1 availability during the DNA damage response to plausibly prevent extensive DNA resectioning at the damage site (Sofie *et al* 2012). The 14-3-3 proteins have recently been reported to bind to the central region of Exo1, and that Exo1 association with 14-3-3 proteins

limits its damage recruitment and DNA end resection activity (Chen, *et al*,. 2015).

So far, most biochemical studies have been focused on the NH_2-terminal region of hExo1, one of the two key nucleases (the other being Dna2) involve in DNA double strand break resection. The NH_2-terminal region of hExo1 is named HEX-N2, which represents 1-395 of the 846 amino acid residues of the full-length hExo1. Orans, *et al* (2011) have purified the HEX-N2 variant from bacteria; they have reported that it contains an active exonuclease domain and also further characterized it by using crystallography (*Fig. 1.8*). Full-length hExo1 has only been partially characterized, and this has been limited due its biochemical activity at various salt temperatures and the necessary pH conditions (Bregenhorn & Jiricny, 2014). To date, there has been no report on the biophysical characterization of full-length hExo1, hence, there is a need for further biochemical and biophysical characterizations of hExo1 to understand how this protein is able to carry out its function and how it is regulated.

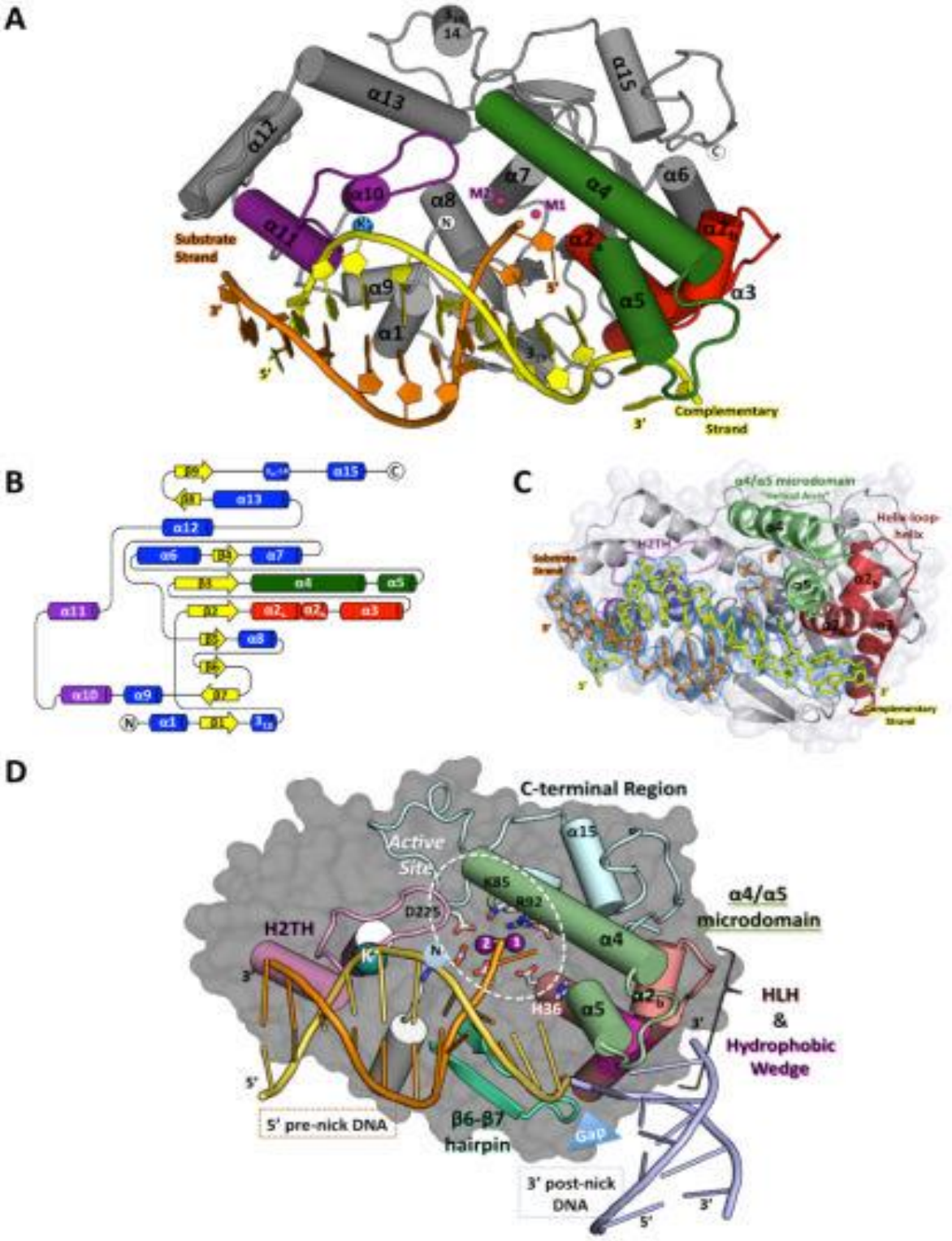

A
α13
α15
α12
α10
α8
α7
α4
α6
α11
α9
α1
α5
α3
α2
Substrate Strand
Complementary Strand
B
C
α4/α5 microdomain
H2TH
Helix-loop-helix
D
C-terminal Region
Active Site
α4/α5 microdomain
H2TH
HLH & Hydrophobic Wedge
β6-β7 hairpin
5' pre-nick DNA
3' post-nick DNA

Figure 1.8. Structure of the hExo1 catalytic domain in complex with a 5'-recessed end substrate

(A) Structure of the hExo1 catalytic domain bound to a gapped DNA substrate mimic. Conserved DNA binding motifs are indicated: α4-α5 micro-domain ("helical arch"), green; α2-α3 helix-loop-helix, red; K+ ion-binding site (blue) in helix-two-turn-helix (H2TH), purple. Two active-site metal ions are shown (red). (B) Topology map of secondary structure elements in the hExo1 catalytic domain. (C) Simulated-annealing omit electron density map calculated to 2.5 Å resolution contoured at 1σ around DNA of the hExo1 D173A complex. Note the ~90° bend of the 3' complementary DNA strand. DNA binding motifs are colored as in A. (D) Key functional features of the of hExo1-DNA complex. DNA binding motifs are coloured as in B. C-terminal region is blue; hydrophobic wedge region of α2-α3 is shown in magenta; β6-β7 hairpin is teal. hExo1 DNA substrate is orange and yellow; modelled post-nick DNA from *A. fulgidus* FEN-1 structure (PDB 1RXW) is blue. A gap between the pre and post- nick region is highlighted with a blue triangle. Active site residues are shown as sticks. Mn2+ (magenta) and K+ ions (blue) are highlighted. **(Figure reproduced with permission from the publishers of Cell)**

1.6. Proliferating Cell Nuclear Antigen (PCNA)

In all domains of life, DNA sliding clamp proteins can be found. These proteins have homogenous structures from bacteria, archaea and eukaryotes, although they share a sparse sequence homology. They all form ring-shaped proteins that encircle double-stranded DNA. These sliding clamps are widely known for their ability to confer high processivity to classical DNA polymerases that are mostly involved in normal DNA replication and repair. Sliding clamps, are, however, known to go far beyond this; they recruit many of the DNA replication, repair and recombination enzymes by forming a mobile platform on the DNA itself.

The sliding clamp protein in eukaryotes is part of proliferating cell nuclear antigens (PCNA). Referred to as the '*maestro of the replication fork'* (Moldovan, *et al*., 2007), PCNA integrates the recruitment of many proteins to sites of DNA replication and in many cases, regulates their activities. PCNA plays a crucial role in a vast majority of nuclear processes including DNA replication, translesion DNA synthesis, base excision repair, nucleotide excision repair, mismatch repair, recombination, chromatin assembly and remodelling, sister chromatid cohesion, and cell cycle control (Tsurimoto, 1999; Maga & Hubscher, 2003; Moldovan, *et al*., 2007; Naryzhny, 2008; Zhuang & Ai, 2010).

The X-ray crystal structure of eukaryotic PCNA was first determined in 1994 (Krishna, *et al*., 1994). Since then, a diverse range of X-ray crystal structures of PCNA bound to peptides derived from PCNA-binding proteins have been solved. More recently, X-ray structures and lower-resolution structures of PCNA bound to full-length protein partners have additionally been resolved. These structures have contributed a critical understanding into how PCNA recognizes and recruits its binding protein partners to replication forks. Eukaryotic PCNA is a ring-shaped homo-trimer with each sub-unit containing two domains. As revealed by the X-ray crystal structure of eukaryotic PCNA, each sub-unit consists of

two independent and similarly folded domains (*Fig. 1.9*) (Krishna, *et al*., 1994).

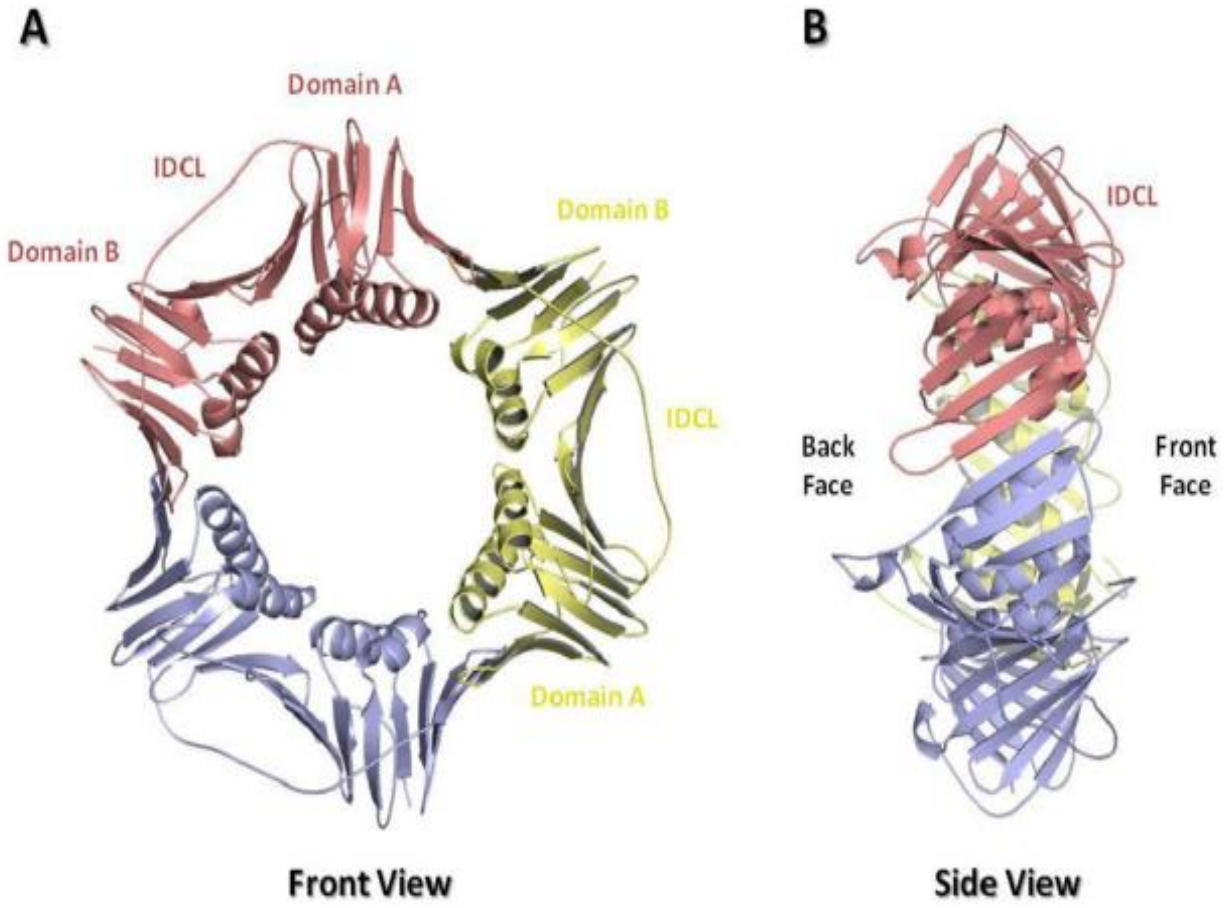


Figure 1.9. The Ribbon diagram of the PCNA trimer (PDB ID: 1PLQ)

Shown from the front (**A**) and the side (**B**) with the individual PCNA subunits colored red, yellow and blue. The inter-domain connector loop (IDCL) is indicated.

PCNA contributes a molecular platform which coordinates a diverse series of processes required in the maintenance, duplication and transmission of the genome (Moldovan, *et al*., 2007). To achieve these processes, PCNA promotes a multiple protein–protein and protein–DNA interactions at the replication fork. The inner channel of PCNA is sufficiently large enough (~35 Å), to allow DNA (~24 Å) to pass through, and the central cavity has a net positive electrostatic charge that allows the PCNA to go across the duplex in a sequence-independent approach (Ivanov, *et al*., 2006). The passage of duplex DNA through the clamp is in a slanted mode, which may facilitate the proper orientation required by PCNA-bound proteins to execute their activity. However, it is not yet clear if these structural studies have accurately showed the active nature of the movement of PCNA on DNA. The conformation of PCNA-bound proteins may also be altered on the PCNA which might be critical for distinct enzymatic functions, as proposed for the polymerizing and editing modes of DNA polymerase in *Pyrococcus furiosus* (Georgescu, *et al*., 2008; Mayanagi, *et al*., 2011).

PCNA has a superfluity of interacting proteins that must be controlled in a spatio-temporal mode in order to aid their roles in a variety of DNA-related processes (Moldovan, *et al*., 2007). The PCNA–protein interaction is governed by a motif referred to as the PCNA-interacting protein (PIP) box. At least 200 or more human proteins contain this short sequence motif (PIP box). The consensus for the PIP box sequence is Q-x-x-[ILM]-x-x-[FY]-[FY]; in some cases, this is flanked by an upstream K-A motif (Xu, *et al*., 2001).

A key question is how the PIP box interactions with PCNA are controlled, considering the fact that this motif is found in a diverse range of proteins. Does the PIP box sequence itself impart inherent hierarchy? This may be true to a certain extent; for example, when isothermal titration calorimetry (ITC) experiments were carried out on PIP box-containing peptides from p21CIP1/ WAF1, DNA polymerase δ

(Pol δ), sub-unit p66 and flap endonuclease1 (FEN1), it was discovered that p21CIP1/WAF1 binds to PCNA with a much greater affinity (~200-fold) than the other peptides (Bruning & Shamoo, 2004). When the crystal structures of the PIP box-containing peptides of p21, p66 and FEN1 bound to PCNA were compared, it was revealed that the PIP box is able to pack itself into the hydrophobic surface of PCNA and that this strongly determined the affinity for binding. p21CIP1/WAF1 exhibited the most extensive efficiency in packing (Bruning & Shamoo, 2004). PIP boxes are therefore said to demonstrate an elegant hierarchy of sequence, and the ability for PIP boxes to fit into the hydrophobic surface of PCNA is a worthwhile estimate of the protein–protein interaction strength.

Rasmussen and colleagues have shown that a peptide containing a PIP-Box-like sequence in the C-terminus of Exo1 can interact with PCNA (Liberti, *et al*., 2011). Recently, experiments carried out using human cells (U2OS), *Xenopus* egg nuclear extracts and purified proteins have demonstrated that PCNA promotes the exonuclease resection activity of human Exo1 by promoting its damage association and processivity (Chen, *et al*., 2013).

1.7. The 14-3-3 proteins

Phosphorylation was the first post-translational modification of protein to be described (Burnett & Kennedy, 1954). Approximately one third of all cellular proteins are affected by phosphorylation (Gough & Foley, 2010). In 1967, Moore and Perez discovered a family of proteins abundant in bovine brain extracts and they named them "14-3-3" which is due to their particular pattern of elution on a two-dimensional DEAE-cellulose chromatography and starch gel electrophoresis. The first biological role of 14-3-3 proteins elucidated in 1996, was that they interact with phosphorylated partners (phospho-serine or-threonine), which is a way to read the post-translational modification state in signalling cascades (Muslinetal *et al*., 1996). The 14-3-3 protein family is comprised of ~30 kDa acidic proteins that are ubiquitous among eukaryotes. The 14-3-3 proteins are essential components of phosphorylation-mediated signalling in concert with kinases and phosphatases.

In yeast, there are two highly conserved 14-3-3 paralogues. In mammals, there are seven paralogues [Beta (β), Epsilon (ε), Eta (η), Gamma (γ), Tau (τ) Zeta (ζ) sigma (σ)] and in plants, there are up to fifteen paralogues in plants (Aitken, 2006). With the exception of the sigma isoform, all of the mammalian 14-3-3 protein paralogues can form both homo and heterodimers (Wilker *et al*., 2005; Benzinger *et al*., 2005; Gardino *et al*., 2006). In mammalian phyla, the number of paralogues and their primary sequences are invariable. The two closest paralogues are ζ and β (86.5% identical), and the most divergent are ζ and ε (66% identical). Their differences do not affect the tri-dimensional structure, especially in the binding groove, in which all the paralogues contain the K49, R56, and R127 residues that are crucial for their binding activity (Aitken, 2002).

The 14-3-3 proteins are dimeric and highly helical. This was revealed by the first crystal structures of human 14-3-3 ε (Liu *et al*., 1995) and 14-3-3 τ (Xiao *et al*., 1995). A bundle of nine anti-parallel helices (H1 – H9) are contained in each monomer and an amphipathic ligand binding groove is present in the concave surface which is formed by α-helices H3, H5, H7 and H9 (*Fig. 1.10A*). The dimeric molecule is in a cup-like shape with a large central channel approximately 35 Å broad, 35 Å wide and 20 Å deep. The dimer interface and inner line walls of the central channel are formed by the invariant residues, while the outer convex surface contained more of the variable residues which are distributed across it (*Fig. 1.10B*).

The C-terminal loop, which is disordered in all available structures, contained the utmost sequence variability. To date, the crystal structures of seven mammalian 14-3-3 isoforms are available (Yang *et al*., 2006). Even though in both apo and ligand-bound form, all of the structures are very much uniform, though comparative studies have elucidated various structural variations (Gardino *et al*., 2006; Yang *et al*., 2006). The relative position of the monomers are different in individual structures and this results from the alterations in angles between the two sub-units (*Fig. 1.11A*) (Yang *et al*, 2006). The 14-3-3 proteins can bind the ligands of different sizes and shapes, and this could be facilitated by the flexibility of their dimeric state. There are other structural differences found in the loop regions among the 14-3-3 isoforms that includes various lengths and conformations (especially loops between α-helices H3 and H4 as well as H8 and H9) and the length of α-helices H3 and H4 (*Fig. 1.11B*) (Benzinger *et al*., 2005; Gardino *et al*., 2006).

It was initially discovered that 14-3-3 proteins recognize a specific novel phosphoserine-containing motif (Muslin *et al*., 1996). This was refined further and two consensus binding motifs were identified using an oriented peptide library. These motifs were: RSxpS/TxP (mode I),

and RxxxpS/TxP (mode II) where *x* stands for any amino acid. A third consensus binding motifs was identified: pS/TX-COOH (mode 3) (Muslin *et al*., 1996; Yaffe *et al*., 1997; Ganguly *et al*., 2005; Coblitz *et al*., 2006), and it has been explained that ligands with the mode III sequence motif exhibit weaker binding affinity to 14-3-3 compared to the mode I and II motifs (Wurtele *et al*., 2003; Ganguly *et al*., 2005; Coblitz *et al*., 2005; Coblitz *et al*., 2006).

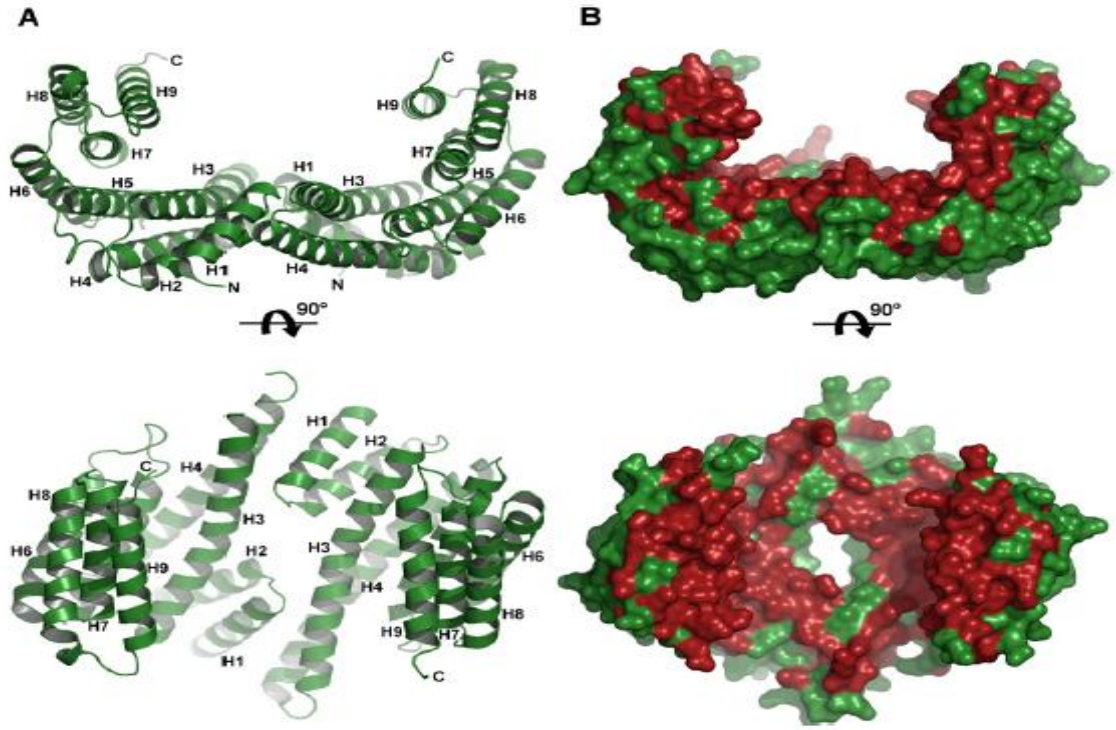


Figure 1.10. Crystal structure of the 14-3-3 protein (human ζ isoform, PDB ID code 1QJB [29]). (A) A ribbon representation. (B) The surface representation. Residues that are totally conserved among all seven human isoforms are shaded in dark red.

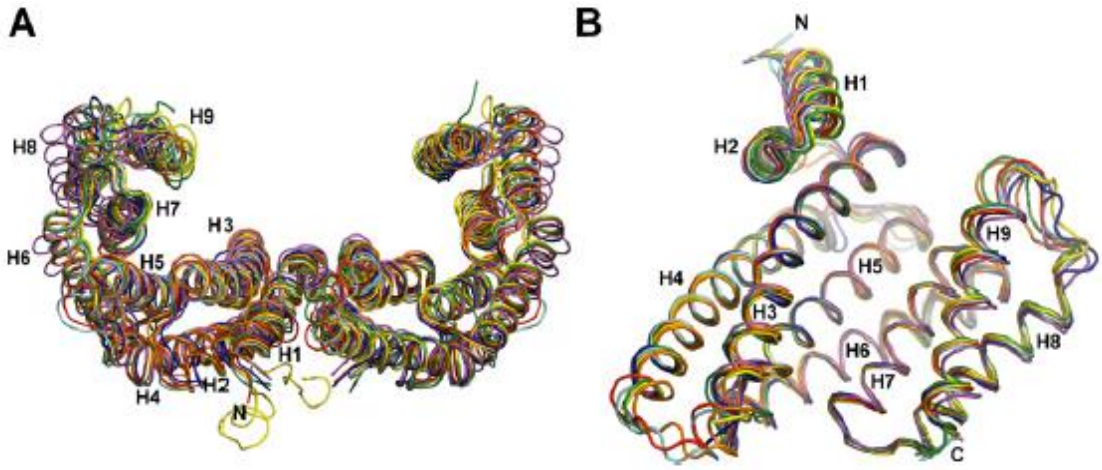


Figure 1.11. Structural comparison of all seven human 14-3-3 protein isoforms. (A) Superimposition of 14-3-3 dimers. The beta isoform (PDB ID 2C23) is shown in magenta, gamma (2B05) in red, epsilon (2BR9) in orange, zeta (1QJB) in green, eta (2C74) in cyan, sigma (1YWT) in blue and tau (2BTP) in yellow. Bound peptides were removed for better clarity. (B) Comparison of monomers. Only one monomer from each crystal structure was used for this superimposition.

The 14-3-3 proteins can also bind un-phosphorylated ligands. The Exoenzyme S (ExoS) cytotoxin and the R18 peptide derived from a phage-display library are two good examples of ligands with such a binding mode (Fu *et al*., 1993; Masters *et al*., 1999; Wang *et al*., 1999; Henriksson *et al*., 2000). As revealed by the crystallographic studies, R18 binds in a uniform fashion as with the phosphorylated peptides through the amphipathic sequence, WLDLE, whose two acidic groups interact with a cluster of basic residues within the ligand binding groove (Petosa *et al*., 1998). On the other hand, the crystal structure of the 14-3-3ζ:ExoS complex revealed that the ExoS peptide bound in a reverse orientation that depended primarily on the hydrophobic contacts between the four leucine residues of ExoS and the "roof" of the 14-3-3 ζ ligand binding grove (Ottmann *et al*., 2007).

Bioinformatics analyses have proved that 14-3-3 binding sites are often found within disordered regions either in the N- and C-terminal tails, or bordering on the functional domains (Bustos & Iglesias, 2006; Oldfield *et al*., 2008; Johnson *et al*., 2010). Functionally, the elasticity of the intrinsically disordered regions can provide various advantages for signalling proteins. These advantages may include the proficiency to bind to multiple binding partners and/or the fine control over the binding affinities involved (reviewed by Wright & Dyson 2009; Shoemaker *et al*., 2000). Shoemaker *et al*. (2000) suggested that an intrinsically disordered or partially disordered protein would have an advantage of having a greater 'capture radius' that paves the way for a diffusive search for a binding target than as would be in a more closely packed, folded protein with restricted conformational plasticity (Shoemaker *et al*. 2000). The more numerous binding sites for the 14-3-3 proteins within the unstructured regions also suggests that the disorder-to-order transition of the ligand molecule's structure might be a common binding aspect for the 14-3-3 proteins (Bustos & Iglesias,

2006). All of these aspects might be significant for binding interactions between the 14-3-3 proteins and their ligands.

It has been reported that in budding yeast, Exo1 interacts with two of the isoforms of the 14-3-3 proteins and that the 14-3-3 proteins suppress the Exo1 processing of stalled replication forks intermediates (Engels, *et al*., 2011). Using yeast two-hybrid assay, human Exo1 was reported to interact with at least six of the seven human isoforms of the 14-3-3 protein. But the significance of Exo1 function in this interaction in the DSB resection has not been determined (Andersen, *et al*., 2012). However, the 14-3-3 proteins have recently been reported to bind to the central region of human Exo1 and in that, the Exo1 association with 14-3-3 proteins limits its damage recruitment and DNA end resection activity (Chen, *et al*,. 2015).

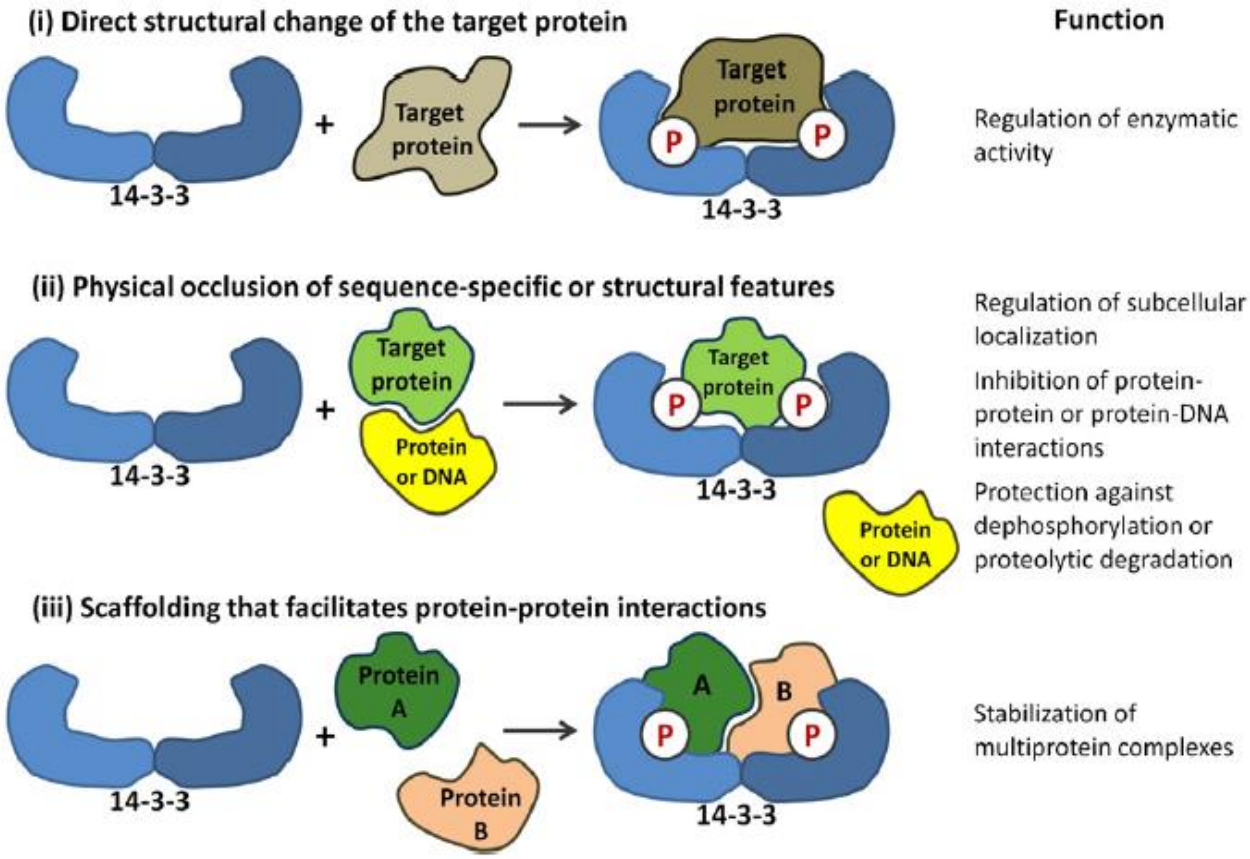


Figure 1.12. Modes of 14-3-3 protein action.

The 14-3-3 protein binding can: (i) induce a conformational change of the target protein; (ii) mask a specific region in the target protein; or (iii) facilitate the interaction between two other proteins. **(Figure reproduced with permission from Seminars in Cell & Developmental Biology publishers).**

1.8. Intrinsically disordered proteins

Intrinsically disordered proteins (IDPs) and intrinsically disordered protein regions (IDPRs) have, in recent times, drawn much attention. This is as a result of the existence of these non-3D-structured biologically functional molecules which contradicts the old tradition of the *'one protein–one structure–one function'* paradigm (Dunker *et al*. 1998; Wright & Dyson, 1999; Uversky *et al*., 2000; Dunker *et al*., 2001; Tompa, 2002; Daughdrill *et al*., 2005; Uversky & Dunker, 2010). These highly dynamic and biologically important functional proteins were, at many times, discovered and rediscovered before they were recognized and accepted to be a unique extension of the protein kingdom. These proteins were depicted with various different terms as a result of a lengthy and complex pathway to their recognition. They were referred to as floppy, pliable, rheomorphic (Holt & Sawyer, 1993), flexible (Pullen *et al*., 1975), mobile (Cary *et al*., 1978), partially folded (Linderstrom & Schellman 1959), natively denatured (Schweers *et al*., 1994), natively unfolded (Uversky *et al*., 2000; Weinreb *et al*., 1996), natively disordered (Daughdrill et al., 2005), intrinsically unstructured (Wright & Dyson, 1999; Uversky *et al*., 2000), intrinsically denatured, (Schweers *et al*., 1994) intrinsically unfolded (Weinreb *et al*., 1996), intrinsically disordered (Dunker *et al*., 2001), vulnerable (Chen *et al*., 2008), chameleon (Uversky, 2003), malleable (Fuxreiter *et al*., 2008 16), 4D (Tsvetkov *et al*., 2008), protein clouds (Dunker & Uversky, 2010), and dancing proteins (Livesay, 2010), among various other terms.

This trail of terms may be considered to be the prehistory of intrinsic disorder. In the earlier periods, researchers have found that biologically active non-folded proteins are far different from the globular, transmembrane, and fibrous proteins referred to as "normal''. For a decade, each of such proteins was conceded to be an exception to a general rule that each unique sequence defined a unique 3D-structure

which was central for a unique function. The collection of terms used in characterizing IDPs in earlier times not only revealed the creativity of the researchers, but also highlighted the difficult task encountered in trying to come up with an appropriate term that would properly describe the proteins. Despite the fact that none of the proposed terms was perfect in defining the biologically active proteins that had no unique structure, 'intrinsically disordered protein' is the current and most frequently used term than any other.

Based on systematic bioinformatics analyses, IDPs have been clearly demonstrated to be highly sufficient in any given proteome (Dunker *et al*., 2000; Dunker *et al*., 2001; Ward *et al*., 2004; Uversky & Dunker, 2010; Uversky, 2010;). These proteins have therefore shifted from being ambiguous and attenuated to novel types of proteins, whose functionality is predisposed by the absence of a stable structure, and which are conventional in nature. IDPs/IDPRs functions are approbatory to ordered proteins and domain functions (Dunker *et al*., 2001; Uversky, 2002; Radivojac *et al*., 2007), with IDPs/IDPRs involved in a typically important biological functional roles such as regulation, signalling and control pathways (Lakoucheva *et al*., 2002; Uversky *et al*., 2005). Due to their important functional roles, the malfunction of IDPs has been correlated with diverse human diseases such as cancer, amyloidosis cardiovascular and neurodegenerative diseases (Uversky *et al*., 2008).

1.9. Disorder prediction in hExo1

In an attempt to distinguish between the ordered and intrinsically disordered regions in proteins, a neural network predictors of naturally disordered regions has been developed (Romero *et al*., 1997; Li *et al*., 1999; Dunker *et al*., 2001; Romero *et al*., 2001). It uses several amino-acid attributes such as coordination number, hydropathy, and flexibility. The predictor VL-XT of the PONDR program was applied to the entire hEXo1 protein. As shown in *Fig. 1.13a*, hExo1 is predicted to have three main disordered regions located in the C-terminal region. In fact, about two-thirds of the hExo1 is predicted to be disordered with a score higher than the 0.5 threshold or conversely, barely below the threshold (*Fig. 1.13a* and *b*). The region encompassing residues 1–345 is strongly predicted not to be disordered. With these predictions, it is imperative to investigate the biophysical characteristics of hExo1 using techniques such Small Angle X-ray Scattering (SAXS), Analytical Ultracentrifugation (AUC), Circular Dichroism Spectroscopy (CD) and Dynamic Light Scattering (DLS).

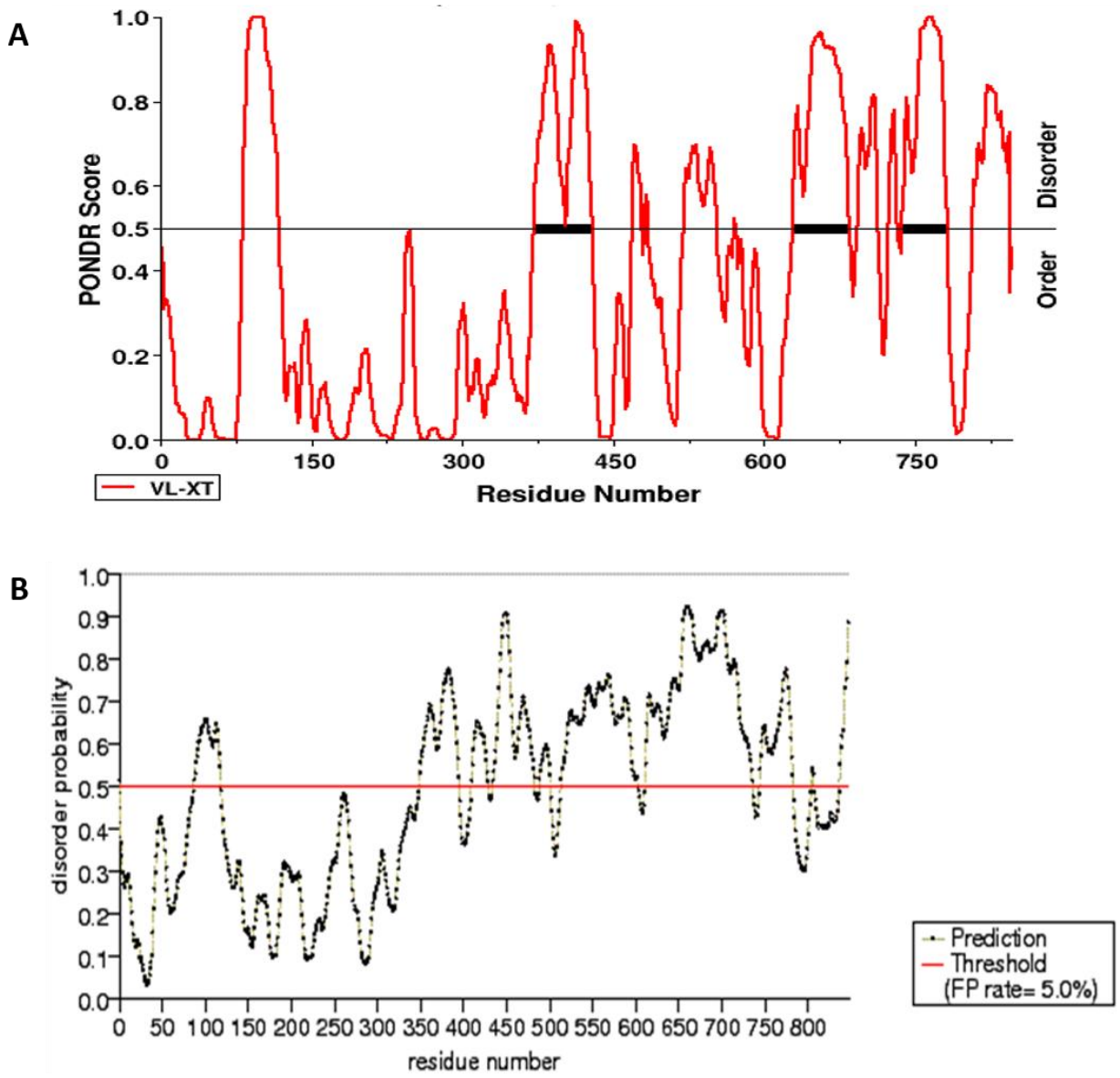


Figure. 1.13. Prediction of unstructured regions. (a) PONDR prediction of unstructured regions in hExo1, using VL-XT predictor (Li *et al*., 1999; Romero *et al*., 1997, 2001). The prediction score is plotted against residue number. Residues with a score above a threshold of 0.5 are considered disordered. The disordered regions are marked by thick bars. (b) PrDOS prediction of unstructured regions in hExo1 (Ishida1 and Kinoshita, 2007).

1.10. Analytical Ultracentrifugation (AUC)

Analytical ultracentrifugation (AUC) has proven to be a useful method for the characterization of macro-molecules in solution and a very useful tool for quantitative studies on the interaction of macro-molecules (Hansen *et al*., 1994; Hensley, 1996; Cole & Hansen, 1999; Scott & Schuck, 2005; Howlett *et al*., 2006). AUC has a broad range of applications. It can be used to analyse the solution behaviour of various types of molecules in a broad range of solvents and solute concentrations.

In analytical ultracentrifugation, the samples are characterized in their native state and under biologically relevant solution conditions unlike most of the commonly used methods. AUC experiments are performed in a free solution, thereby eliminating any complications due to interactions with gel matrices or surfaces. There are two complementary views of solution behaviour in AUC. Sedimentation velocity provides first-principle, hydrodynamic information about the size and shape of molecules (Laue & Stafford, 1999; Lebowitz *et al*., 2002; Howlett *et al*., 2006) and sedimentation equilibrium which provides first-principle, thermodynamic information about the solution molar masses, stoichiometries, association constants, and solution non-ideality (Laue, 1995; Howlett *et al*., 2006).

AUC is a valuable tool for studying protein interactions due to its various virtues. Unlike spectroscopic techniques which give a superposition of the signals from all species, AUC allows for hydrodynamic separation and the identification of different species by size due to a size-dependent migration of complexes that occurs, and yet, AUC differs from chromatographic approaches because the migration occurs in a free solution which enables quantification based on first principles. This is usually carried out in a process that enables the complexes to remain as their constituent species throughout the period of the analysis, and for an exchange between all species to

proceed in a way that reflects the kinetic and equilibrium properties of the interacting system.

1.11. Small Angle X-ray Scattering (SAXS)

Small Angle X-ray Scattering (SAXS) is a powerful method for the analysis of biological macro-molecules in solution. Profound advances in instrumentation and computational methods over the last decade have led to new developments in the application of SAXS to structural biology. SAXS is widely able to provide low resolution structural information about flexible proteins in solution that can complement crystallographic analyses. Despite not being a high resolution method, vast information about bio-macromolecules, advances in computing power and continued developments in algorithms has enabled the derivation of much more detailed information from SAXS data analysis (Chacon *et al*., 1998; Petoukhov & Svergun, 2003; Takahashi *et al*., 2003; Zipper & Durchschlag, 2003; Petoukhov & Svergun, 2005). SAXS is a hybrid method because when combined with other structural information, it can elucidate considerable biological information about the conformations of proteins in solution.

When matter is irradiated by an X-ray beam, one of the primary interactions is the elastic scattering of X-rays by the electrons. X-rays thus are scattered by spatially correlated electron pairs constructively and destructively interfere in accordance with Bragg's law. The longer the electron pair distance, the smaller the angle at which interference effects are observable. This is readily apparent when contrasting the scattering profiles of the large proteins relative to the smaller proteins. Large proteins will scatter more strongly at smaller angles than small proteins, and much more strongly than any buffer. In the last case, the electrons are exclusively correlated on small length scales.

Traditionally, SAXS was defined by scattering at angles where the small angle cosine and sine approximations applied. However,

practically, SAXS analysis may use scattering at angles up to the primary scattering peak of water at a momentum transfer of ≈2 $Å^{-1}$ which thereafter overwhelms all other signals. (Momentum transfer $s = (4\pi/\lambda)\sin(\theta/2)$ where λ is the wavelength of X-rays and θ is the scattering angle relative to the incident beam) (*Fig. 1.14*).

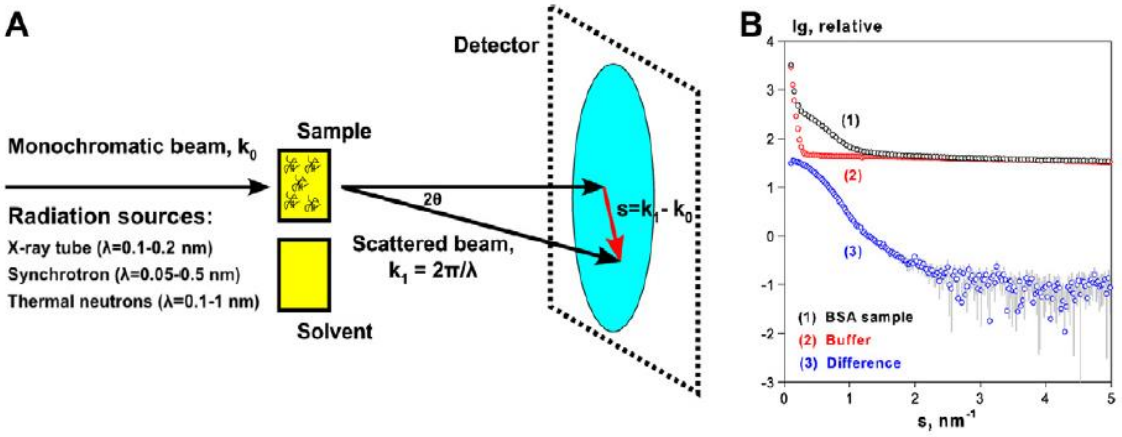


Figure 1.14. Schematic representation of a typical SAXS experiment and radially averaged data. (A) Standard scheme of a SAS experiment. (B) X-ray scattering patterns from a solution of BSA measured at X33 (DORIS, Hamburg) in 50 mM HEPES, pH 7.5, solvent scattering and the difference curve (containing the contribution from the protein alone, scaled for the solute concentration, 5 mg/ml). **(Figure reproduced with permission from Journal of Structural Biology publishers)**

1.12. Circular Dichroism (CD)

Proteins are optically active macro-molecules, and therefore they exhibit differential absorption of circular polarized light. The far-UV circular dichroism (CD) spectroscopy of proteins and peptides (180–250 nm) is primarily based on the excitation of electronic transitions in amide groups. The peptide backbone in proteins forms a characteristic secondary structure such as α-helices, β-pleated sheets, turns, and disordered regions with specific Φ, Ψ dihedral angles and H-bond patterns affecting the CD spectrum (Woody, 1995). Circular dichroism spectroscopy has been exploited in the studies of protein folding and stability, inter-molecular interactions, and ligand binding, and recently, CD has also been applied in protein disorder investigation assays (Matsuo, *et al*., 2007; Wallace, 2009). A primary use is in analysing the secondary structure or conformation of macro-molecules, particularly proteins, as their secondary structure is sensitive to its environment, temperature or pH. Circular dichroism can be used to observe how the secondary structure changes with certain environmental conditions or on interaction with other molecules. Structural, kinetic and thermodynamic information about the macro-molecules can be derived from circular dichroism spectroscopy.

1.13. Dynamic Light Scattering (DLS)

Dynamic Light Scattering is also known as Photon Correlation Spectroscopy. This technique is one of the most popular methods used to determine the size of particles. Shining a monochromatic light beam, such as a laser, onto a solution with spherical particles in the Brownian motion causes a Doppler Shift when the light hits the moving particle, changing the wavelength of the incoming light. This change is related to the size of the particle. It is possible to compute the sphere size distribution and to give a description of the particle's motion in the medium, measuring the diffusion coefficient of the particle and using the auto-correlation function. Although dynamic scattering is, in

principle, capable of distinguishing whether a protein is a monomer or dimer, it is much less accurate for distinguishing small oligomers than classical light scattering or sedimentation velocity. The advantage of using dynamic scattering is the possibility to analyse the samples containing broad distributions of species of widely-differing molecular masses (e.g. a native protein and various sizes of aggregates), and to detect very small amounts of a higher mass species (<0.01% in many cases). Dynamic light scattering (DLS) is a technique based on measuring the fluctuations in the intensity of light scattered from particles in a solution without perturbing the system (Chu, 1974). It has been used to determine the diffusion coefficients and the sizes of particles in a solution rapidly and exactly (Kalpand *et al*., 1994; Nispa *et al*., 1999).

We have now seen a distinct picture of Exonuclease1 as a multi-functional protein involved in biological events monitoring and preserving genomic ability. These multi-functions includes, double strand break (DSB) repair through homologous recombination (HR), mismatch repair (MMR), replication, genome maintenance, meiosis, telomere regulation, class switch recombination (CSR), somatic hypermutation (SH) in lymphocytes, gene conversion, post-replication repair (PRR), telomere processing, and apoptosis signalling.

1.14. PROJECT OUTLINE

Exo1 plays a critical role in DNA double strand break (DSB) resection which is an important step in DSB repair through homologous recombination. Insufficient resection of broken double stranded DNA hinders HR and ATR checkpoint activation but excessive resection can have deleterious consequences, because ssDNA is more prone to degradation, also breakage of the 3' strand DNA could cause loss of genetic information (Chen *et al*, 2013). Likewise, persistent checkpoint signalling induced by excessive ssDNA could lead to cell death (Rossiello *et al,* 2014). Exonuclease1 interacts with various partner proteins such as PCNA, 14-3-3, MRN/MRX, BLM, RPA, SOSS1 and 9-1-1.

Despite hExo1's critical importance in inducing the overall DNA damage response, the mechanisms and regulation of the hExo1 resection pathway remain incompletely understood. Two thirds of hExo1 is predicted to be intrinsically disordered, and it is in this region that many post-translational modifications and binding events are known to occur.

How hExo1's function and/or regulation are properly coordinated with respect to its structure is not yet known. To date, there is no experimental evidence relating hExo1 structure to its function and/or regulation. This work aimed to investigate the biophysical characteristics and *in vitro* regulation of DNA resection activity of both full-length hExo1 and N-terminal hExo1 proteins. This work has a particular focus on PCNA and 14-3-3s as hExo1 binding partner candidates, since the previous studies have shown evidence of binding and some degree of activity modulation by both PCNA and 14-3-3s as depicted in *Figure. 1.15*.

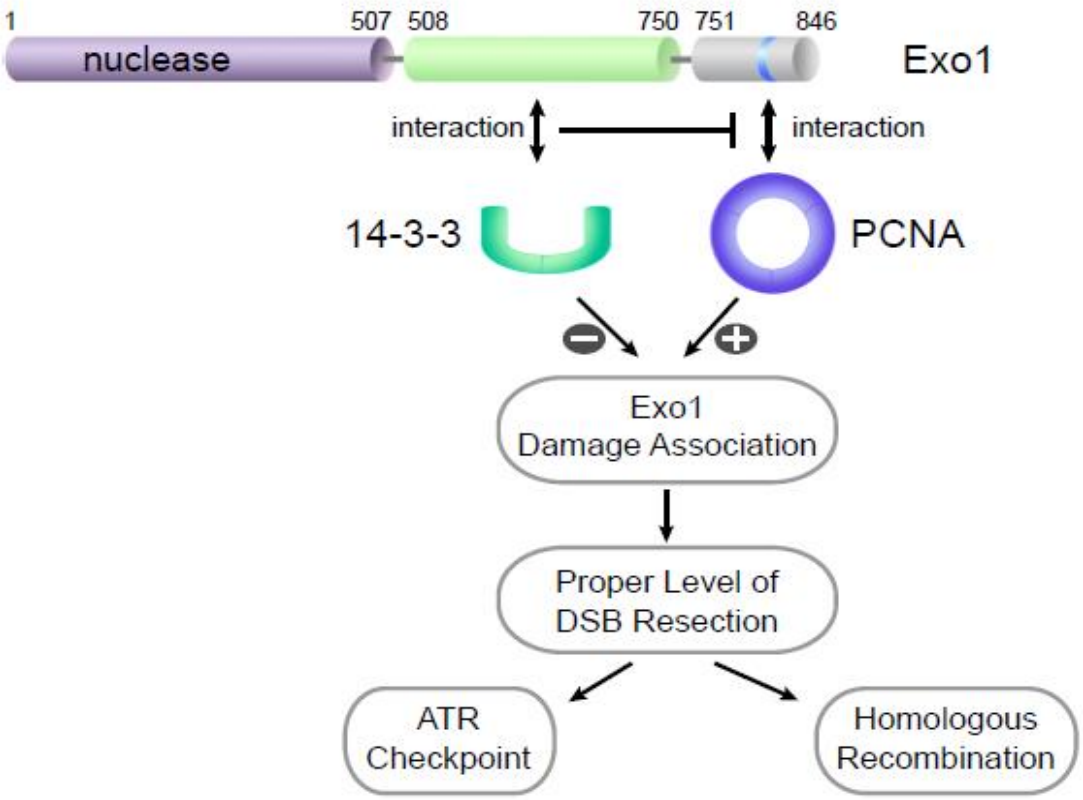


Figure 1.15. Depiction of human Exo1 association with PCNA and 14-3-3s

PCNA interact with the PIP box on the C-terminal region of hExo1 and promote damage association. 14-3-3s bind to the central region of hExo1 and restrain hExo1 damage association and subsequently affect proper level of DSB resection. **(Adapted from Chen *et al*., 2015).**

AIMS:

- Cloning of hExo1 and binding partner proteins (PCNA, 14-3-3ζ and 14-3-3ε) genes
- Optimize the expression and purification of hExo1 (Insect cells and bacterial expression systems) and binding partner proteins (Bacterial expression)
- Study the thermodynamic and kinetic properties of hExo1 in DNA end resection
- Establish the regulatory roles of PCNA, 14-3-3ζ and 14-3-3ε on hExo1 activity in DNA end resection
- Biophysical characterization of hExo1

OBJECTIVES:

(a) Express and purify the hExo1 protein and binding partners (PCNA, 14-3-3s)

(b) Test hExo1 *in vitro* DNA end resection activity under different temperature, pH and salt conditions

(c) Test how PCNA and 14-3-3s regulate hExo1 activity in DNA end resection (*in vitro*)

(d) Determine the secondary structure content, folding, spatial distribution of the hExo1 protein Sedimentation Velocity Analytical Ultracentrifugation (SV-AUC), Small Angle X-ray Scattering (SAXS), Circular Dichroism (CD) and Dynamic Light Scattering (DLS).

CHAPTER TWO: MATERIALS AND METHODS

2.1 MATERIALS

The full-length clone for the human Exo1 splice variant (*hExo1* cDNA) in a pFastBacI plasmid (pFastbacI-hExo1) and human *PCNA* cDNA in pET28a vector (pET28a-PCNA) were kindly provided by Professor Paul Modrich, (HHMI & Department of Biochemistry, Box 3711, Rm 159 Nanaline Duke Bldg Duke University Medical Centre Durham NC 27710, 919-684-2775). A yeast two-hybrid vector harbouring each of the 14-3-3 isoforms coding region (pHAF633 pJG 14-3-3 zeta and pRRS305 pJG 14-3-3 epsilon) were kindly provided by Professor Lene Juel Rasmussen, Centre for Healthy Aging, Department of Cellular and Molecular Medicine, University of Copenhagen, 2200 Copenhagen, Denmark. MAX Efficiency® DH10Bac™ Competent *E. coli* was purchased from Invitrogen. Unless stated otherwise all other chemicals/reagent used in insect cell protein expression were obtained from Invitrogen. All restriction enzymes were purchased from New England Biolabs. Phusion High-Fidelity PCR Master Mix was purchased from New England Biolabs (NEB). Platinum® Taq polymerase (Invitrogen) PureLink Quick Gel Extraction and PCR Combo Kit and PureLink™ HiPure Plasmid DNA Miniprep Kit were purchased from Invitrogen. All antibiotics were purchased from Sigma Aldrich. IMPACT™ Kit (contained pTXB1 vector) was purchased from New England Biolabs and pET28a vector was purchased from Novagen. GeneJET Plasmid Miniprep Kit was purchased from Fisher Thermo Scientific.

2.2. METHODS

This chapter presents the detailed methods used in cloning hExo1 in pTXB1 vector and Nt-hExo1, PCNA, 14-3-3s in pET28a (+) vector. It also presents the methods used in over-expression and purification of all the recombinant proteins.

2.2.1. Cloning

2.2.1.1. Propagation of pFastbacI-hExo1 plasmid

A 2 µL aliquot of the pFastBacI-hExo1 plasmid DNA (50 ng/µL) was added into 50 µL aliquot of competent *E. coli* DH5α cells and placed on ice for 30 min. Cells were heat-shocked at 42^{o}C for 30 seconds and placed immediately onto ice. An aliquot of 250 µL pre-warmed SOC media (Invitrogen) was added into each tube and incubated at 37^{o}C for 60 min so that the cells could recover. The culture was plated out on LB agar (Sigma Aldrich) + 100 ug/ml ampicillin and incubated at 37^{o}C overnight.

2.2.1.2. Miniprep

To obtain pure plasmid DNA, a GeneJET Plasmid Miniprep Kit (Thermo Scientific) was used. Using a flame-sterile technique the selected colony was inoculated into 10 ml of LB broth + 150 ug/ml ampicillin and incubated at 37^{o}C overnight with shaking at 200 rpm. A 2 ml of bacterial overnight culture was pelleted by centrifugation at 10,000 rpm for 2 minutes. Pelleted bacterial cells were re-suspended in 250 µL of the resuspension solution and resuspended completely by vortexing until no cell clumps remained. The cell suspension was then transferred to a microcentrifuge tube. The lysis solution (250 µL) was added and mixed thoroughly by inverting the tube 4-6 times until the solution became viscous and slightly clear. A neutralization solution (350 µL) was added and mixed immediately and thoroughly by inverting the tube 4-6 times.

To separate the plasmid from the cell debris and chromosomal DNA, the solution was centrifuged at 13,000 rpm for 5 minutes. The supernatant containing the plasmid DNA was transferred to the supplied GeneJET spin column (contained in the GeneJET Plasmid Miniprep Kit from Thermo Scientific) by decanting and centrifuged at 13,000 rpm for 1 min, flow-through was discarded the column placed back into the same collection tube. The wash solution (500 µL) was added to the GeneJET spin column and centrifuged at 13,000 rpm for 1 minute and the flow-through was discarded, column was placed back into the same collection tube and repeated the wash procedure using 500 µL of the wash solution. The flow-through was discarded and column was centrifuged for an additional 1 min to remove residual wash solution. GeneJET spin column was transferred into a fresh 1.5 mL micro centrifuge tube. A 50 µL of the elution buffer (contained in the GeneJET Plasmid Miniprep Kit from Thermo Scientific) was added to the centre of GeneJET spin column membrane to elute the plasmid DNA and incubated for 2 min at room temperature followed by centrifugation at 13,000 rpm for 2 min. Eluted sample which contained the purified recombinant plasmid DNA (pFastbacI-hExo1) was stored at -20^{o}C.

2.2.1.3. Transforming DH10Bac™ E. coli

The baculovirus shuttle vector (bacmid), bMON14272 (136 kb), present in DH10Bac™ *E. coli* contained a low-copy number mini-F replicon, Kanamycin resistance marker and a segment of DNA encoding the LacZα peptide from a pUC-based cloning vector into which the attachment site for the bacterial transposon, Tn7 (mini-*att*Tn7) has been inserted. Insertion of the mini-*att*Tn7 does not disrupt the reading frame of the LacZα peptide. The bacmid propagated in *E. coli* DH10Bac™ as a large plasmid that conferred resistance to kanamycin and complemented a lacZ deletion present on the chromosome to form colonies that were black (Lac+) in the presence of a chromogenic

substrate S-gal and the inducer, IPTG. Recombinant bacmids (composite bacmids) were generated by transposing a mini-Tn7 element from a pFastBac™ donor plasmid to the mini-*att*Tn7 attachment site on the bacmid. The Tn7 transposition functions were provided by a helper plasmid. DH10Bac™ *E. coli* also contained the helper plasmid, pMON7124 (13.2 kb), which encoded the transposase and confered resistance to tetracycline. The helper plasmid provided the Tn7 transposition function *in trans* (Barry, 1988).

One vial of MAX Efficiency® DH10Bac™ competent cells was thawed on ice, gently mixed and a 100 µL of the DH10Bac™ cells was transferred into a pre-chilled, 15 mL round-bottom polypropylene tube. About 100 ng plasmid DNA (pFastbac1-hExo1) was added to the cells and mixed gently. Cells were incubated on ice for 30 mins and then heat-shocked in water bath for 45 secs at 42°C without shaking. After the heat shock cells were immediately transferred to ice and chilled for 2 minutes. A room temperature SOC medium was added (900 µL) to the cells and incubated at 37°C with shaking at 225 rpm for 4 hours. After the incubation a 10-fold serial dilutions of the cells (10^{-1}, 10^{-2}, 10^{-3}) was prepared with SOC medium and plated 100 µL of each dilution on S-Gal agar (Sigma Aldrich) plate containing 50 µg/mL kanamycin, 7 µg/mL gentamicin, 10 µg/mL tetracycline, and 40 µg/mL IPTG. Plates were incubated for 48 hours at 37°C. About 10 white colonies were picked and restreaked on fresh S-Gal agar (Sigma Aldrich) plates containing 50 µg/mL kanamycin, 7 µg/mL gentamicin, 10 µg/mL tetracycline, and 40 µg/mL IPTG. The plates were incubated overnight at 37°C. From a single colony confirmed to have a white phenotype on re-streaked plates, a liquid culture containing 50 µg/mL kanamycin, 7 µg/mL gentamicin, and 10 µg/mL tetracycline was inoculated.

2.2.1.4. Isolating recombinant bacmid DNA

Recombinant bacmid DNA was isolated using the PureLink™HiPure Plasmid DNA Miniprep Kit (Invitrogen). 1.5 mL bacterial cells (in LB

broth) was harvested by centrifugation at 9,000 × g for 15 minutes. All medium was removed. 0.4 mL re-suspension Buffer (contained in the PureLink™HiPure Plasmid DNA Miniprep Kit from Invitrogen) containing RNase A was added to the pellet and re-suspended until the cells were homogeneous. Cell suspension was transferred to a centrifuge tube. 0.4 mL Lysis Buffer (contained in the PureLink™HiPure Plasmid DNA Miniprep Kit from Invitrogen) was added and mixed gently by inverting the capped tube five times and incubated at room temperature for 5 minutes. A 0.4 mL Precipitation Buffer (contained in the PureLink™HiPure Plasmid DNA Miniprep Kit from Invitrogen) was then added and mixed immediately by inverting the capped tube until the mixture was homogeneous. The mixture was centrifuged at 15,000 × g at room temperature for 10 minutes. The clear lysate (1.2 mL) was pipetted into a sterile tube and centrifuge at 15,000 × g for 5 minutes at room temperature to remove any remaining cellular debris. The supernatant was loaded onto the equilibrated PureLink™HiPure Mini column and allowed the solution to drain by gravity flow. The column was washed twice with 2.5 mL Wash Buffer (contained in the PureLink™HiPure Plasmid DNA Miniprep Kit from Invitrogen). The solution in the column was allowed to drain by gravity flow after each wash and the flow-through discarded. A sterile centrifuge tube (elution tube) was placed under the column and 0.9 mL Elution Buffer (contained in the PureLink™HiPure Plasmid DNA Miniprep Kit from Invitrogen) was added to the column to elute bacmid DNA. The solution was allowed to drain by gravity flow. Isopropanol (0.63 mL) was added to the elution tube and mixed then placed on ice for 10 minutes. The mixture was centrifuged at 15,000 × g at 4°C for 20 minutes. The supernatant was carefully removed and discarded. The DNA pellet was re-suspended in 1 mL 70% ethanol and centrifuged at 15,000 × g at 4°C for 5 minutes. The supernatant was carefully removed and discarded. The pellet was air-dried for 10 minutes. The DNA pellet was then re-suspended in 40 µL TE Buffer (contained in the

PureLink™HiPure Plasmid DNA Miniprep Kit from Invitrogen) and allowed to dissolve for at least 10 minutes on ice. To avoid shearing the DNA, solution was pipetted only 1–2 times to re-suspend. Bacmid DNA was subsequently stored at 4°C.

2.2.1.5. Analyzing recombinant bacmid DNA by polymerase chain reaction (PCR)

PCR was used to analyse recombinant bacmid DNA to verify successful transposition to the bacmid. The primers used are shown in Table 2.1.

pUC/M13 forward primer	5′-CCCAGTCACGACGTTGTAAAACG-3′
pUC/M13 reverse primer	5′-AGCGGATAACAATTTCACACAGG-3′

Table 2.1. Primers for the PCR of recombinant bacmid DNA

A 50 µL PCR reaction in a 0.5 mL micro-centrifuge tube was set up as shown in table 2.2.

Reagent/Sample	**Amount added**
Recombinant bacmid DNA	1 µL (100 ng/µL)
10x PCR Buffer contained in Platinum Taq Polymerase kit	5 µL
10 mM dNTP Mix	1 µL
50 mM $MgCl_2$	1.5 µL
10 µM forward primer (re-suspended in water)	2.5 µL
10 µM reverse primer (re-suspended in water)	2.5 µL
Platinum® Taq polymerase	0.5 µL (5 units/µL)
Sterile dH_2O	38.5 µL

Table 2.2. PCR reaction set up for the recombinant bacmid DNA

The recombinant bacmid DNA was amplified using the parameters shown in Table 2.3.

Step	Time	Temperature	Cycles
Initial Denaturation	3 minutes	94°C	1x
Denaturation	45 seconds	94°C	30x
Annealing	45 seconds	55°C	
Extension	5 minutes	72°C	
Final extension	7 minutes	72°C	1x

Table 2.3. Polymerase Chain Reaction (PCR) Settings for the recombinant bacmid DNA.

About 5–10 µL was removed from the reaction and the DNA fragment size was assessed by agarose gel electrophoresis.

2.2.1.6. Recombinant baculovirus production

Sf21 insect cells were used for baculovirus production by (transfection with Bacmid DNA). The Sf21 cells were grown in Graces insect cell medium (Invitrogen) supplemented with FBS (foetal bovine serum) and containing penicillin (final concentration 100 µg/ml) and streptomycin (final concentration 100 µg/ml). The Sf21 cells used were confirmed to be in the log phase (1.5–2.5 × 10^6 cells/mL) with greater than 95% viability by measuring the optical density. A 2 mL of unsupplemented Grace's Insect Medium (without antibiotics and serum) was added in each well. Seeds of 8 × 10^5 Sf9 cells per well. Cells were allowed to attach for 15 minutes at room temperature in the laminar flow hood.

Cellfectin® II Reagent was used in the next step (Cellfectin® II Reagent is a proprietary cationic lipid formulation that offers the highest transfection efficiencies and protein expression levels on the widest variety of adherent and suspension insect cell lines, including Sf9 and Sf21 cells). The Cellfectin® II reagent was mixed before use, 8 µL was

diluted in 100 µL unsupplemented Grace's Medium (without antibiotics and serum), vortexed briefly to mix and the mixture kept at room temperature for up to 30 minutes. 1 µg of baculovirus DNA was diluted in 100 µL unsupplemented Grace's Medium (without antibiotics and serum) and mixed gently. The diluted DNA was combined with diluted Cellfectin® II (total volume ~210 µL), mixed gently and incubated for 30 minutes at room temperature. ~210 µL DNA-lipid mixture or transfection mixture was added drop-wise onto the cells and incubated at 27°C for 5 hours. The transfection mixture was removed and replaced with 2 mL of complete growth medium (Grace's Insect Medium). Cells were incubated at 27°C for 72 hours.

2.2.1.7. Isolating P1 viral stock

After 72 hours, the medium containing virus from each well (~2 mL) was collected and transferred to sterile 15 mL snap-cap tubes. The tubes were centrifuged at 500 × g for 5 minutes to remove cells and large debris. Clarified supernatant was transferred to fresh 15-mL snap-cap tubes. This was the P1 viral stock and was stored at 4°C and protected from light.

2.2.1.8. Amplifying baculoviral stock

Sf9 cell suspension was prepared, plated at 2 × 10^6 cells/well and incubated at room temperature for 1 hour to allow attachment. After 1 hour, cells were inspected under an inverted microscope to verify attachment. An appropriate amount of P1 viral stock was added to each well and incubated for 48 hours in a 27°C humidified incubator. After 48 hours post-infection, 2 mL of medium containing virus was collected from each well and transferred to sterile 15 mL snap-cap tubes. Tubes were centrifuged at 500 × g for 5 minutes to remove cells and large debris and to obtain clarified baculoviral stock. The supernatant was transferred to fresh 15 mL snap-cap tubes. This was the P2 viral stock and was stored at 4°C and protected from light.

2.2.1.9. Preparing a viral plaque assay

A 4% (v/v) Agarose Gel (Thermo Fisher) was melted by placing the bottle in a 70°C water bath for 30 mins. While the 4% agarose gel was melting, an empty sterile 100 mL bottle and sf-900 Medium (1.3x) were placed in the 40°C water bath. Working quickly in a sterile hood, the plaquing medium was prepared. 30 mL of 1.3x Sf-900™ II SFM medium (Invitrogen) and 10 mL of the melted 4% Agarose Gel were combined in the empty 100 mL bottle and mixed gently. The bottle of plaquing medium (Invitrogen) was returned to the 40°C water bath until use.

2.2.1.10. Plaque assay procedure

Sf9 cells were harvested and a 30 mL cell suspension prepared at 5×10^5 cells/mL in Sf-900™ II SFM medium (Invitrogen). The cell suspension (2 mL) was transferred into each well of two 6-well plates. Cells were allowed to settle to the bottom of the plate and incubated, covered at room temperature for 1 hour. After 1 hour incubation, the cell monolayers were observed using an inverted microscope. Sf9 cells were found to attach at 50% confluence.

An 8-log serial dilution (10^{-1} to 10^{-8}) of the clarified baculoviral stock in Sf-900™ II SFM medium was prepared by sequential dilution of 0.5 mL of the baculoviral stock into 4.5 mL of the medium in a 12 mL disposable tubes. The 6-well plates containing Sf9 cells and the tubes of diluted virus were moved to the sterile hood and labelled the plates, in columns of 2 (1 sample well plus 1 duplicate) as follows: no virus (negative control), 10^{-4}, 10^{-5}, 10^{-6}, 10^{-7}, 10^{-8}. The medium was removed from each well, discarded, and immediately replaced with 1 mL of the appropriate virus dilution. For a negative control, appropriate medium was added without virus. Cells with virus were incubated for 1 hour at room temperature. After 1 hour incubation, the cells and the bottle of plaquing medium from the 40°C water bath were moved to a sterile hood.

Sequentially, starting from the highest dilution (10^{-8}) to the lowest dilution (10^{-4}), the medium containing virus from the wells was removed and replaced with 2 mL of plaquing medium. Working quickly to avoid dessication of the cell monolayer. Agarose overlay was allowed to harden for 1 hour at room temperature before moving the plates. The cells were incubated in a 27°C humidified incubator for 10 days until plaques were visible and ready to count. A Neutral Red solution (1 mg/mL) (Sigma Aldrich) was prepared in cell-culture grade, distilled water, 0.5 mL of Neutral Red solution was added to each well containing plaquing overlay and incubated for 2 hours at room temperature. Gently excess stain was removed with pipet, plaques appeared as clear spots in a nearly clear gel against a red background. The number of plaques present in each dilution were counted, then the following formula was used to calculate the titre (plaque forming units (pfu)/mL) of the viral stock. The optimal range counted was 3 to 20 plaques per well of a 6-well plate.

Titre (pfu/mL) = number of plaques x dilution factor x 1/mL of inoculum/well.

The expected ranges for P1 and P2 viral stocks were:

1×10^6 to 1×10^7 pfu/mL for P1 viral stocks

1×10^7 to 1×10^8 pfu/mL for P2 viral stocks

2.2.1.11. Cloning of hExo1 into pTXB1 vector

The coding region of hExo1 (codons 1-846) was amplified by PCR using a full-length clone for the human Exo1 splice variant (*hExo1* cDNA) in a pFastBacI plasmid (pFastbacI-hExo1) as template. The forward primer used contained *NdeI* recognition sequence overlap (underlined) and reverse primer contained *SapI* recognition sequence overlap (underlined) as shown in Table 2.4.

Forward primer	5′-GGGAATTCCATATGGGGATACAGGGATTGCTA-3′
Reverse primer	5′-AAGGCCGCTCTTCCGCACATCTGGAATATTGCTCTTTGAACACGG-3′

Table 2.4. Primers for hExo1 PCR

2.2.1.12. PCR

A 50 µL PCR reaction was set up in a 0.5 mL micro-centrifuge tube as described in Table 2.5.

Reagent/Sample	**Amount added**
Plasmid DNA (pFastbacI-hExo1)	2 µL (30 ng/µL)
10 µM forward primer (re-suspended in water)	2.5 µL
10 µM reverse primer (re-suspended in water)	2.5 µL
2x Phusion High-Fidelity PCR master mix	25 µL
Sterile dH_2O	18 µL

Table 2.5. Polymerase Chain Reaction set up for hExo1.

DNA was amplified using the parameters shown in Table 2.6.

Step	Time	Temperature	Cycles
Initial Denaturation	3 minutes	94°C	1x
Denaturation	45 seconds	94°C	30x
Annealing	45 seconds	55°C	
Extension	3 minutes	72°C	
Final extension	7 minutes	72°C	1x

Table 2.6. Polymerase Chain reaction settings for hExo1

A 10 µL of the finished reaction was removed and analysed by 1% agarose gel electrophoresis to check the fragment size. PCR product was then purified away from the PCR components using the PureLink™ PCR clean-up/Quick Gel Extraction System (Invitrogen). The PCR product was digested using *NdeI* and *SapI* and then inserted between the *NdeI* and *SapI* sites of the pTXB1 plasmid (New England Biolabs) to construct a gene fusion between hExo1 and a self-cleaving affinity tag that is composed of an Mxe intein fragment and the chitin-binding domain (El-Shemerly, *et al* 2005).

2.2.1.13. Restriction digest

A 20 µL restriction digest was set up as shown in Table 2.7.

Reagent/Sample	Amount added
10x Buffer	5 µL
Vector or PCR fragment	5 µL (100 ng)
NdeI	1 µL (20 units)
SapI	1 µL (20 units)
dH_2O	8 µL

Table 2.7. Set up for the restriction digest of hExo1 PCR product

The reaction was incubated for 1 hour at 37°C. Then cleaned-up with PureLink™ PCR clean-up/Quick Gel Extraction System (Invitrogen). The vector was treated with Shrimp Alkaline Phosphatase (SAP) to remove the terminal phosphate so as to prevent vector re-ligation. The reaction was set up as shown in Table 2.8.

Reagent/Sample	**Amount added**
10x Buffer	5 µL
Shrimp Alkaline Phosphatase	2 µL
Vector DNA	43 µL (~90 ng)

Table 2.8. Set up for the Shrimp Alkaline Phosphatase treatment of the restriction digested pTBX1 vector.

The reaction was incubated at 37°C for 30 mins. Then the DNA was purified away from the reaction components using the PureLink™ PCR clean-up/Quick Gel Extraction System (Invitrogen).

2.2.1.14. Ligation of the hExo1 PCR product into pTXB1 vector

The pure digested product was then ligated into the *NdeI/SapI* phosphatase-treated pTXB1 vector to construct a translational fusion between hExo1 and a self-cleaving affinity tag that is composed of an Mxe intein fragment and the chitin-binding domain. The ligation reactions were set up in ratios of 1:1 and 1:10 vector/insert DNA end concentrations and a negative control as shown in Table 2.9.

Reagent Or Sample	**Amount added (negative control)**	**Amount added (1:1)**	**Amount added (1:10)**
Vector	4 µL (5 ng/µL) (4.5 nM)	4 µL (5 ng/µL) (4.5 nM)	4 µL (5 ng/µL) (4.5 nM)
Insert	0 µL	4 µL (7.5 ng/µL) (4.5 nM)	10 µL (30 ng/µL) (45 nM)
10x T4 ligase buffer	1 µL	1 µL	1 µL
T4 ligase	1 µL	1 µL	1 µL
dH_2O	4 µL	0 µL	0 µL

Table 2.9. Set up for the ligation of hExo1 PCR product into pTXB1 vector.

The reactions were left at room temperature overnight.

2.2.1.15. Transformation of bacteria with ligated vector

An aliquot of 5 µL ligation reaction was added into competent *E. coli* DH5α cells and placed on ice for 30 minutes. Cells were heat-shocked on a heating block at 42°C for 30 seconds and placed immediately onto ice. A pre-warmed SOC media (250 µL) was added into each tube and incubated at 37°C for 60 minutes so that the cells can recover. The culture was plate out on LB agar + 150 µg/ml ampicillin + 25 µg/ml chloramphenicol and incubated at 37°C overnight.

2.2.1.16. Colony PCR screen for the ligated inserts

About 10 colonies were selected which were circled and numbered on the plate to take note of their identity. Each of the selected colonies was touched with a sterile pipette tip and agitated in 0.5 ml tube containing 20 µL dH_2O and heated at 100°C on a heating block for 5 minutes. Tubes were pulse-centrifuged. An aliquot of 3 µL supernatant was transferred to PCR tube and set up the PCR reaction. (The PCR set up and conditions the same as described in table 2.6). PCR product was analysed on 1% agarose gel to identify for the correct fragment. Once the correct fragment was identified the colony that contained such a fragment was selected for miniprep.

2.2.1.17. Miniprep of the pTXB1-hExo1 plasmid

GeneJET Plasmid Miniprep Kit (Thermo Scientific) was used. Using flame sterile technique the selected colony was agitated into 10 ml of LB + 150 µg/ml ampicillin + 25 µg/ml chloramphenicol and incubated at 37°C overnight with shaking at 200 rpm. 2 ml of bacterial overnight culture was pelleted by centrifugation at 10,000 rpm for 2 minutes. Pelleted bacterial cells were resuspended in 250 µL of the resuspension solution (contained in the GeneJET Plasmid Miniprep Kit from Thermo Scientific) and re-suspended completely by vortexing until no cell

clumps remained. Cell suspension was transferred to a 2 mL micro centrifuge tube.

A 250 µL of the lysis solution (contained in the GeneJET Plasmid Miniprep Kit from Thermo Scientific) was added and mixed thoroughly by inverting the tube 4-6 times until the solution became viscous and slightly clear. A 350 µL neutralization solution (contained in the GeneJET Plasmid Miniprep Kit from Thermo Scientific) was added and mixed immediately and thoroughly by inverting the tube 4-6 times. To pellet cell debris and chromosomal DNA, the solution was centrifuged at 13,000 rpm for 5 minutes. The supernatant was transferred to the supplied GeneJET spin column by decanting and centrifuged at 13,000 rpm for 1 min, flow-through was discarded the column placed back into the same collection tube. The wash solution (500 µL) was added to the GeneJET spin column and centrifuged at 13,000 rpm for 1 minute and the flow-through was discarded, the column was placed back into the same collection tube and repeated the wash procedure using 500 µL of the wash solution. The flow-through was discarded and column was centrifuged for an additional 1 min to remove residual wash solution. GeneJET spin column was transferred into a fresh 1.5 mL micro centrifuge tube. An elution buffer (50 µL) was added to the centre of GeneJET spin column membrane to elute the plasmid DNA and incubated for 2 min at room temperature followed by centrifugation at 13,000 rpm for 2 min. Eluted sample which contained the purified recombinant plasmid DNA (pTXB1-hExo1) was stored at -20^{o}C. The construct was then verified by sequencing (Eurofins Genomics).

2.2.1.18. Cloning N-terminal domain of hExo1 (Nt-hExo1) into pET28a vector

The coding region of N-terminal hExo1 (codons 1-391) was amplified by PCR using full length clone for the human Exo1 splice variant in a pFastBacI plasmid (pFastbacI-hExo1) as template and the primers used are shown in Table 2.10.

Forward primer	5'-GGGAATTCCATATGGGGATACAGGGATTGCTA-3'
Reverse primer	5'-AAGGCCGCGGCCGCCTTCAATTGTGGGGCATCTGA-3'

Table 2.10. Primers for the PCR of Nt-hExo1

The forward primer contained *NdeI* recognition sequence overlap (underlined) and reverse contained *NotI* recognition sequence overlap (underlined).

PCR (as described in Table 2.6), and restriction digests were carried out as described earlier but with *NdeI* and *NotI* restriction enzymes in this case, the pure digested product was ligated into the *NdeI/NotI* phosphatase treated pET28a (+) vector to produce pET28a-Nt-hExo1, transformation of bacteria with the ligated vector, colony PCR screens for ligated inserts and minipreps were all carried out as described earlier for the cloning of hExo1 into pTXB1 vector. The construct was first analysed on 0.8% agarose gel and then sent for sequencing (Eurofins Genomics).

2.2.1.19. Cloning of PCNA, 14-3-3ζ and 14-3-3ε into pET28a (+) vector

The coding region for each of PCNA, 14-3-3ζ and 14-3-3ε was amplified by PCR. For PCNA protein, human *PCNA* cDNA was used as a template and for the 14-3-3 isoforms, a yeast two-hybrid vector harbouring either of the 14-3-3 isoforms coding region (pHAF633 pJG 14-3-3ζ and pRRS305 pJG 14-3-3ε) as templates. Primers were designed with an *NdeI* recognition sequence overlap in forward primers

and *NotI* recognition sequence overlap in reverse primers as shown in Table 2.11.

PCNA primers	Forward	5'-GGGAATTCCATATGTTCGAGGCGCGCCTG-3'
	Reverse	5'-AAGGCCGCGGCCGCCTAAGATCCTTCTTCA-3'
14-3-3 zeta (ζ) primers	Forward	5'-GGGAATTCCATATGGATAAAAACGAGCTGG-3'
	Reverse	5'-AAGGCCGCGGCCGCTTAATTTTCCCCTCCTTCTCC-3'
14-3-3 epsilon (ε) primers	Forward	5'-GGGAATTCCATATGGATGATCGGGAGGAT C-3'
	Reverse	5'-AAGGCCGCGGCCGCTCATCTTCCACATCCTGCAGC-3'

Table 2.11. Primers for the PCR of PCNA, 14-3-3ζ and 14-3-3ε.

PCR (as described in Table 2.6), and restriction digests were carried out as described earlier (Table 2.7) but with *NdeI* and *NotI* restriction enzymes in this case. Each of the pure digested PCR products was ligated (as described in Table 2.9) into the *NdeI/NotI* phosphatase treated pET28a to produce pET28a-PCNA, pET28a-14-3-3ζ and pET28a-14-3-3ε. Transformation of bacteria with the ligated vector, colony PCR screens for the ligated inserts and miniprep were all carried out as described earlier for cloning hExo1 into pTXB1 vector. The constructs were first analysed on 0.8% agarose gel and then sent for sequencing (Eurofins Genomics).

2.2.2. RECOMBINANT PROTEIN EXPRESSION

2.2.2.1. Expression of hExo1 protein from insect cells

A 500 mL High Five™, insect cells were cultured in serum-free HyQ-SFX medium (HyClone, Inc.) supplemented with glutamine (final concentration 20 mM) and 50 µg/ml gentamicin. The culture was incubated in a humidified incubator at 27°C. At a density of 1–1.5×10^6 cells/ml the culture was infected with baculovirus expressing hExo1 at a MOI of approximately 10 and incubation was continued for 72 hours. The cells were harvested by centrifugation after 72 hours post-infection. After harvesting, cells were rinsed once with serum-free medium and re-suspended in 50 ml lysis buffer (20 mM HEPES pH 7.5, 190 mM KCL, 10% v/v glycerol, 0.1mM EDTA) and stored at -80°C.

This work was carried out at Harwell Research Complex with an assistance given by Mr. Jay Zhang and Dr Stephen Carr.

2.2.2.2. Expression of hExo1 protein from bacteria

The pTXB1 derived *hExo1* construct was transformed into *E. coli* strain BL21-CodonPlus (DE3)-RIL (Agilent technologies) for protein expression. An aliquot of 2 µL plasmid DNA (50 ng/µL) was added into competent BL21-CodonPlus (DE3)-RIL *E.coli* cells and placed on ice for 30 minutes. The cells were heat-shocked on a heating block at 42°C for 30 seconds and placed immediately onto ice. A 250 µL of pre-warmed SOC media (Invitrogen) was added into each tube and incubated at 37°C for 60 minutes so that the cells can recover. The culture was plate out on LB agar + 150 µg/ml ampicillin + 25 µg/ml chloramphenicol and incubated at 37°C overnight.

From a single colony on LB agar plate a 100 mL LB + 150 µg/ml ampicillin + 25 µg/ml chloramphenicol starter culture was inoculated using flame sterile technique. The culture was incubated overnight at 37°C (rotation 250 rpm). A 100 mL starter culture was transferred to a 1 L LB + 150 µg/ml ampicillin + 25 µg/ml chloramphenicol and grown

to an OD_{600} = 0.3 at 37°C (rotation 250 rpm) and protein expression was induced by addition of IPTG (0.2 mM final) incubator temperature was switched to 18ºC and culture was allowed to grow overnight (rotation 250 rpm). The following day, cells were harvested by centrifugation at 5000 rpm for 10 minutes at 4°C in Beckman Coulter centrifuge using JA-10 rotor. Cell pellets were re-suspended in 50 ml pre-chilled (4°C) CH buffer (20 mM Tris pH 8.0, 500 mM NaCl, 0.1% v/v Triton X100, 1 mM EDTA, 10% v/v glycerol) supplemented with 0.1 mM PMSF and Roche complete inhibitor cocktail.

2.2.2.3. Expression of Nt-hExo1 protein

The pET28a derived *Nt-hExo1* construct was transformed into *E. coli* strain BL21-CodonPlus (DE3)-RIL (Agilent technologies) for protein expression. As described earlier for hExo1.

2.2.2.4. Expression of PCNA, 14-3-3ζ and 14-3-3ε proteins

The *E. coli* (BL21 DE3) was transformed with either of the constructs (pET28a-PCNA, pET28a-14-3-3ζ or pET28a-14-3-3ε). An aliquot of 5 µL of plasmid DNA was added into competent BL21 (DE3) *E.coli* cells and placed on ice for 30 minutes. Cells were heat-shocked on a heating block at 42°C for 30 seconds and placed immediately onto ice. A 250 µL aliquot of pre-warmed SOC media was added into each tube and incubated at 37°C for 60 minutes so that the cells can recover. The culture was plated out on LB agar + 50 µg/ml kanamycin and incubated at 37°C overnight. From a single colony on LB agar plates a 100 mL LB + 50 µg/ml kanamycin starter culture was inoculated using flame sterile technique, culture was incubated overnight at 37°C (rotation 250 rpm). A 100 mL starter culture was transferred to a 1 L LB + 50 µg/ml kanamycin and grown to an OD_{600} = 0.6 at 37°C (rotation 250 rpm) and protein expression was induced by addition of IPTG (0.2 mM final) and culture was allowed to grow overnight (rotation 250 rpm) at 37°C. The following day, cells were harvested by centrifugation at 5000 rpm for 10

minutes at 4°C in JA-10 rotor. Cell pellets were re-suspended in 50 ml pre-chilled (4°C) lysis buffer (20 mM Tris pH 7.4, 500 mM NaCl, 50 mM imidazole, 10% v/v glycerol) supplemented with 0.1 mM PMSF and Roche complete inhibitor cocktail.

2.2.3. PROTEIN PURIFICATION

2.2.3.1. Purification of hExo1 protein expressed from insect cells

Insect cells were lysed using Insect Cell Protein Extraction Reagent (I-PER) (Thermo Scientific) according to the manufacturer's protocol. Cells were pelleted by centrifugation at 5000 g for 10 minutes, 4mL of I-PER Reagent per gram of cell pellet was added to the cell pellet and the suspension was pipetted up and down until it was homogeneous. The suspension was incubated for 15 minutes at room temperature. The lysate was centrifuged at 15,000 × g for 30 minutes in JA-20 rotor to separate soluble proteins from the insoluble proteins.

Using a peristaltic pump the cleared supernatant was loaded onto 5 ml HiTrap Heparin HP column (GE Healthcare Life Sciences) pre-equilibrated with binding buffer as described previously (Orans *et al*., 2011) (20 mM HEPES pH 7.5, 190 mM KCL, 10% v/v glycerol, 0.1 mM EDTA) at a rate of 5 mL per minute. The column was washed with 20 times column volume (100 mL) of binding buffer followed by elution with 50 mL elution buffer (20 mM HEPES pH 7.5, between 250 mM to 1 M KCl, 10% v/v glycerol, 0.1mM EDTA). Eluted sample containing hExo1 was spin concentrated using Spin-X UF concentrator (Corning) and loaded on to a 1 ml pre-equilibrated HiTrap SP FF cation-exchange column (GE Healthcare Life Sciences) which was equilibrated with 10 times column volume equilibration buffer (20 mM HEPES pH 7.5, 0.1 mM EDTA, 50 mM NaCl, 1 mM DTT, 10% v/v glycerol) with a peristaltic pump at the rate of 1 mL per minute. The column was washed with 20 times column volume equilibration buffer followed by elution with the 20 ml elution buffer (20 mM HEPES pH 7.5, 0.1 mM EDTA, between 200mM to 500mM KCl, 1 mM DTT, 10% v/v glycerol). Eluted samples containing hExo1 were pooled together and spin concentrated down to 1 mL with Spin-X UF concentrator (Corning) and passed through a Superose 12 10/300 (GE Health care life sciences) gel filtration column using an AKTA prime protein purification system, column was pre-equilibrated

with reaction buffer (20mM HEPES pH 7.5, 100mM KCl, 10% glycerol) and the column washed with the same buffer. After gel filtration, hExo1 containing fractions were pooled together and concentrated with spin-x UF concentrator (Corning) and snap-frozen in liquid nitrogen, then stored at -80^{o}C.

2.2.3.2. Purification of hExo1 protein expressed from *E. coli* BL21-CodonPlus-(DE3)-RIL

Protein purification was conducted as described previously but with some modifications (El-Shemerly, *et al*., 2005). The bacterial suspension was sonicated by a continuous sonication on ice, 1 min at maximum power followed by 1 min incubation on ice, this was repeated 5 times and PMSF was added after sonication. Sonicated bacterial suspension was centrifuged at 18000 rpm for 45 minutes at 4^{o}C in JA-20 rotor.

The cleared supernatant containing the fusion protein of interest was saved at 4^{o}C. A 10 mL of chitin-beads suspension (New England Biolabs) an affinity matrix for the isolation of target proteins fused to an intein-chitin binding domain fusion was poured in a frit-equipped plastic column (Bio-Rad) and allowed the storage solution to drain by gravity flow, the column was equilibrated by passing 100 ml of CH buffer (20 mM Tris pH 8.0, 500 mM NaCl, 0.1% v/v Triton X100, 1 mM EDTA, 10% v/v glycerol) + PMSF by gravity flow. 50 ml soluble fraction containing hExo1-Intein was loaded onto the column and allowed to flow slowly (~ 0.5 ml/min) by gravity flow, the column was washed with 200 mL CH buffer + PMSF.

The on column proteolytic cleavage of the Intein tag was then triggered. The column was closed and 5 mL of CH buffer + PMSF + 30 mM DTT was poured onto the column and the beads stirred gently with a sterile glass rod. This was allowed to incubate over night at 4^{o}C. The next day the column was opened and the first 5 mL fraction containing hExo1 was recovered by gravity flow using a tube placed on ice,

another 5 mL CH buffer + PMSF was poured in the column and recover a second 5 mL fraction, this step was repeated until 5 fractions were recovered. All the eluted fractions were pooled together and concentrated down using spin-x UF concentrator.

The concentrated sample containing hExo1 was diluted at 5 times sample volume with heparin column binding buffer (20mM HEPES pH 7.5, 190mM KCL, 10% v/v glycerol, 0.1mM EDTA). Using a peristaltic pump the sample was loaded onto 5 ml HiTrap Heparin HP column (GE Health care life sciences) pre-equilibrated with binding buffer (20 mM HEPES pH 7.5, 190 mM KCL, 10% v/v glycerol, 0.1 mM EDTA) at a rate of 5 mL per minute. Column was washed with 20 times column volume (100 mL) binding buffer followed by elution with 100 mL elution buffer (20 mM HEPES pH 7.5, 1 M KCl, 10% v/v glycerol, 0.1mM EDTA).

Eluted sample containing hExo1 was spin concentrated using Spin-X UF concentrator (Corning) and passed through a Superose 12 10/300 (GE Healthcare Life Sciences) gel filtration column using an AKTA prime protein purification system, column was pre-equilibrated with reaction buffer (20 mM HEPES pH 7.5, 100mM KCl, 10% v/v glycerol) and the column washed with the same buffer. After gel filtration, hExo1 containing fractions were pooled together and concentrated with Spin-X UF concentrator (Corning) and snap-frozen in liquid nitrogen, then stored at -80^{o}C.

2.2.3.3. Purification of His-tagged Nt-hExo1, PCNA, 14-3-3ζ and 14-3-3ε proteins

B-PER® Bacterial Protein Extraction Reagent (Thermo Scientific) was used for protein extraction. Bacterial cells were pelleted by centrifugation at 5000 rpm for 10 minutes. A 4 mL of B-PER reagent was added per gram of cell pellet. The suspension was pipetted up and down until it was homogeneous and incubated for 10-15 minutes at room temperature. The suspension was centrifuged at 13,000 rpm for 5 minutes to separate soluble proteins from the insoluble proteins.

Using a peristaltic pump (Pharmacia), soluble lysates were loaded onto a 5 mL HisTrap HP (GE Health care) affinity column which was pre-equilibrated with 10 column volume binding buffer (20 mM Tris pH 7.5, 500 mM NaCl, 50 mM imidazole) at a flow rate of 5 mL per minute. The column was washed with 50 column volume binding buffer. His-tagged recombinant proteins were eluted with 50 mL elution buffer (20 mM Tris pH 7.5, 500 mM NaCl, 500 mM imidazole). Eluted samples were spin concentrated and loaded on a PD10 desalting column (GE Health care) to remove imidazole by buffer exchange in to a reaction buffer (20 mM HEPES pH 7.5, 100 mM KCl, 10% v/v glycerol). Samples were then spin concentrated and stored at -80^{o}C.

2.2.4. MASS SPECTROMETRY

The identity of the purified recombinant proteins was verified by mass spectrometry as follows:

2.2.4.1. Gel Piece Processing and Tryptic Digestions

Samples were prepared and separated by SDS-PAGE and stained using coomassie colloidal blue. Samples were excised from gels using a sterile scalpel and the protein sample was processed in gel pieces using the Proteome Works Mass PREP robotic liquid handling station (Waters, Elstree, UK). The samples were incubated three times in 100 µl of de-stain solution (50 mM ammonium bicarbonate, 50% v/v acetonitrile) for 10 minutes at room temperature.

Following removal of the final aliquot, the sample was dehydrated by incubation at room temperature in 50 µl of acetonitrile for 5 minutes, acetonitrile was removed and the gel plugs incubated for 10 minutes to allow evaporation. The sample was further processed by incubation at room temperature in 50 µl of reducing solution (10 mM dithiothreitol, 100 mM ammonium bicarbonate) for 30 minutes and, following removal of the reducing solution, incubation at room temperature in 50 µl of alkylation solution (55 mM iodoacetamide, 100 mM ammonium bicarbonate) for 20 minutes. The gel pieces were then washed at room temperature in 50 µl of 100 mM ammonium bicarbonate for 10 minutes, 50 µl of acetonitrile for 5 minutes and dehydrated by double room temperature washes in 50 µl of acetonitrile for 5 minutes and evaporation for 5 minutes. The microtitre plate containing the gel plugs was cooled to 6°C for 10 minutes before addition of 25 µl per well of trypsin gold (Promega), diluted to 10 ng µl-1 in trypsin digestion buffer (25 mM ammonium bicarbonate). The plate was incubated at 6°C for a further 15 minutes to permit trypsin entry into the gel plugs with minimal autocatalysis before incubation at 40°C for 5 hours.

2.2.4.2. Mass Spectrometry

Samples were analysed by LC-ESI-tandem MS on a Q-TOF2 mass spectrometer fitted with a nanoflow ESI (electrospray ionization) source (Waters Ltd). Peptides were delivered on-line to the MS via a CapLC HPLC system, with peptide trapping on a C18 PepMap100 (5 µm, 100 Å) µ-Precolumn 300 µm i.d., 5 mm (Thermo). The mass spectrometer was operated with a capillary voltage of 3000 V in positive ion mode, using argon as the collision gas. Tandem MS data were acquired using automated data-dependent switching between MS and MS/MS scanning based upon ion intensity, mass and charge state (data directed analysis (DDATM)). In this automated acquisition type of experiment, a method was created in the MassLynx 4.0 software in which charge state recognition was used to select doubly, triply and quadruply charged precursor peptide ions for fragmentation. One precursor mass at a time was chosen for tandem MS acquisition. A collision energy was automatically selected based on charge and mass of each precursor and varied from 15 to 55 eV.

2.2.4.3. Data Processing and Database Searching

Protein Lynx Global Server version 2.0 (Waters, Ltd) was used to process the uninterpreted MS data into peak list (pkl) files which were searched against all entries in the NCBInr database (version 20140228) using the web version of the MASCOT MS/MS ions search tool (http://www.matrixscience.com/). Carbamidomethylation of cysteine and oxidation of methionine were set as variable modifications. One missed cleavage by trypsin was accepted. Other than file type (Micromass pkl) and instrument type (ESI-QUAD-TOF), all remaining search values were the preset defaults.

Recombinant proteins were confirmed from the data search results as human exonuclease1 (hExo1), human proliferating cell nuclear antigen (PCNA), human 14-3-3ζ and human 14-3-3ε. The mass spectrometry

was carried out by Dr. Susan Liddell, School of Biosciences, University of Nottingham, Sutton Bonington campus, UK.

2.2.5. *IN VITRO* DNA END RESECTION ASSAYS

Resection assays with linearized plasmid DNA substrate was performed as described by Nicolette *et al*, (2010) but with some modifications. The 4.8-kb plasmid pFastBac-HTA was linearized with *SphI,* which generated a 4 nucleotides long 3' overhang dsDNA. Reactions were performed in a volume of 20 µL that contained between 1-30 nM hExo1 protein, between 10-50 nM linearized plasmid DNA and reaction buffer (20 mM HEPES pH 7.0, 100 mM KCl, 5 mM $MgCl_2$, 1 mM ATP, 10% v/v glycerol). Reactions were incubated at 37°C for 1 hr unless indicated otherwise. All the reaction components were assembled in a 0.5 mL microfuge tube on ice and reactions were activated by transferring the tubes onto a heating block pre-set at 37^{o}C. Reactions were stopped by the addition of stop buffer (2% w/v SDS, 10 mM EDTA), supplemented with 1 µg proteinase K and incubated for 1 hour 37°C. Reaction products were separated on 1% agarose gels eluted with Tris-acetate-EDTA (40 mM Tris-acetate, 1 mM EDTA) buffer, gel was incubated in 1x staining solution (1x SYBR gold in TAE buffer) with gentle agitation at room temperature for 30 minutes. Stained gel was visualized with Gel Doc XR+ system (BioRad).

2.2.5.1. DNA resection assay at different salt concentrations

Resection assays were conducted as described above but with various salt concentrations in the reaction buffer (50, 100, 150, 200, 250, 300, 350, 400, 450 and 500 mM KCl).

2.2.5.2. DNA resection assay at Different pH conditions

Reaction conditions were the same as above except that these were carried out at various pH conditions of the reaction buffer (pH 5.0, 5.5, 6.0, 6.5, 7.0, 7.5, 8.0, 8.5 and 9.0).

2.2.5.3. DNA resection assay at different temperature conditions

The reaction conditions were the same as above except that these were conducted at different temperature conditions (on ice, 4^{o}C, room temperature, 25^{o}C, 30^{o}C and 37^{o}C).

2.2.5.4. DNA resection assay after pre-incubation of hexo1 at different temperatures

The reaction conditions are the same as above except that these were conducted after hExo1 was pre-incubated at different temperature conditions (ice, 4^{o}C, room temperature, 25^{o}C, 30^{o}C, 37^{o}C, 45^{o}C and 50^{o}C) prior to reaction set up.

2.2.5.5. DNA resection assay with blunt-end and 5’ overhang dsDNA substrates

The same reaction conditions that were used with the resection assay described earlier, but in this case different types of dsDNA substrates were used. Either a blunt end dsDNA substrate generated with *StuI* restriction enzyme or a 5’ overhang dsDNA substrate generated with *BamHI* restriction enzyme was used instead of the 3’ overhang dsDNA substrate.

2.2.5.6. DNA resection assay at different reaction incubation time

In this case reactions were incubated at 37^{o}C and reactions were terminated at different times (1 minute, 5, 10, 15, 30 and 60 minutes).

2.2.5.7. DNA resection assay in the presence or absence of ATP and Mg^{2+}

Reactions were set up in the presence or absence of ATP and Mg^{2+} and in the presence of GTP and Ca^{2+} as substitutes to ATP and Mg^{2+}.

2.2.5.8. DNA resection assay with Nt-hExo1 (N-terminal domain of hExo1)

Resection assays with plasmid DNA substrate was performed as described by Nicolette *et al*, (2010) but with some modifications. The 4.5-kb plasmid pFastBacHTA was linearized with *SphI* which generate 4 nucleotide 3' overhangs. Reactions were performed in a volume of 20 µL that contained between 20 nM Nt-hExo1 protein, 30 ng linearized plasmid DNA, reaction buffer (20 mM HEPES pH 7.0, 100 mM KCl, 5 mM MgCl2, 1 mM ATP, 10% v/v glycerol) and were incubated at 37°C for 1 hour. All the reaction components were assembled in a 0.5 mL microfuge tube on ice and reactions were activated by transferring the tubes onto a heating block pre-set at 37°C. Reactions were stopped by the addition of stop buffer (2% w/v SDS, 10 mM EDTA), supplemented with 1 µg proteinase K and incubated for 1 hour 37°C. Reaction products were analysed on 1 % native agarose gels run in 1x Tris-acetate-EDTA (TAE; 40 mM Tris-acetate, 1 mM EDTA) buffer, and visualized with SYBR gold (Invitrogen).

2.2.5.9. DNA resection assay with hExo1 and Nt-hExo1 in the presence of PCNA

The same reaction condition with resection assay described earlier but in the presence of 100 nM to 1 uM PCNA.

2.2.5.10. DNA resection assay with hExo1 and Nt-hExo1 in the presence of 14-3-3 proteins

The same reaction condition with resection assay described earlier but in the presence of 100 nM to 1 uM of either 14-3-3ζ or 14-3-3ε.

2.2.5.11. Molar ratio assays

Resection assays were set up as described earlier but at different molar ratios of hExo1 to either PCNA (trimer) and/or 14-3-3s (dimers) as follows: 1:1 to 1:10 hExo1/PCNA ratio, and 1:1 to 1:10 hExo1/14-3-3s ratio.

2.2.6. Sedimentation Velocity Analytical Ultracentrifugation (SV-AUC)

All proteins (hExo1, Nt-hExo1, PCNA, Zeta, Epsilon) were subjected to Sedimentation Velocity Analytical Ultracentrifugation (SV-AUC) experiment in 20 mM HEPES at pH 7.5, 100 mM KCl, 1 mM EDTA and 10% v/v glycerol at a concentration of 1 mg/mL using XL-I analytical ultracentrifuge (Beckman-Coulter, Brea, CA). Samples were centrifuged at 40,000 rpm at 4^{o}C over 12 hours with continuous scan from 5.8 to 7.2 cm at 0.003 cm intervals. Data was fitted using the program SedFit (Schuck, 2000) with a continuous distribution model to obtain the experimental molecular weight, Stokes radius and frictional ratios.

2.2.7. Small Angle X-ray Scattering (SAXS)

SAXS data was collected and analyzed at the Diamond Light Source (BL 21 beamline). Data was collected at a wavelength of 1.0 Å and sample-to-detector distance of 1.5 m. SAXS data was collected on 4 serial dilutions for purified hExo1 protein (1.25 mg/mL, 2.5 mg/mL, 5 mg/mL, 7.5 mg/mL) and 2 serial dilutions for Nt-hExo1 protein (1.25 mg/mL and 2.5 mg/mL) for Nt-hExo1 in a buffer (20 mM HEPES pH 7.5, 100 mM KCl, 10% v/v glycerol). Data was collected from 18 times of 3 seconds X-ray exposure at 20°C for proteins and relevant buffer. Scattering profiles were generated by subtracting buffer from sample exposures followed by merging of all the 18 X-ray exposures and averaged in ScÅtter software for SAXS analysis to generate SAXS data including the entire scattering spectrum.

2.2.8. Circular Dichroism (CD)

Circular Dichroism (CD) spectra in the far-UV region (185-260nm) were measured using a Chirascan Plus CD spectropolarimeter (Applied Photophysics Ltd, Leatherhead, UK) using a 0.05cm pathlength cell, 1nm bandwidth, 1 nm step size and 1 s integration time. Proteins were analysed at a concentration of 0.3 mg/mL in 5 mM potassium phosphate pH 7.2 buffer. The secondary structure estimation (SSE) from CD data was carried out applying the CONTINLL program with the sp43 data base set of 43 soluble proteins from CDApps suite of programs developed at Diamond B23 beamline.

2.2.9. Dynamic Light Scattering (DLS)

The sizing of the proteins, their binary, ternary and quaternary complexes was determined by dynamic light scattering (DLS) using a Zetasizer NANO ZSP (Malvern, UK) with 60 µl capacity cuvette. Proteins were analysed in 20 mM HEPES pH 7.2 containing 50 mM KCl, 1 mM EDTA and 5% (v/v) glycerol.

3.0 CHAPTER THREE: RESULTS FOR CLONING AND PROTEIN EXPRESSION STUDIES

The results for the cloning of hExo1 gene into insect cells and bacterial expression vectors together with the cloning studies for the binding partner proteins (PCNA, 14-3-3ζ and 14-3-3ε) are presented in this chapter. Also this chapter presents the results from the studies for expression and purification of hExo1 (Insect cells and bacterial expression systems) and binding partner proteins (Bacterial expression).

3.1.0 CLONING

3.1.1 Plasmid for hExo1 protein expression from insect cells

The plasmid pFastBac-hExo1 was propagated in competent *E. coli* DH5 and isolated by miniprep using a GeneJET Plasmid Miniprep Kit (Thermo Scientific) according to the manufacturer's protocol. Isolated plasmid was analysed on a 0.8% agarose gel. The pFastbac1+hExo1 construct has produced a larger plasmid ~5.2 kb compared to pFastbac1 plasmid alone ~3.1 kb (*Fig. 3.1*) showing that the insert has been ligated.

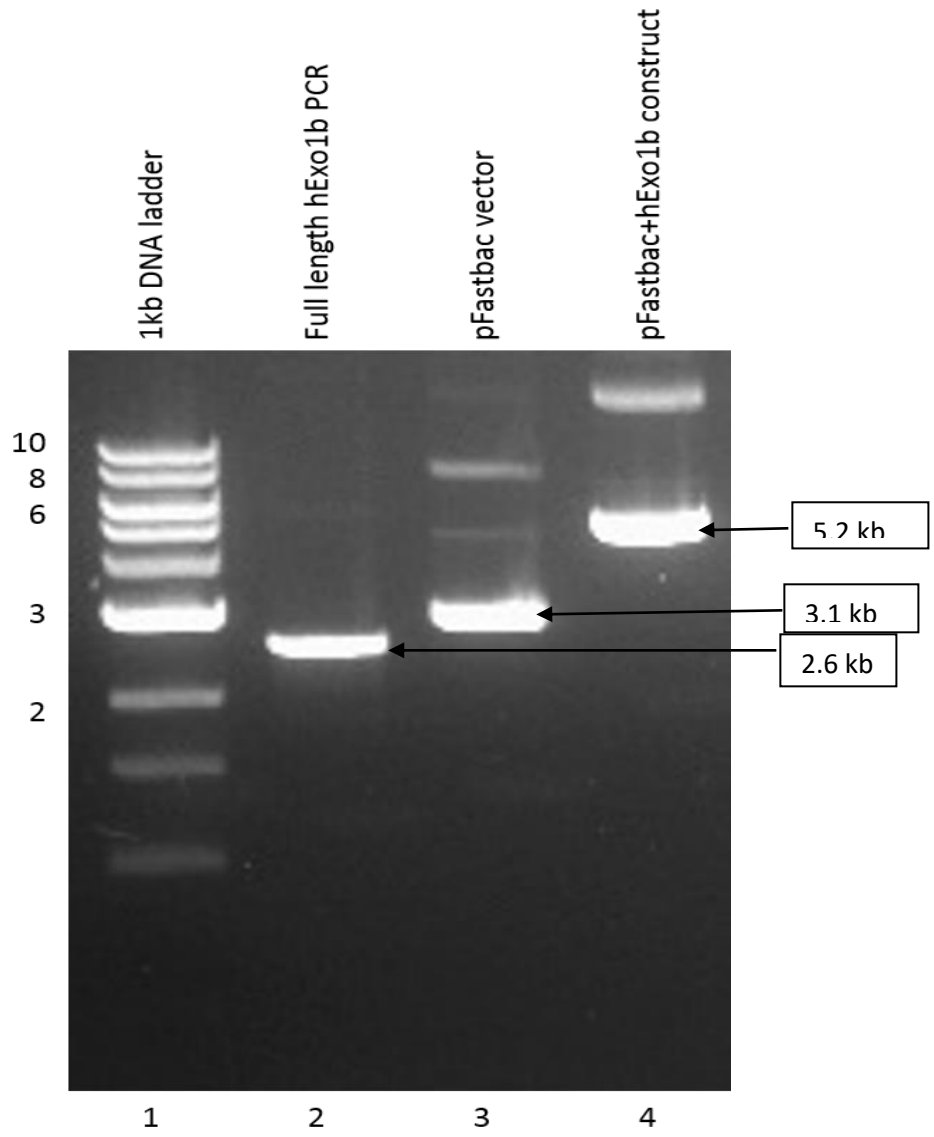


Figure 3.1. Agarose gel image for the analysis of isolated pFastBac-hExo1 plasmid. Lane 1 was a 1 kb DNA ladder, lane 2 is 100 ng of PCR product for hExo1, lane 3 is pFastBac plasmid (100 ng) and lane 4 is the pFastBac+hExo1 construct (100 ng).

3.1.2. Transformation of *E. coli* DH10Bac™

In order to generate a high molecular weight recombinant bacmid DNA for insect cell transformation, MAX Efficiency® DH10Bac™ competent cells (Invitrogen Life Technologies) were transformed according to the manufacturer's instructions. Black/white selection was use to select the colonies that were successfully transformed from an S-Gal agar (Sigma Aldrich) plate containing 50 µg/mL kanamycin, 7 µg/mL gentamicin, 10 µg/mL tetracycline, and 40 µg/mL IPTG (*Fig. 3.2a*). The white colony

phenotype was further verified by re-streaking on a fresh S-Gal agar plate containing 50 µg/mL kanamycin, 7 µg/mL gentamicin, 10 µg/mL tetracycline, and 40 µg/mL IPTG (*Fig. 3.2b*).

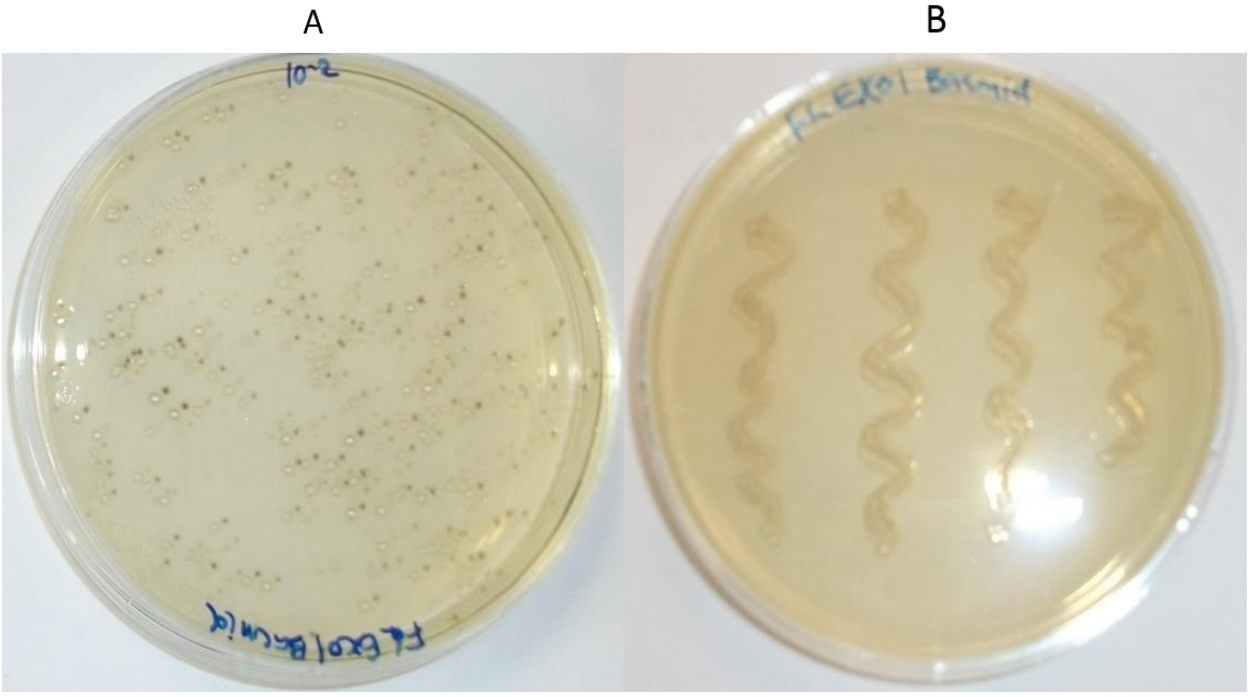


Figure 3.2. (A) S-Gal agar plate showing black/white colonies formed by the transformed DH10Bac™ competent *E. coli* cells (white colonies) and untransformed (black colonies). (B) Verified white phenotype colonies.

Recombinant bacmid DNA was isolated from the verified white colony phenotype using the PureLink™HiPure Plasmid DNA Miniprep Kit (Invitrogen) as instructed by the manufacturer. Recombinant bacmid DNA was greater than 135 kb in size. Since restriction analysis was difficult to perform with DNA of this size, PCR analysis was used to verify the presence of gene of interest in the recombinant bacmid. Forward and reverse pUC/M13 primers that hybridize to sites flanking the mini-*att*Tn7 site within the *lac*Zα-complementation region (*Fig. 3.3*) to facilitate PCR analysis were used.

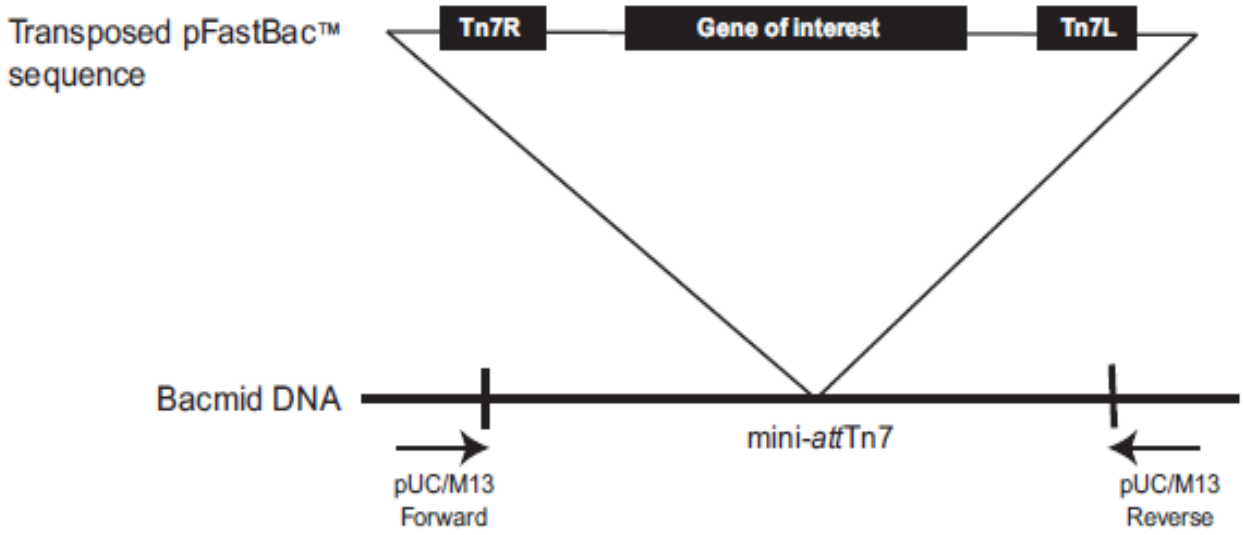


Figure 3.3. Depiction of how forward and reverse pUC/M13 primers hybridize

After the PCR was performed, the PCR product was then analysed on a 0.8% agarose gel and a correctly sized fragment of close to 5 kb was identified (Bacmid transposed with pFastBac™1 ~2300 bp + 2538 bp insert) (*Fig. 3.4*).

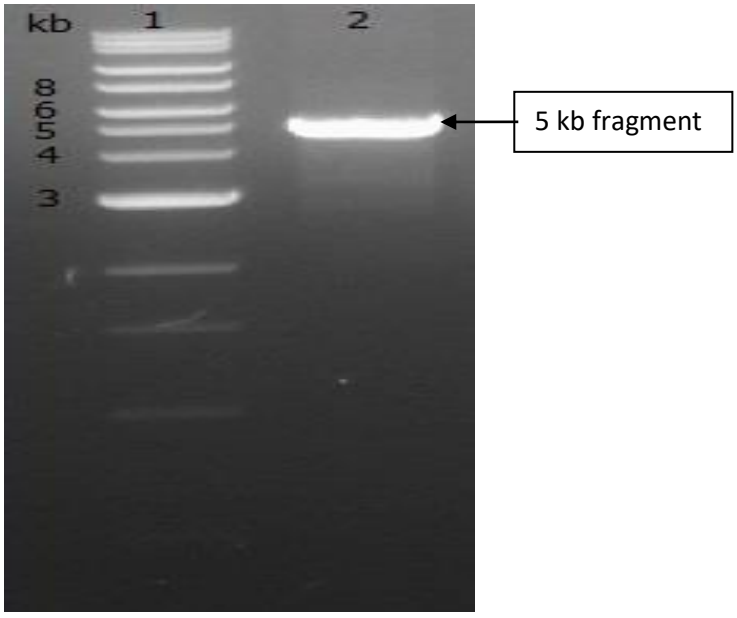


Figure 3.4 Agarose gel image showing the bacmid PCR product (100 ng) lane 2, lane 1 is 1kb plus DNA ladder.

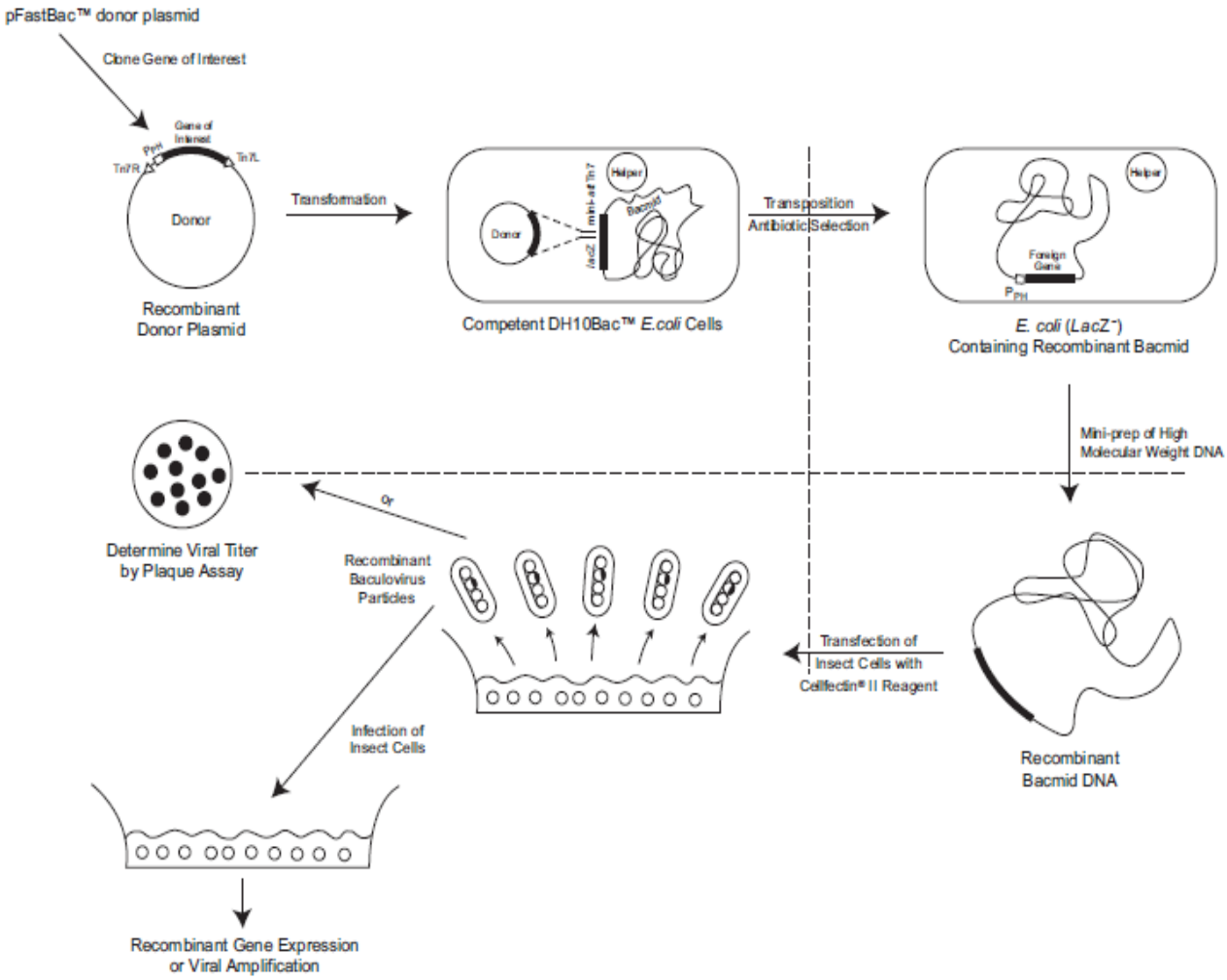


Figure 3.5. Depicts the generation of recombinant baculovirus and the expression of gene of interest using the Bac-to-Bac® Baculovirus Expression System. **(Figure adapted from Invitrogen user guide for Bac-to-Bac® Baculovirus Expression System)**

3.1.3. Plasmid for hExo1 protein expression in *E. coli* cells

The coding region of hExo1 (codons 1-846) was amplified by PCR using a full-length clone for the human Exo1 splice variant (*hExo1* cDNA) in a pFastBacI plasmid (pFastbacI-hExo1) as the template. The PCR product was inserted between the *NdeI* and *SapI* sites of the pTXB1 plasmid (NEB) to construct a translational fusion between hExo1 and a self-cleaving affinity tag that is composed of an Mxe intein fragment and the chitin-binding domain. The construct was first verified by agarose gel analysis and then sent for sequencing (Eurofins Genomics, Germany). The sequencing result matched NCBI sequence ID ref NC_000001.11 with 100% query cover, 0.0 E value and 100% identity, with features as exonuclease 1 isoform b. The pTXB1+hExo1 construct has produced a larger plasmid ~8.6 kb compared to pTXB1 vector alone ~6.3 kb showing that the insert has been ligated (*Fig. 3.6*).

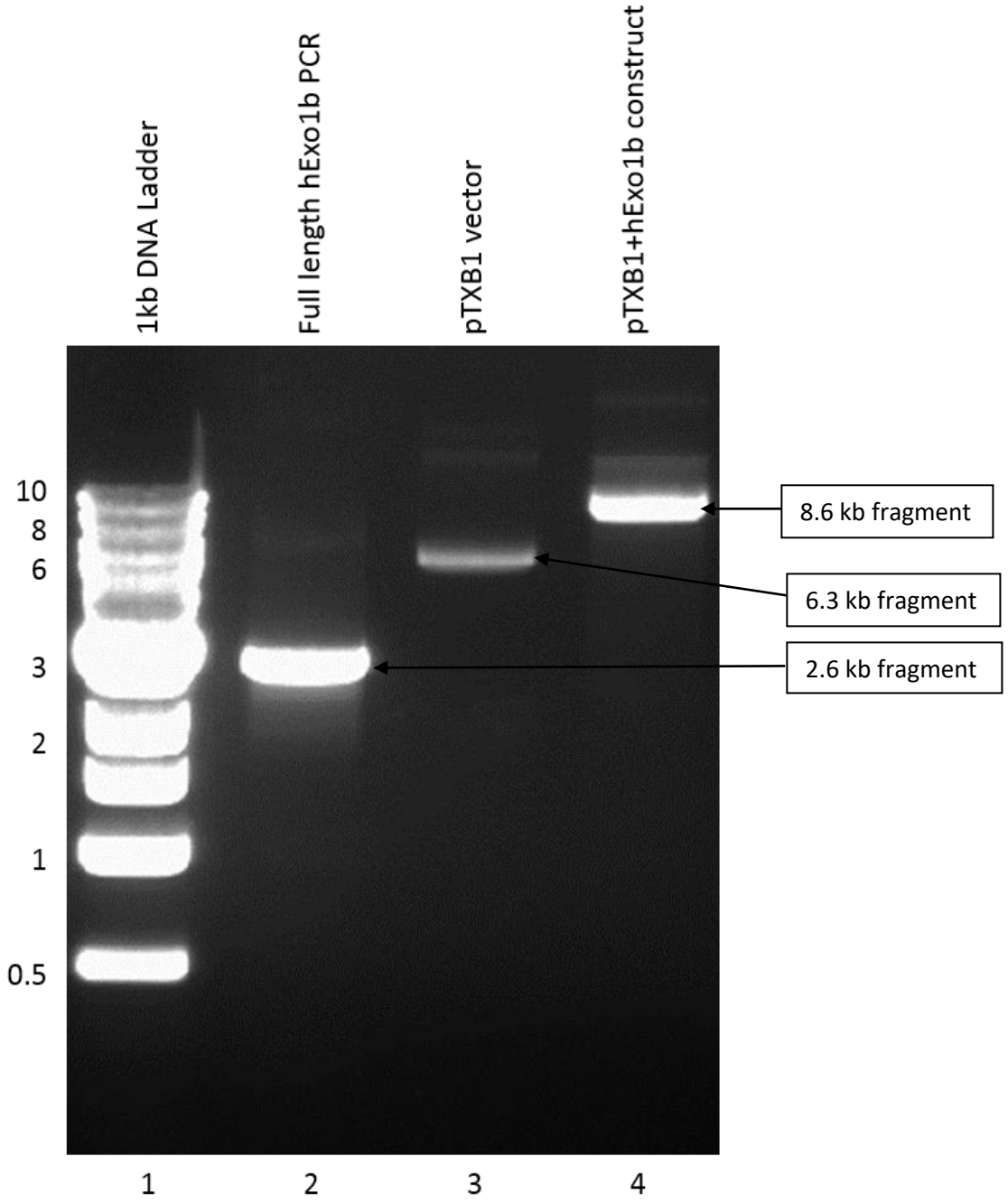


Figure 3.6. Agarose gel image for pTXB1+hExo1 construct. A 100 ng PCR product lane 2, 50 ng vector lane 3 and 100 ng pTXB1+hExo1 construct lane 4.

3.1.4. Cloning of Nt-hExo1 gene into pET28a (+) vector

The coding region of Nt-hExo1 (codons 1-391) was amplified by PCR using full length clone for the human Exo1 splice variant in a pFastBacI plasmid (pFastbacI-hExo1) as template. The PCR product was inserted between the *NdeI* and *NotI* sites of the pET28a plasmid (Novagen) to construct a His-tag translational fusion. The construct was first analysed on a 0.8% agarose gel and then sent for sequencing (Eurofins Genomics). The sequencing result matched NCBI sequence ID ref NC_000001.11 with 100% query cover, 0.0 E value and 100% identity, with features as exonuclease 1 isoform b. The pET28a-Nt-hExo1 construct has produced a larger plasmid ~5.8 kb compared to pET28a vector alone ~4 kb showing that the insert has been ligated (*Fig. 3.7*).

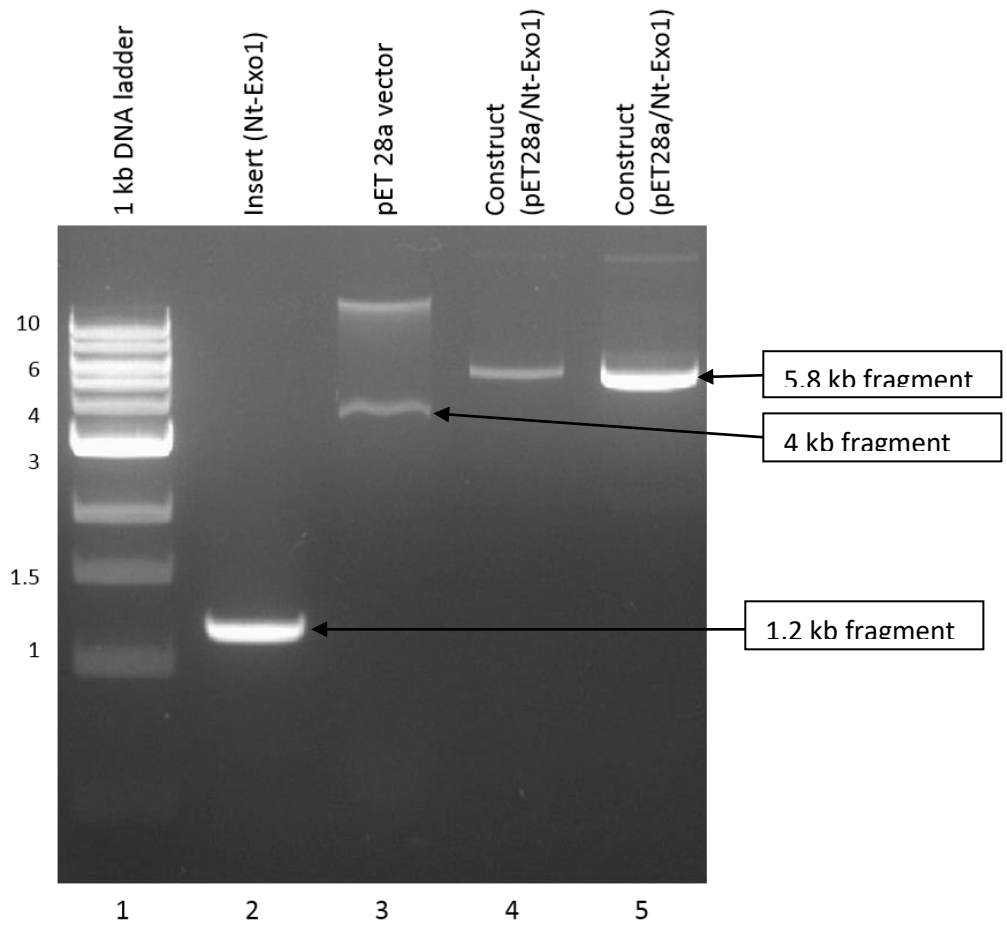


Figure 3.7. Agarose gel analysis for pET-28a+Nt-hExo1 construct. A 100 ng PCR product for Nt-hExo1 lane 2, 30 ng of pET-28a vector lane 3, 30 ng of pET28a+Nt-hExo1 construct lane 4 and 100 ng of pET28a+Nt-hExo1 construct lane 5.

3.1.5. Cloning of PCNA, 14-3-3ζ and 14-3-3ε genes into pET28a (+) vector

The coding region of PCNA, 14-3-3 zeta and 14-3-3 epsilon were PCR amplified individually. For human PCNA, human *PCNA* cDNA was used as a template and for human 14-3-3 isoforms a yeast two hybrid vector harbouring either of the 14-3-3 isoforms coding region (pHAF633 pJG 14-3-3ζ and pRRS305 pJG 14-3-3ε) were used as templates. Primers used contained an *NdeI* recognition sequence overlap in the forward primers and *NotI* recognition sequence overlap in the reverse primers.

The PCR products were inserted between the *NdeI* and *NotI* sites of the pET28a (+) plasmid (Novagen) to construct an N-terminal 6xHis tag translational fusion. The constructs were first analysed on 0.8% agarose gels (*Fig. 3.8*) and then sent for sequencing (Eurofins Genomics Germany). The sequencing result for the human PCNA construct matched NCBI sequence ID ref NC 018931.2 features: proliferating cell nuclear antigen (*Homo sapiens*). For the human 14-3-3ζ the sequencing result matched the NCBI sequence ID NC 018919.2 features: 14-3-3ζ (*Homo sapiens*) and for the 14-3-3ε construct, the sequencing result matched the NCBI sequence ID NC 018928.2 features: 14-3-3ε (*Homo sapiens*).

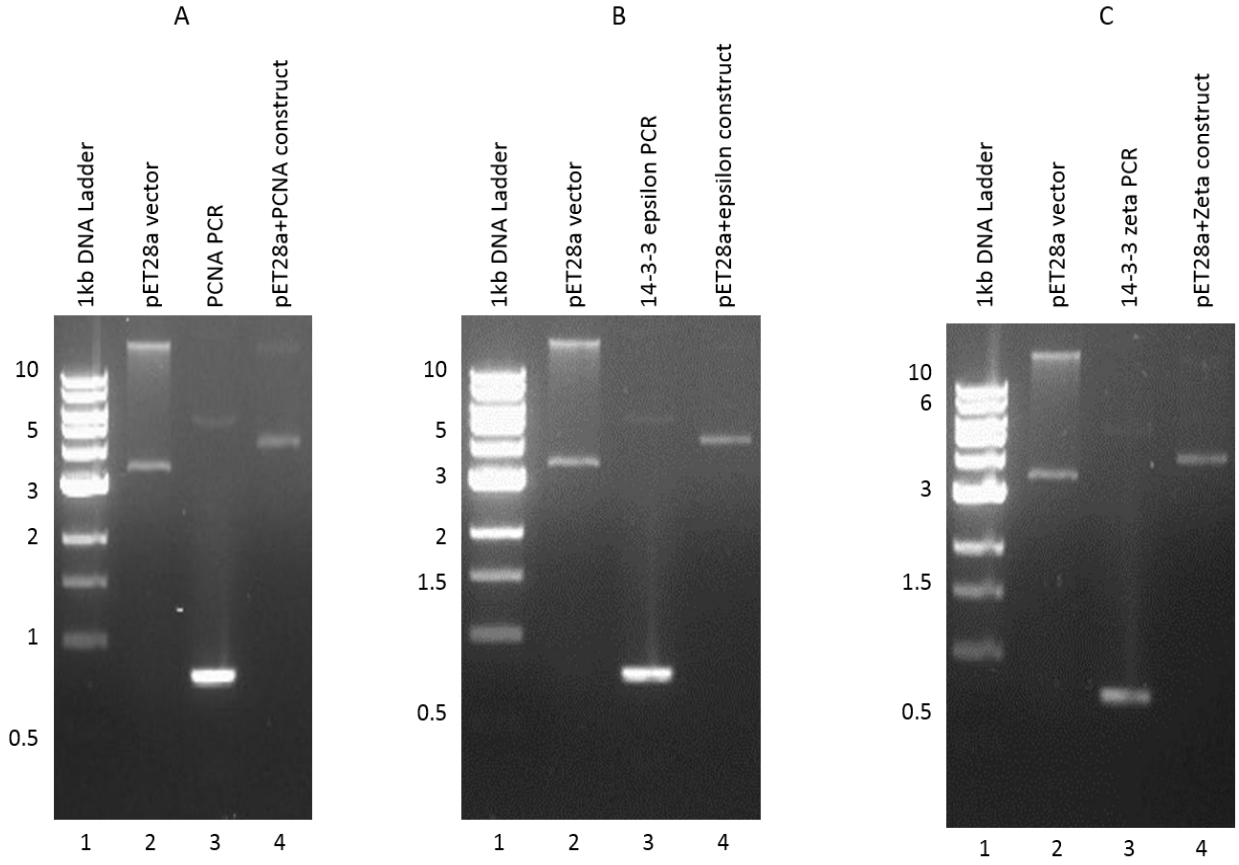


Figure 3.8. Agarose gel analysis of human PCNA (A), human 14-3-3 epsilon (B) and human 14-3-3 zeta (C) constructs. Gels were stained with ethidium bromide and visualized using a GelDoc (BioRad). About 50 ng of each sample was loaded on to the gel.

3.2. EXPRESSION RECOMBINANT PROTEINS

3.2.1. Expression of hExo1 protein

The full-length human exonuclease1 (hExo1) protein was expressed from both High Five™ insect cells using a Bac-to-Bac baculovirus expression system according to manufacturer's guidelines (Invitrogen) and *E. coli* BL21 (DE3) codon plus RIL. The High Five™ cells were infected with baculovirus expressing hExo1 and incubated for 72 hours. The cells were harvested by centrifugation after 72 hours post-infection. After harvesting, cells were rinsed once with serum-free medium and re-suspended in 50 ml lysis buffer (20mM HEPES pH 7.5, 190mM KCL, 10% v/v glycerol, 0.1mM EDTA), 1mL of cell suspension was aliquot to analyse protein expression and the remainder of cell suspension was stored at -80^{o}C. A 1 mL cell suspension was pelleted and cells were lysed using Insect Cell Protein Extraction Reagent (I-PER) (Thermo Scientific) according to manufacturer's protocol. The lysate was centrifuged at 15,000 × *g* for 30 minutes, soluble proteins were separated from the insoluble proteins. Supernatant was analysed using 4-20% Mini-PROTEAN® TGX Stain-Free™ Precast Gels (Bio-Rad UK) (*Fig. 3.9 lane 2*).

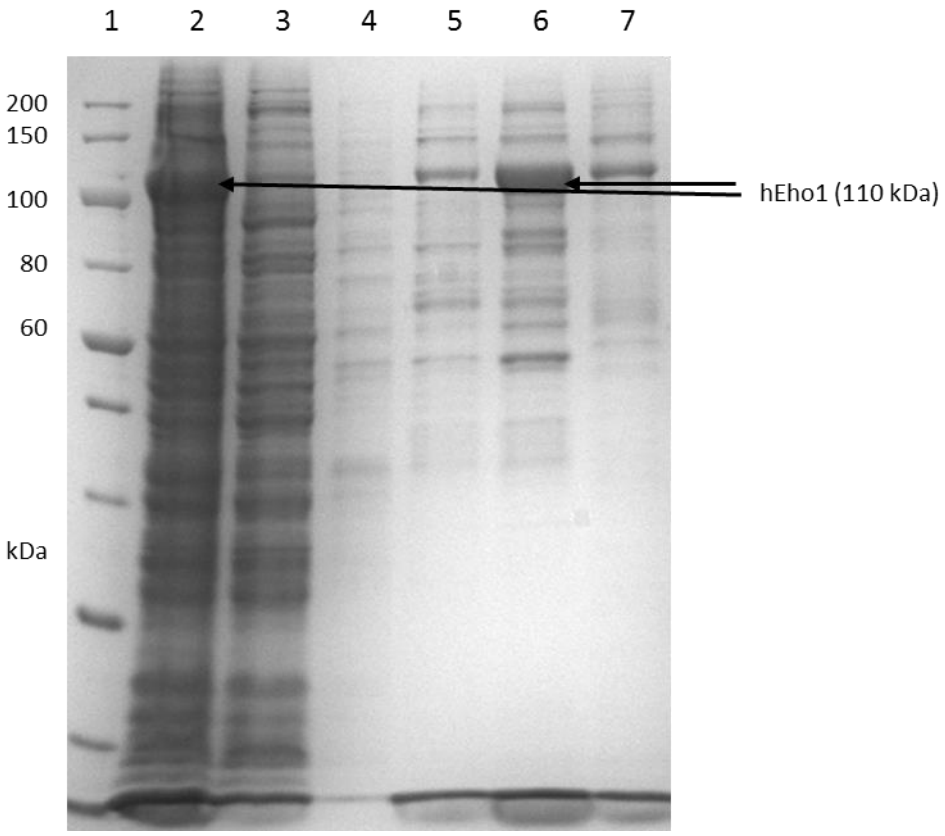


Figure. 3.9. SDS/PAGE analysis of hExo1 expression from High five insect cells. Lane 1 was the 200 kDa protein ladder, lane 2 was the soluble cell lysate and lane 3 was the soluble cell lysate from negative control (cells that do not harbour the pFastBac1+hExo1 plasmid). Lane 4 was the eluted sample from the heparin column after washing through the column with washing buffer, the eluton buffer contained 250 mM KCl, lane 5 was eluted sample with 300 mM KCl in the elution buffer, lane 6 was a 350 mM KCl elution and lane 7 was a 500 mM KCl elution.

For bacterial expression of full length hExo1 protein, transformed *E. coli* BL21 DE3 codon plus RIL was cultured and incubated at 37°C. Protein expression was induced when the cell density reached OD_{600} = 0.3. The incubator was then set at 18°C and allowed the incubation to continue overnight. Overnight culture was centrifuged, supernatant discarded and cells resuspended in CH buffer (20 mM Tris pH 8.0, 500 mM NaCl, 0.1% Triton X100, 1 mM EDTA, 10% glycerol). From 1mL resuspended cells protein expression was analysed by SDS/PAGE (*Fig. 3.10*).

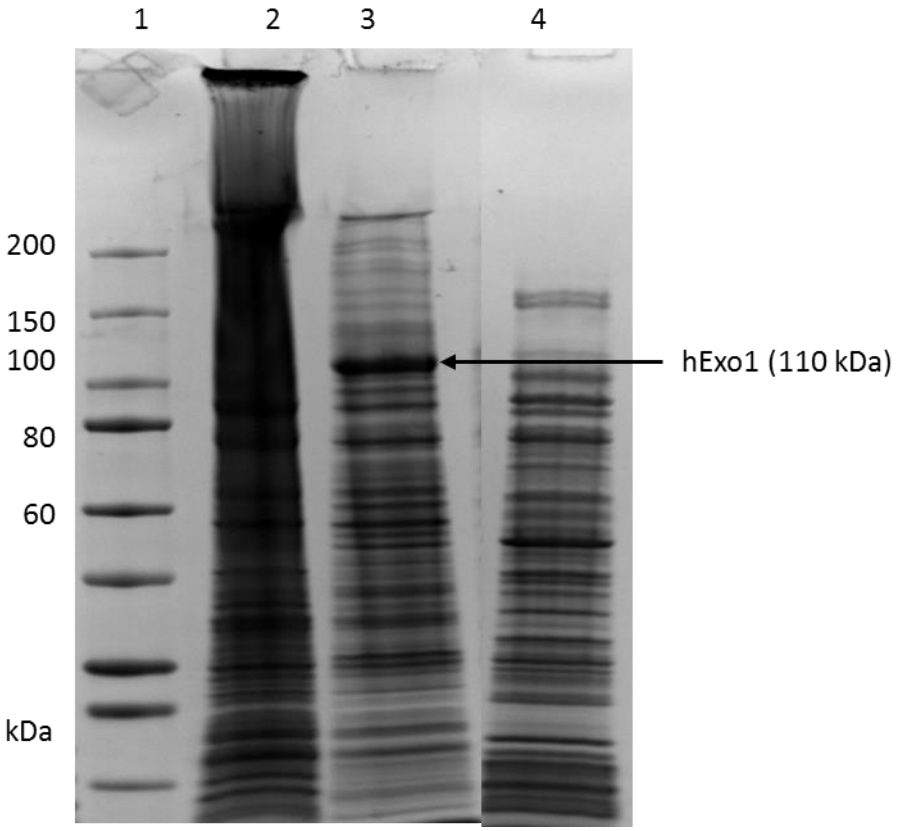


Figure. 3.10. SDS/PAGE analysis of bacterial full length hExo1 protein expression. Lane 1 was the 200 kDa protein ladder, lane 2 was whole cell lysate, lane 3 soluble cell lysate and lane 4 soluble cell lysate from negative control.

3.2.2. Expression of Nt-hExo1 (N-terminal domain of hExo1) protein

Nt-hExo1 protein was expressed from *E. coli* BL21 DE3 codon plus RIL as described above for the full length hExo1 protein expression in bacteria. Overnight culture was centrifuged, supernatant discarded and cells were resuspended in lysis buffer (20 mM Tris pH 7.4, 500 mM NaCl, 50 mM imidazole, 10% v/v glycerol). From 1mL resuspended cells, protein expression was analysed by SDS/PAGE (*Fig. 3.11 lane 3*).

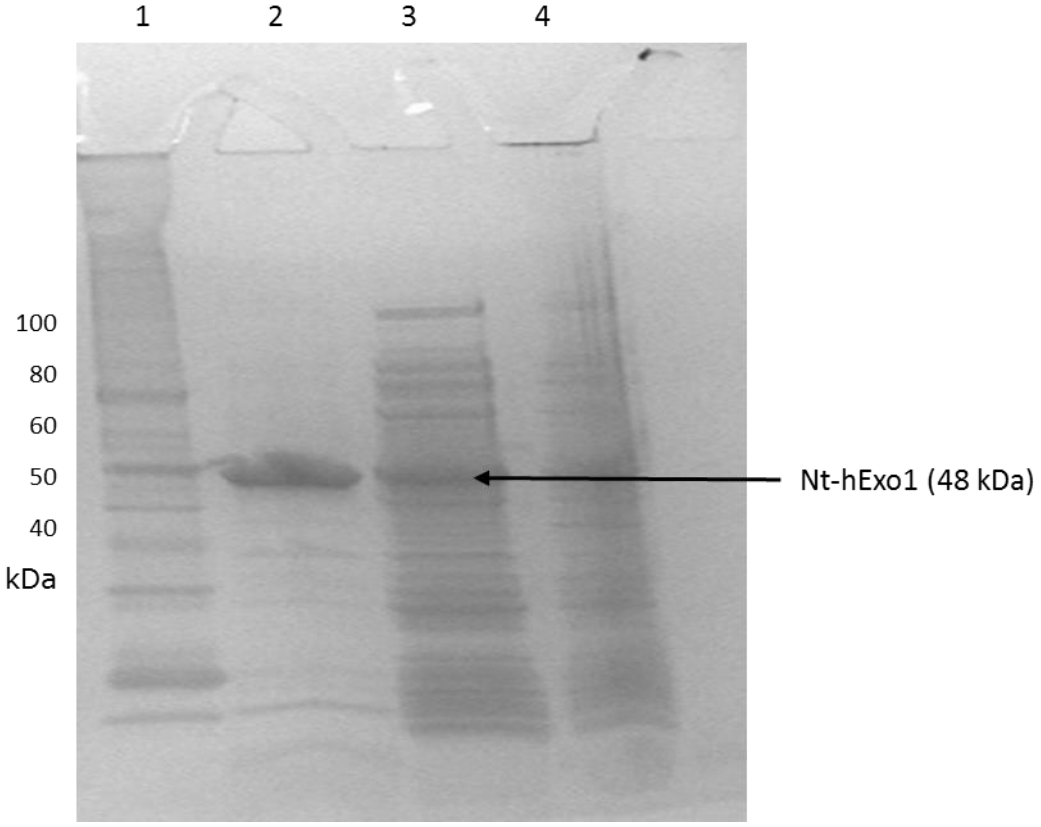


Figure. 3.11. SDS/PAGE analysis of Nt-hExo1 protein expression. Lane 1 protein ladder, lane 2 partially purified Nt-hExo1 protein, lane 3 soluble cell lysate and lane 4 whole cell lysate.

3.2.3. Expression of PCNA, 14-3-3ζ and 14-3-3ε proteins

PCNA, 14-3-3ζ and 14-3-3ε proteins were individually expressed from *E. coli* BL21 DE3. Cells were cultured in LB growth media and incubated at 37^{o}C, proteins expression was induced when culture density reached OD_{600} = 0.6 and then the incubation was allowed to continue overnight at 37^{o}C. The overnight culture was centrifuged and supernatant discarded. The cells were resuspended in lysis buffer (20 mM Tris pH 7.4, 500 mM NaCl, 50 mM imidazole, 10% v/v glycerol). Protein expression was analysed by SDS/PAGE using 20 µL of resuspended cells (*Fig. 3.12 and 3.13*).

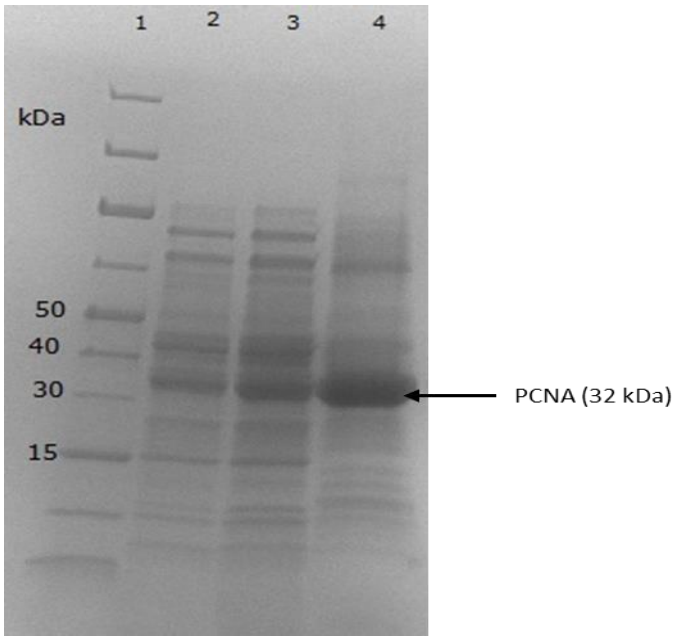


Figure 3.12. SDS/PAGE analysis for PCNA protein expression. Lane 1 protein ladder, lane 2 soluble lysate after one hour induction, lane 3 after 3 hours induction and lane 4 is overnight from overnight induction.

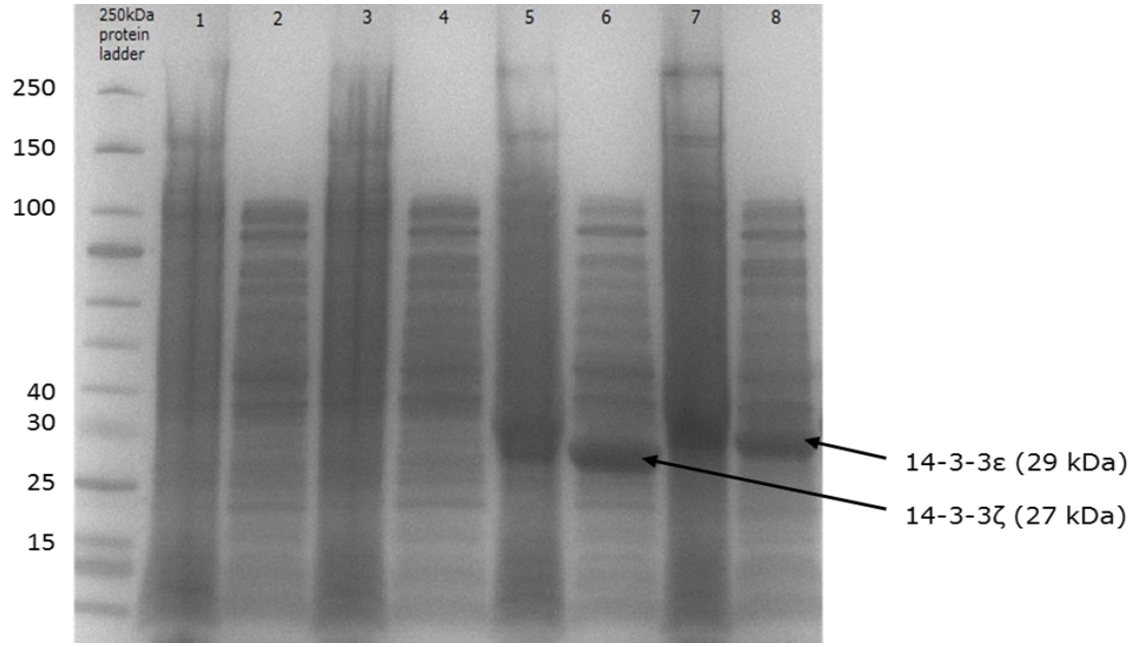


Figure 3.13. SDS/PAGE analysis from 14-3-3 zeta and epsilon protein expression. Lane 1 and 3 were for the whole cell lysate from negative control, lane 2 and 4 were for the soluble lysate from negative control, lane 5 and 6 were whole cell lysate and soluble cell lysate from the 14-3-3 zeta expression respectively, while lane 7 and 8 were for the whole cell lysate and soluble cell lysate from 14-3-3 epsilon expression respectively.

3.3. PURIFICATION OF PROTEINS

Having identified that expression of the target protein had occurred, the next step was to purify the protein from large scale growth of the host (insect cells and/or bacterial cells).

3.3.1. Purification of hExo1 protein

Human Exo1 was purified to near homogeneity using a strategy previously described (El-Shemerly *et al*., 2005; Andersen *et al*., 2012) but with some minor modifications that were found to be essential to consistently obtain pure protein as described in chapter two. After size-exclusion chromatography, fractions where the chromatogram peak appeared with higher intensity were collected and analysed by SDS/PAGE (*Fig. 3.14*). Human Exo1 has a molecular weight of 94 kDa, but migrated similar to proteins of about 115 kDa in size in the presences of sodium dodecyl sulfate (*Fig. 3.14a and b*), this migration behaviour of hExo1 was observed in previous studies (Genschel *et al*., 2002; El-Shemerly *et al*., 2005; Chen *et al*., 2013; Bregenhorn & Jiricny, 2014). This is most likely due to the unusual amount of charged amino acids found in the intrinsically disordered portion of the protein that have adverse effects on the amount of SDS bound to the protein during electrophoresis and hence lead to anomalous migration of the protein.

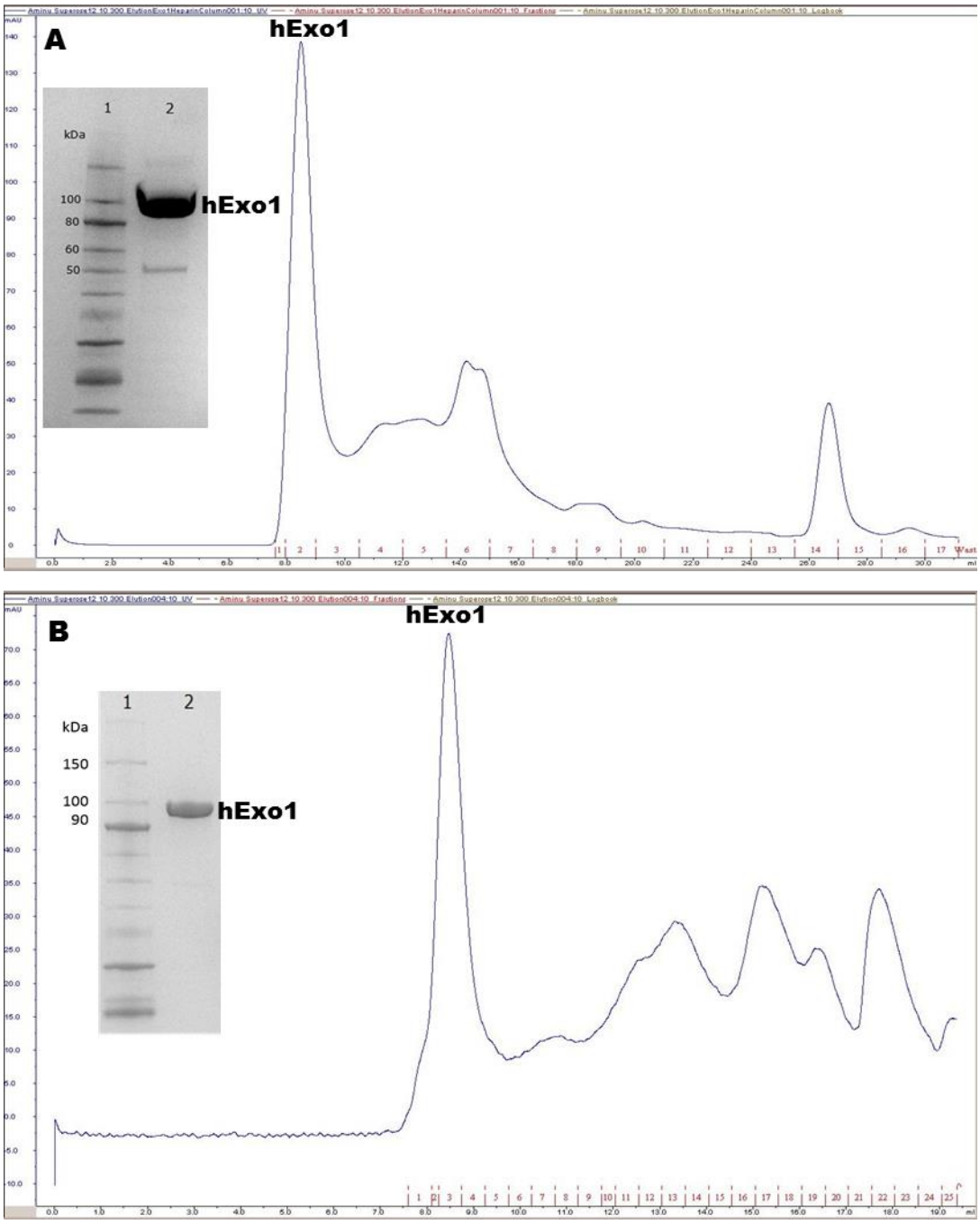


Figure. 3.14. (A) Chromatogram profile of hExo1 after size-exclusion chromatography using Superose 12 10/300 column (protein expressed from insect cells) and SDS/PAGE analysis of 10 µg purified hExo1 protein (inset) lane 2. (B) Chromatogram profile of hExo1 after size-exclusion chromatography using Superose 12 10/300 column (protein expressed from bacteria) and SDS/PAGE analysis of 10 µg purified hExo1 protein (inset) lane 2.

3.3.2. Purification of Nt-hExo1 protein

Nt-hExo1 was affinity purified using a HisTrap HP affinity column, eluted sample was further purified with Superose 12 10/300 gel filtration column using an AKTA prime protein purification system. After gel filtration, Nt-hExo1 containing fractions were pooled together and concentrated, 10µL was aliquot and SDS/PAGE analysed (*Fig. 3.15*). The remainder of sample was snap-frozen in liquid nitrogen and then stored at -80^{o}C.

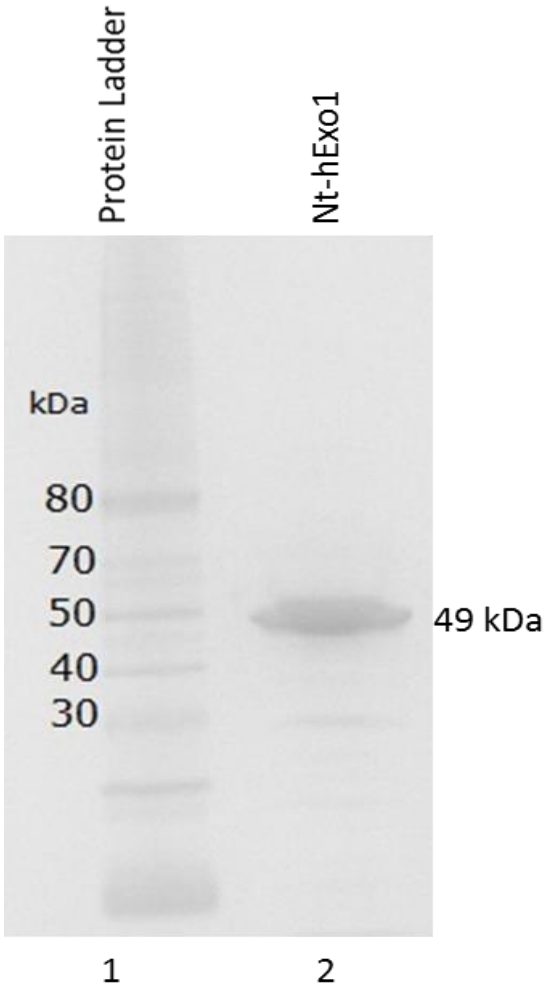


Figure. 3.15. SDS/PAGE analysis for purified Nt-hExo1. About 2 µg of Nt-hExo1 preparations was subjected to polyacrylamide gel electrophoresis in the presence of sodium dodecyl sulfate and stained with Coomassie Brilliant Blue. Protein ladder lane 1, purified Nt-hExo1 lane 2.

3.3.3. Purification of His-tagged PCNA, 14-3-3ζ and 14-3-3ε proteins

PCNA, 14-3-3ζ and 14-3-3ε were all affinity purified using a HisTrap HP affinity column. 10µL of each purified protein was aliquot and SDS/PAGE analysed (*Fig. 3.16*). The remainder of samples were snap-frozen in liquid nitrogen and stored at -80°C.

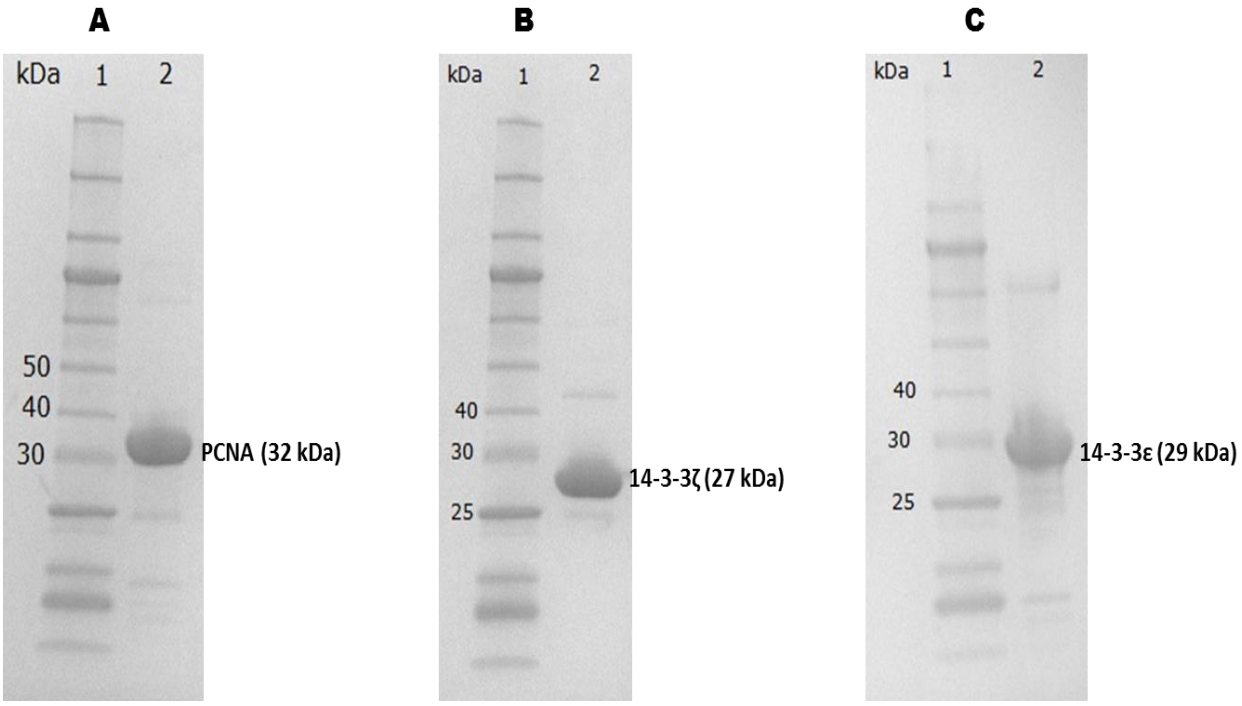


Figure. 3.16. SDS/PAGE analysis for His-tag PCNA, 14-3-3 zeta and 14-3-3 epsilon proteins. 10 µg of each of the proteins preparations were subjected to polyacrylamide gel electrophoresis in the presence of sodium dodecyl sulfate and stained with Coomassie Brilliant Blue (a) Protein ladder lane 1, purified PCNA lane 2. (b) Protein ladder lane 1, purified 14-3-3ζ lane 2. (c) Protein ladder lane 1, purified 14-3-3ε lane 2.

3.3.4. Protein Quantification and Identification

All the purified proteins were quantified using a NanoDrop ND-1000 Spectrophotometer (Labtech UK) at 280 nm settings. All proteins were quantified after all the purification steps from 1 litre growth of the hosts. The quantity obtained for each protein are shown in Table 3.1.

Protein	Quantity (mg)
hExo1	12 (insect cells)
	5 (bacterial cells)
Nt-hExo1	17
PCNA	22
14-3-3ζ	25
14-3-3ε	23

Table 3.1. Quantities of recombinant proteins obtained

4.0 CHAPTER FOUR: KINETIC STUDIES AND REGULATION OF HUMAN EXONUCLEASE1 DNA END RESECTION ACTIVITY ASSAYS

This chapter aimed to verify the kinetic parameters of hExo1 and to test exonuclease activity of hExo1 on DNA substrate under different conditions such as the ionic strength, temperature, pH and using different substrates. The effect of hExo1 binding partners on the nuclease activity was also tested.

4.1. KINETIC STUDIES

4.1.1. Ionic strength assay of hExo1

The ionic strength of hExo1 during its exonuclease DNA resection activity was tested and the reaction products were separated on 1% agarose gels eluted with TAE buffer and visualized using a GelDoc. Human Exo1 was tolerant to KCl in the range from 50 mM to 150 mM (*Fig. 4.1 lanes 2-4*) and thus active under physiological salt conditions. At 200 mM salt concentration, hExo1 activity decreased slightly (*Fig. 4.1 lane 5*). Nuclease activity of hExo1 drastically reduced when the reactions were conducted in the presence of 250-500 mM salt concentrations (*Fig. 4.1 lanes 6-9*). Likewise, at low salt concentration (5-10 mM KCl) hExo1 nuclease activity significantly decreased (*Fig. 4.1 lanes 10-11*).

Further assays of hExo1 exonuclease activities were conducted in the reaction buffer (20 mM HEPES pH 7.5, 5 mM $MgCl_2$, 1 mM ATP, 1 mM DTT, 100 ug/uL BSA, 10% v/v glycerol) in the presence of 100 mM KCl to stabilize the DNA configurations, by reducing thermo-breathing of DNA forming transient 5’ flap at dsDNA. The reaction products were separated on 1% agarose gels eluted with TAE buffer and then stained with SyBr gold DNA stain, thereafter, the gels were visualized using a GelDoc.

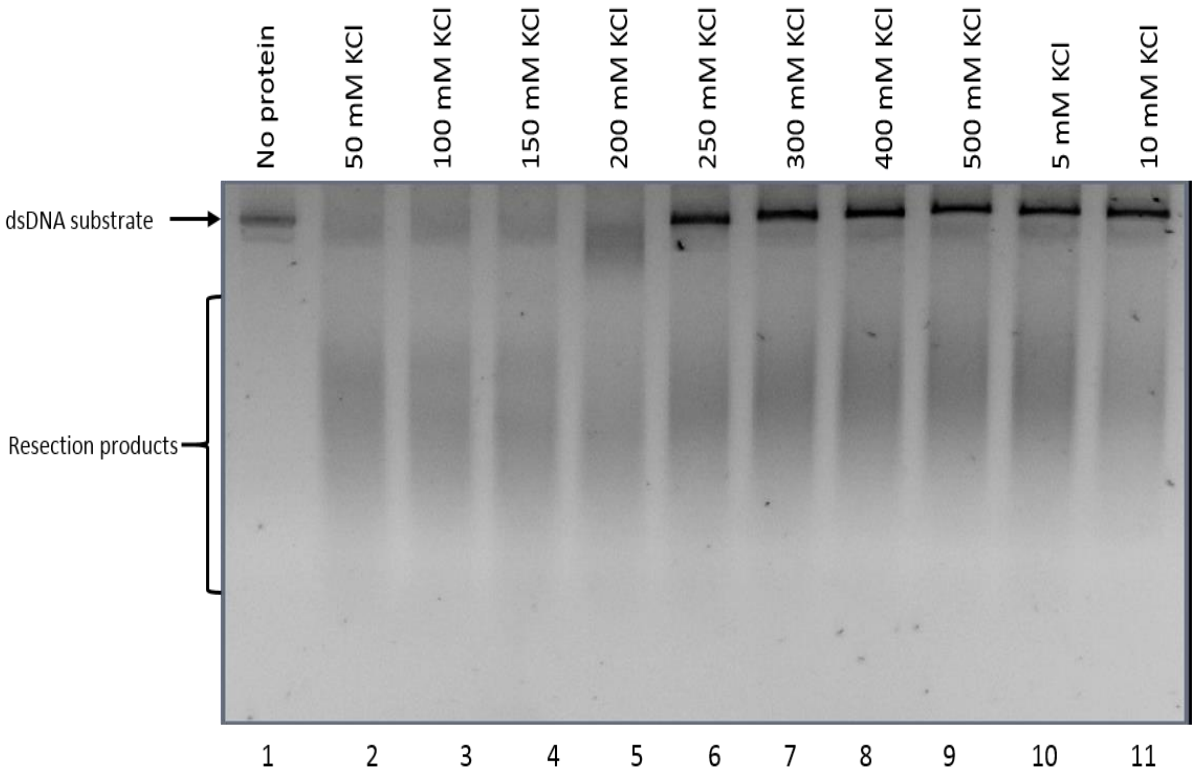


Figure 4.1. Ionic strength assay. Representative 1% agarose gel of three independent replicates of experiments showing exonuclease activities on a 3' overhang 4.8kb dsDNA substrate by incubation with 15 nM purified recombinant hExo1. Lane 1 was substrate control, no hExo1 enzyme was added. Lanes 2–11 contain 15 nM of hExo1 in the presence of salt concentrations as indicated on the gel image above. Assay was set up on ice and reaction was activated by transferring reaction tubes to 37°C and incubated for 60 min.

4.1.2. Human Exonuclease1 is temperature sensitive

To examine if hExo1 is temperature sensitive, hExo1 activity was tested at six different temperatures as follows: ice, 4°C, room temperature (RT), 25°C, 30°C and 37°C. The resection activity of hExo1 was observed to be higher at room temperature that at both 4°C and when incubated on ice (*Fig. 4.2 lanes 2,3 and 4*). The activity increased when reaction was incubated at 25°C and further increased activity was observed at 30°C and 37°C (*Fig 4.2, lanes 5, 6 and 7*).

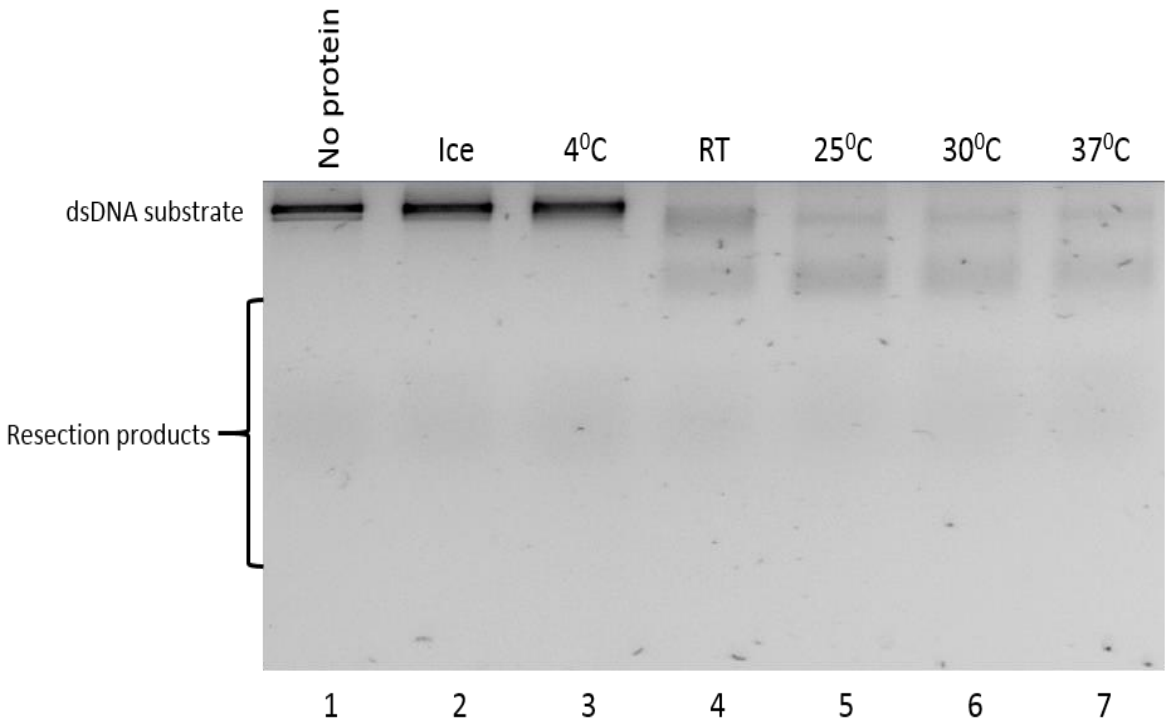


Figure 4.2. Temperature sensitivity assay. Representative 1% agarose gel of three independent replicates of experiments showing hExo1 exonuclease activities on a 3' overhang 4.8kb dsDNA substrate. Lane 1 was substrate control, no hExo1 enzyme was added. Lanes 2–7 contain 15 nM hExo1 incubated at different temperatures as indicated on the gel image above. Assay was set up on ice and reaction was activated by transferring reaction tubes to different assay temperatures and incubated for 60 min.

4.1.3. Human exonuclease1 protein is not stable at high temperature

To determine the stability of hExo1 protein at various temperatures, hExo1 was pre-incubated at various temperatures as follows: 50°C, 45°C, 40°C, 37°C, 30°C, 25°C, 4°C and on ice for one hour prior to the assay set up. Thereafter, the assay was set up using a 4.8kb dsDNA substrate (*Fig. 4.3*). Pre-incubation of hExo1 at 4°C and on ice (*Fig. 4.3, lanes 8 & 9*) increased exonuclease activity compared pre-incubation at 37°C (*Fig. 4.3. lane 5*) while pre-incubation at 50°C, 45°C and 40°C drastically decreased exonuclease activity and pre-incubation at 30°C and 25°C, (*Fig. 4.3. lanes 6 and 7*) mildly decreased exonuclease activity.

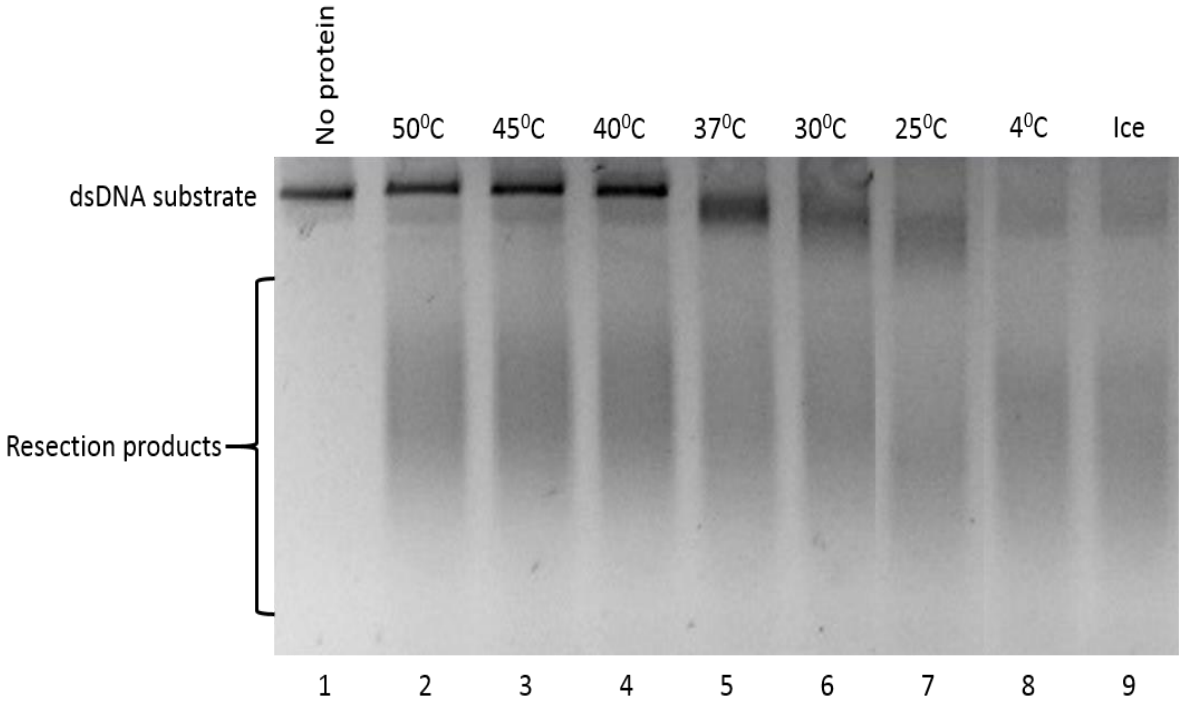


Figure 4.3. Temperature stability assay. Representative 1% agarose gel of three independent replicates of experiments showing hExo1 exonuclease activities on a 3′ overhang 4.8kb dsDNA substrate. Lane 1 was substrate control, no hExo1 enzyme was added. Lanes 2–9 contain 15 nM pre-incubated hExo1 at different temperatures as indicated on the gel image above. Assay was set up on ice and reaction was activated by transferring reaction tubes to different assay temperatures and incubated for 60 min.

4.1.4. Human exonuclease1 is pH sensitive

To determine if full length hExo1 is sensitive to pH, hExo1 activity was tested at nine different pH condition of the reaction buffer (20 mM HEPES pH 7.0, 100 mM KCl, 5 mM MgCl2, 1 mM ATP, 10% v/v glycerol) as follows: 5, 5.5, 6, 6.5, 7, 7.5, 8, 8.5, and 9. It was observed that hExo1 exonuclease activity was higher and almost nearly the same across the pH ranges 7-8 (*Fig. 4.4 lanes 6,7 and 8*). HEPES buffer has a pKa_1 as 3 and pKa_2 as 7.5 at 25°C.

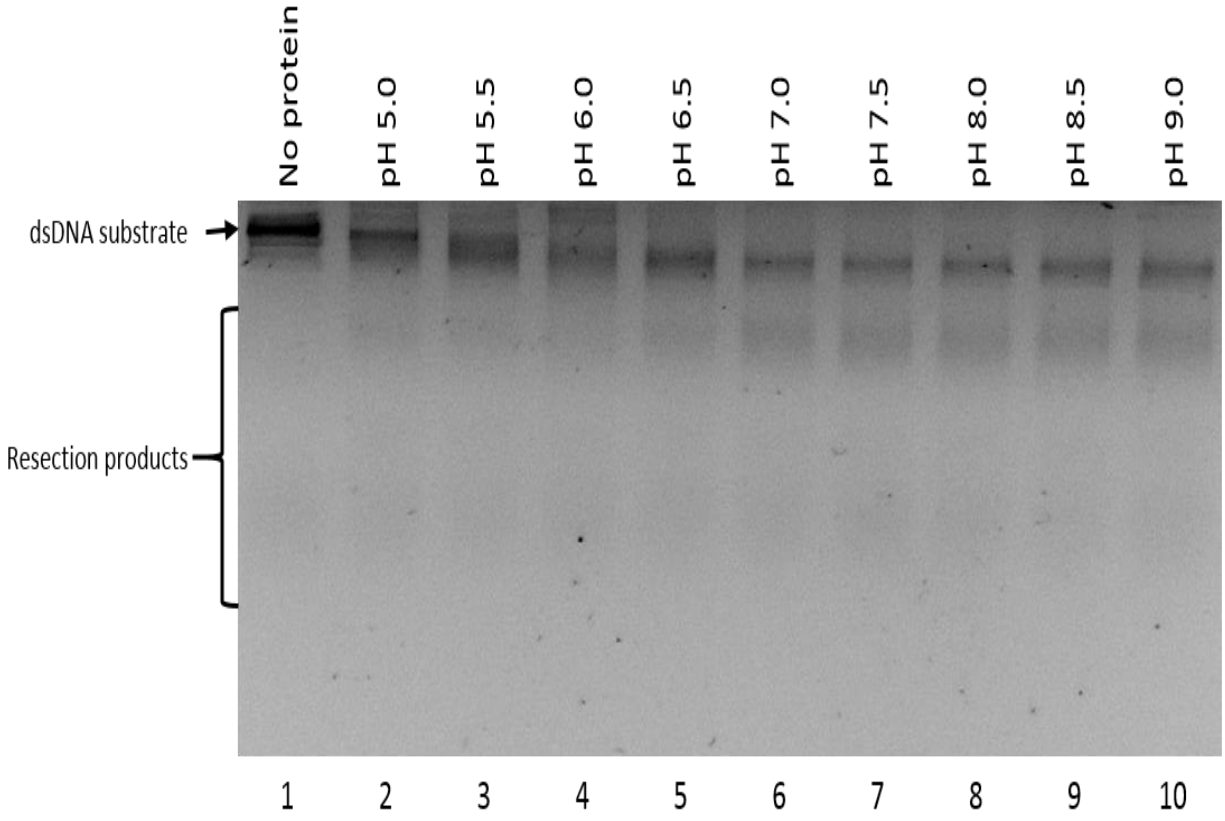


Figure 4.4. pH sensitivity assay. Representative 1% agarose gel of three independent replicates of experiments showing hExo1 exonuclease activities on a 3' overhang 4.8kb dsDNA substrate. Lane 1 was a substrate control; no hExo1 enzyme added. Lanes 2–10 contained 10 nM hExo1 incubated at different pH as indicated on the gel image above. Assay was set up on ice and reaction was activated by transferring reaction tubes to 37°C and incubated for 60 min.

4.1.5. Human exonuclease1 resection activity is specific to 3’ overhang DNA substrate

To test if hExo1 was specific to a 3’ overhang substrate, an assay was carried out with different substrate types, 3’ overhang, 5’ overhang and blunt end 4.8kb dsDNA substrates. The results suggested that hExo1 is specific to 3’ overhang dsDNA substrate (*Fig. 4.5, lane 2*). No substrate degradation was observed in reactions that contained either of 5’ overhang or blunt end dsDNA substrate (*Fig. 4.5, lanes 3 and 4*).

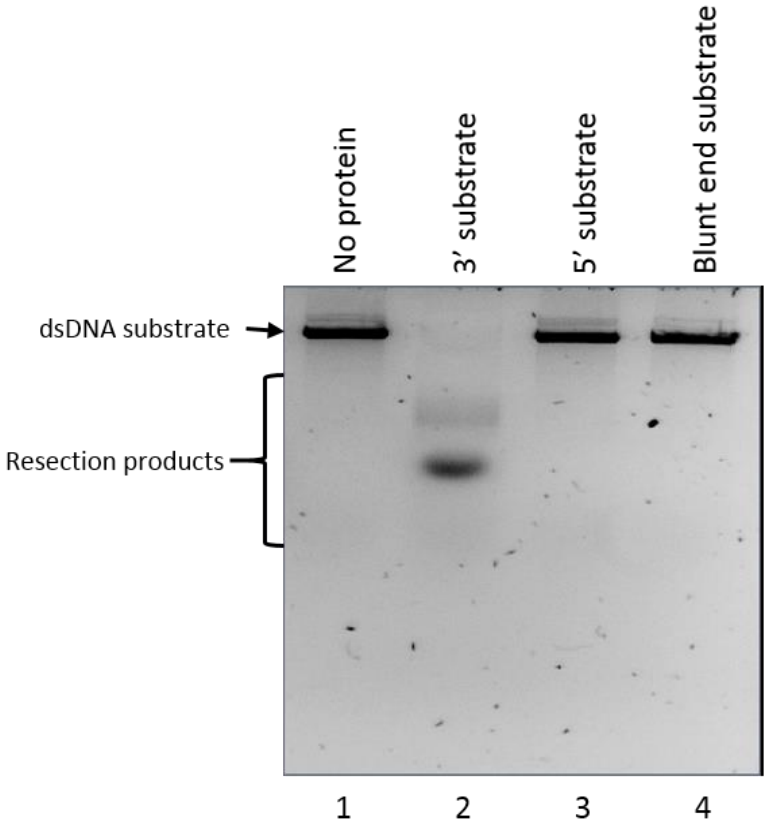


Figure 4.5. Substrate specificity assay. Representative 1% agarose gel of three independent replicates of experiments showing hExo1 exonuclease activities on different 4.8kb dsDNA substrate type. Lane 1 was a substrate control; no hExo1 enzyme added. Lanes 2–4 contained 15 nM hExo1 incubated at different pH as indicated on the gel image above. Assay was set up on ice and reaction was activated by transferring reaction tubes to 37^{o}C and incubated for 60 min.

4.1.6. The role of reaction incubation time on DNA resection activity of hExo1

This study investigated the role of reaction incubation time to ascertain how long hExo1 could remain active in the reaction. Six different resection reactions were set up, incubated and terminated at different times as shown in Table 4.1.

Reaction	Incubation period (Minute)
1	1
2	5
3	10
4	15
5	30
6	60

Table 4.1. Resection assays incubation time

Reaction results revealed that hExo1 remained active over a period of 60 minutes and degraded the substrate almost completely after 60 minutes (*Fig. 4.6, lane 7*). Resection products appeared right from the first minute of reaction (*Fig. 4.6, lane 2*). These data suggest that Exo1 is active in reaction mixture after 60 min at 37^{o}C. This is contrary to what was reported previously: which was that hExo1 was inactive in reaction at 37^{o}C after 15 minutes (Keijzers *et al*., 2015).

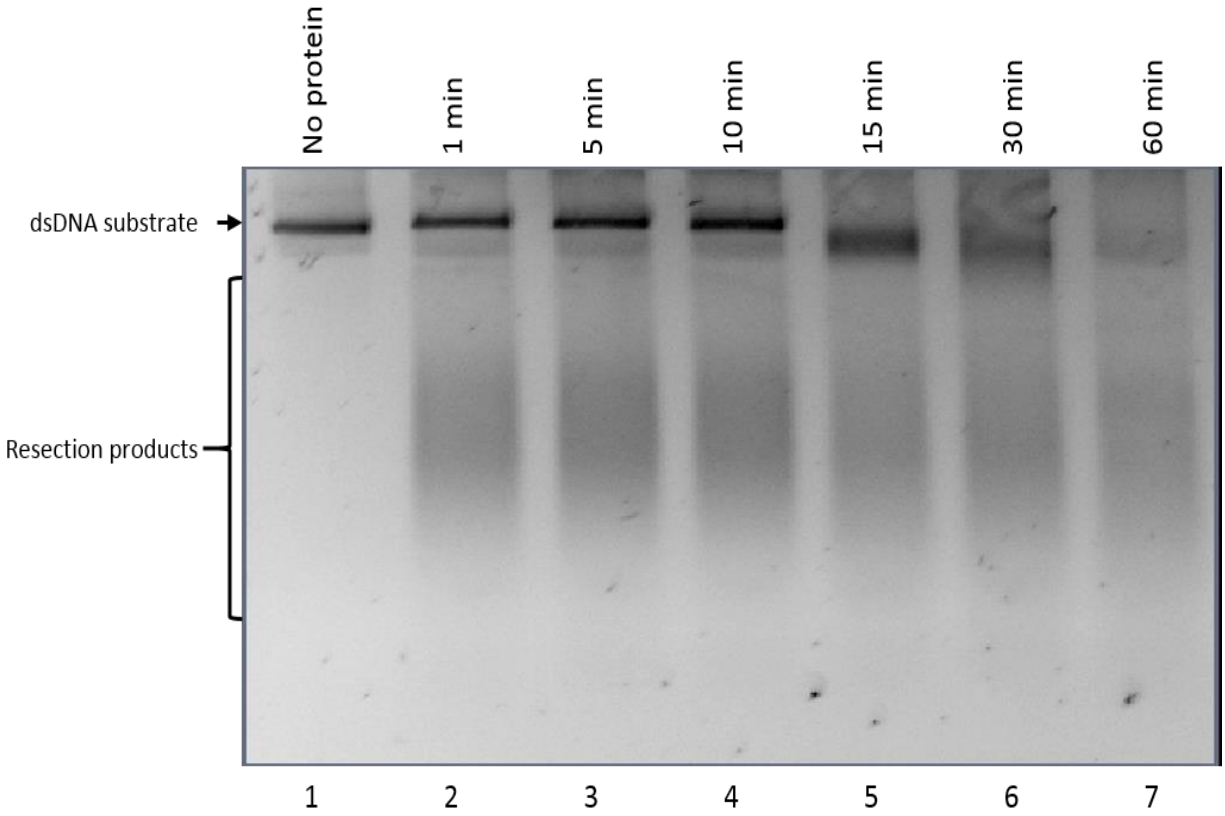


Figure 4.6. Time course assay. Representative 1% agarose gel of three independent replicates of experiments showing hExo1 exonuclease activities on a 15nM 3' overhang 4.8kb dsDNA substrate at different time course. Lane 1 was a substrate control; no hExo1 enzyme was added. Lanes 2–7 contained 5nM hExo1 incubated for different period of times as indicated on the gel image above.

4.1.7. Human exo1 resection activity depend on the presence of ATP and Mg^{2+}

To examine if hExo1 has an absolute requirement for ATP and Mg^{2+}, reactions were set up in the presence or absence of either both or one of ATP and Mg^{2+}. Another set of reactions were set up in the presence of GTP and Ca^{2+} as a substitutes to ATP and Mg^{2+}. Resection activity on a 3' overhang dsDNA substrate was only observed when both ATP and Mg^{2+} were present in the reaction (*Fig. 4.7, lane 2*). This result suggests that hExo1 resection activity on a 3' overhang dsDNA substrate require the presence of both ATP and Mg^{2+}.

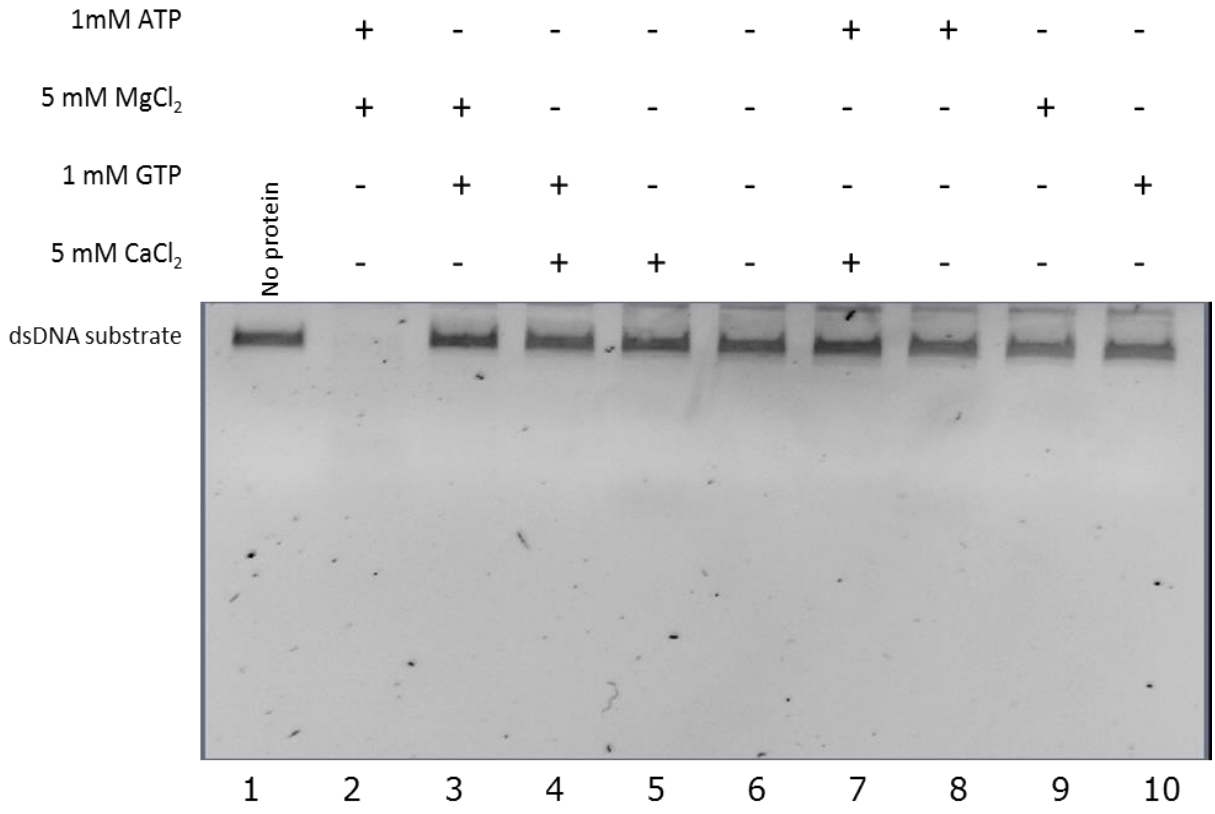


Figure 4.7. ATP and Mg^{2+} requirement assay. Representative 1% agarose gel of three independent replicates of experiments showing hExo1 exonuclease activities on a 3' overhang 4.8kb dsDNA substrate in the presence or absence of both ATP and Mg^{2+}. Lane 1 was substrate control; no hExo1 enzyme was added. Lanes 2–10 contained 20 nM hExo1 and 40 nM of a 3' overhang 4.8kb dsDNA. Assays were set up on ice and reaction was activated by transferring reaction tubes to 37°C and incubated for 60 min.

4.2. REGULATION OF hExo1 DNA RESECTION ACTIVITY

4.2.1. PCNA enhances hExo1 resection activity on DNA

PCNA is a ring-shaped clamp that can encircle dsDNA and can slide across the DNA. PCNA was also previously reported to directly interact with hExo1 (Chen, *et al*., 2013), there is a possibility that PCNA promotes hExo1 activity by tethering hExo1 to the DNA substrate, thereby increasing its exonuclease activity on the DNA substrate. To test this hypothesis more directly, first, a DNA end resection reaction was reconstituted using purified, recombinant hExo1 and PCNA proteins and a 3’ overhang 4.8 kb dsDNA fragment as resection substrate. PCNA drastically enhanced resection of the DNA fragment by full-length hExo1. Result of this assay revealed that the resection reaction was almost carried out to completion when PCNA was present in the reaction as can be seen from the gel image (*Fig. 4.8, lanes 7-10*). More resection product appeared with the increase in hExo1 concentration (*Fig. 4.8, lanes 2-5*). In the presence of PCNA the resection product appeared to have migrated all the way down the bottom of the gel and that made it difficult to see on the gel unlike in those reaction that did not contained PCNA where they appeared as a smear on the gel (*Fig. 4.8, lanes 2-5*).

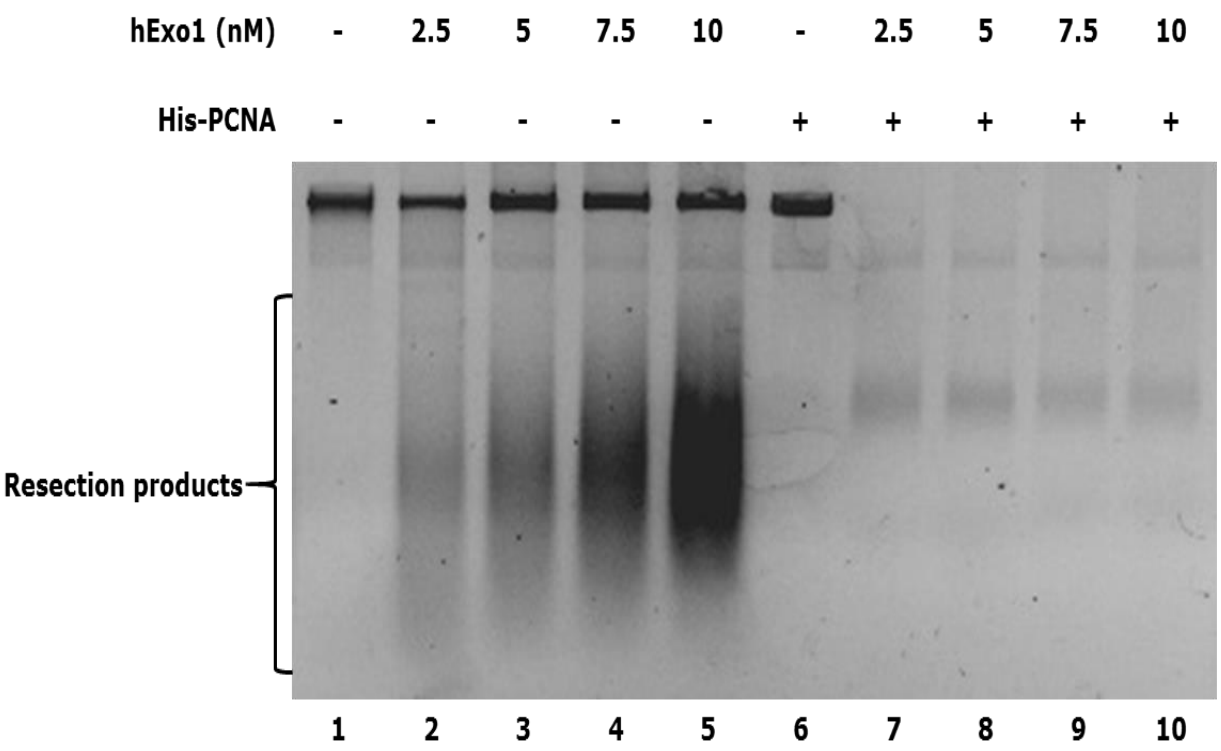


Figure 4.8. PCNA stimulates exonuclease activity of hExo1. Representative 1% agarose gel of four independent replicates of experiments showing that PCNA enhanced hExo1 resection activity on a 3' overhang 4.8kb dsDNA substrate. Lane 1 was substrate control; no hExo1 protein added. Lanes 2–5 contained 30 nM dsDNA substrate and a varying concentrations of hExo1 ranging from 2.5-10 nM as indicated on the gel image above, lane 6 contained 100 nM PCNA only, no hExo1 protein, while lanes 7-10 contained 100 nM PCNA and varying concentration of hExo1 protein as indicated on the gel image above. Assay was set up on ice and reaction was activated by transferring reaction tubes to 37^{o}C and incubated for 60 min.

4.2.2. PCNA hinders DNA resection activity of Nt-hExo1

Nt-hExo1 (hExo1 nuclease domain) is devoid of a PIP-Box and therefore cannot interact directly with PCNA. To verify if the stimulation effect of PCNA on full-length hExo1 is as a result of direct interaction between the two proteins (hExo1 and PCNA), resection assay was reconstituted using purified recombinant Nt-hExo1 and PCNA proteins and a 3' overhang 4.8 kb dsDNA fragment as resection substrate. In clear contrast, PCNA did not enhance, but actually hindered Nt-hExo1 resection activity on dsDNA substrate. Comparing lanes 2 and 3 in Figure 4.9 it clearly showed a difference in the resection activity of Nt-hExo1 in the presence and absence of PCNA.

The results clearly indicated that PCNA enhances the full-length hExo1 mediated DNA resection activity by direct interaction between PCNA and PIP-Box on the C-terminal domain of full-length hExo1. PCNA could indirectly inhibit Nt-hExo1; for instance, when PCNA occupy the DNA fragment it may protect the DNA substrate from being attacked by Nt-hExo1.

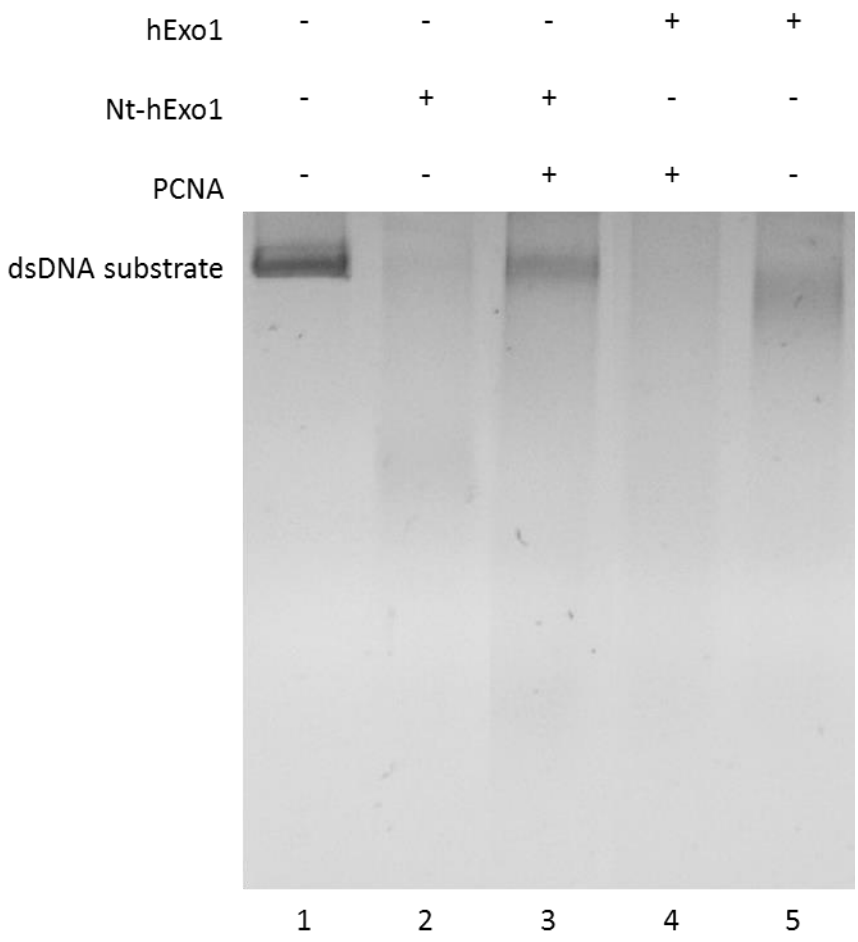


Figure 4.9. PCNA hinders Nt-hExo1 DNA end resection activity. Representative 1% agarose gel of four independent replicates of experiments showing PCNA enhances hExo1 exonuclease activities on a 3' overhang 4.8kb dsDNA substrate (lane 4) but hinders Nt-hExo1 nuclease activity (lane 3). Lane 1 was substrate control; no protein added. Lanes 2 contained 15 nM Nt-hExo1, while lane 3 contained 15 nM Nt-hExo1, 30 nM 3' overhang dsDNA and 100 nM PCNA. Lane 4 contained 10 nM full-length hExo1, 30 nM 3' overhang dsDNA and 100 nM PCNA. Assay was set up on ice and reaction was activated by transferring reaction tubes to 37^{o}C and incubated for 60 min.

4.2.3. The 14-3-3 proteins inhibit hExo1-mediated DNA resection

The 14-3-3 proteins bind to a wide variety of proteins to regulate and coordinate a diverse array of cellular processes. Human Exo1 was reported to interact with at least six of the seven human isoforms of the 14-3-3 proteins (Andersen, *et al*., 2012).

The question was whether 14-3-3 proteins exert an inhibitory, stimulatory or no effect on hExo1 resection activity on dsDNA substrate. To address this question, a resection assay was reconstituted using purified recombinant hExo1, 14-3-3ζ and 14-3-3ε proteins with a 3′ overhang 4.8 kb dsDNA fragment as resection substrate. Consequently, both the two 14-3-3 isoforms (ζ and ε) inhibited the resection activity of hExo1 on a 3′ overhang dsDNA fragment (*Fig.4.10*). 14-3-3ζ appeared to have slightly stronger inhibitory effect than 14-3-3ε as seen on the gel where the resection products are more in the presence of 14-3-3ε indicating that resection activity of hExo1 occurred more in the presence of 14-3-3ε than in the presence pf 14-3-3ζ (*Fig. 4.10, lanes 2-5*).

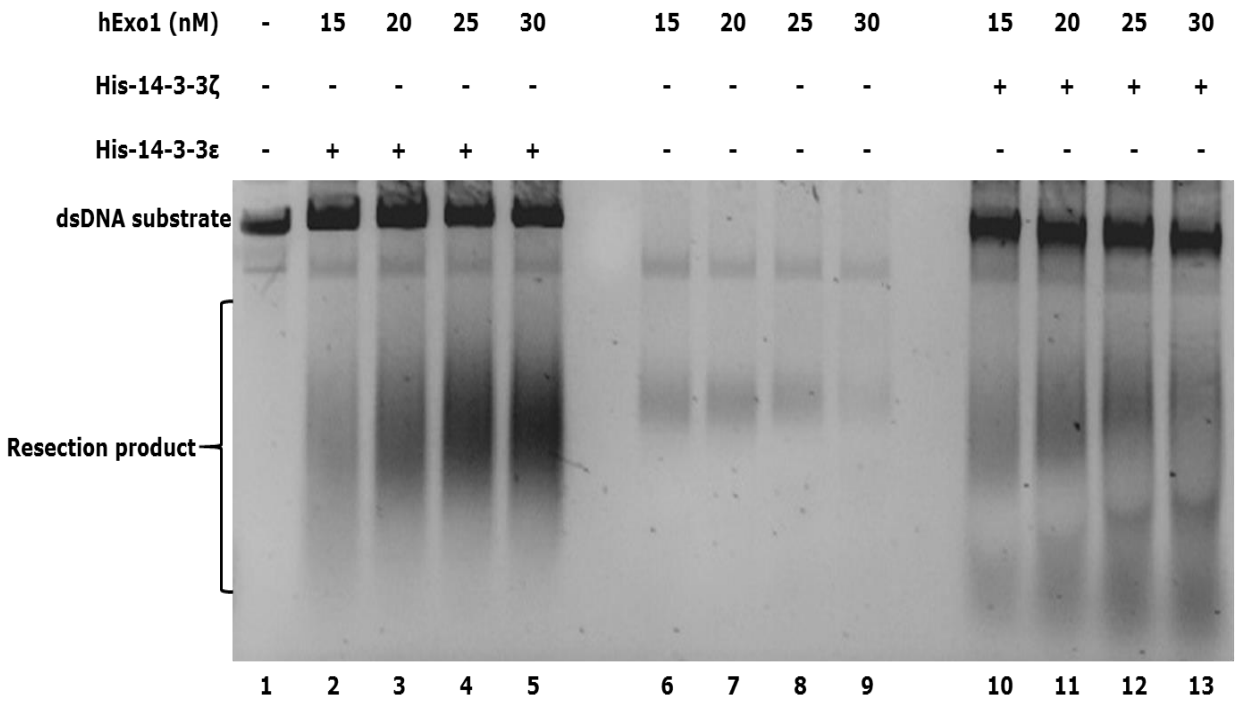


Figure 4.10. 14-3-3s inhibits hExo1 resection activity. Representative 1% agarose gel of four independent replicates of experiments showing 14-3-3s inhibits hExo1 resection activities on a 3' overhang 4.8kb dsDNA substrate (lanes 2-5 and 10-13). Lane 1 was a substrate control; no protein added. Lanes 2-13 each contained 30 nM 3' overhang dsDNA and varying concentrations of hExo1 as indicated on the gel image above. Lanes 2-5 100 nM 14-3-3ε and lanes 10-13 contained 100 nM 14-3-3ζ. Assay was set up on ice and reaction was activated by transferring reaction tubes to 37^{o}C and incubated for 60 min.

4.2.4. The 14-3-3 proteins interact with hExo1 within the C-terminal region of the hExo1

The next question was, which region on the hexo1 protein interact with the 14-3-3 proteins. To address this question, a resection assay was reconstituted using purified recombinant Nt-hExo1 (nuclease domain of hExo1, residues 1-391) and 14-3-3ζ and 14-3-3ε proteins with a 3’ overhang 4.8 kb dsDNA fragment as resection substrate. Neither of the 14-3-3 isoforms inhibits the resection activity of Nt-hExo1 but hExo1 resection activity was inhibited by both 14-3-3ζ and 14-3-3ε isoforms (*Fig. 4.11*). These results suggest that 14-3-3 proteins bind within the C-terminal region (residues 392-846) on hExo1 and restrain its activity. It was also observed that, 14-3-3ζ exhibited stronger inhibitory effect on hExo1 resection activity (*Fig. 4.11 lane 4*) compared to 14-3-3ε (*Fig. 4.11, lane 6*).

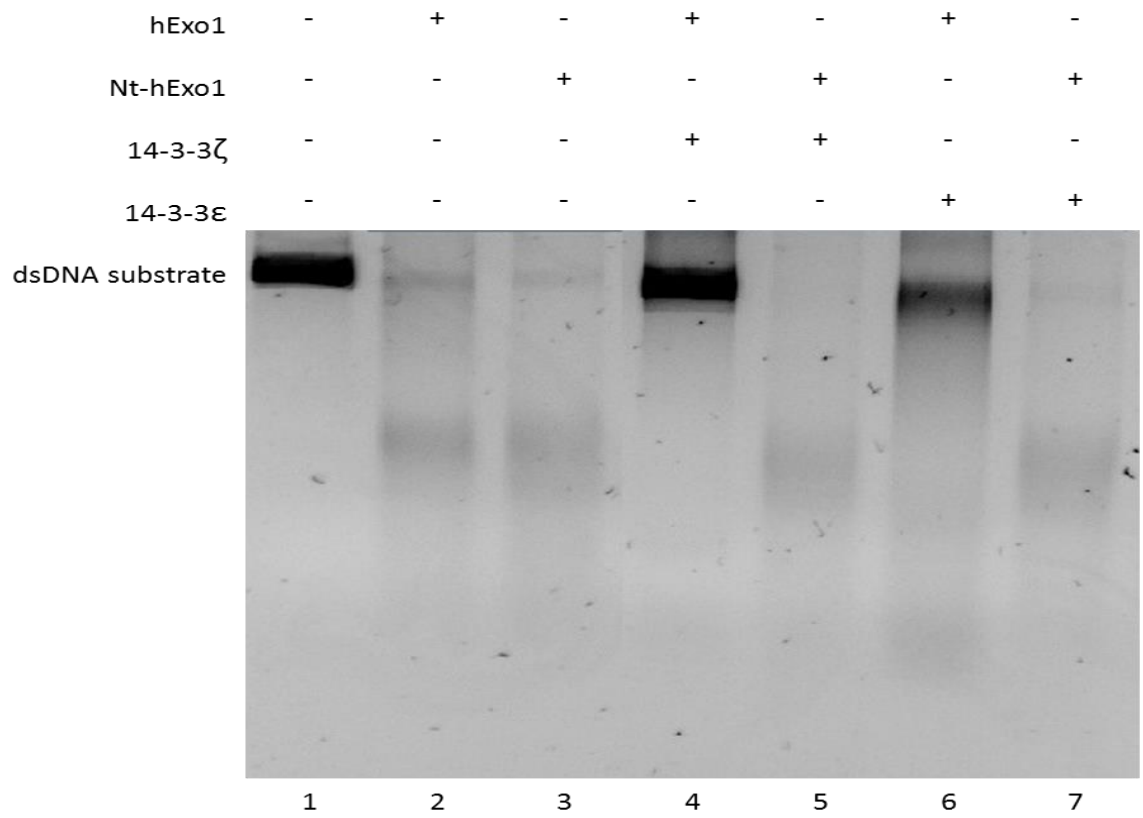


Figure 4.11. 14-3-3s inhibits full length hExo1 but not Nt-hExo1 resection activity. Representative 1% agarose gel of four independent replicates of experiments showing 14-3-3s inhibits hExo1 but not Nt-hExo1 resection activities on a 3' overhang 4.8kb dsDNA substrate. Lane 1 was a substrate control; no protein added. Lane 2 contained 15 nM hExo1 (full-length). Lane 3 contained 15 nM Nt-hExo1. Lane 4 contained 15 nM hExo1 (full-length) and 100 nM 14-3-3ζ. Lane 5 contained 15 nM Nt-hExo1 and 100 nM 14-3-3ζ. Lane 6 contain 15 nM full-length hExo1 and 100 nM 14-3-3ε while lane 7 contained 15 nM Nt-hExo1 and 100 nM 14-3-3ε. Each of the reaction tubes contained 30 nM 3' overhang dsDNA substrate. Assays were set up on ice and reactions were activated by transferring reaction tubes to 37^{o}C and incubated for 60 min.

4.2.5. 14-3-3 proteins suppress PCNA binding to hExo1

Since both PCNA and 14-3-3s interact with hExo1 within its C terminal region, it is possible that binding of 14-3-3 to hExo1 may interfere with the binding PCNA or vice versa. To confirm this, a resection assay was reconstituted using purified recombinant hExo1, PCNA, 14-3-3ζ and 14-3-3ε proteins with a 3' overhang 4.8 kb dsDNA fragment as resection substrate. In these assays, reactions were set up as described earlier but in this case hExo1 and PCNA were added in the presence of the substrate and incubated for 5 minutes then either of 14-3-3ζ or 14-3-3ε was added and reaction allowed to continue for one hour. Another reaction was set up in a reverse manner of adding hExo1 with either 14-3-3ζ or 14-3-3ε and allowed to incubate for 5 minutes followed by addition of PCNA. Also, the same procedure was carried out between hExo1 and 14-3-3s. The results of these assays revealed that indeed both 14-3-3ζ and 14-3-3ε suppresses PCNA binding to hExo1 (*Fig. 4.12*).

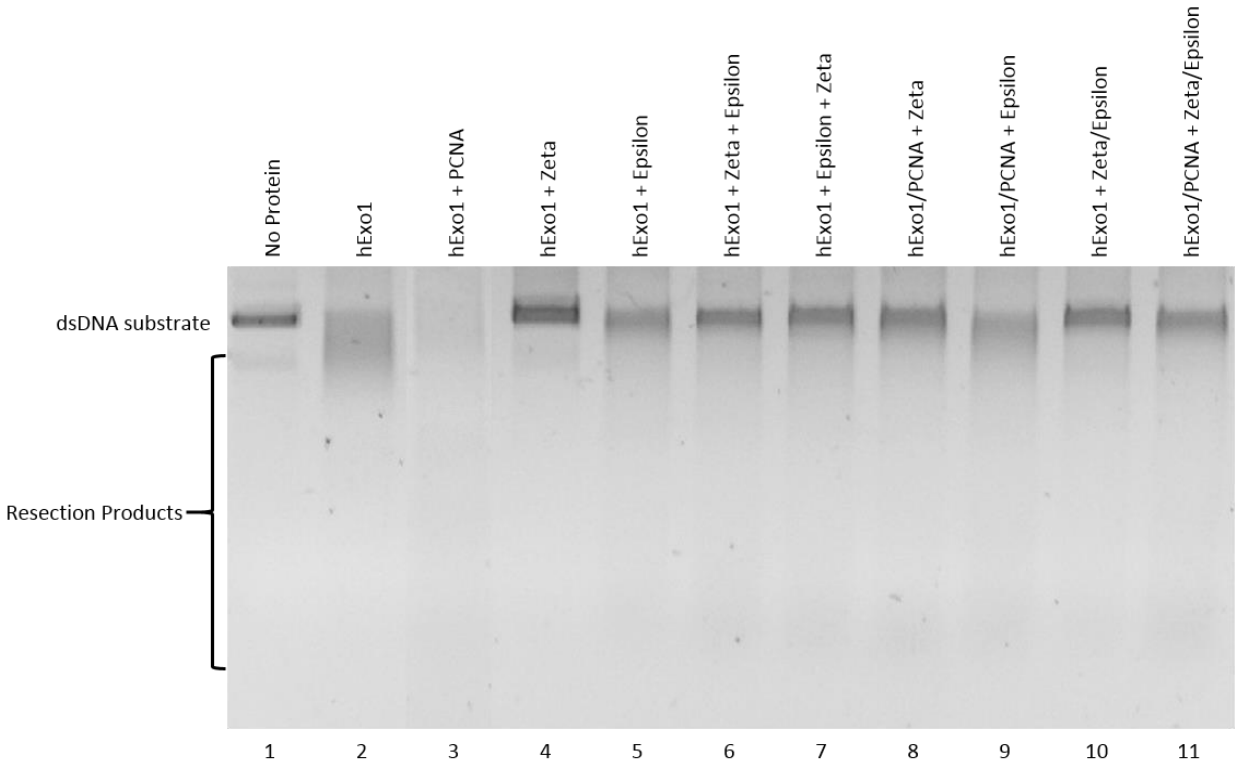


Figure 4.12. 14-3-3s Suppress PCNA Binding to hExo1. Representative 1% agarose gel of three independent replicates of experiments showing 14-3-3ζ suppress PCNA binding to hExo1 in resection activities on a 3′ overhang 4.8kb dsDNA substrate. Lane 1 was a substrate control; no protein was added. Lane 2 contained 5 nM hExo1. Lane 3 contained 5 nM hExo1 and 50 nM PCNA. Lane 4 contained 5 nM hExo1 and 50 nM 14-3-3ζ. Lane 5 contained 5 nM hExo1 and 50 nM 14-3-3 epsilon. Lane 6 contained 5 nM hExo1, 50 nM PCNA and 50 nM 14-3-3ζ, lane 7 contained 5 nM hExo1, 50 nM PCNA and 50 nM 14-3-3ε. Lanes 8 and 9 have the same content as lanes 6 and 7 but only differ in order of proteins addition. Lanes 10 and 11 also have same content as lanes 6 and 7 but 14-3-3ζ and 14-3-3ε were pre-mixed prior to addition. Each reaction tube contained 20 nM 3′ overhang dsDNA substrate. Assays were set up on ice and reactions were activated by transferring reaction tubes to 37°C and incubated for 60 min.

4.2.6. Molar ratio of PCNA binding to hExo1

Human exonuclease1 has low abundance in cells (El-Shemerly *et al*., 2005). The *in vivo* molar ratio of hExo1 to other binding partner proteins is not well clear due to the lack of properly established experimental evidence. It is therefore, imperative to understand the molar ratio binding of hExo1 to its binding partner proteins. To address this, an *in vitro* resection assay was reconstituted with purified recombinant proteins (hExo1 and PCNA). Proteins were added to the reaction in a molar ratio of hExo1 to PCNA (trimer) 1:0.5 to 1:10. From the assay result (*Fig. 4.13*) an increase in hExo1 resection activity was observed when the ratio of hExo1 to PCNA (trimer) was 1:2 which remained consistent through to ratio 1:10 (hExo1 to PCNA) (*Fig. 4.13, lanes 5-13*), no increase in hExo1 resection activity was observed when hExo1 to PCNA ratio was 1:0.5 and 1:1, lanes 3 and 4 in Figure 4.13 compared to where PCNA was not added to the reaction (*Fig. 4.13 lane 2*).

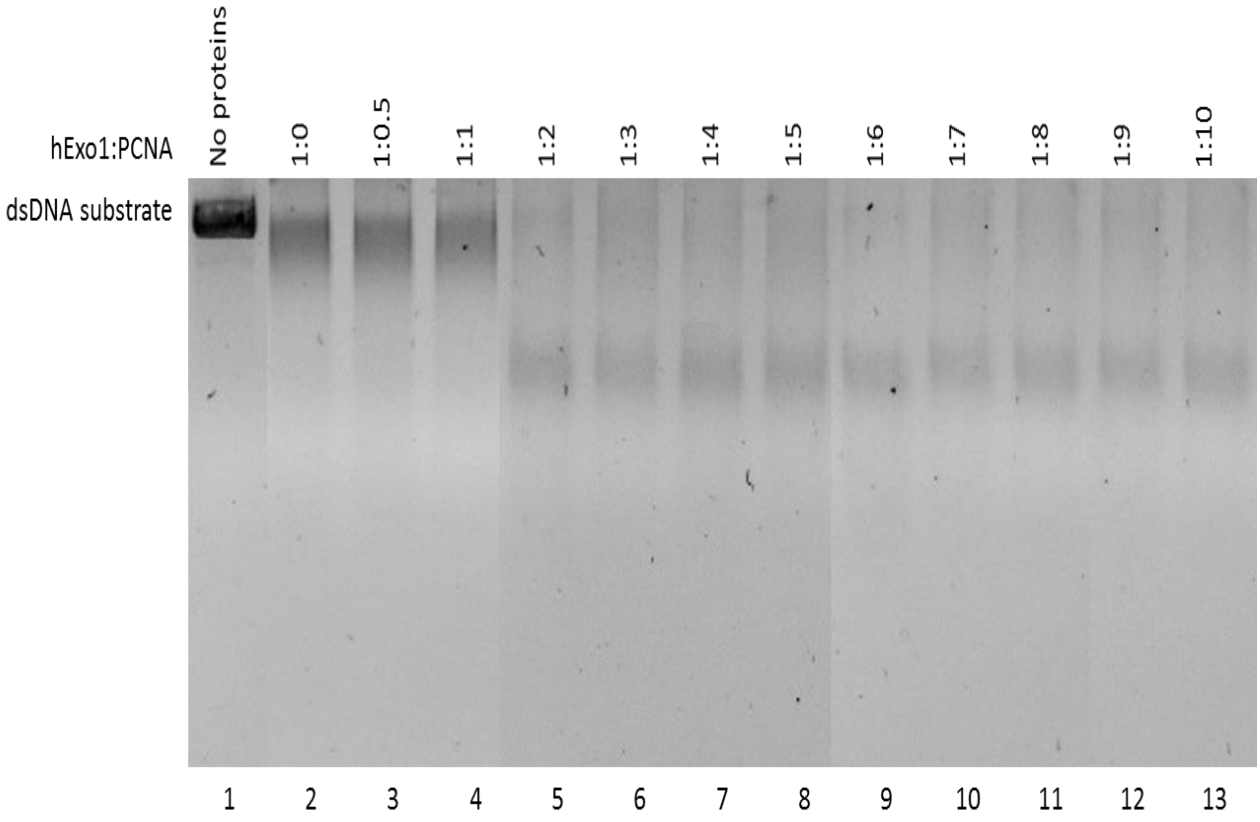


Figure 4.13. Molar ratio of PCNA binding to full length hExo1. Representative 1% agarose gel of three independent replicates of experiments showing molar ratios of PCNA binding to hExo1 in resection activities on a 3' overhang 4.8kb dsDNA substrate. Lane 1 was a substrate control; no protein was added. Lanes 2-13 contained 10 nM hExo1 and varying concentrations (molar ratio to hExo1) of PCNA as indicated on each lane.

4.2.7. Molar ratio of 14-3-3ζ binding to hExo1

To test the affinity of 14-3-3ζ binding to hExo1 and to ascertain at what molar ratio it can affect the resection activity of hExo1, *in vitro* resection assays were conducted on 4.8 kb dsDNA substrate with purified recombinant hExo1 and 14-3-3ζ. Proteins were added to the reaction in a molar ratio of hExo1 to 14-3-3ζ (dimer) 1:05 to 1:10. It was observed that 14-3-3ζ begins to inhibit hExo1 DNA end resection activity at 1:1 molar ratio (*Fig. 4.14, lane 4*), at ratio 1:0.5 14-3-3ζ did not inhibit hExo1 (*Fig. 4.14, lane 3*). 14-3-3ζ inhibition on hExo1 resection activity increases with an increase in molar ratio for 14-3-3ζ (*Fig. 4.14, lanes 5-13*).

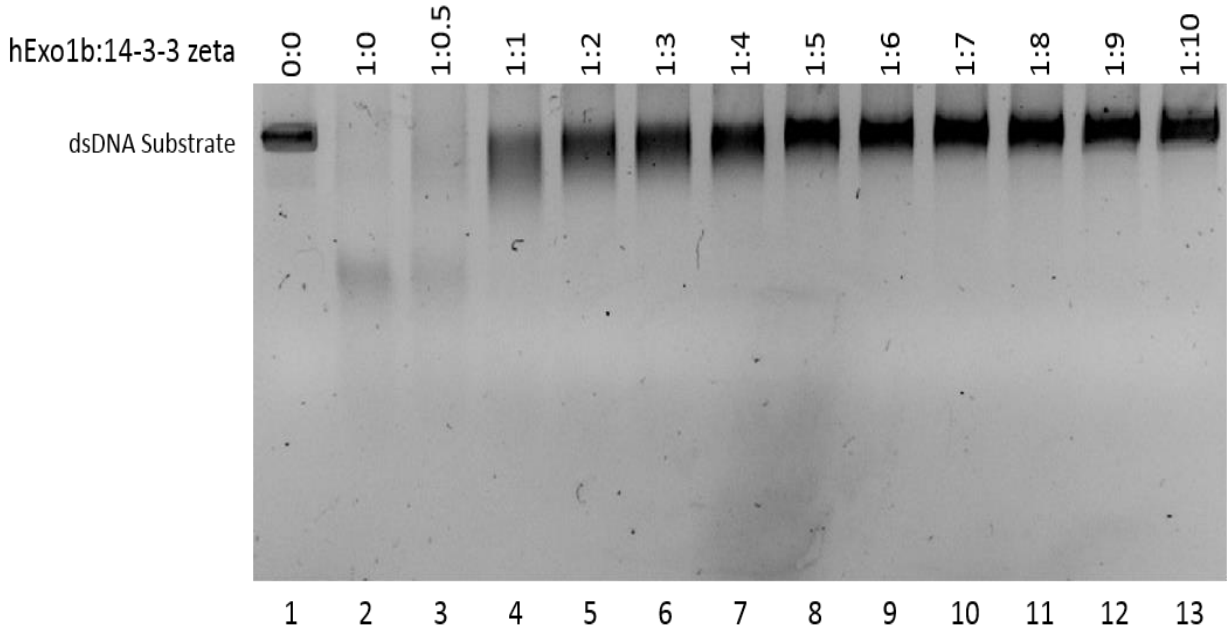


Figure 4.14. Molar ratio of 14-3-3ζ binding to full length hExo1. Representative 1% agarose gel of three independent replicates of experiments showing molar ratios of 14-3-3ζ binding to hExo1 in resection activities on a 3' overhang 4.8kb dsDNA substrate. Lane 1 is substrate control, no protein was added. Lanes 2-13 contained hExo1 and 14-3-3ζ in a molar ratio as indicated on each lane. From lane 2 to lane 13 hExo1 concentration was 20 nM in each lane. Lane 2 contained 0 nM 14-3-3ζ, from lane 3 to lane 13 contained 10, 20, 40, 60, 80, 100, 120, 140, 160, 180, 200 nM 14-3-3ζ (dimer) respectively. In each case, 30 nM DNA substrate was used.

4.2.8. Molar ratio of 14-3-3ε binding to hExo1

Next, the molar ratio of 14-3-3ε binding to hExo1 was tested. *In vitro* resection assays were carried out on 4.8 kb dsDNA substrate with purified recombinant hExo1 and 14-3-3ε. Proteins were added to the reaction in a molar ratio of hExo1 to 14-3-3ε (dimer) 1:1 to 1:10. Inhibition effect of 14-3-3ε on hExo1 resection activity was observed at 1:3 hExo1:14-3-3ε ratio (*Fig. 4.15, lane 5*), at hExo1 14-3-3ε ratio 1:1 and 1:2 14-3-3ε did not inhibit hExo1 (*Fig. 4.15, lanes 3 and 4*). The 14-3-3ε inhibition on hExo1 resection activity increases as the molar concentration increase (*Fig. 4.15, lanes 6-11*) as observed with 14-3-3ζ. These results suggests that 14-3-3ζ has a stronger affinity for hExo1 while 14-3-3ε has weaker affinity for hExo1 binding.

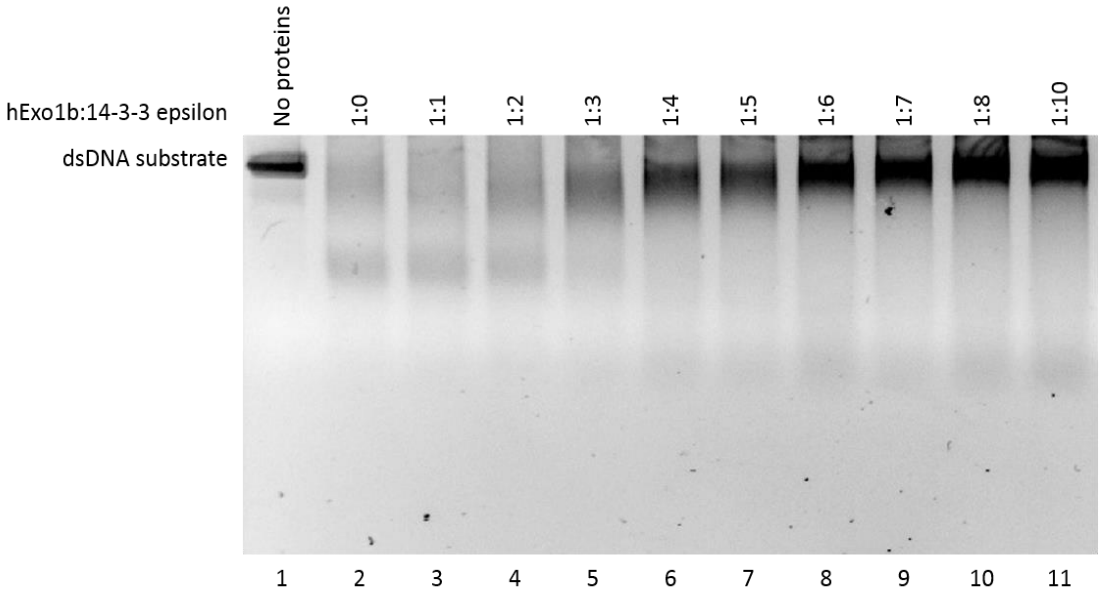


Figure 4.15. Molar ratio of 14-3-3ε to full length hExo1. Representative 1% agarose gel of three independent replicates of experiments showing molar ratios of 14-3-3Ɛ binding to hExo1 in resection activities on a 3' overhang 4.8kb dsDNA substrate. Lane 1 is substrate control, no protein was added. Lanes 2-11 contained hExo1 and 14-3-3Ɛ in a molar ratio as indicated on each lane. From lane 2 to lane 11 hExo1 concentration was 20 nM in each lane. From lane 2 to lane 11 contained 20, 40, 60, 80, 100, 120, 140, 160, 200 nM 14-3-3 epsilon (dimer) respectively. In each case, 30 nM DNA substrate was used.

4.2.9. The 14-3-3 proteins exhibit cooperative binding to hExo1

Exonuclease1 belongs to the RAD2 family of structure specific endonucleases (Lieber, 1997), the N-terminal and internal nuclease domains of which are highly conserved from bacteriophage to human (Lieber, 1997; Ceska & Sayers, 1998). Exonuclease1 possesses 5′ → 3′ exonuclease and flap endonuclease activities (Lee & Wilson, 1999) that share the same active site, with two Mg^{2+} atoms coordinated by five aspartate residues. In human exonuclease1, these are D30, D152, D171, D173 and D225 (Orans, *et al*., 2001).

From the results of *in vitro* assays conducted, this work found that 14-3-3 proteins bind to hExo1 in the C-terminal region and inhibit hExo1 DNA end resection activity (*Fig. 4.10*) but do not interact or inhibit the DNA end resection activity of the Nt-hExo1 (residue 1-391) (*Fig. 4.11*) which is the N-terminal nuclease domain of hExo1, suggestive that 14-3-3 proteins binds to other sites on hExo1 other than the active site.

The next question was whether or not hExo1 contains more than one binding site for the 14-3-3 proteins. To address this, the intensity of bands (substrate and product bands) on the gel images in Figures 4.14 and 4.15 were quantitated. The data was fitted to a cooperative ligand-binding equation (Hill equation) (Eq. 4.2) using the programme Grafit5 (Erithacus Software) to determine the equilibrium binding constant (K_d) and Hill coefficient (n) for each 14-3-3 protein. The binding curve obtained is sigmoidal (*Fig. 4.16*), which indicate that there is positive cooperative behaviour involving more than one binding site for 14-3-3 proteins on hExo1. 14-3-3ζ binds marginally tighter to hExo1 with a K_d of 67.5 nM compared to K_d of 79 nM for 14-3-3ε. Both show cooperativity (n>1) but 14-3-3ε has double the cooperativity of 14-3-3ζ: it binds ~4 dimers compared to ~2 dimers. The binding curve obtained deviated from the rectangular hyperbola (Eq. 1) behaviour instead it exhibits a sigmoidal behaviour (Eq. 2) which is an indication

that there are more than one binding sites for 14-3-3 proteins on hExo1.

$$v_0 = \frac{V_{max}[S]}{K_m + [S]} \qquad (4.1)$$

where V is the reaction velocity, V_{max} is the maximum reaction velocity, and $[S]$ is the substrate concentration. The constant K is analogous to the Michaelis constant (K_m)

$$\theta = \frac{[L]^n}{K_d + [L]^n} = \frac{[L]^n}{K_a^n + [L]^n} \qquad (4.2)$$

θ is the fraction of ligand binding sites filled, $[L]$ is the ligand concentration, K_d is the apparent dissociation constant derived from the law of mass action (equilibrium constant for dissociation), K_a is the ligand concentration producing half occupation (ligand concentration occupying half of the binding sides), that is also the microscopic dissociation constant, n is the Hill coefficient that describes the cooperativity. When $n = 1$ no cooperativity, $n > 1$ positive cooperativity and $n < 1$ negative cooperativity.

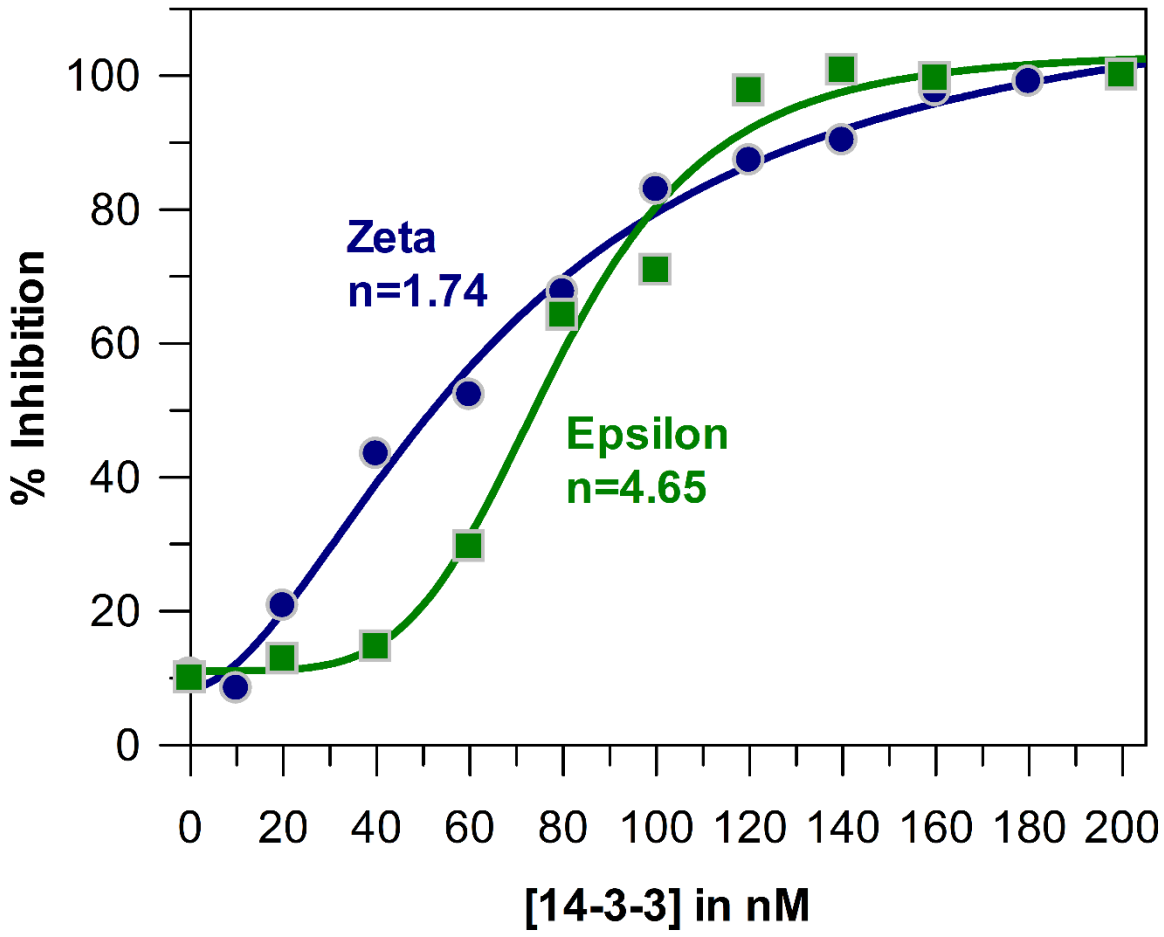


Figure 4.16. Binding curve. Cooperative binding of 14-3-3 to hExo1.

Combining these results, it can be said that hExo1 is an exonuclease enzyme that possesses 5′ → 3′ exonuclease activity and also it is specific to a 3′ overhang DNA substrate. This enzyme was temperature sensitive and exhibited instability temperature between 40^{o}C and 50^{o}C. Exonuclease activity of hExo1 was found to be enhanced by PCNA and inhibited by both 14-3-3ζ and 14-3-3ε which agrees with previous reports (Chen *et al*, 2013; Chen *et al*, 2015).

Previously, it was reported that hExo1 binds all the seven isoforms of 14-3-3 proteins (Andersen *et al*, 2012), this study found that 14-3-3 epsilon binds to hExo1 with less affinity and exhibited weaker inhibitory effect on hExo1 than 14-3-3 zeta which binds hExo1 with high affinity and exhibited stronger inhibitory effect on hExo1. These results showed that the binding sites for 14-3-3 proteins on hExo1 are situated away from the nuclease domain (active site) as seen in the resection assays using the truncated hExo1 (Nt-hExo1) in which 14-3-3 did not interact or exhibit any inhibitory effect on the resection activity of Nt-hExo1 and this confirms that 14-3-3 protein likely binds hExo1 in its C-terminal domain. This is in agreement with previous report on 14-3-3 proteins binding to central domain of hExo1 (Chen *et al*, 2015). At least 3 molecules of 14-3-3 proteins bind one hExo1 and their binding to hExo1 is cooperative, as seen from the binding curve. 14-3-3 proteins also disrupt PCNA association with hExo1, this event may rather arise from the conformational change that 14-3-3 binding can induce on hExo1 upon binding than a case of displacement as it was recently proved that 14-3-3 proteins and PCNA have different binding sites on hExo1 (Chen, *et al*., 2015).

5.0 CHAPTER FIVE: RESULTS FOR THE BIOPHYSICAL STUDIES

This chapter presents the results for biophysical studies that aimed to determine the flexibility, secondary structure content, folding, and spatial distribution of the hExo1 protein using biophysical techniques including Analytical Ultracentrifugation (AUC), Small angle X-ray scattering (SAXS), Circular Dichroism (CD) and Dynamic Light Scattering (DLS).

5.1. Characterization of proteins by Sedimentation Velocity Analytical Ultracentrifugation (SV-AUC)

Sedimentation velocity analytical ultracentrifugation (SV-AUC) technique was employed to characterize proteins (hExo1, Nt-hExo1, PCNA, 14-3-3ζ and 14-3-3ε). SV-AUC on the purified proteins allowed determination of their experimental molecular weights as presented in table 5.1. The experimental molecular weights were determined using the relationship:

$$M = SN_o(6\pi\eta R_s)/(1 - v_2\rho) \qquad (5.1)$$

M is the mass of the protein molecule in Dalton; N_o is Avogadro's number, 6.023×10^{23}; v_2 is the partial specific volume of the protein; typical value is 0.73 cm^3/g; ρ is the density of solvent (1.0 g/cm^3 for H_2O); η is the viscosity of the solvent (0.01 g/cm^{-s} for H_2O).

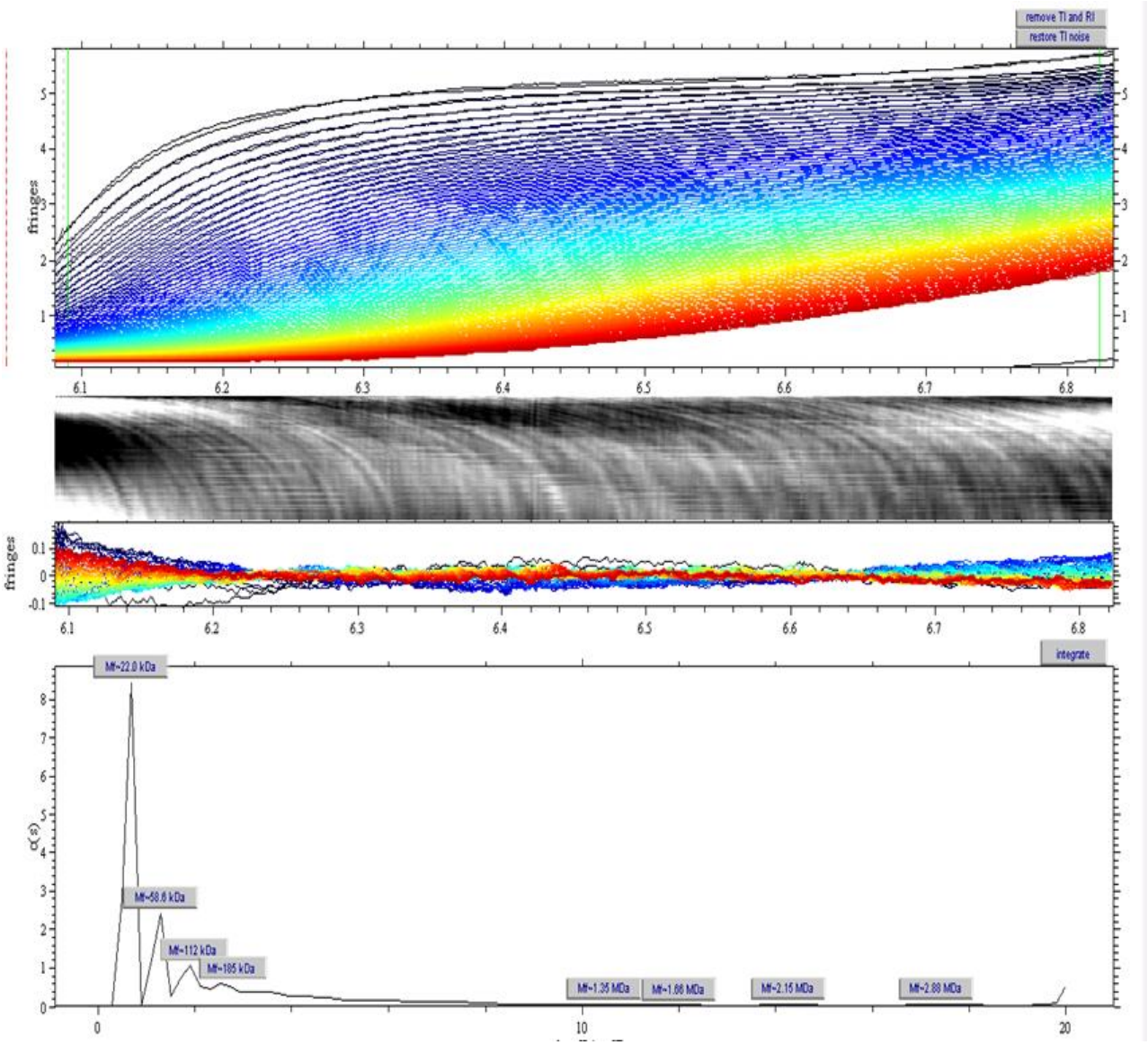


Figure 5.1. Sedimentation velocity analytical ultracentrifugation of purified hExo1. hExo1 was subjected to analytical ultracentrifugation experiment in 20 mM HEPES at pH 7.5, 100 mM potassium chloride, 1 mM EDTA and 10% (v/v) glycerol at a concentration of 1 mg/mL at 4°C with cells scanned every 10 minutes for 8 hours. Data was fit to the continuous distribution model to obtain the experimental molecular weight, Stokes radius and frictional ratio of hExo1. Raw data from the time-course measurement of interference of the sample along the sample cell length (Upper plot). Residuals after fitting the data to the continuous size distribution model (Middle plot). Sedimentation coefficient distributions c(s) calculated from the sedimentation profile (Lower plot). The sedimentation coefficient axis has been corrected for buffer conditions.

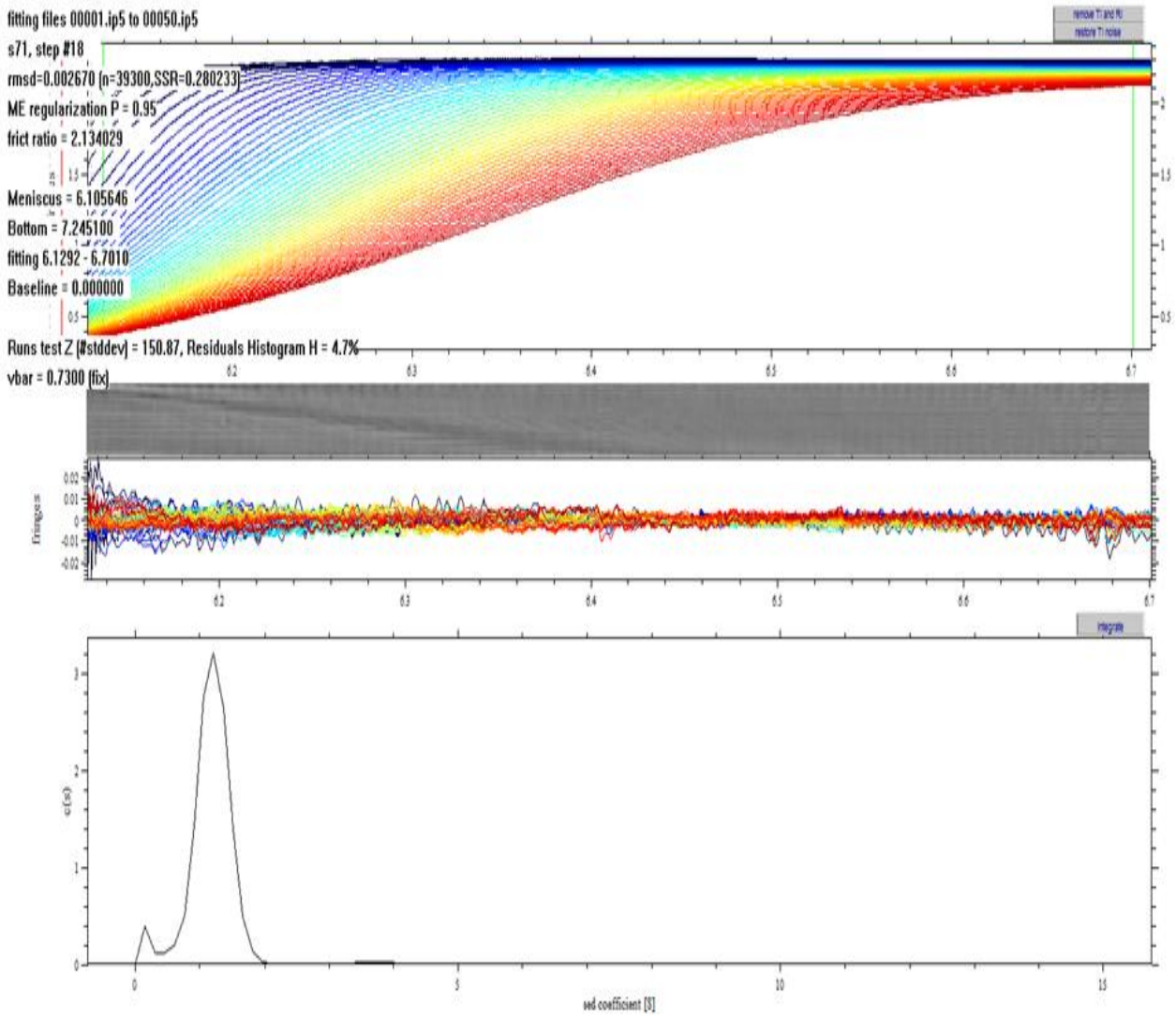


Figure 5.2. Sedimentation velocity analytical ultracentrifugation of purified Nt-hExo1. NtΔhExo1 was subjected to analytical ultracentrifugation experiment in 20 mM HEPES at pH 7.5, 100 mM potassium chloride, 1 mM EDTA and 10% (v/v) glycerol at a concentration of 1 mg/mL at 4°C with cells scanned every 10 minutes for 8 hours. Data was fit to the continuous distribution model to obtain the experimental molecular weight, Stokes radius and frictional ratio of hExo1. Raw data from the time-course measurement of interference of the sample along the sample cell length (Upper plot). Residuals after fitting the data to the continuous size distribution model (Middle plot). Sedimentation coefficient distributions c(s) calculated from the sedimentation profile (Lower plot). The sedimentation coefficient axis has been corrected for buffer conditions.

With the calculated molecular weight of 112 kDa, this result confirms that hExo1 exists as a monomer, PCNA as trimer and both 14-3-3ζ and 14-3-3ε as dimers in solution, with 14-3-3ε showing an evidence of tetramer and hexamer. SV-AUC also allows calculation of the Stokes radius of the samples, which represents the hydrodynamic radius (R_H) of a protein molecule. From the SV-AUC data, the R_H of proteins were calculated (Table 5.1). The frictional ratio (f/f_0) of proteins were also calculated from the SV-AUC data (Table 5.1). Frictional ratio is an indicator of size and shape of a protein. Empirically, it has been reported that a frictional ratio of around 1.2 to 2.0 are exhibited by a nearly globular protein, whereas an elongated or branched protein has a frictional ratio of 2.0 to 3.0 (Erickson, 2009).

Proteins	**Experimental Molecular Weight (kDa)**	**Stoke Radius (Å)**	**Sedimentation Coefficient (S)**	**Frictional ratio (f/f_0)**
hExo1 (Monomer)	20.0, 56.8 and 110.	112	0.9	3
Nt-hEXo1 (Monomer)	64	84.57	1.8	2.15
PCNA (Trimer)	85.5	55.86	3.5	1.42
14-3-3ζ (Dimer)	63.2	61.1	2.7	1.5
14-3-3ε (Dimer)	61.7	53	2.7	1.3

Table 5.1. Calculated SV-AUC experimental parameters

Another parameter to look at in an SV-AUC experiment was the sedimentation coefficient (S). The rate at which the sedimentation boundary moves is a measure of the sedimentation coefficient (S) of the protein. The sedimentation coefficient depends on the molecular weight (larger proteins sediment faster) and also on molecular shape. Unfolded proteins or one with highly elongated shapes will experience more hydrodynamic friction, and thus will have smaller sedimentation

coefficients than a folded, globular protein of the same molecular weight (http://www.ap-lab.com/sedimentation_velocity.htm). The sedimentation coefficient of each of the proteins is presented in table 5.1.

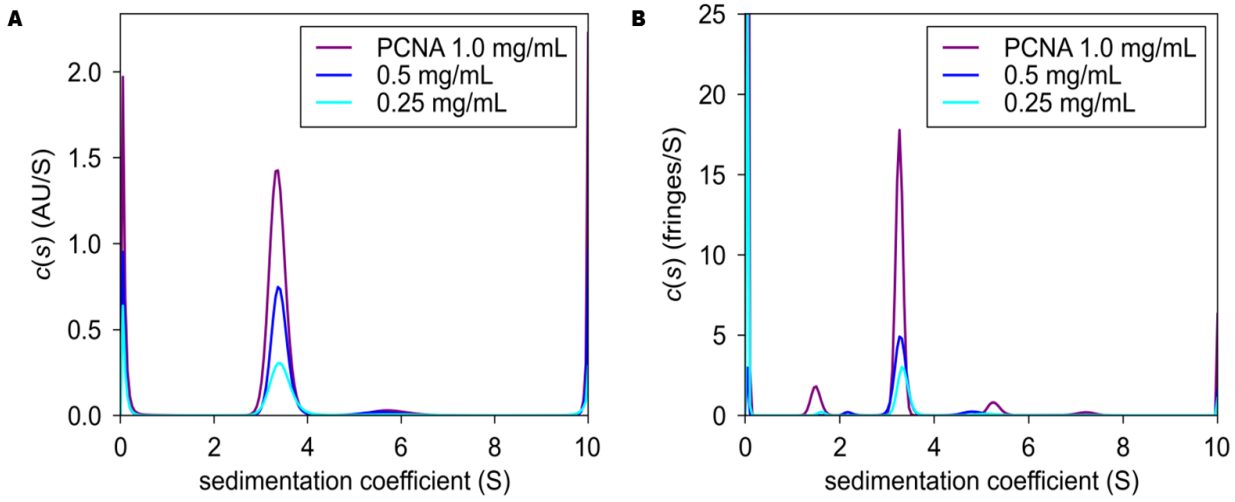


Figure. 5.3. Sedimentation coefficient distributions c(s) for PCNA calculated from the absorbance sedimentation profile (A) and interference sedimentation profile (B) for three different concentrations of PCNA protein. The sedimentation coefficient axis has been corrected for buffer conditions.

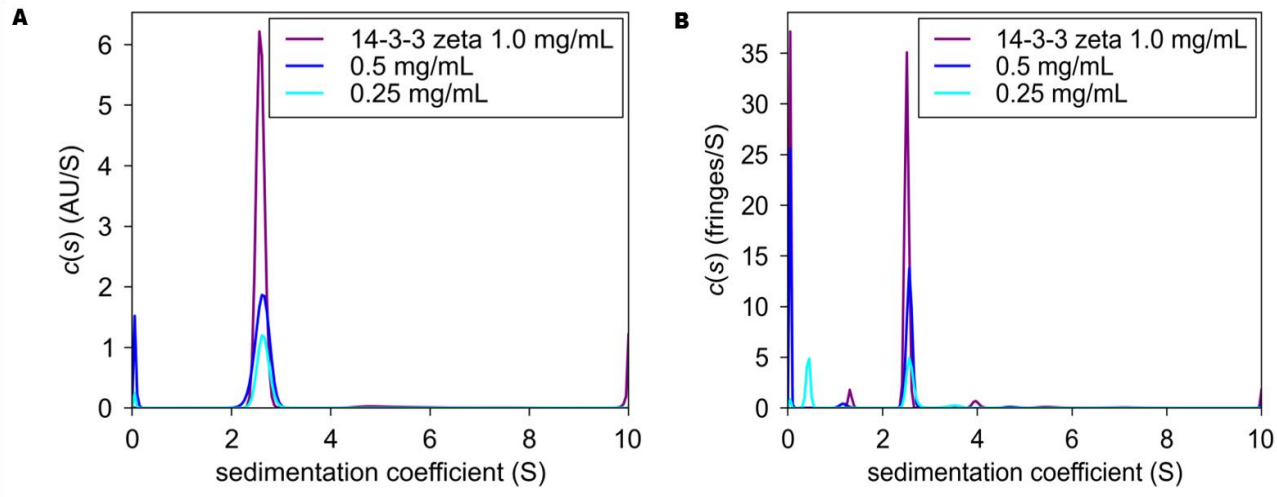


Figure. 5.4. Sedimentation coefficient distributions c(s) for 14-3-3 zeta calculated from the absorbance sedimentation profile (A) and interference sedimentation profile (B) for three different concentration of 14-3-3 zeta protein. The sedimentation coefficient axis has been corrected for buffer conditions.

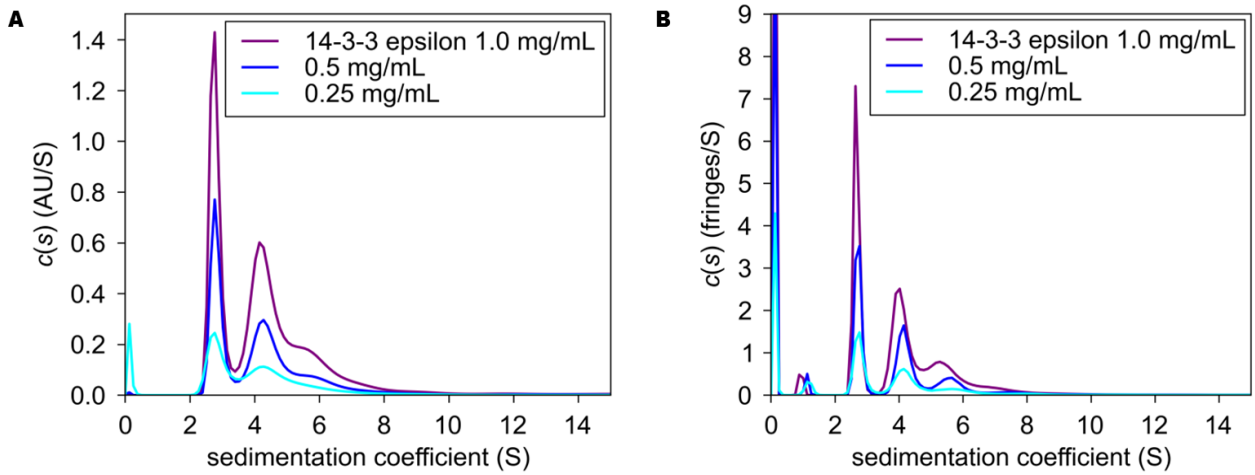


Figure. 5.5. Sedimentation coefficient distributions c(s) for 14-3-3 zeta calculated from the absorbance sedimentation profile (upper plot) and interference sedimentation profile (lower plot) for three different concentration of 14-3-3 zeta protein. The sedimentation coefficient axis has been corrected for buffer conditions.

From these results, it can be suggested that hExo1 is an intrinsically partially disordered monomeric protein that persists in a heterogeneous ensemble of partly elongated prolate forms. It has an expanded R_H compared to folded proteins of the same length. In studies of intrinsically disordered proteins, this solvated radius has routinely been obtained (Adkins & Lumb, 2002; Kalthoff *et al*., 2002; Denning *et al*., 2003; Sanchez-Puig *et al*., 2005; Batra-Safferling *et al*., 2006; Paz *et al*., 2008; Rajasekar *et al*., 2010) from size-exclusion chromatography experiments by comparing its elution characteristics with those for globular proteins with defined Stokes radii (Laurent & Killander, 1964; Siegel & Monty, 1966).

The frictional ratio (f/f_0) is a structure parameter that can be obtained independent of the molecular mass, is the ratio of the Stokes radius to its unsolvated counterpart (R_u). In that case, a larger friction ratio is indicative of protein asymmetry. Nonetheless, as proteins are constantly hydrated to certain degree, the Stokes radius give forth another contribution to solute volume. Therefore, a larger frictional ratio for globular proteins indicates asymmetry. Traditionally, the frictional ratio

values for intrinsically disordered proteins are relatively high: 2.8 for nucleoporin (Denning *et al*., 2003), 2.1 for securing (Sanchez-Puig *et al*., 2005), 1.9 for KorB (Rajasekar *et al*., 2010), 1.6 for neuroligin (Paz *et al*., 2008) and 2.23 for CasSD (Hotta, *et al*., 2014). From all the calculated SV-AUC experimental parameters it can be seen that the nuclease domain of hExo1 (Nt-hExo1) exhibited a different characteristics from that of the full length hExo1, with the frictional ratio less than that of full length (2.15 compared to 3), stoke radius of 84.57 Å compared to 118 Å for the full length and sedimentation coefficient (S) of 1.8 compared to 0.9 for the full length (*Figs. 5.1, 5.2*), with these it can be suggested that the nuclease domain of hExo1 (Nt-hExo1) is more compact than the full length.

Whether the higher values of f/f_0 reflect asymmetry of a compact protein or a larger value of δ (the extent of solvation) for an unstructured species cannot be determined by analytical ultracentrifugation. Instead, spectral techniques such as small-angle X-ray scattering (SAXS) circular dichroism (CD) and nuclear magnetic resonance (NMR), must be used to obtain evidence of any regular and rigid structure. Failure to detect such characteristics (regular and rigid structure) of detailed structure has thus provided the major criterion for classifying the macromolecules under consideration as intrinsically disordered proteins (Tompa, 2010; Uversky & Longhi, 2010).

5.2. Characterization of proteins by Small Angle X-ray Scattering (SAXS)

To ascertain whether or not the higher values of f/f_0 reflect asymmetry of a compact protein or a larger value of δ (the extent of solvation) for an unstructured species small angle x-ray scattering was employed to further characterize hExo1 and Nt-hExo1.

For proteins randomly oriented in solution, all configurations of the macromolecule are sampled during the experiment and the scattering profile is azimuthally symmetric around the primary beam. Because the signal difference between buffer and protein is small, the scattering profile of the buffer solution must be subtracted from that of the protein. This also removes background due to parasitic scattering of the primary beam, a ''halo'' of X-rays surrounding the primary beam, and ultimately the limiting factor on the smallest angles attainable at a given instrument. The scattering profile is dependent on the size and shape of the macromolecule and is a unique ''signature'' of the protein. In their study of the protein data bank, Sokolova and co-workers have shown that no two unique structures have identical calculated scattering profiles (Sokolova *et al*., 2003a,b).

The first step in analyzing SAXS data is to assess the scattering data using model-independent methods. This also gives an insight into the quality of data and might also unveil the effects of concentration or aggregation in the data. The first characteristics that are usually inferred from scattering data without requiring any modeling are radius of gyration, Kratky plot ($q^2I(q)$ vs. q), which directly reports on the compact or unstructured nature of the polypeptide chain and distance distribution function P(r), which is the histogram of the distances within a protein.

The radius of gyration is the first parameter yielded by SAXS and provides information on the average size of the scattering object in

solution. Because IDPs are prone to adopt large extended conformations, the radius of gyration is a particularly relevant parameter to evaluate an IDP using SAXS. To determine the radius of gyration for the hExo1 and Nt-hExo1 proteins from the SAXS data collected at Diamond (BL21), 18 X-ray exposures for each of samples and buffer were first averaged and buffer scattering subtracted from samples scattering.

Using the program ScÅtter for SAXS analysis, experimental SAXS curves were plotted and the scattering pattern for each of the samples (different concentration), buffer and buffer-subtracted samples was determined (Fig. 5.6 A, B, C and D; Fig. 5.7 A and B). Using the Guinier approximation, the radius of gyration for each of the different sample concentration was calculated from the experimental SAXS curves (Table 5.2)

Sample	**Concentration (mg/mL)**	**Calculated R_g**
hExo1	1.25	75.4
	2.5	75.2
	5	80.3
	7.5	75.6
Nt-hExo1	1.25	42.4
	2.5	47.6

Table 5.2. The calculated radius of gyration for hExo1 and Nt-hExo1

The Kratky plot gives an insightful representation of the scattering intensity for a quick assessment of the globular nature of a polypeptide chain. The Kratky plot plots the scattering pattern as $q^2I(q)$ versus q. For a globular protein with a well-defined solvent accessible surface, the scattering intensity $I(q)$ follows the Porod law and decreases as q^{-4} in the large q region. As a result, the corresponding Kratky plot exhibits a typical bell-shape with a well-defined maximum. In contrast, the scattering intensity for a random chain has a limiting behaviour of q^{-2} at high q, as indicated by the Debye law. The Kratky plot of a fully

unfolded protein will exhibit a plateau in *q* region, sometimes followed by an increase as *q* increases, depending on the local rigidity of the chain. Regardless, this representation is incapable to discern between fully folded and partially unfolded proteins containing structured regions of significant size, which also results in bell-shaped Kratky plots.

Therefore, it is highly recommended to plot a dimensionless Kratky plot (Durand, *et al*., 2009). In this dimensionless Kratky plot, the intensity $I(q)$ is normalized to the forward scattering intensity $I(0)$, and *q* is normalized to the radius of gyration of the protein. Multiplying *q* by the radius of gyration makes the angular scale independent of protein size, while $I(q)$ divided by $I(0)$ becomes independent of the molecular weight of the protein as $I(0)$ is proportional to the molecular weight. This normalization enables the comparison between a Kratky plots of globular and unstructured proteins, irrespective of their size, and this will infer an insightful information from this representation. For a globular protein, the scattering pattern in a normalized Kratky plot manifests a maximum value of 1.104 for $qR_g=\sqrt{3}$, regardless of the protein size (Fig 5.8). While for unstructured protein, the curve rises with increasing angle to reach a nearly flat region at a value between 1.5 and 2 followed at high *q* values (typically $q > 0.2\text{-}0.3$ $Å^{-1}$) by a further increase depending on the rigidity of the polypeptide chain (*Fig. 5.8*).

Dimensionless Kratky plots of partially unstructured proteins exhibits distinctive intermediate profiles between the two extremes (*Fig. 5.8*). From the experimental SAXS data for hExo1 and Nt-hExo1 a dimensionless Kratky plot was plotted with ScÅtter program. From the plot, hExo1 protein exhibited the behaviour of a multi domain comprising a compact and an extended domains (*Fig. 5.9A*) while Nt-hExo1 exhibited the behaviour of a partially folded protein (*Fig. 5.9B*).

Several intrinsically disordered proteins have been characterized biophysically with scattering techniques, MeCP2 62.5 ± 4.5 Å (Yang *et*

al., 2011), Msh6 N-term 56 ± 2 Å (Shell *et al*., 2007), Ki-1/57 47.5 ± 1.0 Å (Bressan *et al*., 2008), Synthetic Resilin 50 ± 5 Å Nairn *et al* 2008) and Tau ht40 65 ± 3 Å (Mylonas, *et al* 2008). In all these cases, a monotonic increase in Kratky plots as well as large R_g values and expanded $p(r)$ functions with very large D_{max} values were the key SAXS features used to identify intrinsically disordered proteins.

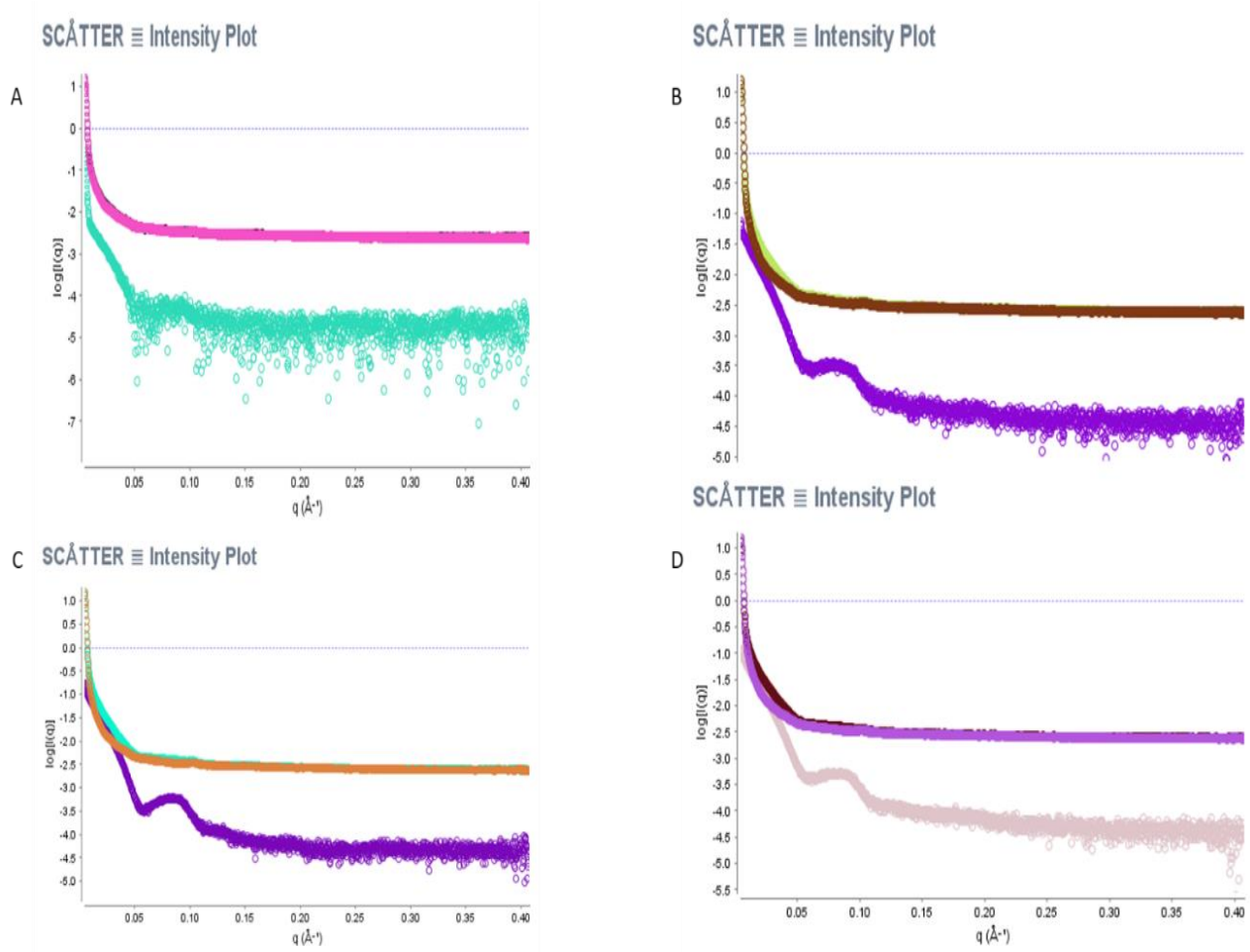


Figure 5.6. SAXS scattering curves. SAXS scattering profiles for hExo1 protein measured at BL21 (Diamond) in 20 mM HEPES, pH 7.5, 100 mM KCl and 10% glycerol. Solvent scattering and the difference curve (containing the contribution from the protein alone, scaled for the solute concentration). (A) Scattering profile for 1.25 mg/ml hExo1 sample, buffer only (pink), sample (purple) and scattering from buffer-subtracted sample (aqua). (B) Scattering profile for 2.5 mg/ml hExo1 sample, buffer only (brown), sample (green-yellow) and buffer-subtracted sample (purple). (C) Scattering profile for 5 mg/ml hExo1 sample, buffer only (chocolate), sample (aqua) and buffer-subtracted sample (purple). (D) Scattering profile for 7.5 mg/ml hExo1 sample, buffer only (violet), sample (maroon) and buffer-subtracted sample (thistle).

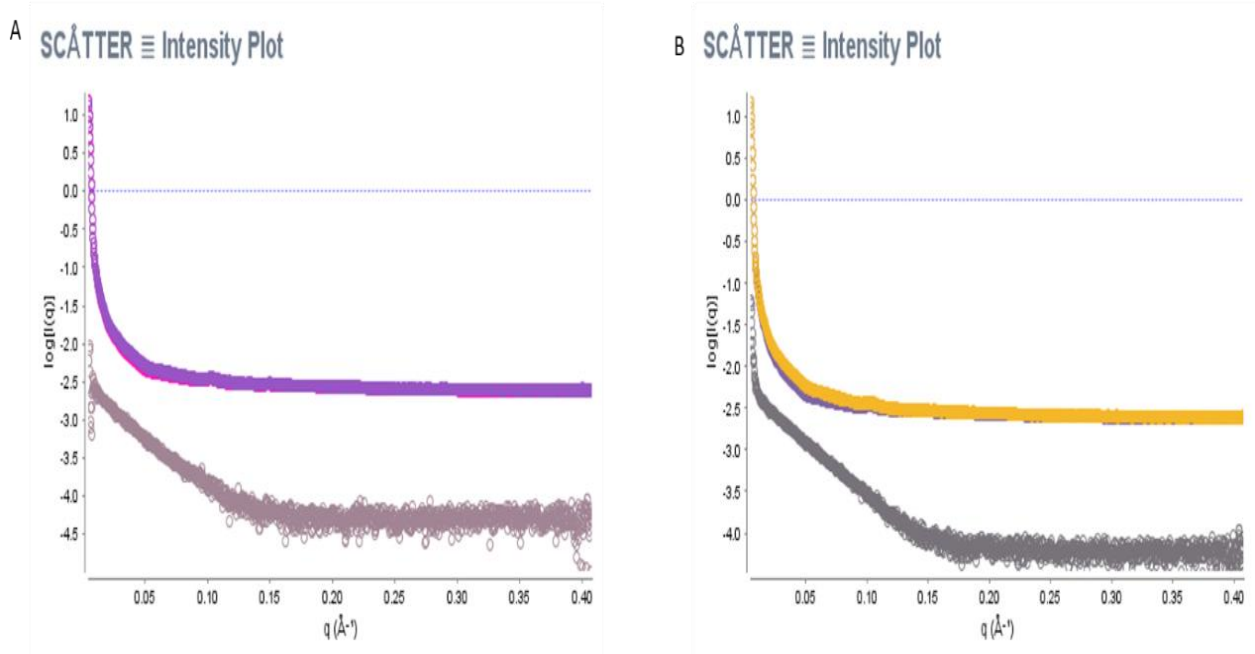


Figure 5.7. SAXS scattering curves. SAXS scattering profiles for NΔhExo1 protein measured at BL21 (Diamond) in 20 mM HEPES, pH 7.5, 100 mM KCl and 10% glycerol. Solvent scattering and the difference curve (containing the contribution from the protein alone, scaled for the solute concentration). (A) Scattering profile for 1.25 mg/ml NΔhExo1 sample, buffer only (purple), sample (pink) and scattering profile for buffer-subtracted sample (grey). (B) Scattering patterns from 2.5 mg/ml NΔhExo1 sample, buffer only (yellow), sample (purple) and buffer subtracted sample (dark grey).

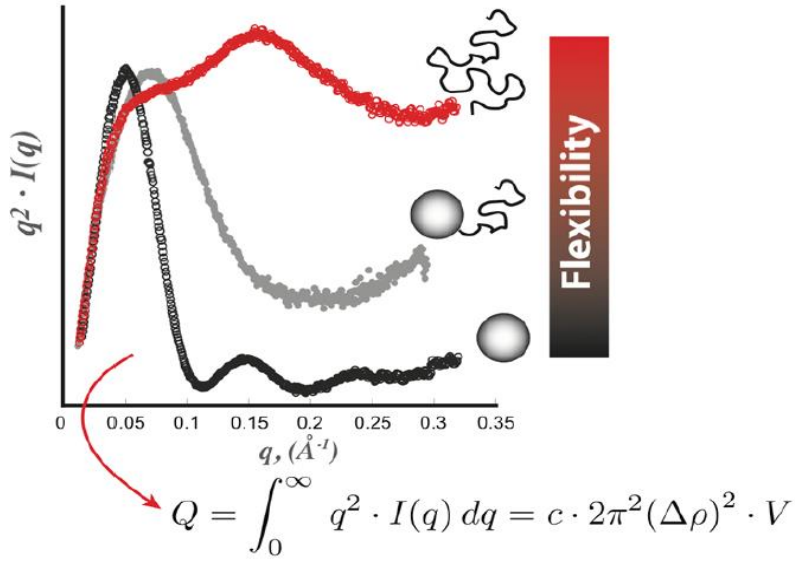


Figure 5.8. Kratky plot of scattering data illustrating changes in the behaviour of the curve for folded (sphere), partially folded (sphere-random coil) and completely unfolded particles (random coil). For a folded particle, the integrated area under the curve determines the Porod invariant, Q, and is scaled by concentration, c. **(Figure Copied from Rambo and Tainer, 2011)**

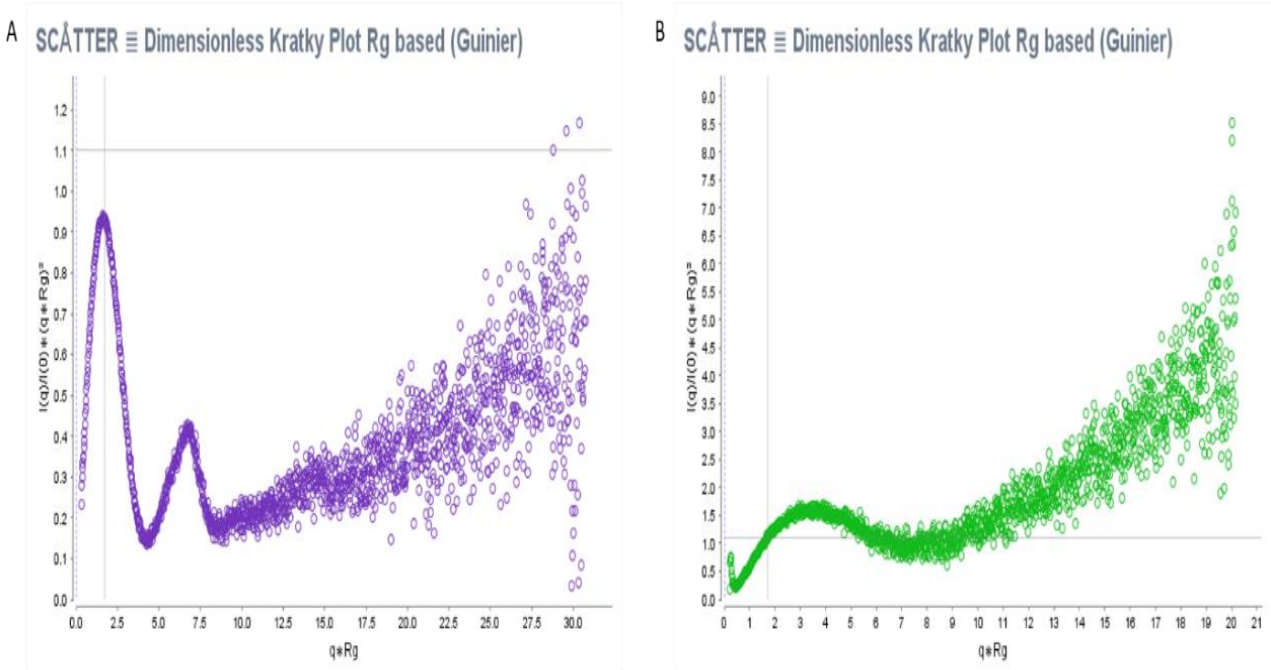


Figure 5.9. Normalised Kratky plots. Normalised Kratky plot from the experimental scattering data illustrating changes in the behaviour of the curve for hExo1 in (A) and Nt-hExo1 in (B).

The Guinier law can theoretically be applied to any particle whatever its shape. The radius of gyration is inferred from the slope of the Guinier plot, which represents the logarithm of the scattering intensity versus q^2. A Guinier plot is only linear over a restricted region (*Fig. 5.10*) of the scattering spectrum: $qR_g < 1.0$. This region may sometimes be extended to $qR_g < 1.3$ for well-folded proteins, but for an IDP, the region is actually reduced to $qR_g<0.8$ and is sometimes even smaller (Putnam, *et al*., 2007; Moncoq, *et al*., 2004) because of the multiple sizes adopted by an IDP. Therefore, there may only be a few usable points in the experimental spectrum, thus limiting the accuracy of the measured R_g. From the comparison between the Guinier fitting for the experimental SAXS data (*Fig. 5.10*) and the reference Guinier fitting (*Fig. 5.11*), the presence of aggregates was detected in both hExo1 and Nt-hExo1 samples. This is in agreement with the SV-AUC experiment in which aggregation was detected in both samples. Scattering from aggregated samples strongly influence the entire data set, it is therefore strongly advised not to rely on interpreted data set from aggregated samples.

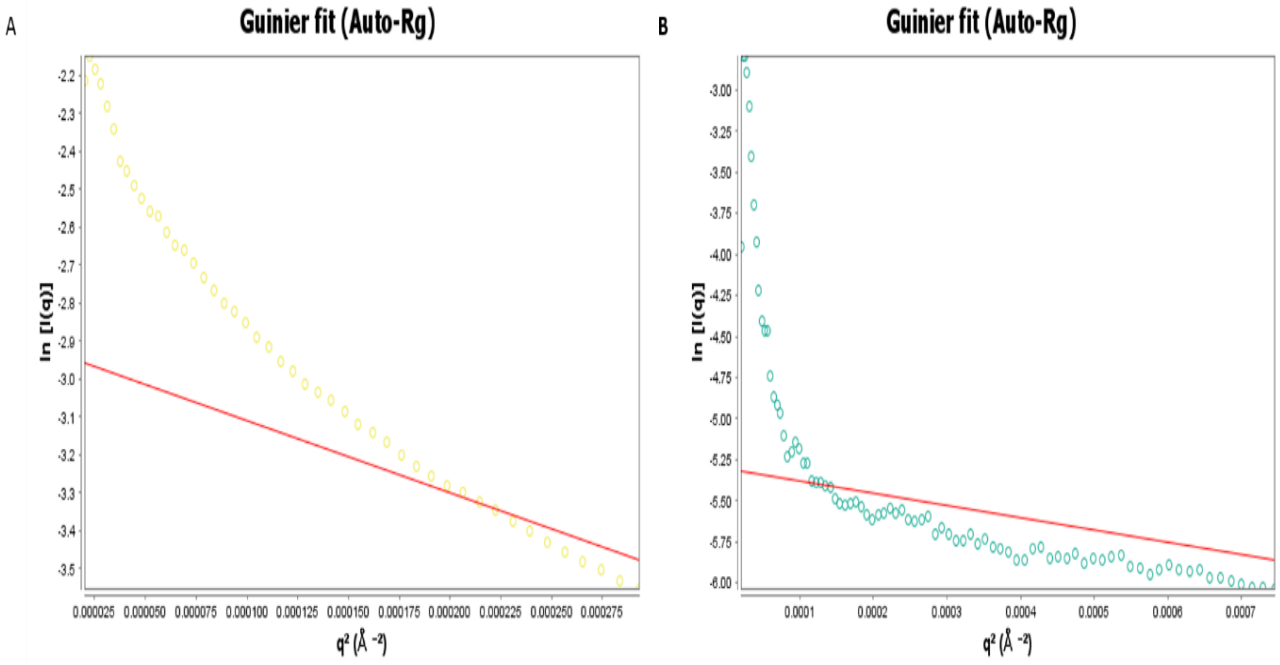


Figure 5.10. Guinier fit plots. Guinier fit plot for hExo1 (A) and Nt-hExo1 (B) SAXS results directly discerned aggregation based on low angle Guinier regions for the two protein samples (hExo1 and Nt-hExo1).

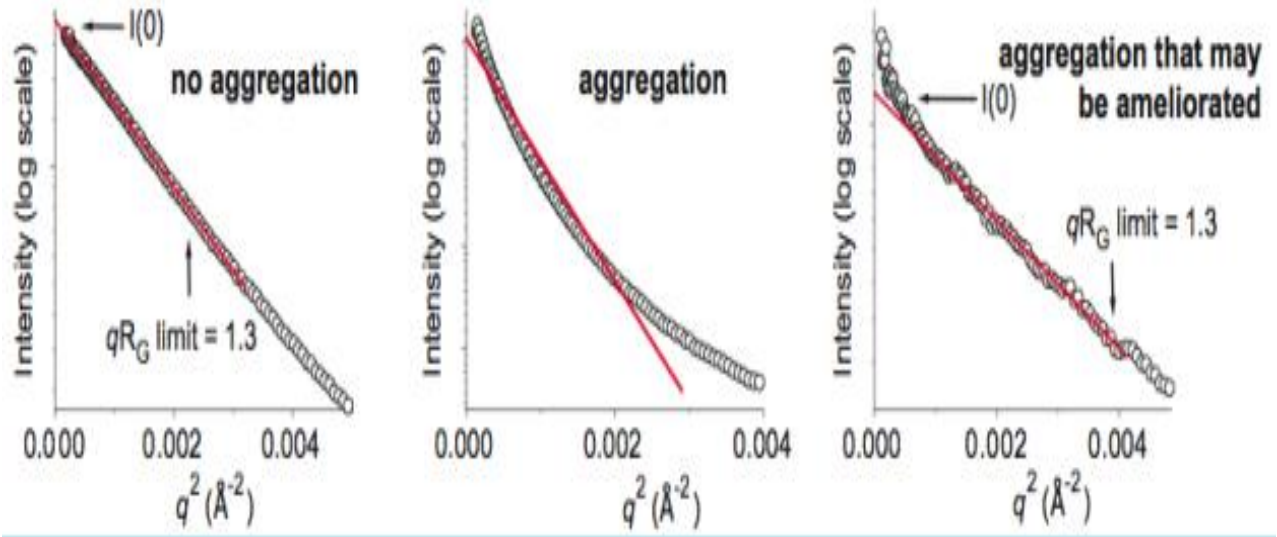


Figure 5.11. Guinier plot. A non-linear dependence of log (I(q)) vs q^2 indicates the presence of aggregation. (Copied from http://bioisis.net)

5.3. Characterization of proteins by Circular Dichroism (CD) Spectroscopy and Dynamic Light Scattering (DLS).

As the SAXS data analysis for hExo1 and Nt-hExo1 cannot be relied upon due to the poor quality of the data and the presence of aggregates as detected from Guinier fitting, further biophysical analysis was required to characterize hExo1 and Nt-hExo1 to determine whether or not hExo1 was intrinsically disordered protein or partly disordered. To address this, Circular Dichroism (CD) Spectroscopy and Dynamic Light Scattering (DLS) techniques were employed to further characterize proteins. This work was carried out at Diamond Light Source (Beamline B23) UK.

The interaction properties of hExo1, 14-3-3ζ, 14-3-3ε and PCNA proteins, were studied by CD spectroscopy and DLS measuring first the proteins alone, their binary and ternary combinations and finishing with their quaternary mixture.

The model of hExo1 predicted from amino acid folding propensity consists of two domains, a long extended tail (150 amino acids) and a globular core, Nt-hExo1, which showed a CD spectrum indicative of a significant α-helix content (*Fig. 5.12A*) that was estimated to be 23% (Table 5.2). Nt-hExo1 was also found to be lesser photo-stable (*Fig. 5.13A*) than the other proteins, hExo1, 14-3-3ζ, 14-3-3ε and PCNA under the same condition of UV irradiation conducted in four consecutive repeated scans (data not shown).

The striking aspect of the CD spectrum of hExo1 was its very small overall intensity with a magnitude range of just 0.8 mdeg that compared to those of the other proteins of figure 1A with the same concentration of about 0.3 mg/ml in a 0.05cm pathlength cell was about 40 to 120 times smaller. Such a small intensity could be the result of cancellation between spectral features of almost opposite sign.

In figure 5.13A, the zoomed spectra of hExo1 and Nt-hExo1, first and forth scan, revealed the same crossover at about 202nm. For comparison, the spectrum of hExo1 was normalized to that of Nt-hExo1 at about 210nm by multiplying the latter by 42.7 (*Fig. 5.13A*). The spectra were super-imposable in the 195-210nm region (crossover at about 200nm) but not in the 220-240nm region, likely due to different aromatic side-chain CD contributions. From these clues, it is conceivable to assume that Nt-hExo1 retains the same folding (23% α-Helix, 26% β-Strand, 21% Turn and 29.8% Unordered, see Table 5.2) in the full protein (hExo1), behaving as a proper domain.

In view of this, the subtraction of the CD spectrum of Nt-hExo1 (1st scan) from that of the full protein (hExo1) revealed the CD spectrum of the remaining hExo1 protein, the extended tail (Fig. 5.13B) that was estimated to be 44.6% β-strand, 21.1% Turn and 33.9% Unordered (Table 5.2). Another way of look at it is that the right handedness of the α-Helix and β-Strand conformations (Pauling & Corey, 1951) of the globular domain of hExo1 (N-terminal) was cancelled by the left-handedness of the β-Strand, polyproline of type II and turn of type II conformations (Adzhubei & Sternberg 1993; Doose, *et al*., 2007; Moradi, *et al*., 2009) of the extended tail (C-terminal) of hExo1 protein. As a result, the CD of these two domains mirroring each other resulting in the very small intensity CD spectrum observed for hExo1 (*Figs. 5.12 and 5.14*).

For each of the following binary mixtures at 1:1 molar ratios: hExo1+14-3-3ε, hExo1+14-3-3ζ and hExo1+PCNA, the diameter size measured by DLS was found to be intermediate between the sizes of the individual proteins for each of the corresponding binary combinations (*Fig. 5.14B*, Table 5.3). Protein hExo1 appeared to be in a soluble associated form (aggregate) of 396nm (*Fig. 5.12B*) that reverted to the 7.5-11.7nm range when interacting with the other proteins as binary and ternary complexes (*Fig. 5.14B*). The fact that

the globular domain of hExo1, the Nt-hExo1 retained the same size as that of full protein (hExo1) (*Fig. 5.12B*, Table 5.2) was ruling out the extended tail as the cause of the protein large association.

Interestingly the less photo-stable Nt-hExo1 4th scan revealed an even larger association form (825nm) (*Fig. 5.12B*, Table 5.3). On the other hand, the size of PCNA (10.1nm) and epsilon (7.5nm) being bigger than that of zeta (4.5nm) despite all having similar molecular weights was implying that PCNA was a trimer, 14-3-3ε was dimers whilst 14-3-3ζ was a monomer (*Fig. 5.12B*, Table 5.3). The observed CD spectra of the binary complexes were slightly smaller than those calculated from the sum of the corresponding individual proteins indicating that the small spectral changes were related to small folding losses upon the formation of the binary complexes (*Fig. 5.14A*).

Analogously for the following ternary mixtures: hExo1+14-3-3ε+PCNA, hExo1+14-3-3ζ+PCNA and hExo1+14-3-3ε+14-3-3ζ, the diameter size measured by DLS was also found to be intermediate between the sizes of the individual proteins for each of the corresponding ternary combinations (*Fig. 5.15D*, Table 5.3) being consistent with the formation of ternary complexes. For each of the ternary complexes, the CD spectra were compared to various simulated spectra obtained in different manners: the sum of 3 individual proteins and the sum of various binary complexes with the third missing protein as illustrated in figures 5.15A, 5.15B and 5.15C. Although the differences between the observed and simulated spectra were small like the one observed for the binary complexes, the ternary complex hExo1+14-4-4ε+PCNA, nevertheless, showed bigger differences than hExo1+14-3-3ζ+PCNA with hExo1+14-3-3ε+14-3-3ζ the least (*Figs. 5.15A, B and C*).

For the quaternary mixture of hExo1 with 14-3-3ζ and 14-3-3ε and PCNA the size was also found to be intermediate between the individual proteins (*Fig. 5.16B*), though, not as clear cut discriminating as for the

binary (*Fig. 5.14B*) and ternary complexes (*Fig. 5.15D*). The size of the quaternary mixture of 7.5nm was the same as that of 14-3-3ε indicating that the quaternary mixture could be a mixture of the ternary complex hExo1+14-3-3ζ+PCNA (1:1:1) and 14-3-3ε (1), though the peaks of quaternary mixture and epsilon are not quite superimposed. On the other hand, the observed CD spectrum was significantly smaller than the three simulated spectra from different ternary combinations and mixture of individual proteins (*Fig. 5.16A*) was more consistent with the formation of a quaternary complex.

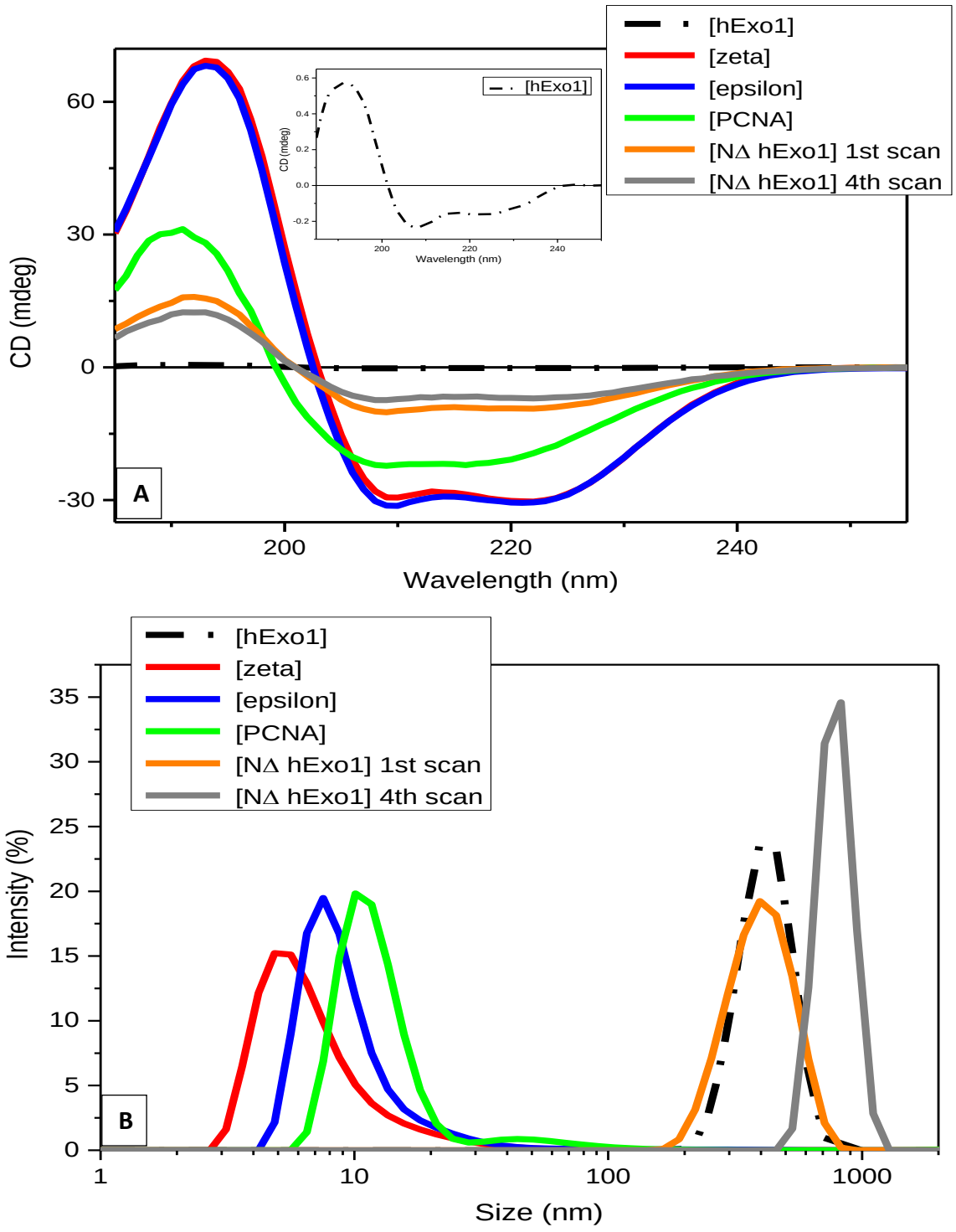


Figure 5.12. Far-UV CD spectra (**A**) and DLS data size in nm (**B**) of hExo1 (dash-dot black), 14-3-3ζ (red), 14-3-3ε (blue), PCNA (green), Nt-hExo1 1st scan (orange) and Nt-hExo1 4st scan (grey). The insert of **A** is the far UV CD spectrum of hExo1 (dash-dot black) zoomed to show the helical features despite the small intensity of the spectrum that with the larger scale is not visible.

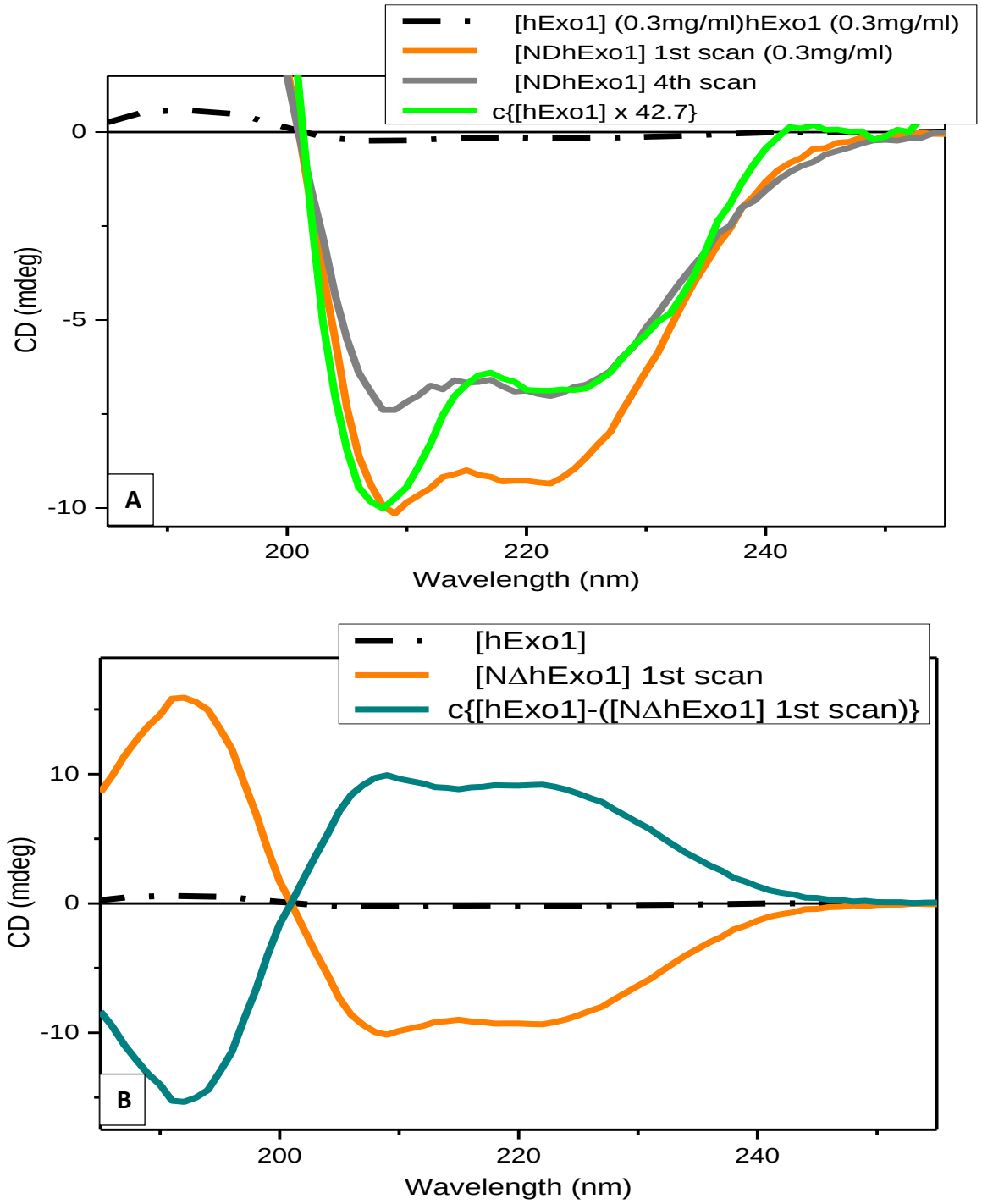


Figure 5.13. **A**) Far CD spectra of hExo1 (dash-dot black) and Nt-hExo1 (orange) and Nt-hExo1 (grey), and normalised spectrum of hExo1 calculated by multiplied by 42.7 factor (c[hExo1] x 42.7) (green) at smaller scale to highlight the identical crossover. **B**) Far-UV CD spectra of hExo1 (dash-dot black), Nt-hExo1 1st scan and the simulated spectrum of the extended tail of hExo1 (c x hExo1 - Nt-hExo1 aqua) calculated by subtracting the spectrum of Nt-hExo1 from that of hExo1.

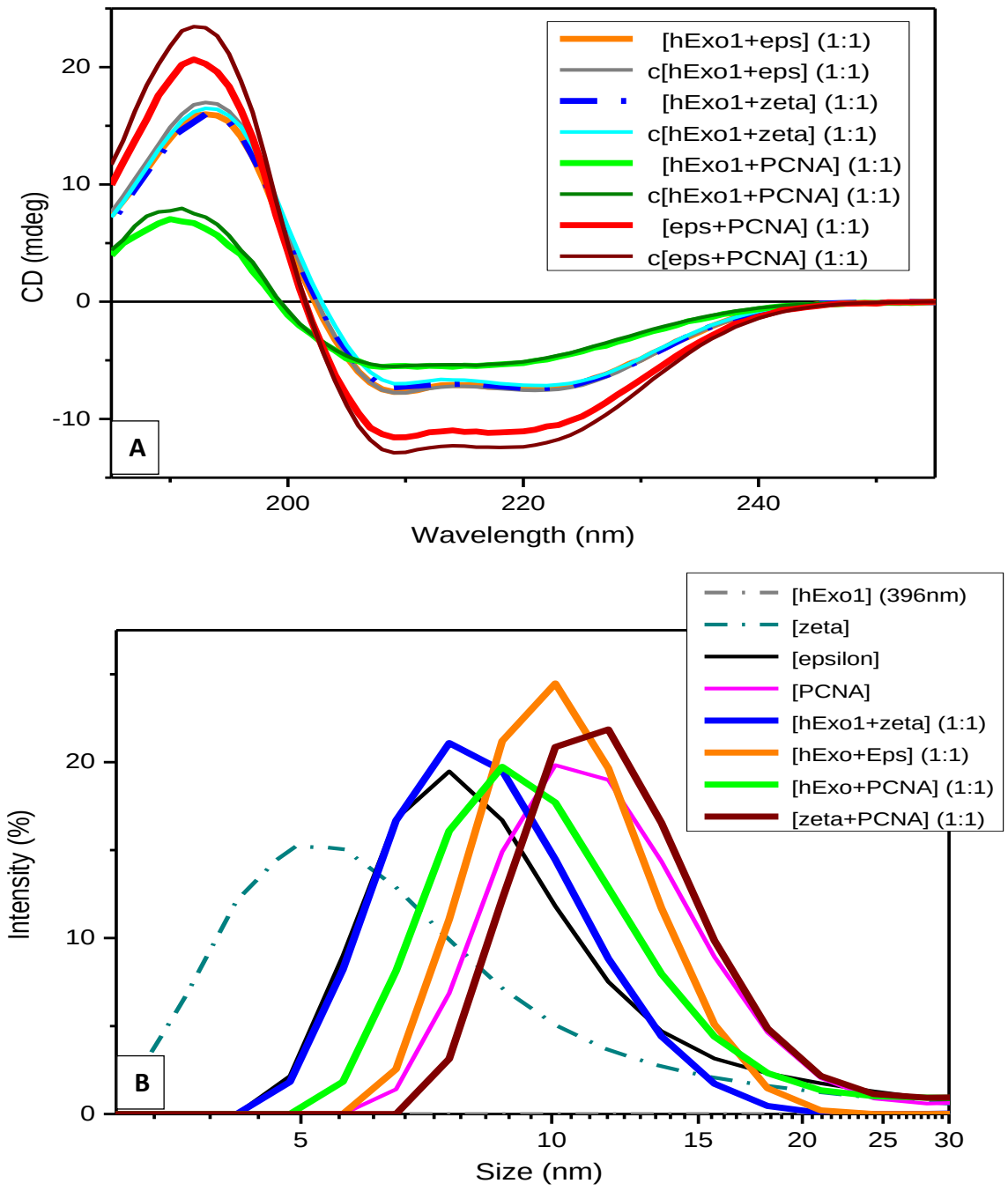
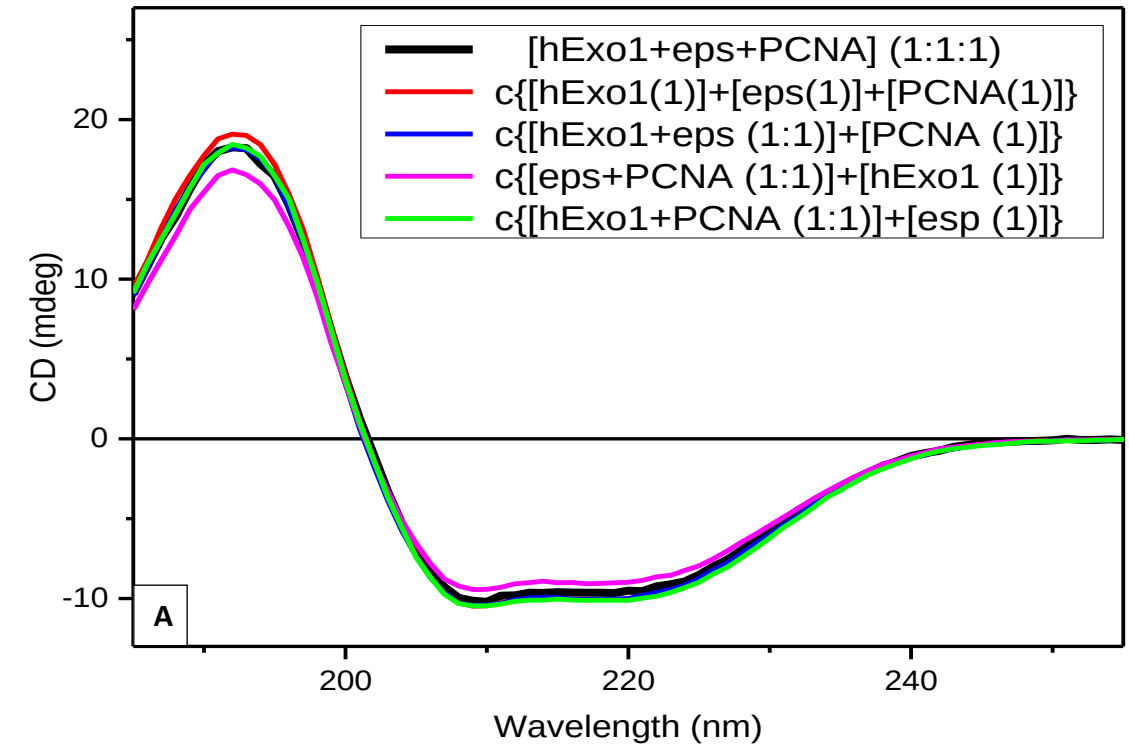
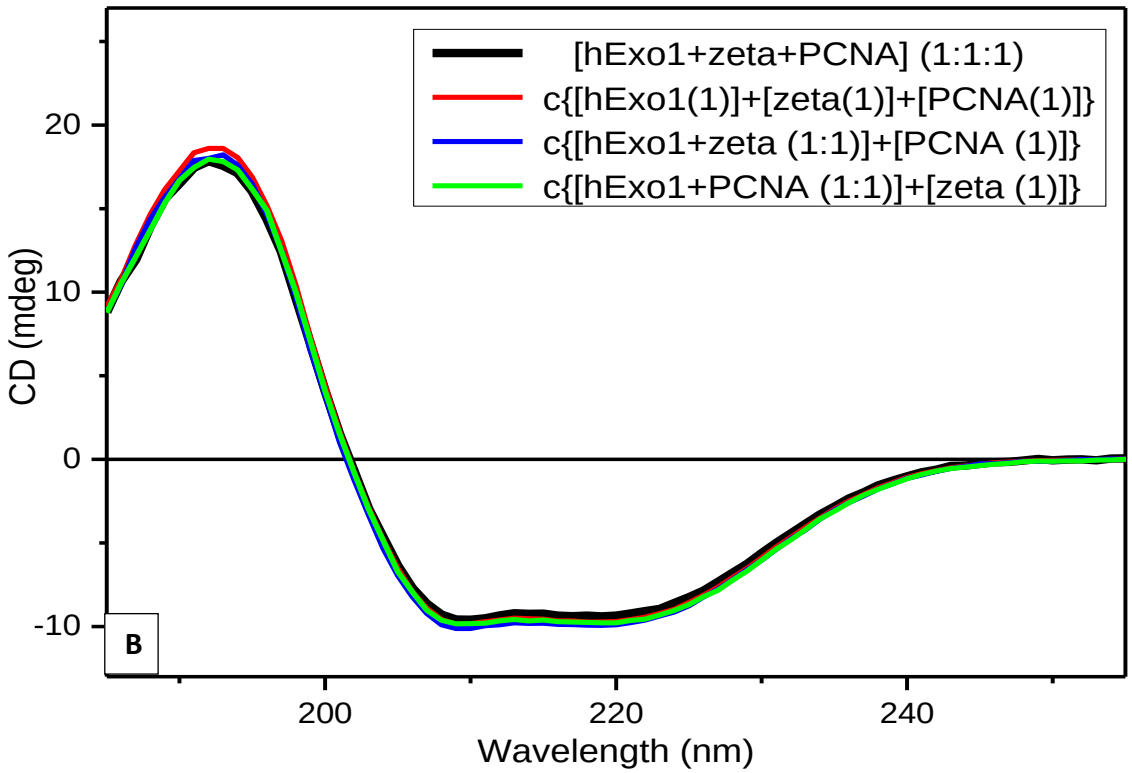
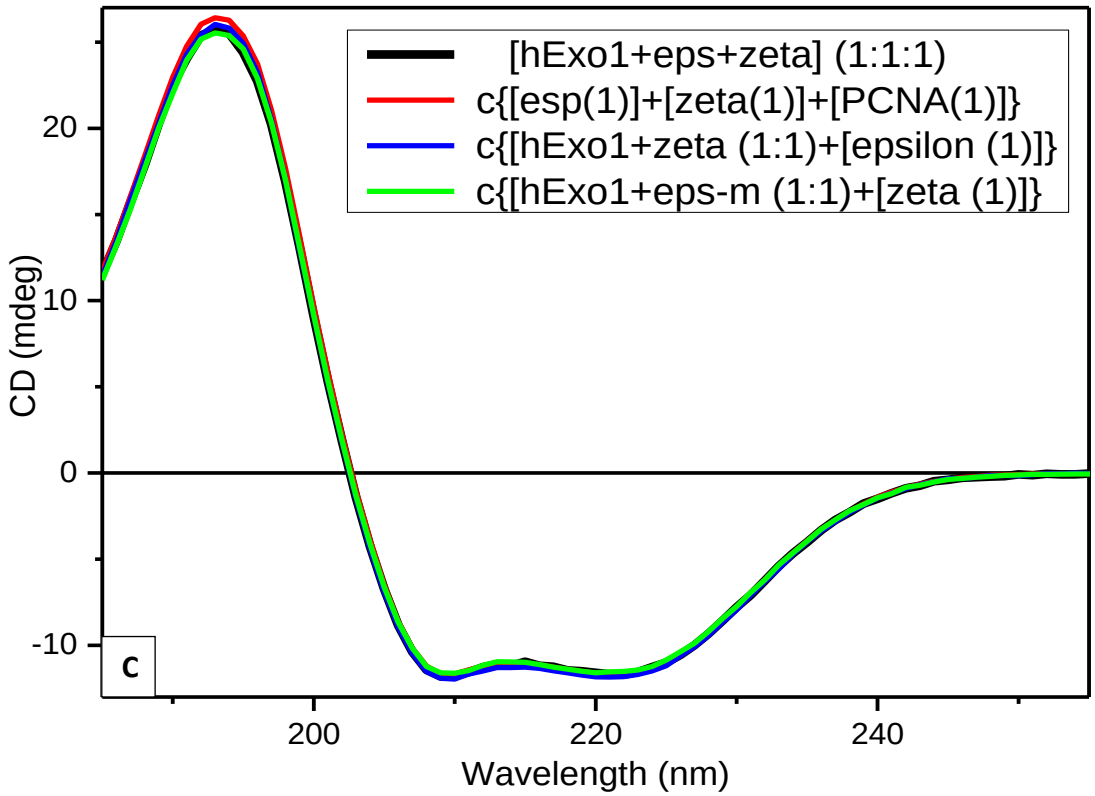


Figure 5.14. **A**) Far-UV CD spectra of binary complexes of hExo1+epsilon (observed orange, simulated grey), hExo1+14-3-3ζ (observed blue, simulated cyan), hExo1+PCNA (observed green, simulated dark green), and 14-3-3ε+PCNA (observed red, simulated brown). The simulated spectra were calculated by adding together the spectra of individual proteins at the same concentration of those of the binary complexes. **B**) DLS data reported in terms of size of hExo1 (396nm), 14-3-3ζ (aqua), 14-3-3ε (black), PCNA (magenta), hExo1+14-3-3ζ (blue), hExo1+14-3-3ε (orange), hExo1+PCNA (green), and 14-3-3ζ+PCNA (brown).


[hExo1+eps+PCNA] (1:1:1)
c{[hExo1(1)]+[eps(1)]+[PCNA(1)]}
c{[hExo1+eps (1:1)]+[PCNA (1)]}
c{[eps+PCNA (1:1)]+[hExo1 (1)]}
c{[hExo1+PCNA (1:1)]+[esp (1)]}
CD (mdeg)
20
10
0
-10
A
200
220
240
Wavelength (nm)


[hExo1+zeta+PCNA] (1:1:1)
c{[hExo1(1)]+[zeta(1)]+[PCNA(1)]}
c{[hExo1+zeta (1:1)]+[PCNA (1)]}
c{[hExo1+PCNA (1:1)]+[zeta (1)]}
CD (mdeg)
20
10
0
-10
B
200
220
240
Wavelength (nm)


[hExo1+eps+zeta] (1:1:1)
c{[esp(1)]+[zeta(1)]+[PCNA(1)]}
c{[hExo1+zeta (1:1)+[epsilon (1)]}
c{[hExo1+eps-m (1:1)+[zeta (1)]}
CD (mdeg)
20
10
0
-10
C
200
220
240
Wavelength (nm)

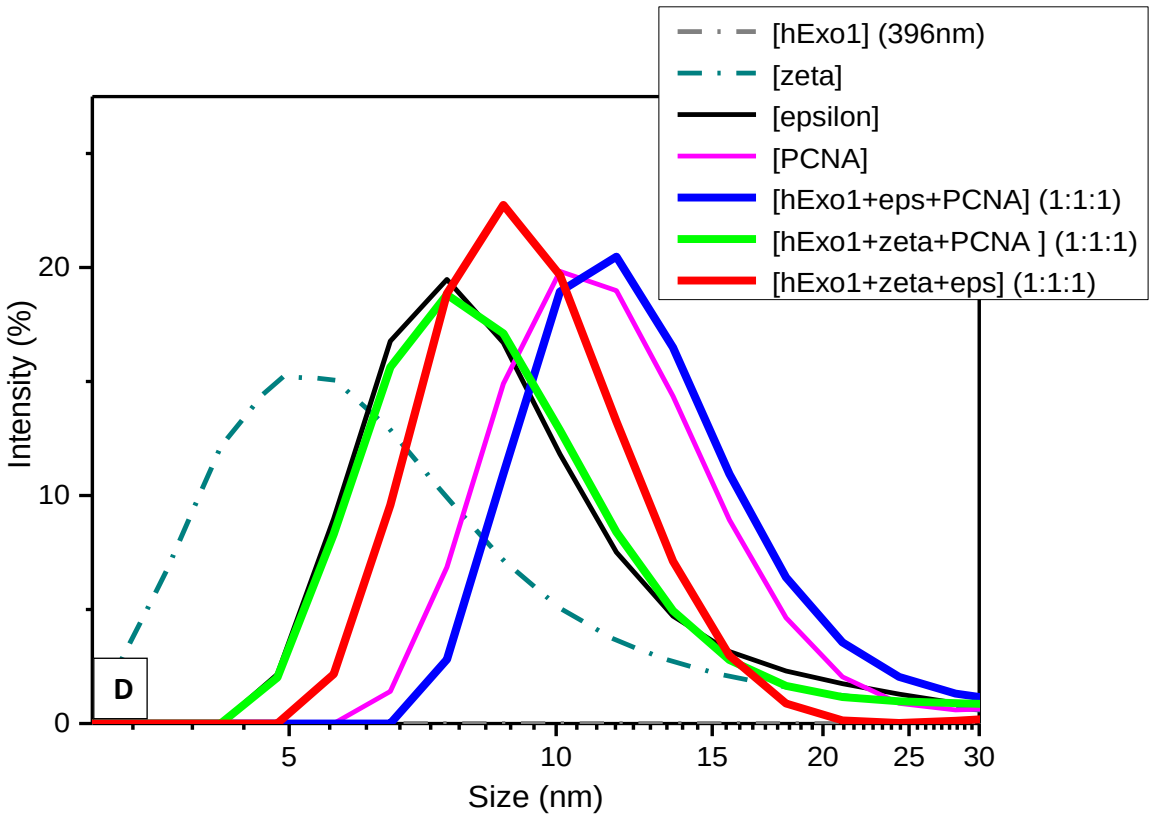

[hExo1] (396nm)
[zeta]
[epsilon]
[PCNA]
[hExo1+eps+PCNA] (1:1:1)
[hExo1+zeta+PCNA] (1:1:1)
[hExo1+zeta+eps] (1:1:1)
Intensity (%)
20
10
0
D
5
10
15
20
25
30
Size (nm)

Figure 5.15. Far-UV CD spectra of ternary complexes and their corresponding simulated spectra. **A**) Observed spectrum hExo1+epsilon+PCNA (1:1:1) (black) and calculated spectra obtained as follows: i) by the sum of the individual spectra of hExo1(1) with 14-3-3ε(1) and PCNA(1) c(hExo1)(1)+14-3-3ζ(1)+PCNA(1) (red). ii) by the sum of the binary complex c(hExo1+14-3-3ζ)(1:1) with PCNA(1) c(hExo1)+14-3-3ζ(1:1)+PCNA(1) (blue). iii) by the sum of the binary complex c(14-3-3ε)+PCNA(1:1) with hExo1(1) c(14-3-3ε)+PCNA(1:1)+hExo1(1) (magenta). iv) by the sum of the binary complex c(hExo1)+PCNA(1:1) with 14-3-3ε(1) c(hExo1)+PCNA(1:1)+14-3-3ε(1) (green). **B**) Observed spectrum hExo1+zeta+PCNA (1:1:1) (black) and calculated spectra obtained as follows: i) by the sum of the individual speεctra of hExo1(1) with 14-3-3ζ(1) and PCNA(1) c(hExo1)(1)+14-3-3ζ(1)+PCNA(1) (red). ii) c(hExo1)+14-3-3ε(1:1)+PCNA(1) (blue). iii) c(hExo1)+PCNA(1:1)]+14-3-3ε(1) (green). **C**) Observed spectrum hExo1+14-3-3ε+14-3-3ζ (1:1:1) (black) and calculated spectra obtained as follows: i) by the sum of the individual spectra of hExo1(1) with 14-3-3ε(1) and 14-3-3ζ(1) c(hExo1)(1)+14-3-3ε(1)+14-3-3ζ(1) (red)). ii) c(hExo1)+14-3-3ζ(1:1)+14-3-3ε(1) (blue). iii) c(hExo1)+14-3-3ε(1:1)]+14-3-3ζ(1) (green). **D**) DLS data reported in terms of size of hExo1 (396nm), 14-3-3ζ (aqua), 14-3-3ε (black), PCNA (magenta), hExo1+14-3-3ε+PCNA (1:1:1) (blue), hExo1+14-3-3ζ+PCNA (1:1:1) (green), and hExo1+14-3-3ζ+14-3-3ε (1:1:1) (red).

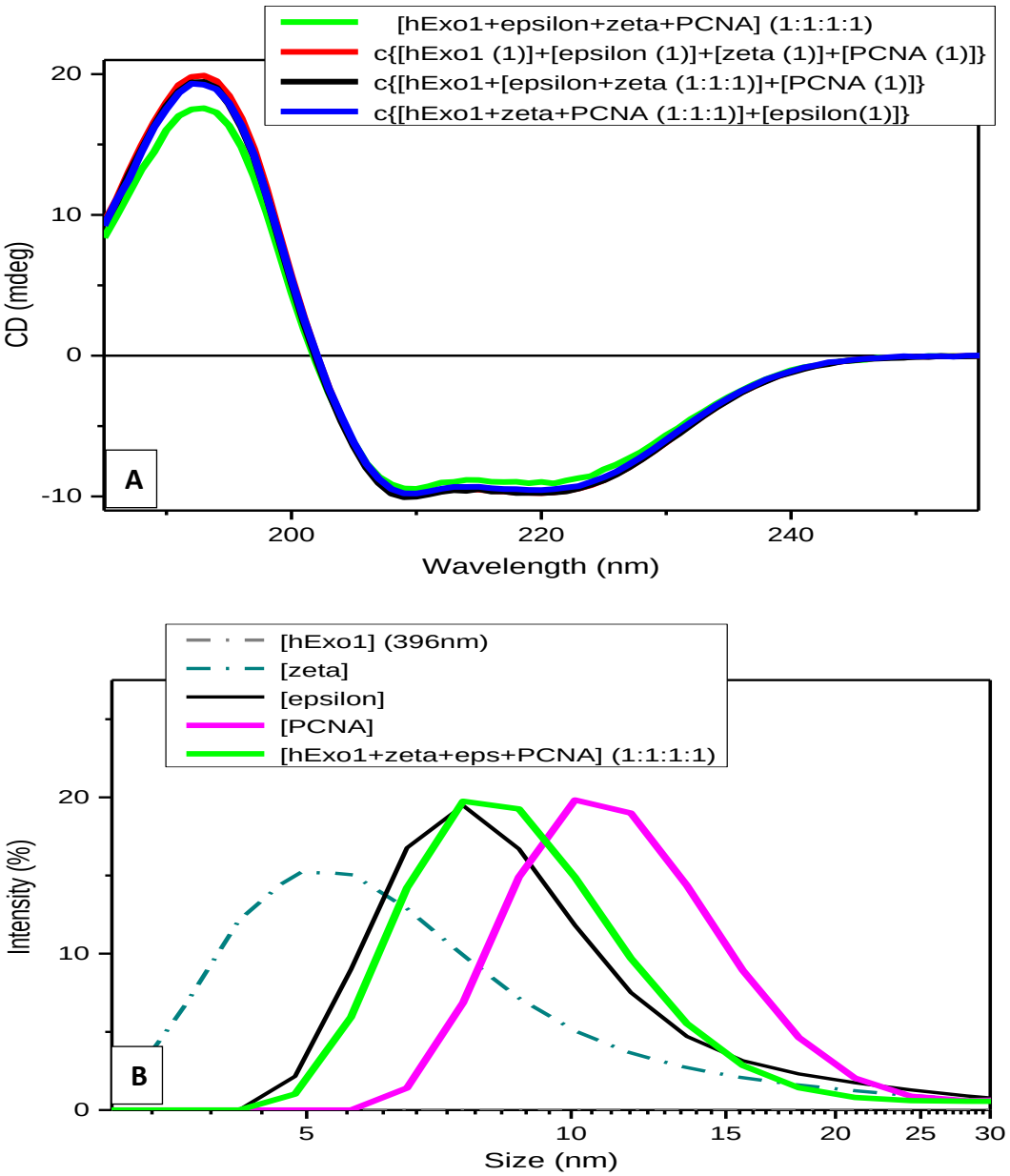


Figure 5.16. **A**) Far-UV CD spectrum of the quaternary mixture hExo1+14-3-3ε+14-3-3ζ+PCNA (1:1:1:1) (green) and calculated spectra obtained as follows: i) by the sum of the individual spectra of hExo1(1) with 14-3-3ε(1) and 14-3-3ζ(1) and PCNA(1) c(hExo1+14-3-3ε(1)+14-3-3ζ(1)+PCNA(1) (red). ii) by the sum of the ternary complex c(hExo1+14-3-3ε+14-3-3ζ(1:1:1) with PCNA(1) c(hExo1+14-3-3ε(1)+14-3-3ζ(1:1:1)+PCNA(1) (blue)). iii) by the sum of the ternary complex c(hExo1+14-3-3ζ(1)+PCNA(1:1) with 14-3-3ε(1) c(hExo1+14-3-3ζ+PCNA(1:1:1)+14-3-3ε(1) (blue)). **B**) DLS data reported in terms of size of hExo1 (396nm), 14-3-3ζ (aqua), 14-3-3ε (black), PCNA (magenta) and quaternary mixture hExo1+14-3-3ζ+14-3-3ε+PCNA (1:1:1:1) (green).

SSE – CONTINNL –SP43	α-Helix	β-Strand	Turn	Unordered	Standard Deviation
14-3-3ζ	74.6	1.8	7.2	16.4	0.011
PCNA	32.7	17.7	21.3	28.3	0.046
Nt-hExo1 1st scan	23.1	26.1	21.0	29.8	0.033
Nt-hExo1 4th scan	21.1	28.6	21.2	29.2	0.029
hExo1	3.7	42.5	21.5	32.3	0.691
14-3-3ε	75.7	1.5	6.8	16.0	0.012
tail* cal(hExo1)-(Nt-hExo1)	0.5	44.6	21.1	33.9	0.073

Table 5.3. Secondary Structure Estimation (SSE) by CONTINNL using SP43 data set (soluble proteins).

Complexes	**Individual proteins**			
hExo1+14-3-3ζ (1:1) (**7.5**)	hExo1 (**396**)	14-3-3ζ (**4.5**)		
hExo1+PCNA (1:1) (**8.7**)	hExo1 (**396**)			PCNA (**10.1**)
hExo1+14-3-3ε (1:1) (**10.1**)	hExo1 (**396**)		14-3-3ε (**7.5**)	
14-3-3ζ+PCNA (1:1) (**11.7**)		14-3-3ζ (**4.5**)		PCNA (**10.1**)
hExo1+14-3-3ζ+PCNA (1:1:1) (**7.5**)	hExo1 (**396**)	14-3-3ζ (**4.5**)		PCNA (**10.1**)
hExo1+14-3-3ζ+14-3-3ε (1:1:1) (**8.7**)	hExo1 (**396**)	14-3-3ζ (**4.5**)	14-3-3ε (**7.5**)	
hExo1+14-3-3ε+PCNA (1:1:1) (**11.7**)	hExo1 (**396**)		14-3-3ε (**7.5**)	PCNA (**10.1**)
hExo1+14-3-3ζ+14-3-3ε+PCNA (1:1:1:1) (**7.5**)	hExo1 (**396**)	14-3-3ζ (**4.5**)	14-3-3ε (**7.5**)	PCNA (**10.1**)
	Nt-hExo1 *1st scan* (**396**)			
	Nt-hExo1 *4st scan* (**825**)			

Table 5.4. Sizes of hExo1, 14-3-3ζ, 14-3-3ε, and PCNA proteins, their binary, ternary and quaternary mixtures and Nt-hExo1 first scan and fourth scan by DLS (Zetasizer Nano ZSP).

The formation of the protein-protein complexes for the binary and ternary combinations of the four proteins hExo1, zeta, epsilon and PCNA were unambiguously determined by DLS data. Surprisingly, the large association of hExo1 in solution was disrupted upon binding to the other proteins either as binary, ternary or quaternary complexes. This association/aggregation of hExo1 was not due to the extended tail but to the globular core as observed for the Nt-hExo1 protein, which was also the least photo-stable protein. The extended tail of hExo1 was found to be primarily of left-handedness folding that almost cancelled out the signal from the right-handedness folding of the globular core. Very small conformational changes were observed upon formation of the binary and ternary complexes. However, CD spectroscopy was more discriminating and revealing of the formation of the quaternary complex than DLS. In summary this research work highlights the powerful combination of CD spectroscopy and DLS for protein-protein interaction studies.

6.0 CHAPTER SIX: DISCUSSION AND CONCLUSIONS

6.1. DISCUSSION

6.1.1. Thermodynamic and kinetic properties of hExo1

This study successfully cloned and expressed hExo1 protein in two different expression hosts (Insect cells and Bacterial hosts). Previously hExo1 was expressed from either insect cells or bacterial hosts (Genschel *et al*., 2002; El-Shemerly *et al*., 2005; Andersen *et al*., 2012; Chen *et al*., 2013; Bregenhorn & Jiricny, 2014). This project discovered that hExo1 was overexpressed more in the insect cell host (~12 mg/mL per 1 litre of expression host) than in the bacterial host (~5 mg/mL per 1 litre of expression host), these values referred to the concentrations of protein obtained after all the purification steps. This may be due to the fact hExo1 is a eukaryotic protein which may make its expression more suitable in eukaryotic expression host.

Understanding the structural, biochemical and thermodynamic properties of a protein is the basis to comprehensive molecular understanding of its structure and function. There are very limited reports in the literature describing the characterization of full-length human Exo1 protein, and most of these are confined almost entirely to its enzymatic activity. As such, characterization of hExo1 exonuclease resection activity alongside its thermodynamic properties will lead to a novel insight into how hExo1 mediates its activity. Recently, it was suggested that NH_2-terminal tagging of Exo1 inhibited nuclease activity (Shao *et al*., 2014). Therefore, this project studied the thermodynamics, kinetics, biochemical and biophysical properties of full-length hExo1, without affinity tags.

The ionic strength assay for full-length hExo1 was conducted in order to understand the role of ionic strength in its enzymatic function. In previous studies it was reported that truncated HEX-N2 which represents amino acids 1-395 of the full length Exo1, exhibited optimal

activity at 50 mM KCl (Lee & Wilson, 1999). Likewise, in recent studies, full-length Exo1 was reported to exhibit a reduced nuclease activity at 40 mM and 180 mM KCl (Bregenhorn & Jiricny 2014).

This study show that full-length hExo1 is tolerant to KCl in the range from 50 mM to 200 mM with a slight decreased in resection activity at 200 mM KCl, therefore, hExo1 is active under physiological salt conditions (*Fig. 4.1, lanes 2-5*). High concentrations of KCl (250–500 mM) reduced hExo1 exonuclease resection activity (*Fig. 4.1, lanes 6-9*). Similarly, low concentrations of KCl (5 mM and 10 mM) drastically reduced hExo1 enzymatic exonuclease resection activity (*Fig. 4.1, lanes 10-11*).

This study confirms that hExo1 is temperature sensitive. The exonuclease resection activity of hExo1 was tested at six different temperatures, on ice, 4^{o}C, room temperature, 25^{o}C, 30^{o}C and 37^{o}C (*Fig. 4.2*). It was observed that hExo1 exhibited optimal exonuclease resection activity at 37^{o}C. This is contrary to what Keijzers and colleagues (2015) observed that Exo1 has approximately a 2-fold increase in enzymatic activity at 25^{o}C and 30^{o}C compared with 37^{o}C (Keijzers *et al*., 2015). Also, this study observed that hExo1 protein is not stable at temperature ranges from 40^{o}C to 50^{o}C, hExo1 was pre-incubated at either on ice, 4^{o}C, 25^{o}C, 30^{o}C, 37^{o}C, 40^{o}C, 45^{o}C or 50^{o}C for 60 min, followed by an exonuclease resection assay using a dsDNA substrate *(Fig. 4.3*). Pre-incubation of hExo1 on ice and at 4^{o}C (*Fig. 4.3, lanes 9 and 8*) significantly increased exonuclease resection activity compared to pre-incubation at 37^{o}C (*Fig. 4.3, lane 5*). When hExo1 was pre-incubated at 40^{o}C, 45^{o}C or 50^{o}C prior to resection assay, resection activity of hExo1 drastically decreased. This is further evidence that hExo1 is sensitive to high temperature and these observations agrees to what was previously reported (Keijzers *et al*., 2015). Next, the enzymatic requirements of hExo1 revealed that the pH range for its

optimal exonuclease resection activity is in the range 7–8 (*Fig. 4.4, lanes 6, 7 and 8*).

Further to this, the enzymatic exonuclease resection function of hExo1 was dependent on the presence Mg^{2+} and ATP (*Fig. 4.7*) at concentrations of 5 mM and 1 mM respectively. Dependence of exonuclease resection function on divalent metal ion for the truncated Exo1 was previously reported (Lee & Wilson, 1999). A more detailed look at the substrate preferences of hExo1 revealed that this protein degrades 3'-overhang duplex substrates while no substrate degradation was observed when a blunt end and 5'-overhang dsDNA substrates were used (*Fig. 4.5*). Lee and Wilson (1999) report that the truncated Exo1 (HEX1-N2) degrades both 5' and 3' ^{32}P labelled blunt end duplex substrates (Lee & Wilson, 1999). The disagreement between the results found in this study and the previously reported (Lee & Wilson, 1999) with regards to substrate specificity of hExo1 may be due to the fact that this study used a full-length protein, and persistently checked its integrity before and after the assay by SDS/PAGE analysis. However, this does not appear to be the case in other assays. There is also a mixture of conditions in the published assays: some were done with protein of unspecified purity but this study used a single band purity. Also, some previous studies used phosphorylated protein, whereas in this study hExo1 was always un-phosphorylated. In this study, obtaining the same unphosphorylated protein was rigorous throughout the study: many literature studies are unclear as to whether this criteria was met.

Next, the role of resection reaction incubation time was investigated in this study. This study examined whether the hExo1 protein would remain active after 1, 5, 10, 15, 30 and 60 minutes in reaction (*Fig. 4.6*). The resection reaction was assayed at 37^{o}C and found that hExo1 degraded 3' overhang dsDNA substrate from the very first few second of starting the reaction and continued resection of the 3' overhang

dsDNA substrate for up to 60 minutes. These data suggest that hExo1 is active in resection reaction mixture after 60 min at 37^{o}C. These data contradicts what was reported previously that hExo1 was inactive in reaction mixture after 10 min at 37^{o}C (Keijzers *et al*., 2015). This may be due to different substrates used in both studies, while a 5'-radioactive labelled 42-mer dsDNA was used as a substrate (Keijzers *et al*., 2015), here a linearized 4.8 kb non radio labelled dsDNA was used, which is a much larger DNA target and hence there is more substrate upon which to act (5 nM hExo1 protein against 15 nM dsDNA substrate). These observations are important for the design of *in vitro* experiments and biophysical studies involving hExo1.

6.1.2. Regulation of hExo1 DNA resection activity by PCNA and 14-3-3 proteins

This study has unveiled key elements of a mechanism for the regulation of hExo1-mediated DNA end resection following DNA double strand break, and how hExo1 DNA end resection activity is a prerequisite for both DNA repair and the activation of checkpoint. This study suggest that hExo1 function in DNA end resection is controlled through protein-protein interactions. Although interaction with PCNA enhances hExo1 activity in DNA resection, interaction with 14-3-3 proteins inhibits the DNA end resection activity of hExo1 (*Figs. 4.8 and 4.10*) (Chen *et al*., 2013; Chen *et al*., 2015). At least, the mechanism through which 14-3-3s hinders hExo1-mediated DNA end resection is established, by interrupting the binding of hExo1 to PCNA (*Fig. 4.12*). This coordinated control safeguard the DNA end resection which is critical for genome maintenance and the survival of cells following DNA lesion.

Even though the role of PCNA in DNA double strand break resection has only been reported recently (Chen *et al*., 2013), its role in DNA synthesis during DNA replication has been reported significantly. In the event of DNA replication, PCNA is loaded onto the ssDNA–dsDNA

junctions and serves as a processivity factor for DNA polymerases δ and ε. PCNA enhances processive DNA synthesis by tethering DNA polymerases δ and ε to the DNA template (Majka & Burgers, 2004; Moldovan, *et al*., 2007). Further to DNA replication, in the event of homologous recombination PCNA function as a processivity clamp for DNA polymerase δ during the elongation of the invaded 3' ssDNA end (Li *et al*., 2009). A recent study by Chen and colleagues strongly suggested that PCNA plays an analogous role in DNA resection (Chen *et al*., 2013). According to this study, PCNA acts to increase the processivity of Exo1 in resection by tethering Exo1 to the DNA substrate (Chen *et al*., 2013).

Interestingly, similar to PCNA, human MRN was also reported to enhance the *in vitro* processivity of Exo1 in resection (Nimonkar *et al*., 2011). These processivity factors availability has at least in part, given a hint for the critical Exo1 input into the *in vivo* DNA resection despite its low abundance in cells and limited *in vitro* processivity (Szankasi & Smith, 1992; Fiorentini *et al*., 1997). It was recently suggested that, in addition to PCNA function in tethering Exo1 to the DNA substrate it may also modulate Exo1 nuclease activity in cells (Chen *et al*., 2013). A recent study on the N-terminal nuclease domain of Exo1 suggests the possibility that the C-terminus of Exo1 may serve as an autoinhibitory domain that binds (directly or indirectly) and suppresses the N-terminal nuclease activity of Exo1, and that the binding of MMR proteins such as the Msh2-Msh6 complex to the C-terminus of Exo1 relieves the inhibitory effects (Orans *et al*., 2011). Even though this model does not carry any experimental validation, it was however, suggested that there is a possibility that the PCNA interaction with the C-terminus of Exo1 may stimulate Exo1 nuclease activity through a similar derepressing mechanism during double strand break end resection (Chen *et al*., 2013).

The positive regulation on hExo1 by PCNA ensures that an efficient DNA end resection is attained, which is required for prompt HR and ATR checkpoint activations. Even though inadequate resection hampers the activation of HR and ATR, excessive resection can cause certain defective consequences. Uncontrolled over resection of dsDNA will generate excessive ssDNA, this in turn may drain the RPA protein pool. Further lesion can occur when an uncoated 3’ ssDNA is exposed, which can lead to genomic instability with a possible compromise of the genetic information (Chen *et al*., 2013; Toledo *et al*., 2013).

Results obtained in this study from biophysical characterization of hExo1 using SV-AUC, SAXS, and DLS techniques have all revealed that hExo1 associates to a large complex in solution, which was subsequently changed by further protein/protein interactions. The formation of the protein-protein complexes for the binary and ternary combinations of the four proteins hExo1, 14-3-3ζ 14-3-3ε, and PCNA were unambiguously determined by DLS data. It is surprising, that the large association of hExo1 in solution was disrupted upon binding to the other proteins either as binary, ternary or quaternary complexes. This association/aggregation of hExo1 was not due to the extended C-terminal tail but to the globular N-terminal core as observed for the Nt-hExo1 protein, which was also the least photo-stable protein. This research project therefore proposes, on the basis of Dynamic Light Scattering measurement that apart from tethering hExo1 on the DNA substrate, PCNA binds to the C-terminal region on hExo1 and disrupt the aggregation state of hExo1 thereby stabilizing monomeric hExo1 which is more active, and hence which subsequently increases hExo1 resection activity on the dsDNA substrate.

The activities of hExo1 and Dna2 can potentially result in over active resection of DNA which must be regulated adequately to enhance proficient DNA repair with a minimal loss of DNA sequence. The outlined results in this study showed that 14-3-3 proteins play a significant

function in restraining the resection of DNA by hExo1. Through direct binding to the intrinsically disordered C-terminal domain of hExo1, 14-3-3s restrain DNA end resection hExo1. The 14-3-3 proteins did not bind Nt-hExo1, hence did not restrain DNA end resection activity of Nt-hExo1 protein (*Fig. 4.11*) which is further evidence that 14-3-3s bind to C-terminal domain of hExo1. These data are in agreement with the recently emerging evidence that 14-3-3s bind to the central domain (residues 508-750) of hExo1 (Chen *et el*., 2015).

Mechanistically, this study discovered that 14-3-3s inhibits hExo1 DNA end resection activity by hindering hExo1 binding to PCNA (*Fig. 4.12*). Suppression in hExo1 binding to PCNA may be attained directly by inducing a conformational changes in hExo1 or by an indirect process of modifying hExo1 following 14-3-3s binding. Recently, it was suggested that 14-3-3s do not modulate the nuclease activity of Exo1 at the sites of DNA damage but, instead, decrease the recruitment and retention of Exo1 at sites of DNA damage (Chen *et al*., 2015) because 14-3-3 proteins do not localize to sites of DNA damage (Chen *et al*., 2015) and because 14-3-3η and 14-3-3σ which interacts with Exo1 did not affect the nuclease activity of recombinant Exo1 *in vitro* (Andersen *et al*., 2012).

The negative regulation of hExo1 resection by 14-3-3s found in this study is consistent with the genetic study conducted in budding yeast (Engels *et al.* 2011), which showed that 14-3-3 proteins suppressed processing of stalled replication forks that is mediated by Exo1 in budding yeast. When the two 14-3-3 genes were deleted in yeast, it was observed that ssDNA gaps generated by Exo1 accumulated behind the replication forks, suggesting that the resection activity of Exo1 regulated by 14-3-3s during replication (Engels *et al*., 2011). From the resection assays (*Figs. 4.14, 4.15*) results and the binding curve (*Fig. 4.16*) obtained, this study postulate that 14-3-3 proteins allosterically inhibit hExo1 resection activity on a 3’ overhang dsDNA substrate *in*

vitro, there are at least more than one binding site for 14-3-3s on hExo1 and that 14-3-3s bind to hExo1 cooperatively.

The extensive role of Exo1 in DNA resection is conserved in yeast and vertebrates, there are some regulatory differences in Exo1 resection activity among the organisms. For instance, the binding region for 14-3-3 on human Exo1 protein is not conserved in the Exo1 protein of budding yeast. Furthermore, whereas PCNA binds Exo1 directly and enhances Exo1 DNA end resection activity in vertebrates, in yeast Exo1, no PCNA-binding sequence have yet been determined (Chen *et al*., 2013; Ngo *et al*., 2014). Intriguingly, the 9-1-1 complex is another DNA clamp that regulate both human and yeast Exo1 via an unknown mechanism (Karras *et al*., 2013; Ngo *et al*., 2014). Several other regulatory candidates for Exo1 function in DNA double strand break resection have been determined either directly or indirectly in human cells or yeast, including MRN, CtIP, Ku, RPA, SOSS1, BLM, SWR1, ATM, ATR, Rad53, and CDK (Cotta-Ramusino *et al*., 2005; Morin *et al*., 2008; Segurado & Diffley, 2008; El-Shemerly *et al*., 2008; Nimonkar *et al*., 2008; Bolderson *et al*., 2010; Eid *et al*., 2010; Mimitou & Symington, 2010; Shim *et al*., 2010; Nicolette *et al*., 2010; Engels *et al*., 2011; Nimonkar *et al*., 2011; Langerak *et al*., 2011; Sun *et al*., 2012; Cannavo *et al*., 2013; Yang *et al*., 2013; Adkins *et al*., 2013; Andersen *et al*., 2014; Tomimatsu *et al*., 2014).

In this study, the identification of the key functional domains in hExo1 and their direct binding partners has given a mechanistic framework to understand how hExo1 regulators are coordinated in the process of DNA end resection control. In contrast, the Dna2 pathway is not controlled by 14-3-3s (Chen *et al*., 2015), instead, Dna2 resection activity is suppressed directly or indirectly by FANCD2 in human cells, RAD9 in budding yeast, and Pxd1 in fission yeast (Karanja *et al*., 2014; Zhang *et al*., 2014; Bonetti *et al*., 2015). How these two DNA end resection pathways (hExo1 and Dna2) are coordinately controlled to safeguard a

proper level of DNA end resection following a DNA double strand break repair is yet to be unveiled. The stringent control of cellular nucleases is critical for proper DNA repair and the survival of the cell (Tsutakawa *et al*., 2014).

Recently, it was demonstrated that regulation of hExo1 resection by 14-3-3s is important for cell survival following a DNA damage (Chen *et al*., 2015). In the absence of 14-3-3-mediated control of hExo1 resection activity, a decreased in cell viability was observed, this may be caused by the toxic aberrant repair products following uncontrolled DNA end resection or from decoupling of homology mediated repair from DNA resection (Chen *et al*., 2015). A previous study reported that deletion of Exo1 in yeast and mice can rescue various phenotypes that result from disruption of the functions of the checkpoint kinase Rad53 or telomerase, such as DNA damage hypersensitivity, chromosomal instability, and aging (Bertuch & Lundblad, 2004; Maringele & Lydall, 2004; Cotta-Ramusino *et al*., 2005; Schaetzlein *et al*., 2007; Morin *et al*., 2008; Segurado & Diffley, 2008).

It will be important to ascertain whether uncontrolled Exo1 resection contributes to these phenotypes and whether regulation by 14-3-3 plays any role in relation to these. Results of this study also suggest that the process of DNA end resection can be taken advantage of for the treatment of cancer. Considering the replication stress and genomic instability in the majority of cancers, it can be conceived that small molecule inhibitors that specifically target the interaction of 14-3-3 proteins with hExo1 might be effective as chemosensitizers for cancer therapy.

6.1.3. Biophysical studies and disorder prediction of hExo1 protein

This research work uncovers for the first time the model of hExo1 protein predicted from amino acid folding propensity that it consists of two domains, a long extended tail and a globular core. Looking at how hExo1 and Nt-hExo1 exhibited the same crossover at about 202nm (*Fig. 5.13A*) and were super-imposable in the 195-210nm region (where the signal is predominately from secondary structure elements) but not in the 220-240nm region (where the signal is contributed to by tertiary structural elements), it is conceivable to assume that Nt-hExo1 retains the same folding in the full length hExo1 protein and behaving as a proper domain, and indeed this is confirmed by its ability to be crystallised for protein crystallographic studies (Orans *et al*., 2011). On the other hand, the subtraction of the CD spectrum of Nt-hExo1 (1st scan) from that of the full length hExo1 protein revealed the CD spectrum of the remaining hExo1 protein (C-terminus), which exhibited a CD spectra of an extended polypeptide (*Fig. 5.13B*). In view of this, this study propose that hExo1 protein is a multi-domain protein that contain an N-terminus globular core (1-345 amino acid residues) and an extended flexible C-terminus domain (346 - 846 amino acid residues). Furthermore, this study is of the view that 14-3-3 proteins regulate hExo1 resection activity by a mechanism of disorder-to-order transition of the hExo1 C-terminus domain.

The experimental results obtained during this study showed that the C-terminal region of hExo1 is devoid of α-helix and classical β-sheet structures but contains significant local left-handed β-Strand, polyproline of type II (PPII) and turn of type II conformations that almost cancelled out the right handedness of the α-Helix and β-Strand conformations of the globular N-terminal domain of hExo1 protein. As a result, the CD of these two domains mirroring one each other resulting

in the very small intensity CD spectrum observed for hExo1 (*Figs. 5.12*).

Functionally, the elasticity of intrinsically disordered regions can provide various advantages for signalling proteins, this may include the proficiency to bind to multiple binding partners and/or the fine control over the binding affinities (reviewed by Shoemaker *et al*., 2000; Wright & Dyson 2009). Shoemaker and colleagues (2000), suggested that intrinsically disordered or partially disordered protein would have an advantage of having a greater 'capture radius' that pave the way for the diffusive search for a binding target than in a closely packed, folded protein with restricted conformational plasticity (Shoemaker *et al*. 2000). The often found presence of binding sites for the 14-3-3 proteins within the unstructured regions of protein partners also suggests that the utilisation of intrinsic disorder of the ligand molecule's structure might be a common binding aspect to the 14-3-3 proteins (Bustos & Iglesias, 2006).

Proteins are dynamic flexible molecules in solution, and conformational changes are often as important for protein function as the catalytic active site. Flexibility allows allosteric control of proteins by either post-translational modification, small molecules or other proteins, this study found that 14-3-3 proteins regulate hExo1 resection activity allosterically. Flexibility enables proteins to be multi-functional in a coordinated manner.

Exonuclease1 protein function has been implicated in a wide range of biological processes, including genome maintenance, meiosis, and telomere regulation, as well as somatic hyper-mutation (SH) in lymphocytes (Bardwell *et al*, 2004; Tran *et al*, 2004). Human exonuclease 1 (hExo1) is a nuclease that plays a vital role in a variety of DNA metabolic processes like double strand break (DSB) repair through homologous recombination (HR), mismatch repair (MMR) and replication (Qiu *et al*., 1999; Genschel *et al*., 2002; Nielson *et al*., 2004;

Gravel *et al*., 2008; Eid *et al*., 2010; Bolderson *et al*., 2010; Liberti *et al*., 2011). Class switch recombination (CSR), gene conversion, post-replication repair (PRR), telomere processing, and apoptosis signaling following DNA damage are all prominent cellular functions associated with human Exonuclease1 (hExo1) and its mouse and yeast homologs indicated by various studies (Maringele & Lydall, 2002; Bardwell *et al*., 2004; Schaetzlein *et al*., 2007; Tran *et al*., 2007; Bolderson *et al*., 2009; Dherin *et al*., 2009; Tinline *et al*., 2009; Vallur & Maizels, 2010).

Flexibility also allows proteins to interact with multiple structurally distinct partners through the same region that can mold to different shapes. Also, it enables the proteins to have reversible interactions through entropic disorder-to-order transitions and to have increased processivity or specificity by molding to the substrate or to the interacting partner (Dyson & Wright, 2002). Exonuclease1 have been reported to interact with various protein partners including RecQ1 and WRN helicases, MRN/MRX, BLM, RPA, PCNA, SOSS1 and 9-1-1 (Sharma *et al*., 2003; Doherty *et al*., 2005; Nimonkar *et al*., 2008; Nicolette *et al*., 2010; Nimonkar *et al*., 2011; Cannavo *et al* 2013; Yang *et al* 2013; Chen, *et al*., 2013; Ngo, *et al*., 2014). The multi functionality of Exo1 and ability to bind multiple protein partners could be attributed to the flexible intrinsically disordered C-terminal region on Exo1.

Human exonuclease1 protein forms aggregates in solution. This behaviour of hExo1 protein was discovered from the results of SV-AUC, SAXS and DLS experiments obtained. Protein hExo1 on its own appeared to be in a soluble associated form with a measured diameter of 396nm (*Fig. 5.12B*) but this large length of hExo1 protein reverted to the 7.5-11.7nm range when interacting with the other proteins as binary and ternary complexes (*Fig. 5.14B*). The fact that the globular domain of hExo1 (Nt-hExo1) retained the same size as that of full-length hExo1 (*Fig. 5.12B*, Table 5.2) ruled out the extended tail (C-terminus) as the cause of the protein large association. Protein

aggregates play a central role in several degenerative disorders including amyloidosis in the central nervous system, observed for Alzheimer's and Parkinson's diseases. *In vitro* as *in vivo*, proteins can form different aggregates of various sizes and morphologies (amorphous aggregates, oligomers, protofibrils, amyloid fibrils), which have distinct physiological effects depending on the environmental conditions (Selkoe, 2003; Orbán *et al*., 2010). The DLS result was consistent with the results obtained from the other different techniques, both SV-AUC and SAXS experiments employed by this study revealed that hExo1 protein form aggregates in solution. Therefore, it is imperative to further study the nature and roles of this (aggregates) feature exhibited by hExo1 protein.

6.2. CONCLUSIONS

Although Exonuclease1 protein has been previously studied, and despite growing evidence for the crucial role of Exo1 in DNA double strand break repair, no structural studies have been performed on this protein. On the basis of results obtained during this research study, the following conclusions are deduced: Human exonuclease1 protein is a multi-domain protein that consists of a globular core and an extended tail and that these two domains move relative to each other. The extended tail of hExo1 was found to be primarily of left-handedness folding that almost cancelled out the signal from the right-handedness folding of the globular core.

PCNA positively regulated hExo1 resection activity by tethering hExo1 on DNA substrate and also by disrupting the aggregation state of hExo1 through binding to the disordered C-terminal region of hExo1. The C-terminal region of hExo1 may not serve as an autoinhibitory rather it may contribute to the large association state of hExo1 and at the same time serve as a point through which the aggregation can be disrupted, thereby making hExo1 a more active nuclease. The 14-3-3 proteins allosterically and negatively control hExo1 resection activity by modulating hExo1 structure through the disordered C-terminal region of hExo1 in a disorder-to-order transition. Results from this work provide crucial insights into pioneering process of the DNA end resection regulation and may be implicative in cancer treatment. This research work, provide an important information on the conformational state of hExo1 using SV-AUC, SAXS, CD and DLS. A combination of powerful techniques for the analysis of conformation, shape, and dimensions of biopolymers in solution. This research work highlighted the powerful combination of CD spectroscopy and DLS for protein-protein interaction studies.

6.3. FUTURE STUDIES

In the future, it will be interesting to determine whether the functions of PCNA and 14-3-3 proteins in hExo1-mediated resection are conserved in other organisms other than vertebrates. It will also be interesting to find out whether or not PCNA serves as a co-factor of hExo1 in other processes such as DNA replication, mismatch repair (MMR), and telomere control in which Exo1 function is also reported (Tran *et al*,. 2004). Further to PCNA and 14-3-3, Exo1 activity in DNA end resection is controlled by other proteins, including CtIP, BLM, Ku, ATM, ATR, MRN, SOSS1 and RPA (Cotta-Ramusino *et al*., 2005; El-Shemerly *et al*., 2008; Morin *et al*., 2008; Segurado & Diffley, 2008;Nimonkar *et al*., 2008; Nicolette *et al*., 2010; Bolderson *et al*., 2010; Shim *et al*., 2010; Mimitou & Symington, 2010; Eid *et al*., 2010; Langerak *et al*., 2011; Nimonkar *et al*., 2011; Engels *et al*., 2011; Andersen *et al*., 2012; Sun *et al*., 2012; Yang *et al*., 2013; Cannavo *et al*.,2013). In yeast, Exo1 resection is also regulated by Rad53 (Cotta-Ramusino *et al*., 2005; Morin *et al*., 2008; Segurado & Diffley, 2008). Albeit, the related roles between these proteins in Exo1 DNA end resection activity is not yet clear, the myriad of control for the Exo1 pathway ostensibly safeguard proficient DNA end resection to enable proper DNA repair and checkpoint activation, and further prevents unscheduled resection or over-resection that could result to a deleterious consequences. As a result of hExo1 protein aggregation that limits the interpretation of the SAXS data in this study, it will be interesting in the future to further assess the degree of disorder in hExo1 and to determine the level of structure modulation impose on hExo1 upon PCNA and 14-3-3 proteins binding by SAXS experiment.

REFERENCES

ABRAHAM R.T. (2001) Cell cycle checkpoint signaling through the ATM and ATR kinases. *Genes. Dev.*, 15, 2177–2196.

ADKINS, J. N., & LUMB, K. J. (2002). Intrinsic structural disorder and sequence features of the cell cycle inhibitor p57Kip2. Proteins, 46, 1–7.

ADKINS, N. L., NIU, H., SUNG, P., AND PETERSON, C. L. (2013) Nucleosome dynamics regulates DNA processing. *Nat. Struct. Mol. Biol.* 20, 836–842.

ADZHUBEI A.A AND STERNBERG MJE. (1993) "Left-handed Polyproline II Helices Commonly Occur in Globular Proteins", *J. Mol. Biol.*, **229**, 472-493.

AGGARWAL, M., SOMMERS, J.A., MORRIS, C. AND BROSH, R.M. (2010) Delineation of WRN helicase function with EXO1 in the replicational stress response. *DNA Repair* (Amst.) 9, 765–776.

AGUILERA, A., B. GOMEZ-GONZALEZ, (2008). Genome instability: a mechanistic view of its causes and consequences, *Nat. Rev. Genet*. 9 204–217.

AITKEN, A. (2002). Functional specificity in 14-3-3 isoform interactions through dimer formation and phosphorylation. Chromosome location of mammalian isoforms and variants. *PlantMol.Biol.* 50, 993–1010.

AMIN N.S., NGUYEN M.N., OH S. AND KOLODNER R.D. (2001) Exo1- Dependent mutator mutations: model system for studying functional interactions in mismatch repair. *Mol. Cell. Biol.,* 21, 5142–5155.

AMUNDSEN, S.K., G.R. SMITH, (2003). Interchangeable parts of the *Escherichia coli* recombination machinery, *Cell* 112, 741–744.

ANDERSEN, S.D., KEIJZERS, G., RAMPAKAKIS, E., ENGELS, K., LUHN, P., EL-SHEMERLY, M., NIELSEN, F.C., DU, Y., MAY, A., BOHR, V.A. *et al*. (2012) 14-3-3 checkpoint regulatory proteins interact specifically with DNA repair protein human exonuclease 1 (hEXO1) via a semi-conserved motif. *DNA Repair* (Amst.) 11, 267–277.

AYLON, Y., B. LIEFSHITZ, M. KUPIEC, (2004). The CDK regulates repair of double-strand breaks by homologous recombination during the cell cycle, *EMBO J.* 23, 4868–4875.

BAKKENIST C.J. AND KASTAN M.B. (2004) Initiating cellular stress responses. *Cell,* 118, 9–17.

BARDWELL, P.D., WOO, C.J., WEI, K., LI, Z., MARTIN, A., SACK, S.Z., PARRIS, T., EDELMANN, W. AND SCHARFF, M.D. (2004) Altered somatic hypermutation and

reduced class-switch recombination in exonuclease 1-mutant mice. *Nat. Immunol*. 5, 224–229.

BASSING C.H. AND ALT F.W. (2004). The cellular response to general and programmed DNA double strand breaks. *DNA Repair (Amst),* 3, 781–796.

BATRA-SAFFERLING, R., ABARCA-HEIDEMANN, K., K€ORSCHEN, H. G., TZIATZIOS, C., STOLDT, M., BUDYAK, I., ET AL. (2006). Glutamic acid-rich proteins of rod photoreceptors are natively unfolded. *The Journal of Biological Chemistry*, 281, 1449–1460.

BENZINGER A, POPOWICZ GM, JOY JK, MAJUMDAR S, HOLAK TA, HERMEKING H. (2005). The crystal structure of the non-liganded 14-3-3sigma protein: insights into determinants of isoform specific ligand binding and dimerization. *Cell Res*;15:219–27.

BERNSTEIN K.A. AND ROTHSTEIN R. (2009). At loose ends: resecting a double-strand break. *Cell*, 137, 807–810.

BERTUCH, A. A., AND LUNDBLAD, V. (2004). EXO1 contributes to telomere maintenance in both telomerase proficient and telomerase-deficient Saccharomyces cerevisiae. *Genetics* 166, 1651-1659.

BOLDERSON E., RICHARD D., EDELMANN W., KHANNA K. (2009). Involvement of Exo1b in DNA damage-induced apoptosis, *Nucl. Acids Res.* 37, 3452–3463.

BOLDERSON, E., TOMIMATSU, N., RICHARD, D. J., BOUCHER, D., KUMAR, R., PANDITA, T. K., BURMA, S., AND KHANNA, K. K. (2010) Phosphorylation of Exo1 modulates homologous recombination repair of DNA double-strand breaks*. Nucleic Acids Res* 38, 1821-1831.

BONETTI, D., VILLA, M., GOBBINI, E., CASSANI, C., TEDESCHI, G., AND LONGHESE, M. P. (2015) Escape of Sgs1 from Rad9 inhibition reduces the requirement for Sae2 and functional MRX in DNA end resection. *EMBO Rep* 16, 351-361.

BREGENHORN, S. AND JIRICNY, J. (2014) Biochemical characterization of a cancer-associated E109K missense variant of human exonuclease 1. *Nucleic Acids Res*. 42, 7096–7103.

BRUNING, J. B. & SHAMOO, Y. (2004). Structural and thermodynamic analysis of human PCNA with peptides derived from DNA polymerase-δ p66 subunit and flap endonuclease-1. *Structure* 12, 2209–2219.

BUSTOS DM, IGLESIAS AA. (2006). Intrinsic disorder is a key characteristic in partners that bind 14-3-3 proteins. *Proteins*; 63:35–42.

CANNAVO E., CEJKA, P. AND KOWALCZYKOWSKI S.C. (2013) Relationship of DNA degradation by *Saccharomyces cerevisiae* Exonuclease 1 and its stimulation by RPA and Mre11-Rad50- Xrs2 to DNA end resection*. Proc. Natl Acad. Sci. USA*, 110, E1661–E1668.

CEJKA, P., E. CANNAVO, P. POLACZEK, T. MASUDA-SASA, S. POKHAREL, J.L. CAMPBELL, S.C. KOWALCZYKOWSKI, (2010). DNA end resection by Dna2–Sgs1–RPA and its stimulation by Top3–Rmi1 and Mre11–Rad50–Xrs2, *Nature* 467, 112–116.

CESKA T.A. AND SAYERS J.R. (1998) Structure-specific DNA cleavage by 5′ nucleases. *Trends Biochem. Sci.,* 23, 331-336.

CHACON, P., MORAN, F., DIAZ, J.F., PANTOS, E., ANDREU, J.M., (1998). Low resolution structures of proteins in solution retrieved from X-ray scattering with a genetic algorithm. *Biophysical Journal* 74, 2760–2775.

CHEN XIAOQING, IN-KWON KIM, YUCHI HONAKER, SHARAD C. PAUDYAL, WON KYUN KOH, MELANIE SPARKS, SHAN LI, HELEN PIWNICA-WORMS, TOM ELLENBERGER AND ZHONGSHENG YOU. (2015) 14-3-3 Proteins Restrain the Exo1 Nuclease to Prevent Over-resection. *The Journal of Biological Chemistry*, 290, 12300-12312.

CHEN, H., LISBY, M., AND SYMINGTON, L. S. (2013) RPA coordinates DNA end resection and prevents formation of DNA hairpins. *Mol Cell* 50, 589-600.

CHEN, X., PAUDYAL, S. C., CHIN, R. I., AND YOU, Z. (2013) PCNA promotes processive DNA end resection by Exo1. *Nucleic Acids Res* 41, 9325-9338.

CHU, B. (1974) *Laser Light Scattering*, Academic Press, New York.

CHUNG, W.H., Z. ZHU, A. PAPUSHA, A. MALKOVA, G. IRA, (2010) Defective resection at DNA double-strand breaks leads to de novo telomere formation and enhances gene targeting, *PLoS Genet*. 6.

CICCIA, A., AND ELLEDGE, S. J. (2010) The DNA damage response: making it safe to play with knives. *Mol Cell* 40, 179-204.

CIMPRICH, K. A., AND CORTEZ, D. (2008) ATR: an essential regulator of genome integrity. *Nat Rev Mol Cell Biol* 9, 616-627.

COBLITZ B, SHIKANO S, WU M, GABELLI SB, COCKRELL LM, SPIEKER M, ET AL. (2005) C-terminal recognition by 14-3-3 proteins for surface expression of membrane receptors. *J Biol Chem* 280:36263–72.

COBLITZ B, WU M, SHIKANO S, LI M (2006) C-terminal binding: an expanded repertoire and function of 14-3-3 proteins. *FEBS Lett* 580:1531–1535.

COLE JL, HANSEN JC. (1999) Analytical Ultracentrifugation as a Contemporary Biomolecular Research Tool. *J Biomolecular Techniques* 10:163–174.

COTTA-RAMUSINO, C., FACHINETTI, D., LUCCA, C., DOKSANI, Y., LOPES, M., SOGO, J., AND FOIANI, M. (2005) Exo1 processes stalled replication forks and counteracts fork reversal in checkpoint-defective cells. *Mol Cell* 17, 153-159.

COTTA-RAMUSINO, C., FACHINETTI, D., LUCCA, C., DOKSANI, Y., LOPES, M., SOGO, J., AND FOIANI, M. (2005) Exo1 processes stalled replication forks and counteracts fork reversal in checkpoint-defective cells. *Mol. Cell* 17, 153–159.

DALEY, J.M, P.L. PALMBOS, D. WU, T.E. WILSON, (2005) Non-homologous end joining in yeast, *Annu. Rev. Genet*. 39, 431–451.

DENNING, D. P., PATEL, S. S., UVERSKY, V., FINK, A. L., & REXACH, M. (2003). Disorder in the nuclear pore complex: The FG repeat regions of nucleoporins are natively unfolded. Proceedings of the *National Academy of Sciences* of the United States of America, 100, 2450–2455.

DHERIN C., GUENEAU E., FRANCIN M., NUNEZ M., MIRON S., LIBERTI S., RASMUSSEN L., ZINN-JUSTIN S., GILQUIN B., CHARBONNIER J., BOITEUX S. (2009) Characterization of a highly conserved binding site of Mlh1 required for exonuclease I-dependent mismatch repair, *Mol. Cell Biol.* 29, 907–918.

DIGILIO F.A., PANNUTI A., LUCCHESI J.C., FURIA M., POLITO L.C. (1996) Tosca: a Drosophila gene encoding a nuclease specifically expressed in the female germline, *Dev. Biol.* 178, 90–100.

DILLINGHAM MS, KOWALCZYKOWSKI SC. (2008). RecBCD enzyme and the repair of double-stranded DNA breaks. Microbiol Mol Biol Rev 72: 642–671.

DOHERTY, K.M., SHARMA, S., UZDILLA, L.A., WILSON, T.M., CUI, S., VINDIGNI, A. AND BROSH, R.M. (2005) RECQ1 helicase interacts with human mismatch repair factors that regulate genetic recombination. *J. Biol. Chem*. 280, 28085–28094.

DURAND, D.; VIVÈS, C.; CANNELLA, D.; PÉREZ, J.; PEBAY-PEYROULA, E.; VACHETTE, P.; FIESCHI, F. (2009) NADPH oxidase activator p67(phox) behaves in solution as a multidomain protein with semi-flexible linkers. *J. Struct. Biol.*

DYSON, H.J., WRIGHT, P.E., (2002). Coupling of folding and binding for unstructured proteins. *Current Opinion in Structural Biology* 12, 54–60.

EDELMANN, W., AND RUDOLPH, K. L. (2007) Exonuclease-1 deletion impairs DNA damage signaling and prolongs lifespan of telomere-dysfunctional mice. *Cell* 130, 863-877.

EID, W., STEGER, M., EL-SHEMERLY, M., FERRETTI, L. P., PEÑA-DIAZ, J., KÖNIG, C., VALTORTA, E., SARTORI, A. A., AND FERRARI, S. (2010) DNA end resection by CtIP and exonuclease 1 prevents genomic instability. *EMBO Rep.* 11, 962–968.

EL-SHEMERLY M., JANSCAK P., HESS D., JIRICNY J., FERRARI S. (2005) Degradation of human exonuclease 1b upon DNA synthesis inhibition, *Cancer Res.* 65, 3604–3609.

EL-SHEMERLY, M., HESS, D., PYAKUREL, A. K., MOSELHY, S., AND FERRARI, S. (2008) ATR-dependent pathways control hEXO1 stability in response to stalled forks. *Nucleic Acids Res* 36, 511-519.

ENGELS, K., GIANNATTASIO, M., MUZI-FALCONI, M., LOPES, M., AND FERRARI, S. (2011) 14-3-3 Proteins regulate exonuclease 1-dependent processing of stalled replication forks. *PLoS Genet* 7, e1001367.

FIORENTINI P., HUANG K.N., TISHKOFF D.X., KOLODNER, R. D. AND SYMINGTON L.S. (1997) Exonuclease I of *Saccharomyces cerevisiae* functions in mitotic recombination in vivo and in vitro. *Mol. Cell. Biol*., 17, 2764–2773.

FRANK-VAILLANT, M., S. MARCAND, (2002) Transient stability of DNA ends allows non-homologous end joining to precede homologous recombination, *Mol. Cell* 10, 1189–1199.

FU H, COBURN J, COLLIER RJ. (1993). The eukaryotic host factor that activates exoenzyme S of Pseudomonas aeruginosa is a member of the 14-3-3 protein family. *Proc Natl Acad Sci* USA 90:2320–4.

GANGULY S, WELLER JL, HO A, CHEMINEAU P, MALPAUX B, KLEIN DC. (2005) Melatonin synthesis: 14-3-3-dependent activation and inhibition of arylalkylamine N-acetyltransferase mediated by phosphoserine-205. *Proc Natl Acad Sci* USA 102:1222–7.

GARDINO AK, SMERDON SJ, YAFFE MB. (2006) Structural determinants of 14-3-3 binding specificities and regulation of subcellular localization of 14-3-3-ligand complexes: a comparison of the X-ray crystal structures of all human 14-3-3 isoforms. *Semin Cancer Biol* 16:173–82.

GARG, P., STITH, C.M., SABOURI, N., JOHANSSON, E. AND BURGERS, P.M. (2004) Idling by DNA polymerase delta maintains a ligatable nick during lagging-strand DNA replication. *Genes Dev*. 18, 2764–2773.

GARINIS G.A., VAN DER HORST G.T., VIJG J. AND HOEIJMAKERS J.H. (2008) DNA damage and ageing: new-age ideas for an age-old problem. *Nat. Cell Biol.,* 10, 1241–1247.

GENSCHEL J., BAZEMORE L., MODRICH P. (2002) Human exonuclease I is required for 5′ and 3′ mismatch repair*, J. Biol. Chem.* 277, 13302–13311.

GENSCHEL, J. AND MODRICH, P. (2003) Mechanism of 5'-directed excision in human mismatch repair. *Mol. Cell* 12, 1077–1086.

GEORGESCU, R. E. *et al.* (2008) Structure of a sliding clamp on DNA. *Cell* 132, 43–54.

GLATTER, O.; KRATKY, O. (1982) Small angle x-ray scattering. London; New York: *Academic Press*, 27.

GLICKMAN MS. (2014). Double-strand DNA break repair in mycobacteria, *Microbiol Spectrum* 2(5):MGM2-0024-2013.

GLOOR, J.W., BALAKRISHNAN, L. AND BAMBARA, R.A. (2010) Flap endonuclease 1 mechanism analysis indicates flap base binding prior to threading. *J. Biol. Chem*. 285, 34922–34931.

GLOOR, J.W., BALAKRISHNAN, L., CAMPBELL, J.L. AND BAMBARA, R.A. (2012) Biochemical analyses indicate that binding and cleavage specificities define the ordered processing of human Okazaki fragments by Dna2 and FEN1. *Nucleic Acids Res*. 40, 6774–6786.

GOLDBERG, R. J. (1953). Sedimentation in the ultracentrifuge. *The Journal of Physical Chemistry*, 57, 194–202.

GRAVEL S., CHAPMAN J., MAGILL C., JACKSON S. (2008) DNA helicases Sgs1 and BLM promote DNA double-strand break resection, *Genes Dev.* 22, 2767–2772.

GUIDO KEIJZERS, VILHELM A. BOHR AND LENE JUEL RASMUSSEN. (2015) Human exonuclease 1 (EXO1) activity characterization and its function on flap structures *Bioscience Reports* 35, e00206, doi:10.1042/BSR20150058.

GUINIER A.(1939) *Ann Phys*. 1939; 12:76.

HALAZONETIS, T. D., GORGOULIS, V. G., AND BARTEK, J. (2008). An oncogene-induced DNA damage model for cancer development. *Science* 319, 1352-1355.

HANDA, N., ICHIGE, A. KOBAYASHI, I. (2009) Contribution of RecFOR machinery of homologous recombination to cell survival after loss of a restriction–modification gene complex, *Microbiology* 155, 2320–2332.

HANSEN JC, LEBOWITZ J, DEMELER B. (1994) Analytical ultracentrifugation of complex macromolecular systems. *Biochemistry* 33:13155–13163.

HARPER J.W. AND ELLEDGE S.J. (2007) The DNA damage response: ten years after. *Mol. Cell,* 28, 739–745.

HARRISON JC, HABER JE. (2006) Surviving the Breakup: The DNA Damage Checkpoint. *Annu Rev Genet*. 40:209–235.

HARTSUIKER, E., M.J. NEALE, A.M. CARR, (2009) Distinct requirements for the Rad32 (Mre11) nuclease and Ctp1 (CtIP) in the removal of covalently bound topoisomerase I and II from DNA, *Mol. Cell* 33, 117–123.

HAYDYN D.T. MERTENS, DMITRI I. SVERGUN, (2010). Structural characterization of proteins and complexes using small-angle X-ray solution scattering. *Journal of Structural Biology* 172, 128–141.

HENRIKSSON ML, TROLLER U, HALLBERG B. (2000) 14-3-3 proteins are required for the inhibition of Ras by exoenzyme S. *Biochem J* 349(Pt 3): 697–701.

HENSLEY P. (1996) Defining the structure and stability of macromolecular assemblies in solution: the re-emergence of analytical ultracentrifugation as a practical tool. *Structure*, 4:367–73.

HOEIJMAKERS, J. H. (2009) DNA damage, aging, and cancer. *N Engl J Med* 361, 1475-1485.

HOPKINS, B.B., T.T. PAULL, (2008) The P. furiosus mre11/rad50 complex promotes 5′ strand resection at a DNA double-strand break, *Cell* 135, 250–260.

HOTTA K, RANGANATHAN S, LIU R, WU F, MACHIYAMA H, ET AL. (2014) Biophysical Properties of Intrinsically Disordered p130Cas Substrate Domain — Implication in Mechanosensing. *PLoS Comput Biol* 10(4): e1003532. doi:10.1371/journal.pcbi.1003532

HOWLETT GJ, MINTON AP, RIVAS G. (2006) Analytical ultracentrifugation for the study of protein association and assembly. *Curr Opin Chem Biol* 10:430–6.

HUERTAS, P. (2010) DNA resection in eukaryotes: deciding how to fix the break. *Nat Struct Mol Biol* 17, 11-16

HUERTAS, P., F. CORTES-LEDESMA, A.A. SARTORI, A. AGUILERA, S.P. JACKSON, (2008) CDK targets Sae2 to control DNA-end resection and homologous recombination, *Nature* 455, 689–692.

HUNTER, T. (2009) CtIP links DNA double-strand break sensing to resection. *Mol Cell* 36, 954-969.

HURA, G.L., MENON, A.L., HAMMEL, M., RAMBO, R.P., POOLE, F.L., TSUTAKAWA, S.E., JENNEY, F.E., CLASSEN, S., FRANKEL, K.A., HOPKINS, R.C., YANG, S.J., SCOTT, J.W., DILLARD, B.D., ADAMS, M.W.W., TAINER, J.A., 2009. Robust, high-throughput solution structural analyses by small angle X-ray scattering (SAXS). *Nat. Methods* 6, 606–612.

IRA, G., A. PELLICIOLI, A. BALIJJA, X. WANG, S. FIORANI, W. CAROTENUTO, G. LIBERI, D. BRESSAN, L. WAN, N.M. HOLLINGSWORTH, J.E. HABER, M. FOIANI, (2004) DNA end resection, homologous recombination and DNA damage checkpoint activation require CDK1, *Nature* 431, 1011–1017.

IVANOV, I., CHAPADOS, B. R., MCCAMMON, J. A. & TAINER, J. A. (2006) Proliferating cell nuclear antigen loaded onto double-stranded DNA: dynamics, minor groove interactions and functional implications. *Nucleic Acids Res.* 34, 6023–6033.

J¨AGER, A.C., RASMUSSEN, M., BISGAARD, H.C., SINGH, K.K., NIELSEN, F.C. AND RASMUSSEN, L.J. (2001) HNPCC mutations in the human DNA mismatch repair gene hMLH1 influence assembly of hMutL alpha and hMLH1-hEXO1 complexes*. Oncogene* 20, 3590–3595.

JACKSON, S. P., AND BARTEK, J. (2009) The DNA-damage response in human biology and disease. *Nature* 461, 1071-1078.

JAGMOHAN-CHANGUR, S., POIKONEN, T., VILKKI, S., LAUNONEN, V., WIKMAN, F., ORNTOFT, T.F., MOLLER, P., VASEN, H., TOPS, C., KOLODNER, R.D. ET AL. (2003) EXO1 variants occur commonly in normal population: evidence against a role in hereditary nonpolyposis colorectal cancer. *Cancer Res*. 63, 154–158.

JOHNSON C, CROWTHER S, STAFFORD MJ, CAMPBELL DG, TOTH R, MACKINTOSH C. (2010) Bioinformatic and experimental survey of 14-3-3-binding sites. *Biochem J* 427:69–78.

KALPAND, M.K., GARY, D.F. AND LVAN, L.C. (1994) A Study of the Molecular Sources of Nonideal Osmotic Pressure of Bovine Serum Albumin Solutions as a Function of pH, *Biophys. J.* 66, 153–160.

KALTHOFF, C., ALVES, J., URBANKE, C., KNORR, R., & UNGEWICKELL, E. J. (2002). Unusual structural organization of the endocytic proteins AP180 and epsin 1. *The Journal of Biological Chemistry*, 277, 8209–8216.

KARANJA, K. K., LEE, E. H., HENDRICKSON, E. A., AND CAMPBELL, J. L. (2014) Preventing over-resection by DNA2 helicase/nuclease suppresses repair defects in Fanconi anemia cells. *Cell Cycle* 13, 1540–1550.

KARRAS, G. I., FUMASONI, M., SIENSKI, G., VANOLI, F., BRANZEI, D., AND JENTSCH, S. (2013) Noncanonical role of the 9-1-1 clamp in the error-free DNA damage tolerance pathway. *Mol Cell* 49, 536-546.

KASTAN M.B. AND BARTEK J. (2004) Cell-cycle checkpoints and cancer. *Nature,* 432, 316–323.

KEELAGHER, R.E., V.E. COTTON, A.S. GOLDMAN, R.H. BORTS, (2010) Separable roles for exonuclease I inmeiotic DNA double-strand break repair, *DNA Repair* (Amst).

KEIJZERS, G., MAYNARD, S., SHAMANNA, R.A., RASMUSSEN, L.J., CROTEAU, D.L. AND BOHR, V.A. (2014) The role of RecQ helicases in non-homologous end-joining. *Crit. Rev. Biochem. Mol. Biol.* 49, 463–472.

KIM Y.C., GERLITZ G., FURUSAWA T., CATEZ,F., NUSSENZWEIG A., OH K.S., KRAEMER K.H., SHILOH Y. AND BUSTIN M. (2009) Activation of ATM depends on chromatin interactions occurring before induction of DNA damage. *Nat. Cell. Biol*., 11, 92–96.

KORADI R, BILLETER M, WUTHRICH K. (1996) MOLMOL: a program for display and analysis of macromolecular structures. *J Mol Graph* 14(51–55):29–32.

KRAMER, K.M., HABER, J.E. (1993) New telomeres in yeast are initiated with a highly selected subset of TG1-3 repeats, *Genes Dev*. 7, 2345–2356.

KRISHNA TSR, KONG XP, GARY S, BURGERS PM, KURIYAN J. (1994) Crystal structure of the eukaryotic DNA polymerase processivity factor PCNA. *Cell.* 79:1233–1243.

KUNKEL, T. A., SCHARFF, M. D., AND EDELMANN, W. (2013) Mammalian Exo1 encodes both structural and catalytic functions that play distinct roles in essential biological processes. *Proc Natl Acad Sci* USA 110, E2470-E2479.

LANGERAK, P., MEJIA-RAMIREZ, E., LIMBO, O., AND RUSSELL, P. (2011) Release of Ku and MRN from DNA ends by Mre11 nuclease activity and Ctp1 is required for homologous recombination repair of doublestrand breaks. *PLoS Genet* 7, e1002271.

LAUE TM, STAFFORD WF. (1999) Modern Applications of Analytical Ultracentrifugation. *Ann Rev Biophys Biomol Struct* 28:75–100.

LAUE TM. (1995) Sedimentation Equilibrium as Thermodynamic Tool. *Methods Enzymol* 259:427–452.

LAURENT, T. C., & KILLANDER, J. (1964). A theory of gel filtration and its experimental verification. *Journal of Chromatography*, 14, 317–330.

LEBOWITZ J, LEWIS MS, SCHUCK P. (2002) Modern analytical ultracentrifugation in protein science: A tutorial review. *Protein Sci* 11:2067–2079.

LEE B., WILSON D.R. (1999) The RAD2 domain of human exonuclease 1 exhibits 5′ to 3′ exonuclease and flap structure-specific endonuclease activities, *J. Biol. Chem.* 274, 37763–37769.

LEE BI, B.-I., NGUYEN, L.H., BARSKY, D., FERNANDES, M. AND WILSON, D.M. (2002) Molecular interactions of human Exo1 with DNA. *Nucleic Acids Res.* 30, 942–949.

LEE, B.I. AND WILSON, D.M. (1999) The RAD2 domain of human exonuclease 1 exhibits 5′ to 3′ exonuclease and flap structure-specific endonuclease activities. *J. Biol. Chem*. 274, 37763–37769.

LI, X., ROMERO, P., RANI, M., DUNKER, A. K. AND OBRADOVIC, Z. (1999). Predicting protein disorder for N-, C-, and internal regions. *Genome Inform. Ser. Workshop Genome Inform*. 10:30–40.

LI, X., STITH,C.M., BURGERS,P.M. AND HEYER,W.D. (2009) PCNA is required for initiation of recombination-associated DNA synthesis by DNA polymerase delta. *Mol. Cell*, 36, 704–713.

LIAO, S., T. TOCZYLOWSKI, H. YAN, (2008) Identification of the Xenopus DNA2 protein as a major nuclease for the 5′-3′ strand-specific processing of DNA ends, *Nucleic Acids Res*. 36, 6091–6100.

LIBERTI, S.E., ANDERSEN, S.D., WANG, J., MAY, A., MIRON, S., PERDERISET, M., KEIJZERS, G., NIELSEN, F.C., CHARBONNIER, J.-B., BOHR, V.A. et al. (2011) Bi-directional routing of DNA mismatch repair protein human exonuclease 1 to replication foci and DNA double strand breaks. *DNA Repair* (Amst.) 10, 73–86.

LIEBER M.R. (1997) The FEN-1 family of structure-specific nucleases in eukaryotic DNA replication, recombination and repair. *Bioassays,* 19, 233-240.

LIEBER, M.R. (2010). The mechanism of double-strand DNA break repair by the nonhomologous DNA end-joining pathway. *Annu Rev Biochem* 79:181–211.

LIMBO, O., C. CHAHWAN, Y. YAMADA, R.A. DE BRUIN, C. WITTENBERG, P. RUSSELL, (2007) Ctp1 is a cell-cycle-regulated protein that functions with Mre11 complex to control double-strand break repair by homologous recombination, *Mol. Cell* 28, 134–146.

LIU D, BIENKOWSKA J, PETOSA C, COLLIER RJ, FU H, LIDDINGTON R. (1995) Crystal structure of the zeta isoform of the 14-3-3 protein. *Nature* 376:191–4.

LORD, C. J., AND ASHWORTH, A. (2012) The DNA damage response and cancer therapy. *Nature* 481, 287-294.

LYDEARD, J.R., Z. LIPKIN-MOORE, S. JAIN, V.V. EAPEN, J.E. HABER, (2010) Sgs1 and exo1 redundantly inhibit break-induced replication and de novo telomere addition at broken chromosome ends, *PLoS Genet*. 6, e1000973.

MAGA G, HUBSCHER U. (2003) Proliferating cell nuclear antigen (PCNA): a dancer with many partners. *J Cell Sci.* 116:3051–3060.

MAJKA,J. AND BURGERS,P.M. (2004) The PCNA-RFC families of DNA clamps and clamp loaders. Prog. *Nucleic Acid Res. Mol. Biol.,* 78, 227–260.

MANFRINI, N., I. GUERINI, A. CITTERIO, G. LUCCHINI, M.P. LONGHESE, (2010) Processing of meiotic DNA double strand breaks requires cyclin-dependent kinase and multiple nucleases, *J. Biol. Chem*. 285, 11628–11637.

MARINGELE L., AND LYDALL D. (2002) EXO1-dependent single-stranded DNA at telomeres activates subsets of DNA damage and spindle checkpoint pathways in budding yeast yku70Delta mutants, *Genes Dev.* 16, 1919–1933.

MARINGELE, L., AND LYDALL, D. (2004) Telomerase- and recombination-independent immortalization of budding yeast. *Genes Dev* 18, 2663-2675.

MASTERS SC, PEDERSON KJ, ZHANG L, BARBIERI JT, FU H. (1999) Interaction of 14-3-3 with a non-phosphorylated protein ligand, exoenzyme S of Pseudomonas aeruginosa. *Biochemistry* 38:5216–21.

MASTERS, S. C., AND FU, H. (2001) 14-3-3 proteins mediate an essential anti-apoptotic signal. *J Biol Chem* 276, 45193-45200.

MATSUO K, SAKURADA Y, YONEHARA R, KATAOKA M, GEKKO K (2007) Secondary-structure analysis of denatured proteins by vacuum-ultraviolet circular dichroism spectroscopy. *Biophys J* 92(11):4088–4096.

MAY, Y., A., BOHR, V. A., FERRARI, S., ZANNIS-HADJOPOULOS, M., FU, H., AND RASMUSSEN, L. J. (2012) 14-3-3 checkpoint regulatory proteins interact specifically with DNA repair protein human exonuclease 1 (hEXO1) via a semi-conserved motif. *DNA Repair* 11, 267-277.

MAYANAGI, K. *et al.* Architecture of the DNA polymerase B–proliferating cell nuclear antigen (PCNA)–DNA ternary complex. *Proc. Natl Acad. Sci. USA* 108, 1845–1849 (2011).

MCKINNON P.J. AND CALDECOTT K.W. (2007) DNA strand break repair and human genetic disease. *Annu. Rev. Genomics Hum. Genet.,* 8, 37–55.

MIMITOU E.P. AND SYMINGTON L.S. (2009) DNA end resection: many nucleases make light work. *DNA Repair (Amst),* 8, 983–995.

MIMITOU, E. P., AND SYMINGTON, L. S. (2008) Sae2, Exo1 and Sgs1 collaborate in DNA double-strand break processing. *Nature* 455, 770-774.

MIMITOU, E. P., AND SYMINGTON, L. S. (2010) Ku prevents Exo1 and Sgs1-dependent resection of DNA ends in the absence of a functional MRX complex or Sae2. *EMBO J* 29, 3358-3369.

MODRICH P. (2006) Mechanisms in eukaryotic mismatch repair. *J. Biol. Chem*., 281, 30305–30309.

MOLDOVAN, G.L., PFANDER, B. AND JENTSCH, S. (2007) PCNA, the maestro of the replication fork. *Cell*, 129, 665–679.

MONCOQ, K., BROUTIN, I., CRAESCU, C. T., VACHETTE, P., DUCRUIX, A., DURAND, D. (2004) SAXS study of the PIR domain from the Grb14 molecular adaptor: A natively unfolded protein with a transient structure primer? *Biophys. J.*, *87* (6), 4056-4064.

MORADI M., V. BABIN, C. ROLAND, T. A. DARDEN, AND C. SAGUI, (2009) *Proc. Natl. Acad. Sci*. USA. 106, 20746.

MORIN, I., NGO, H.-P., GREENALL, A., ZUBKO, M.K., MORRICE, N. AND LYDALL, D. (2008) Checkpoint-dependent phosphorylation of Exo1 modulates the DNA damage response. *EMBO J*. 27, 2400–2410.

MORRISON, D. K. (2009) The 14-3-3 proteins: integrators of diverse signaling cues that impact cell fate and cancer development. *TiCB* 19, 16-23.

MOYNAHAN, M. E., AND JASIN, M. (2010) Mitotic homologous recombination maintains genomic stability and suppresses tumorigenesis. *Nat Rev Mol Cell Biol* 11, 196-207.

MUSLIN, A.J., TANNER, J.W., ALLEN P.M., SHAW, A.S. (1996) Interaction of 14-3-3 with signalling proteins is mediated by the recognition of phosphoserine. *Cell* 84:889–897.

MYLONAS, E., A. HASCHER, P. BERNADO´,M. BLACKLEDGE, E. MANDELKOW AND D. I. SVERGUN, (2008) *Biochemistry,* 47, 10345–10353.

NAIRN, K. M., R. E. LYONS, R. J. MULDER, S. T. MUDIE, D. J. COOKSON, E. LESIEUR, M. KIM, D. LAU, F. H. SCHOLES AND C. M. ELVIN, (2008) *Biophys. J.*, 95, 3358–3365.

NARYZHNY, S.N., (2008) Proliferating cell nuclear antigen: a proteomics view. *Cell Molec Life Sci*. 65:3789–3808.

NEALE, M.J., J. PAN, S. KEENEY, (2005) Endonucleolytic processing of covalent protein linked DNA double-strand breaks, *Nature* 436, 1053–1057.

NGO, G. H. P., BALAKRISHNAN, L., DUBARRY, M., CAMPBELL, J.L. AND LYDALL, D. (2014). The 9-1-1 checkpoint clamp stimulates DNA resection by Dna2-Sgs1 and Exo1. *Nucleic Acids Res*. 42, 10516–10528.

NICOLETTE, M.L., LEE, K., GUO, Z., RANI, M., CHOW, J. M., LEE, S. E., AND PAULL, T. T. (2010) Mre11-Rad50- Xrs2 and Sae2 promote 5' strand resection of DNA double-strand breaks. *Nat Struct Mol Biol* 17, 1478- 1485.

NIELSEN F., JÄGER A., LÜTZEN A., BUNDGAARD J., RASMUSSEN L. (2004) Characterization of human exonuclease 1 in complex with mismatch repair proteins, subcellular localization and association with PCNA, *Oncogene* 23, 1457–1468.

NIMONKAR, A.V., GENSCHEL, J., KINOSHITA, E., POLACZEK, P., CAMPBELL, J.L., WYMAN, C., MODRICH, P. AND KOWALCZYKOWSKI, S.C. (2011) BLM-DNA2-RPA-MRN and EXO1-BLM-RPA-MRN constitute two DNA end resection machineries for human DNA break repair. *Genes Dev*. 25, 350–362.

NIMONKAR, A.V., OZSOY A.Z., GENSCHEL J., MODRICH P. AND KOWALCZYKOWSKI S.C. (2008) Human exonuclease 1 and BLM helicase interact to resect DNA and initiate DNA repair. *Proc. Natl Acad. Sci. USA*, 105, 16906–16911.

NISPA, M., ALEX, M.J. AND JOHN, B. (1999) Translational Diffusion Coefficients of Bovine Serum Albumin in Aqueous Solution at High Ionic Strength, *J. Colloid Interface Sci.* 218, 167–175.

NIU, H., W.H. CHUNG, Z. ZHU, Y. KWON, W. ZHAO, P. CHI, R. PRAKASH, C. SEONG, D. LIU, L. LU, G. IRA, P. SUNG, (2010) Mechanism of the ATP-dependent DNA end-resection machinery from Saccharomyces cerevisiae, *Nature* 467, 108–111.

OLDFIELD CJ, MENG J, YANG JY, YANG MQ, UVERSKY VN, DUNKER AK. (2008) Flexible nets: disorder and induced fit in the associations of p53 and 14-3-3 with their partners. *BMC Genomics* 9(Suppl. 1):S1.

ORANS J., MCSWEENEY E.A., IYER R.R., HAST M.A., HELLINGA H.W., MODRICH P., BEESE L.S. (2011) Structures of human exonuclease 1 DNA complexes suggest a unified mechanism for nuclease family, *Cell* 145, 212–223.

ORBÁN G, et al. (2010) Different electrophysiological actions of 24- and 72-hour aggregated amyloid-beta oligomers on hippocampal field population spike in both anesthetized and awake rats. *Brain Res* 1354:227–235.

OTTMANN C, YASMIN L, WEYAND M, VEESENMEYER JL, DIAZ MH, PALMER RH, et al. (2007) Phosphorylation-independent interaction between 14-3-3 and exoenzyme S: from structure to pathogenesis. *Embo J*, 26:902–13.

PAQUES F, AND HABER JE. (1999). Multiple pathways of recombination induced by double-strand breaks in *Saccharomyces cerevisiae*. *Microbiol. Mol. Biol. Rev.* 63:349–404.

PAZ, A., ZEIV-BEN-MORDEHAI, T., LUNDQVIST, M., SHERMAN, E., MYLONAS, E., WEINER, L., et al. (2008). Biophysical characterization of the unstructured cytoplasmic domain of the human neuronal adhesion protein neuroligin 3. *Biophysical Journal*, 95, 1928–1944.

PEI, H., ZHANG, L., LUO, K., QIN, Y., CHESI, M., FEI, F., BERGSAGEL, P. L., WANG, L., YOU, Z., AND LOU, Z. (2011) MMSET regulates histone H4K20 methylation and 53BP1 accumulation at DNA damage sites. *Nature* 470, 124-128.

PENG, C. Y., GRAVES, P. R., THOMA, R. S., WU, Z., SHAW, A. S., AND PIWNICA-WORMS, H. (1997) Mitotic and G2 checkpoint control: regulation of 14-3-3 protein binding by phosphorylation of Cdc25C on serine-216. *Science* 277, 1501-1505.

PEREZ, J., VACHETTE, P., RUSSO, D., DESMADRIL, M., DURAND, D. (2001) Heat induced unfolding of neocarzinostatin, a small all-beta protein investigated by small-angle X-ray scattering. *J. Mol. Biol.*, *308* (4), 721-743.

PETOSA C, MASTERS SC, BANKSTON LA, POHL J, WANG B, FU H, et al. (1998) 14-3-3zeta binds a phosphorylated Raf peptide and an unphosphorylated peptide via its conserved amphipathic groove. *J Biol Chem* 273:16305–10.

PETOUKHOV, M.V., SVERGUN, D.I., (2003). New methods for domain structure determination of proteins from solution scattering data. *Journal of Applied Crystallography* 36, 540–544.

PETOUKHOV, M.V., SVERGUN, D.I., (2005). Global rigid body modeling of macromolecular complexes against small-angle scattering data. Biophysical Journal 89, 1237–1250.

PUTNAM, C.; HAMMEL, M.; HURA, G.; TAINER, J. (2007) X-ray solution scattering (SAXS) combined with crystallography and computation: defining accurate macromolecular structures, conformations and assemblies in solution. *Q. Rev. Biophys.*, *40* (3), 191-285.

QIU, J., QIAN, Y., CHEN, V., GUAN, M.X. AND SHEN, B. (1999) Human exonuclease 1 functionally complements its yeast homologues in DNA recombination, RNA primer removal, and mutation avoidance. *J. Biol. Chem.* 274, 17893–17900.

QIU, J., QIAN, Y., FRANK, P., WINTERSBERGER, U. AND SHEN, B. (1999) Saccharomyces cerevisiae RNase H(35) functions in RNA primer removal during lagging-strand DNA synthesis, most efficiently in cooperation with Rad27 nuclease. *Mol. Cell. Biol*. 19, 8361–8371.

RAJASEKAR, K., MUNTAHA, S. T., TAME, J. R. H., KOMMAREDDY, S., MORRIS, G., WHARTON, C. W., et al. (2010). Order and disorder in the domain organization of the plasmid partition protein KorB. *The Journal of Biological Chemistry*, 285, 15440–15449.

RAWISO, M. (1999). From intensity to structure in physical chemistry of polymers. *J. Physique Iv*, *9* (P1), 147-195.

REINHARDT, H. C., AND YAFFE, M. B. (2013) Phospho-Ser/Thr-binding domains: navigating the cell cycle and DNA damage response. *Nat Rev Mol Cell Biol* 14, 563-580.

ROMERO, P., OBRADOVIC, Z. AND DUNKER, A. K. (1997). Sequence data analysis for long disordered regions prediction in the calcineurin family. *Genome Inform. Ser. Workshop Genome Inform*. 8:110–124.

ROMERO, P., OBRADOVIC, Z. LI, X. GARNER, E. BROWN, C. AND DUNKER A. K. (2001). Sequence complexity of disordered protein. *Proteins*. 42:38–48.

ROSSIELLO, F., HERBIG, U., LONGHESE, M. P., FUMAGALLI, M., AND D'ADDA DI FAGAGNA, F. (2014) Irreparable telomeric DNA damage and persistent DDR signalling as a shared causative mechanism of cellular senescence and ageing. *Curr Opin Genet Dev* 26, 89-95.

ROUND, A.R., FRANKE, D., MORITZ, S., HUCHLER, R., FRITSCHE, M., MALTHAN, D., KLAERING, R., SVERGUN, D.I., ROESSLE, M., (2008). Automated sample-changing robot for solution scattering experiments at the EMBL Hamburg SAXS station X33. J. Appl. Cryst. 41, 913–917.

ROUSE J, JACKSON SP. (2002) Interfaces between the detection, signaling, and repair of DNA damage. *Science*. 297:547–551.

RUDOLPH, C., KUHNEL, F., WEI, K., SCHLEGELBERGER, B., SCHIRMACHER, P., KUNKEL, T. A., GREENBERG, R. A., SANCHEZ-PUIG, N., VEPRINTSEV, D. B., & FERSHT, A. R. (2005). Human full-length securin is a natively unfolded protein. *Protein Science*, 14, 1410–1418.

SCHAETZLEIN S., CHAHWAN R., AVDIEVICH E., ROA S., WEI K., EOFF R.L., SELLERS R.S., CLARK A.B., KUNKEL T.A., SCHARFF M.D. et al. (2013) Mammalian Exo1 encodes both structural and catalytic functions that play distinct roles in essential biological processes. *Proc. Natl Acad. Sci. USA*, 110, E2470–E2479.

SCHAETZLEIN S., KODANDARAMIREDDY N., JU Z., LECHEL A., STEPCZYNSKA A., LILLI D., CLARK A., RUDOLPH C., KUHNEL F., WEI K., SCHLEGELBERGER B., SCHIRMACHER P., KUNKEL T., GREENBERG R., EDELMANN W., RUDOLPH K. (2007) Exonuclease-1 deletion impairs DNA damage signaling and prolongs lifespan of telomere-dysfunctional mice, *Cell* 130, 863–877.

SCHMUTTE C., SADOFF M.M., SHIM K.S., ACHARYA S. AND FISHEL R. (2001) The interaction of DNA mismatch repair proteins with human exonuclease I. *J. Biol. Chem*., 276, 33011–33018.

SCHMUTTE, C., MARINESCU, R.C., SADOFF, M.M., GUERRETTE, S., OVERHAUSER, J. AND FISHEL, R. (1998) Human exonuclease I interacts with the mismatch repair protein hMSH2. *Cancer Res*. 58, 4537–4542.

SCHMUTTE, C., SADOFF, M.M., SHIM, K.S., ACHARYA, S. AND FISHEL, R. (2001) The interaction of DNA mismatch repair proteins with human exonuclease I. *J. Biol. Chem*. 276, 33011–33018.

SCHUCK P (2000) Size-distribution analysis of macromolecules by sedimentation velocity ultracentrifugation and lamm equation modeling. *Biophys J* 78: 1606–1619.

SCOTT, DJ. AND SCHUCK, P. (2005) A brief introduction to the analytical ultracentrifugation of proteins for beginners. In: Scott, DJ.; Harding, SE.; Rowe, AJ., editors. Analytical Ultracentrifugation. *Royal Society of Chemistry*: Cambridge, UK, 1-25.

SEGURADO, M., AND DIFFLEY, J. F. (2008) Separate roles for the DNA damage checkpoint protein kinases in stabilizing DNA replication forks. *Genes Dev* 22, 1816-1827.

SELKOE DJ (2003) Folding proteins in fatal ways. *Nature* 426(6968):900–904.

SHAO, H., BAITINGER, C., SODERBLOM, E.J., BURDETT, V. AND MODRICH, P. (2014) Hydrolytic function of Exo1 in mammalian mismatch repair. *Nucleic Acids Res*. 42, 7104–7112.

SHARMA, S., SOMMERS, J.A., DRISCOLL, H.C., UZDILLA, L., WILSON, T.M. AND BROSH, R.M. (2003) The exonucleolytic and endonucleolytic cleavage activities of human exonuclease 1 are stimulated by an interaction with the carboxyl-terminal region of the Werner syndrome protein. *J. Biol. Chem*. 278, 23487–23496.

SHELL, S. S., C. D. PUTNAM AND R. D. KOLODNER, (2007). *Mol. Cell*, 26, 565–578.

SHILOH, Y., AND ZIV, Y. (2013) The ATM protein kinase: regulating the cellular response to genotoxic stress, and more. *Nat Rev Mol Cell Biol* 14, 197-210.

SHIM, E.Y., CHUNG, W.H., NICOLETTE, M.L., ZHANG, Y., DAVIS, M., ZHU, Z. PAULL, T.T., IRA, G., LEE, S.E. (2010) Saccharomyces cerevisiae Mre11/Rad50/Xrs2 and Ku proteins regulate association of Exo1 and Dna2 with DNA breaks, *EMBO J*. 29, 3370–3380.

SHIOTANI, B., AND ZOU, L. (2009) Single-stranded DNA orchestrates an ATM-to-ATR switch at DNA breaks. *Mol Cell* 33, 547-558.

SHOEMAKER BA, PORTMAN JJ, WOLYNES PG. (2000) Speeding molecular recognition by using the folding funnel: the fly-casting mechanism. *Proc Natl Acad Sci* USA, 97:8868–73.

SHUMAN S, GLICKMAN MS. (2007). Bacterial DNA repair by nonhomologous end joining. *Nat Rev Microbiol* 5:852–861.

SIEGEL, L. M., & MONTY, K. J. (1966). Determination of the molecular weights and frictional ratios of proteins in impure systems by use of gel filtration and density gradient centrifugation: Application to crude preparations of sulfite and hydroxylamine reductases. *Biochimica et Biophysica Acta*, 112, 346–362.

SINHA, K.M., UNCIULEAC, M.C., GLICKMAN, M.S., SHUMAN, S (2009). AdnAB: a new DSB-resecting motor-nuclease from mycobacteria, *Genes Dev.* 23, 1423–1437.

SOKOLOVA, A.V., VOLKOV, V.V., SVERGUN, D.I., (2003a). Prototype of a database for rapid protein classification based on solution scattering data. *Journal of Applied Crystallography* 36, 865–868.

SOKOLOVA, A.V., VOLKOV, V.V., SVERGUN, D.I., (2003b). Database for rapid protein classification based on small-angle X-ray scattering data. *Crystallography Reports* 48, 959–965.

SOULAS-SPRAUEL P, RIVERA-MUNOZ P, MALIVERT L, LE GUYADER G, ABRAMOWSKI V, et al. (2007). V(D)J and immunoglobulin class switch recombinations: a paradigm to study the regulation of DNA end-joining. *Oncogene* 26:7780–91.

STEPHEN P. JACKSON AND JIRI BARTEK, (2009). The DNA-damage response in human biology and disease. *Nature* 22; 461(7267): 1071–1078.

STRACKER, T. H., ROIG, I., KNOBEL, P. A., AND MARJANOVIC, M. (2013) The ATM signaling network in development and disease. *Front Genet* 4, 37.

SUN, J., LEE, K. J., DAVIS, A. J., AND CHEN, D. J. (2012) Human Ku70/80 protein blocks exonuclease 1-mediated DNA resection in the presence of human Mre11 or Mre11/Rad50 protein complex. *J. Biol. Chem.* 287, 4936–4945.

SUN, X., ZHENG, L. AND SHEN, B. (2002) Functional alterations of human exonuclease 1 mutants identified in atypical hereditary nonpolyposis colorectal cancer syndrome. *Cancer Res*. 62, 6026–6030.

SUNG P. AND KLEIN H. (2006) Mechanism of homologous recombination: mediators and helicases take on regulatory functions. *Nat. Rev. Mol. Cell Biol.*, 7, 739–750.

SVERGUN, D.I., KOCH, M.H.J., (2003). Small-angle scattering studies of biological macromolecules in solution. *Reports on Progress in Physics* 66, 1735–1782.

SYMINGTON LS, GAUTIER J. (2011). Double-strand break end resection and repair pathway choice. *Annu Rev Genet* 45:247–271.

SZANKASI P. AND SMITH G.R. (1992) A DNA exonuclease induced during meiosis of *Schizosaccharomyces pombe*. *J. Biol. Chem*., 267, 3014–3023.

SZANKASI P. AND SMITH G.R. (1995) A role for exonuclease 1 from *S. pombe* in mutation avoidance and mismatch correction. *Science,* 267, 1166-1169.

TAKAHASHI, Y., NISHIKAWA, Y., FUJISAWA, T., (2003). Evaluation of three algorithms for ab initio determination of three-dimensional shape from one-dimensional solution scattering profiles. *Journal of Applied Crystallography* 36, 549–552.

TAKASHI ISHIDA AND KENGO KINOSHITA, (2007). PrDOS: prediction of disordered protein regions from amino acid sequence. *Nucleic Acids Research*, Vol. 35 Web Server issue doi:10.1093/nar/gkm363.

TANFORD, C. (1961). Physical chemistry of macromolecules. New York: *Wiley*.

TINLINE-PURVIS H., SAVORY A.P., CULLEN J.K., DAVE A., MOSS J., BRIDGE W.L., MARGUERAT S., BAHLER J., RAGOUSSIS J., MOTT R., WALKER C.A., HUMPHREY T.C.

(2009) Failed gene conversion leads to extensive end processing and chromosomal rearrangements in fission yeast, *EMBO J.* 28, 3400–3412.

TISHKOFF, D.X., BOERGER, A.L., BERTRAND, P., FILOSI, N., GAIDA, G.M., KANE, M.F. AND KOLODNER, R.D. (1997) Identification and characterization of *Saccharomyces cerevisiae* EXO1, a gene encoding an exonuclease that interacts with MSH2. *Proc. Natl. Acad. Sci*. U.S.A. 94, 7487–7492.

TOLEDO, L. I., ALTMEYER, M., RASK, M. B., LUKAS, C., LARSEN, D. H., POVLSEN, L. K., BEKKER-JENSEN, S., MAILAND, N., BARTEK, J., AND LUKAS, J. (2013) ATR prohibits replication catastrophe by preventing global exhaustion of RPA. *Cell* 155, 1088–1103.

TOMIMATSU, N., MUKHERJEE, B., CATHERINE HARDEBECK, M., ILCHEVA, M., VANESSA CAMACHO, C., LOUISE HARRIS, J., PORTEUS, M., LLORENTE, B., KHANNA, K. K., AND BURMA, S. (2014) Phosphorylation of EXO1 by CDKs 1 and 2 regulates DNA end resection and repair pathway choice. *Nat Commun* 5, 3561.

TRAN P.T., ERDENIZ N., SYMINGTON L.S. AND LISKAY R.M. (2004) EXO1-A multi-tasking eukaryotic nuclease. *DNA Repair (Amst)*, 3, 1549–1559.

TRAN P.T., FEY J.P., ERDENIZ N., GELLON L., BOITEUX S., LISKAY R.M. (2007) A mutation in EXO1 defines separable roles in DNA mismatch repair and post-replication repair, DNA Repair *(Amst.)* 6, 1572–1583.

TRAUTMAN, R., & SCHUMAKER, V. N. (1954). Generalization of the radial dilution squared law in ultracentrifugation. *The Journal of Chemical Physics*, 22, 551–554.

TSUBOUCHI, H., OGAWA, H. (2000) Exo1 roles for repair of DNA double-strand breaks and meiotic crossing over in *Saccharomyces cerevisiae*, *Mol. Biol. Cell* 11, 2221–2233.

TSURIMOTO T. (1999) PCNA binding proteins. *Frontiers in Bioscience*. 4:849–858.

TSUTAKAWA, S. E., LAFRANCE-VANASSE, J., AND TAINER, J. A. (2014). The cutting edges in DNA repair, licensing, and fidelity: DNA and RNA repair nucleases sculpt DNA to measure twice, cut once. *DNA Repair* 19, 95–107.

UVERSKY, V., & LONGHI, S. (2010). Instrumental analysis of intrinsically disordered proteins. Hoboken, NJ: *Wiley*.

VALLUR A.C., MAIZELS N. (2010) Distinct activities of exonuclease 1 and flap endonuclease 1 at telomeric g4 DNA, *PLoS ONE* 5, e8908.

WADE J. HARPER AND STEPHEN J. ELLEDGE (2007) The DNA Damage Response: Ten Years After. *Molecular Cell* 28, 739-745.

WALLACE, B.A. (2009) Protein characterization by synchrotron radiation circular dichroism spectroscopy. *Q Rev Biophys* 42(4):317–370.

WALTER, J., SUN, L., AND NEWPORT, J. (1998) Regulated chromosomal DNA replication in the absence of a nucleus. *Mol Cell* 1, 519-529.

WANG B, YANG H, LIU YC, JELINEK T, ZHANG L, RUOSLAHTI E, et al. (1999) Isolation of high affinity peptide antagonists of 14-3-3 proteins by phage display. *Biochemistry*, 38:12499–504.

WEI, K., CLARK, A. B., WONG, E., KANE, M. F., MAZUR, D. J., PARRIS, T., KOLAS, N. K., RUSSELL, R., HOU, H., JR., KNEITZ, B., YANG, G., KUNKEL, T. A., KOLODNER, R. D., COHEN, P. E., AND EDELMANN, W. (2003) Inactivation of Exonuclease 1 in mice results in DNA mismatch repair defects, increased cancer susceptibility, and male and female sterility. *Genes Dev* 17, 603-614.

WILKER EW, GRANT RA, ARTIM SC, YAFFE MB. (2005) A structural basis for 14-3-3sigma functional specificity. *J Biol Chem*, 280:18891–8.

WILLIAMS, R.S., G. MONCALIAN, J.S. WILLIAMS, Y. YAMADA, O. LIMBO, D.S. SHIN, L.M. GROOCOCK, D. CAHILL, C. HITOMI, G. GUENTHER, D. MOIANI, J.P. CARNEY, P. RUSSELL, J.A. TAINER, (2008) Mre11 dimers coordinate DNA end bridging and nuclease processing in double-strand-break repair, *Cell* 135, 97–109.

WILSON D.M., CARNEY J.P., COLEMAN M.A., ADAMSON A.W., CHRITENSEN M. AND LAMERDIN J.E. (1998) Hex1: a new human Rad2 nuclease family member with homology to yeast exonuclease 1. *Nucleic Acids Res.,* 26, 3762-3768.

WOODY, R.W. (1995) Circular dichroism. *Methods Enzymol* 246:34–71.

WRIGHT PE, DYSON HJ. (2009) Linking folding and binding. *Curr Opin Struct Biol*, 19:31–8.

WU, D., TOPPER, L.M. WILSON, T.E. (2008) Recruitment and dissociation of nonhomologous end joining proteins at a DNA double-strand break in *Saccharomyces cerevisiae*, *Genetics* 178, 1237–1249.

WURTELE M, JELICH-OTTMANN C, WITTINGHOFER A, OECKING C. (2003) Structural view of a fungal toxin acting on a 14-3-3 regulatory complex. *Embo J*, 22:987–94.

XIAO B, SMERDON SJ, JONES DH, DODSON GG, SONEJI Y, AITKEN A, et al. (1995) Structure of a 14-3-3 protein and implications for coordination of multiple signalling pathways. *Nature*, 376:188–91.

XU, H., ZHANG, P., LIU, L. & LEE, M. Y. (2001) A novel PCNA-binding motif identified by the panning of a random peptide display library. *Biochemistry* 40, 4512–4520.

Xu, Z., Fulop, Z., Wu, G., Pone, E. J., Zhang, J., Mai, T., Thomas, L. M., Al-Qahtani, A., White, C. A., Park, S. R., Steinacker, P., Li, Z., Yates, J., 3rd, Herron, B., Otto, M., Zan, H., Fu, H., and Casali, P. (2010) 14-3-3 adaptor proteins recruit AID to 5′-AGCT-3′-rich switch regions for class switch recombination. *Nat Struct Mol Biol* 17(9): 1124-1135.

YAFFE, M.B, et al. (1997) The structural basis for 14-3-3:phosphopeptide binding specificity. *Cell* 91:961–971.

YANG C., VAN DER WOERD, M. J., MUTHURAJAN, U. M., HANSEN, J. C AND LUGER, K. (2001) *Nucleic Acids Res*., 39, 4122–4135.

YANG S.H., ZHOU R., CAMPBELL J., CHEN J., HA T. AND PAULL T.T. (2013) The SOSS1 single-stranded DNA binding complex promotes DNA end resection in concert with Exo1. *EMBO J*., 32, 126–139.

YANG X, LEE WH, SOBOTT F, PAPAGRIGORIOU E, ROBINSON CV, GROSSMANN JG, et al. (2006) Structural basis for protein–protein interactions in the 14-3-3 protein family. *Proc Natl Acad Sci* USA, 103:17237–42.

YEELES JT, DILLINGHAM MS. (2010). The processing of double-stranded DNA breaks for recombinational repair by helicase-nuclease complexes. *DNA Repair* 9:276–285.

YOU Z. AND BAILIS J.M. (2010) DNA damage and decisions: CtIP coordinates DNA repair and cell cycle checkpoints. *Trends Cell Biol.*, 20, 402–409.

YOU Z., BAILIS J.M., JOHNSON S.A., DILWORTH S.M. AND HUNTER T. (2007) Rapid activation of ATM on DNA flanking double-strand breaks. *Nat. Cell. Biol*., 9, 1311–1318.

YOU Z., CHAHWAN C., BAILIS J., HUNTER T. AND RUSSELL P. (2005) ATM activation and its recruitment to damaged DNA require binding to the C terminus of Nbs1. *Mol. Cell. Biol*., 25, 5363–5379.

YOU, Z., SHI, L. Z., ZHU, Q., WU, P., ZHANG, Y. W., BASILIO, A., TONNU, N., VERMA, I. M., BERNS, M. W., AND HUNTER, T. (2009) CtIP links DNA double-strand break sensing to resection. Mol Cell 36, 954-969.

ZAKHARYEVICH, K., MA, Y., TANG, S., HWANG, P.Y., BOITEUX, S., HUNTER, N. (2010) Temporally and biochemically distinct activities of Exo1 during meiosis promote

double-strand-break resection and resolution of double-Holliday Junctions into crossovers, *Mol*. *Cell* 40, 1001–1015.

ZHANG Y., YUAN F., PRESNELL S., TIAN K., GAO Y., TOMKINSON A., GU L., LI G. (2005) Reconstitution of 5′-directed human mismatch repair in a purified system, *Cell* 122, 693–705.

ZHANG, J. M., LIU, X. M., DING, Y. H., XIONG, L. Y., REN, J. Y., ZHOU, Z. X., WANG, H. T., ZHANG, M. J., YU, Y., DONG, M. Q., AND DU, L. L. (2014) Fission yeast Pxd1 promotes proper DNA repair by activating Rad16XPF and inhibiting Dna2. *PLoS Biol.* 12, e1001946.

ZHOU BB, ELLEDGE SJ. (2000) The DNA damage response: putting checkpoints in perspective. *Nature.* 408:433–439.

ZHU, Z., CHUNG, W. H., SHIM, E. Y., LEE, S. E., AND IRA, G. (2008) Sgs1 helicase and two nucleases dna2 and exo1 resect DNA double-strand break ends. *Cell* 134, 981-994.

ZHUANG ZH, AI YX. (2010) Processivity factor of DNA polymerase and its expanding role in normal and translesion DNA synthesis. *Biochim Biophys Acta.* 1804:1081–1093.

ZIERHUT, C., DIFFLEY, J.F. (2008) Break dosage, cell cycle stage and DNA replication influence DNA double strand break response, *EMBO J*. 27, 1875–1885.

ZIPPER, P., DURCHSCHLAG, H., (2003). Modeling of protein solution structures. *Journal of Applied Crystallography* 36, 509–514.

ZOU, L., AND ELLEDGE, S. J. (2003) Sensing DNA damage through ATRIP recognition of RPA-ssDNA complexes. *Science* 300, 1542-1548.

APPENDICES

Primary amino acid sequence of hExo1 (846 residues)

MGIQGLLQFIKEASEPIHVRKYKGQVVAVDTYCWLHKGAIACAEKLAKGEPTDR
YVGFCMKFVNMLLSHGIKPILVFDGCTLPSKKEVERSRRERRQANLLKGKQLLRE
GKVSEARECFTRSINITHAMAHKVIKAARSQGVDCLVAPYEADAQLAYLNKAGI
VQAIITEDSDLLAFGCKKVILKMDQFGNGLEIDQARLGMCRQLGDVFTEEKFRY
MCILSGCDYLSSLRGIGLAKACKVLRLANNPDIVKVIKKIGHYLKMNITVPEDYIN
GFIRANNTFLYQLVFDPIKRKLIPLNAYEDDVDPETLSYAGQYVDDSIALQIALGN
KDINTFEQIDDYNPDTAMPAHSRSHSWDDKTCQKSANVSSIWHRNYSPRPES
GTVSDAPQLKENPSTVGVERVISTKGLNLPRKSSIVKRPRSAELSEDDLLSQYSL
SFTKKTKKNSSEGNKSLSFSEVFVPDLVNGPTNKKSVSTPPRTRNKFATFLQRK
NEESGAVVVPGTRSRFFCSSDSTDCVSNKVSIQPLDETAVTDKENNLHESEYGQ
EGKRLVDTDVARNSSDDIPNNHIPGDHIPDKATVFTDEESYSFESSKFTRTISPP
TLGTLRSCFSWSGGLGDFSRTPSPSPSTALQQFRRKSDSPTSLPENNMSDVSQ
LKSEESSDDESHPLREEACSSQSQESGEFSLQSSNASKLSQCSSKDSDSEESD
CNIKLLDSQSDQTSKLRLSHFSKKDTPLRNKVPGLYKSSSADSLSTTKIKPLGPA
RASGLSKKPASIQKRKHHNAENKPGLQIKLNELWKNFGFKKDSEKLPPCKKPLS
PVRDNIQLTPEAEEDIFNKPECGRVQRAIFQ

DNA nucleotide sequence of hExo1 gene (2541 nucleotides)

ATGGGGATACAGGGATTGCTACAATTTATCAAAGAAGCTTCAGAACCCATCCATGTGAGGA
AGTATAAAGGGCAGGTAGTAGCTGTGGATACATATTGCTGGCTTCACAAAGGAGCTATTGC
TTGTGCTGAAAAACTAGCCAAAGGTGAACCTACTGATAGGTATGTAGGATTTTGTATGAAA
TTTGTAAATATGTTACTATCTCATGGGATCAAGCCTATTCTCGTATTTGATGGATGTACTT
TACCTTCTAAAAAGGAAGTAGAGAGATCTAGAAGAGAAAGACGACAAGCCAATCTTCTTAA
GGGAAAGCAACTTCTTCGTGAGGGGAAAGTCTCGGAAGCTCGAGAGTGTTTCACCCGGTCT
ATCAATATCACACATGCCATGGCCCACAAAGTAATTAAAGCTGCCCGGTCTCAGGGGGTAG
ATTGCCTCGTGGCTCCCTATGAAGCTGATGCGCAGTTGGCCTATCTTAACAAAGCGGGAAT
TGTGCAAGCCATAATTACAGAGGACTCGGATCTCCTAGCTTTTGGCTGTAAAAAGGTAATT
TTAAAGATGGACCAGTTTGGAAATGGACTTGAAATTGATCAAGCTCGGCTAGGAATGTGCA
GACAGCTTGGGGATGTATTCACGGAAGAGAAGTTTCGTTACATGTGTATTCTTTCAGGTTG
TGACTACCTGTCATCACTGCGTGGGATTGGATTAGCAAAGGCATGCAAAGTCCTAAGACTA
GCCAATAATCCAGATATAGTAAAGGTTATCAAGAAAATTGGACATTATCTCAAGATGAATA
TCACGGTACCAGAGGATTACATCAACGGGTTTATTCGGGCCAACAATACCTTCCTCTATCA
GCTAGTTTTTGATCCCATCAAAAGGAAACTTATTCCTCTGAACGCCTATGAAGATGATGTT
GATCCTGAAACACTAAGCTACGCTGGGCAATATGTTGATGATTCCATAGCTCTTCAAATAG
CACTTGGAAATAAAGATATAAATACTTTTGAACAGATCGATGACTACAATCCAGACACTGC
TATGCCTGCCCATTCAAGAAGTCATAGTTGGGATGACAAAACATGTCAAAAGTCAGCTAAT
GTTAGCAGCATTTGGCATAGGAATTACTCTCCCAGACCAGAGTCGGGTACTGTTTCAGATG
CCCCACAATTGAAGGAAAATCCAAGTACTGTGGGAGTGGAACGAGTGATTAGTACTAAAGG
GTTAAATCTCCCAAGGAAATCATCCATTGTGAAAAGACCAAGAAGTGCAGAGCTGTCAGAA
GATGACCTGTTGAGTCAGTATTCTCTTTCATTTACGAAGAAGACCAAGAAAAATAGCTCTG
AAGGCAATAAATCATTGAGCTTTTCTGAAGTGTTTGTGCCTGACCTGGTAAATGGACCTAC
TAACAAAAAGAGTGTAAGCACTCCACCTAGGACGAGAAATAAATTTGCAACATTTTTACAA
AGGAAAAATGAAGAAAGTGGTGCAGTTGTGGTTCCAGGGACCAGAAGCAGGTTTTTTTGCA
GTTCAGATTCTACTGACTGTGTATCAAACAAAGTGAGCATCCAGCCTCTGGATGAAACTGC

TGTCACAGATAAAGAGAACAATCTGCATGAATCAGAGTATGGAGACCAAGAAGGCAAGAGA
CTGGTTGACACAGATGTAGCACGTAATTCAAGTGATGACATTCCGAATAATCATATTCCAG
GTGATCATATTCCAGACAAGGCAACAGTGTTTACAGATGAAGAGTCCTACTCTTTTGAGAG
CAGCAAATTTACAAGGACCATTTCACCACCCACTTTGGGAACACTAAGAAGTTGTTTTAGT
TGGTCTGGAGGTCTTGGAGATTTTTCAAGAACGCCGAGCCCCTCTCCAAGCACAGCATTG
CAGCAGTTCCGAAGAAAGAGCGATTCCCCCACCTCTTTGCCTGAGAATAATATGTCTGATG
TGTCGCAGTTAAAGAGCGAGGAGTCCAGTGACGATGAGTCTCATCCCTTACGAGAAGAGGC
ATGTTCTTCACAGTCCCAGGAAAGTGGAGAATTCTCACTGCAGAGTTCAAATGCATCAAAG
CTTTCTCAGTGCTCTAGTAAGGACTCTGATTCAGAGGAATCTGATTGCAATATTAAGTTAC
TTGACAGTCAAAGTGACCAGACCTCCAAGCTACGTTTATCTCATTTCTCAAAAAAAGACAC
ACCTCTAAGGAACAAGGTTCCTGGGCTATATAAGTCCAGTTCTGCAGACTCTCTTTCTACA
ACCAAGATCAAACCTCTAGGACCTGCCAGAGCCAGTGGGCTGAGCAAGAAGCCGGCAAGCA
TCCAGAAGAGAAAGCATCATAATGCCGAGAACAAGCCGGGGTTACAGATCAAACTCAATGA
GCTCTGGAAAAACTTTGGATTTAAAAAAGATTCTGAAAAGCTTCCTCCTTGTAAGAAACCC
CTGTCCCCAGTCAGAGATAACATCCAACTAACTCCAGAAGCGGAAGAGGATATATTTAACA
AACCTGAATGTGGCCGTGTTCAAAGAGCAATATTCCAGTAA

Primary amino acid sequence of PCNA (261 residues)

MFEARLVQGSILKKVLEALKDLINEACWDISSSGVNLQSMDSSHVSLVQLTLRS
EGFDTYRCDRNLAMGVNLTSMSKILKCAGNEDIITLRAEDNADTLALVFEAPNQ
EKVSDYEMKLMDLDVEQLGIPEQEYSCVVKMPSGEFARICRDLSHIGDAVVISC
AKDGVKFSASGELGNGNIKLSQTSNVDKEEEAVTIEMNEPVQLTFALRYLNFFTK
ATPLSSTVTLSMSADVPLVVEYKIADMGHLKYYLAPKIEDEEGS

DNA nucleotide sequence of PCNA (786 nucleotides)

ATGTTCGAGGCGCGCCTGGTCCAGGGCTCCATCCTCAAGAAGGTGTTGGAGGCACTCAAGG
ACCTCATCAACGAGGCCTGCTGGGATATTAGCTCCAGCGGTGTAAACCTGCAGAGCATGGA
CTCGTCCCACGTCTCTTTGGTGCAGCTCACCCTGCGGTCTGAGGGCTTCGACACCTACCGC
TGCGACCGCAACCTGGCCATGGGCGTGAACCTCACCAGTATGTCCAAAATACTAAAATGCG
CCGGCAATGAAGATATCATTACACTAAGGGCCGAAGATAACGCGGATACCTTGGCGCTAGT
ATTTGAAGCACCAAACCAGGAGAAAGTTTCAGACTATGAAATGAAGTTGATGGATTTAGAT
GTTGAACAACTTGGAATTCCAGAACAGGAGTACAGCTGTGTAGTAAAGATGCCTTCTGGTG
AATTTGCACGTATATGCCGAGATCTCAGCCATATTGGAGATGCTGTTGTAATTTCCTGTGC
AAAAGACGGAGTGAAATTTTCTGCAAGTGGAGAACTTGGAAATGGAAACATTAAATTGTCA
CAGACAAGTAATGTCGATAAAGAGGAGGAAGCTGTTACCATAGAGATGAATGAACCAGTTC
AACTAACTTTTGCACTGAGGTACCTGAACTTCTTTACAAAAGCCACTCCACTCTCTTCAAC
GGTGACACTCAGTATGTCTGCAGATGTACCCCTTGTTGTAGAGTATAAAATTGCGGATATG
GGACACTTAAAATACTACTTGGCTCCCAAGATCGAGGATGAAGAAGGATCTTAG

Primary amino acid sequence of the 14-3-3ζ (248 residues)

MDKNELVQKAKLAEQAERYDDMAACMKSVTEQGAELSNEERNLLSVAYKNVVG
ARRSSWRVVSSIEQKTEGAEKKQQMAREYREKIETELRDICNDVLSLLEKFLIPN
ASQAESKVFYLKMKGDYYRYLAEVAAGDDKKGIVDQSQQAYQEAFEISKKEMQ
PTHPIRLGLALNFSVFYYEILNSPEKACSLAKTAFDEAIAELDTLSEES
YKDSTLIMQL LRDNLTLWTS DTQGDEAEAG EGGEN

DNA nucleotide sequence of the 14-3-3ζ (744 nucleotides)

TTCCCCTGGCTGTCTGCCGACCTGGGAGCCAATGGAGCGTTGGCTGCTGCTGGCCACCCG
GGGTTCTCTTGGCATCTGTGTAACCTGTGACCAAGCAAGGGCTGGAAGAGTGGGCGATCG
TCTTCCTCTTCCTGGGGGCTGAGATGCGGACTCCCGAGGGCCTCTCTGTCAGCCTTGGGG
CGGCTGGCAAGCGGCAGGCCGATCCCCTCTGCGCAGGGAAGTAGCACGACTCCGTCACCA
TCTTGGGCCACGCTGGGGGCACCGCCGGACCCCTGTTCTGGGGCTCCGCCTGGATGTCCA
CAAATGCTGAGGCCTGCTTGTGCATCTGGGGCACCCAGAGCCCGAAGCTCTGGGCAGGCT
GATGAGAGGGCAGTGGGAATTCTGGAGCCTCGAGGGCCGCCTCCTCGGCCACCTTCTTAG
CTTCTGGGTATCCAGGTGGGAACCAGCAGGGAGCTGTGGCTCGCAACATCTTGCTGCCTT
CGGGAGCACCGGCCTGGCTCTGCTCCTCTCCCCACTGGCGGCTTCAATCAGTGTCGCGGT
GGTCGCGCATCGCCTTTATATAGGCATGGGTCAGAGTGGGTGGGGCTTCTTCTTGATTAC
GTTGGTACTTTATTCTAATCACACTAAATCTCATCTTCCACCAGACTCCAGCTTCGGAAT
GCCTCAGAGGGTCTGCTAATGGAAGCAACTGGATCTCCTGGTTGCTAACCTTGGAGCTAG
GTTGCTTTTCCTGAGTTAATTTACTGTGCCTGCACAGCAGTCCTATAATGGCTACTGGAA
CTGGGCTACTTAGGAGTAAAATGAGGTTCATGGAGGTTTTTCAACTTGTTCGGGCCCAGA
CAACATCCCACGGACCCAGGACTGGTGCAGCAGTCCGCTGCATGCTGGCGGGCAGGATCT
CTCTGGGGTTGCGTTTCCCTGCTCTGTGCACTCTTCCACTGTGGGCAATTGGAGGACAGG
AAGTGGACCACATCCACTTCTGTCCCAGGACATGGGCAAT

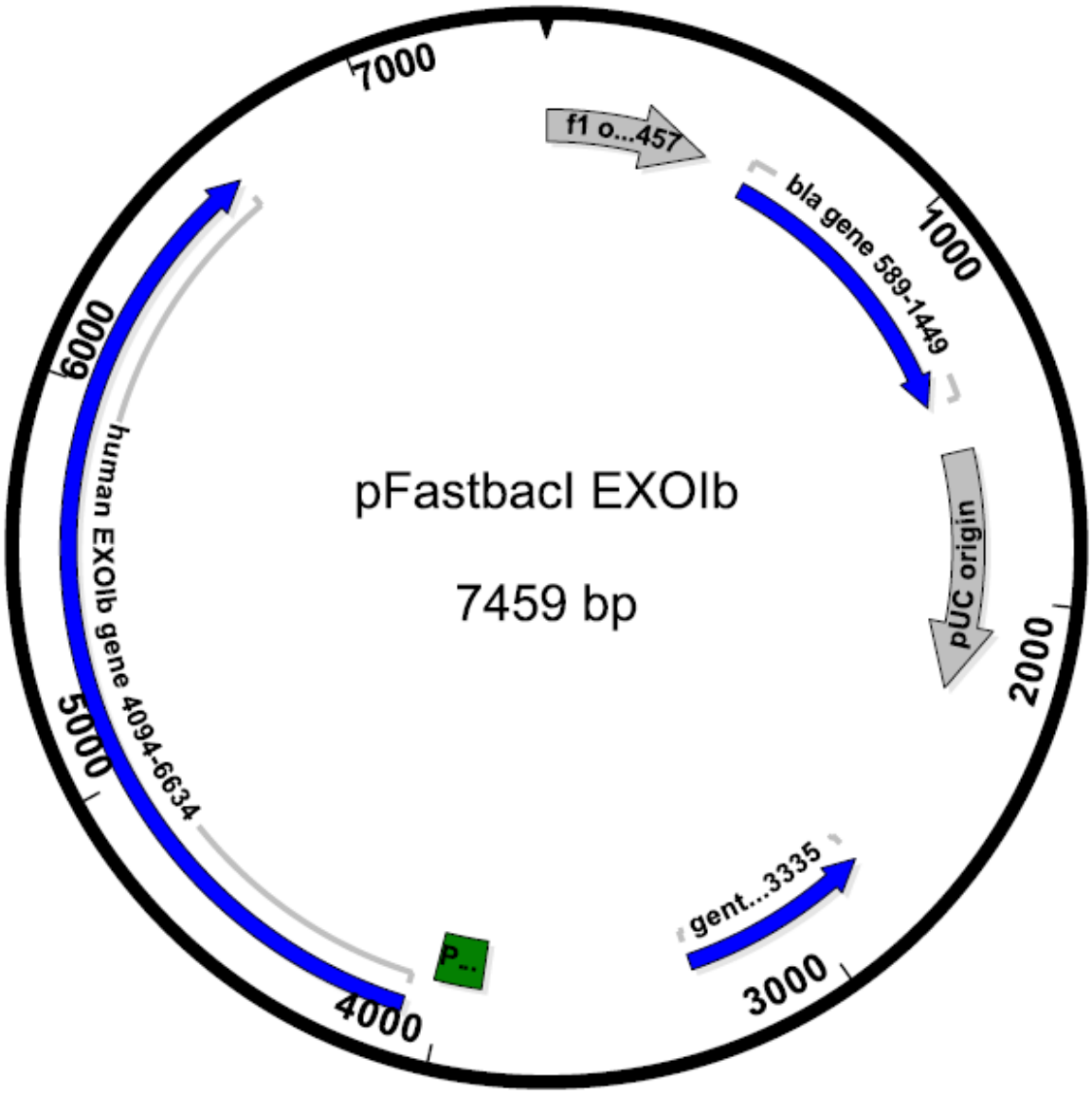
Primary amino acid sequence of the 14-3-3ε (255 residues)

MDDREDLVYQAKLAEQAERYDEMVESMKKVAGMDVELTVEERNLLSVAYKNVI
GARRASWRIISSIEQKEENKGGEDKLKMIREYRQMVETELKLICCDILDVLDKHL
IPAANTGESKVFYYKMKGDYHRYLAEFATGNDRKEAAENSLVAYKAASDIAMTE
LPPTHPIRLGLALNFSVFYYEILNSPDRACRLAKAAFDDAIAELDTLSEESYKDSTL
IMQLLRDNLTLWTSDMQGDGE EQNKEALQDV EDENQ

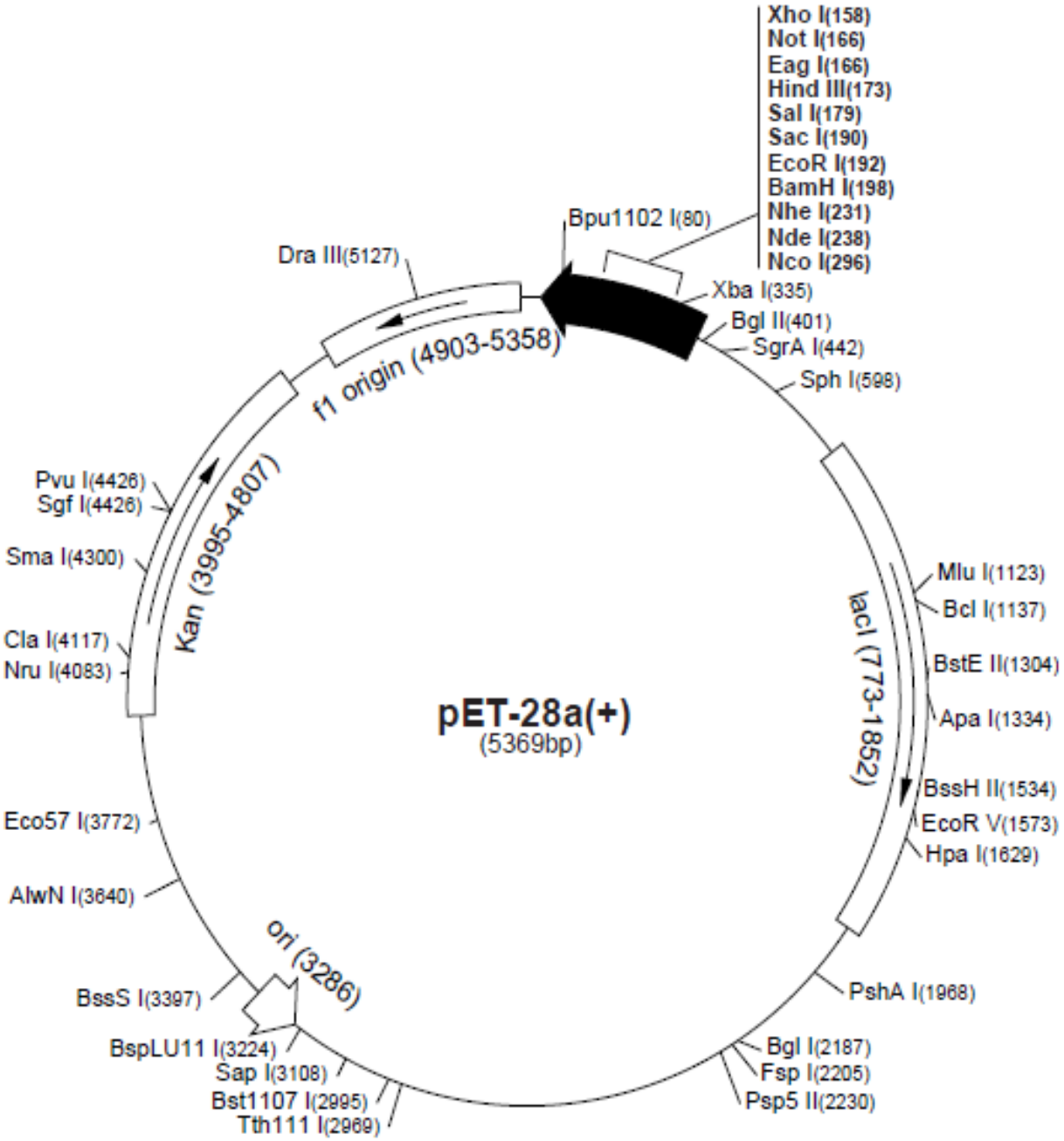
DNA nucleotide sequence of the 14-3-3ε (765 nucleotides)

GGAGGAATTCTTACATCAAACAACATTTGGGCTCTAGAAGCCTCCCAAGGAGTCCTTGTA
AAGAGTCGCGGCCGGGCGCCGTGGCTCACGCCTGTAATCCCGGCACTTTGGGAGGCCGAG
ACGGGTGGATCATGAGGTCAGGAAATCGAGACCATCATGGCTTACAAGGTGAAACCCAGT
CTCTACTAAAAAAAAATACAAAAAAATTAGCCGGACTTGGTGGCGGCAGCCTGCAGTCCC
AGCTACTCGGGAGGCCGGGACAGGAGAATGGCATGAACCCGGGAGGCGGAGCTTGCTGTG
AGCTGAGATCGCGCCACTGCACTCCAGCCTGGGCGACAGAGCGAGACTCCGCCTCAAAAA
AGAAAAAAGAAGAAGAACAAGAAGAATCGCAACCTAATTTAGTATAGAAACAAACTGTAA
ATCTGACTTGGGAATGTATCATGGTAACAAATAGCGGCGGTTCAGCCAATCACATCAGCC
GAGTGTCAGTCAATGGCCGGCAGCCAGCTGTTCAAAACAAGTTCCAAGAAGGCAAATCCG
GGCTGTAACCAGGTCTGTAACCAATCCAGCCACCTCTATACCTCACTTCTGTTTTCTGTA
TGTCACTTTTTTTCTCTGGCTATAAATATAACCCGCACATGTTGTGTGGCAGATCATTCT
GAACCATTTTTGGTCTGGACTGCTGCCTGATTCTAGAACCACAAAAAAAGCCAATTAAGA
TCTGCAAACCCACATTTGTTGTAATTTTGTATTTTAACAGTTGTGCCCTACAAAAGACAT
TAAGCTGAAATTAATTAAAAATCATTTACGGTCATGATTAGGTCATAAAAAATTGTCAAA
CATAACAATTCTTCAAAAAAAGCTAAAAAGTATATTTTAAAAACATTGTTGATGGAAAAA
AGAGTGCAAAAGTAGATAGGAAAATTATGTACAAAACTAAAAACAGAGGAGAAATTAAAA
GTCAAATAATTGCATCAAACTGGAAACCTAGAAAAAATGG

Map of pFastbacI-hExo1 plasmid



Map of pET28a vector



Map of pTXB1 vector

